ZOOM ONLY (CERN)

3. JUNE 2020

Postmerger Gravitational-Wave Signatures of Phase Transitions in Binary Compact Star Mergers

MATTHIAS HANAUSKE

FRANKFURT INSTITUTE FOR ADVANCED STUDIES

JOHANN WOLFGANG GOETHE UNIVERSITÄT

INSTITUT FÜR THEORETIsCHE PHYSIK

ARBEITSGRUPPE RELATIVISTISCHE ASTROPHYSIK

D-60438 FRANKFURT AM MAIN

In collaboration with Lukas Weih, Elias R. Most, L. Jens Papenfort, Luke Bovard, Gloria Montana, Laura Tolos, Jan Steinheimer, Veronica Dexheimer, Horst Stöcker, and Luciano Rezzolla

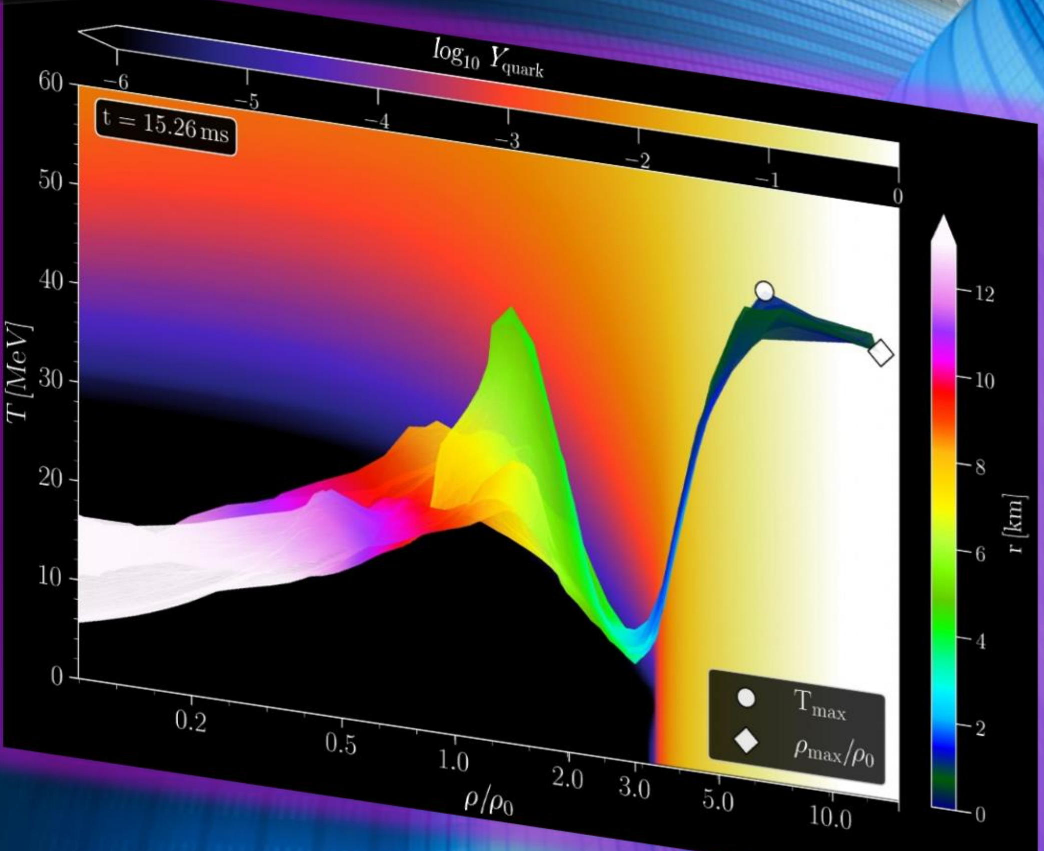

Postmerger gravitational-wave signatures of phase transitions in binary compact star mergers

Postmerger gravitational-wave signatures of phase transitions in binary compact star mergers

- Introduction
- Numerical general relativity of compact star mergers
- The equation of state of compact star matter and the hadron-quark phase transition
- The different phases of a binary compact star merger event
- Gravitational-wave signatures of the hadron-quark phase transition in binary compact star mergers
  - The inspiral and merger phase (premerger signals)
  - Hypermassive hybrid stars (HMHS) within the prompt phase transition scenario (PPT)
  - HMHS within the delayed phase transition scenario (DPT)
  - HMHS within the phase transition triggered collapse scenario (PTTC)
- Summary and Outlook

2015: Gravitational Waves observed by LIGO

Collission of two Black Holes
GW150914

Masses: 36 & 29 Sunmasses

Distance to the Earth 410 Mpc
(1.34 Billion Lightyears)

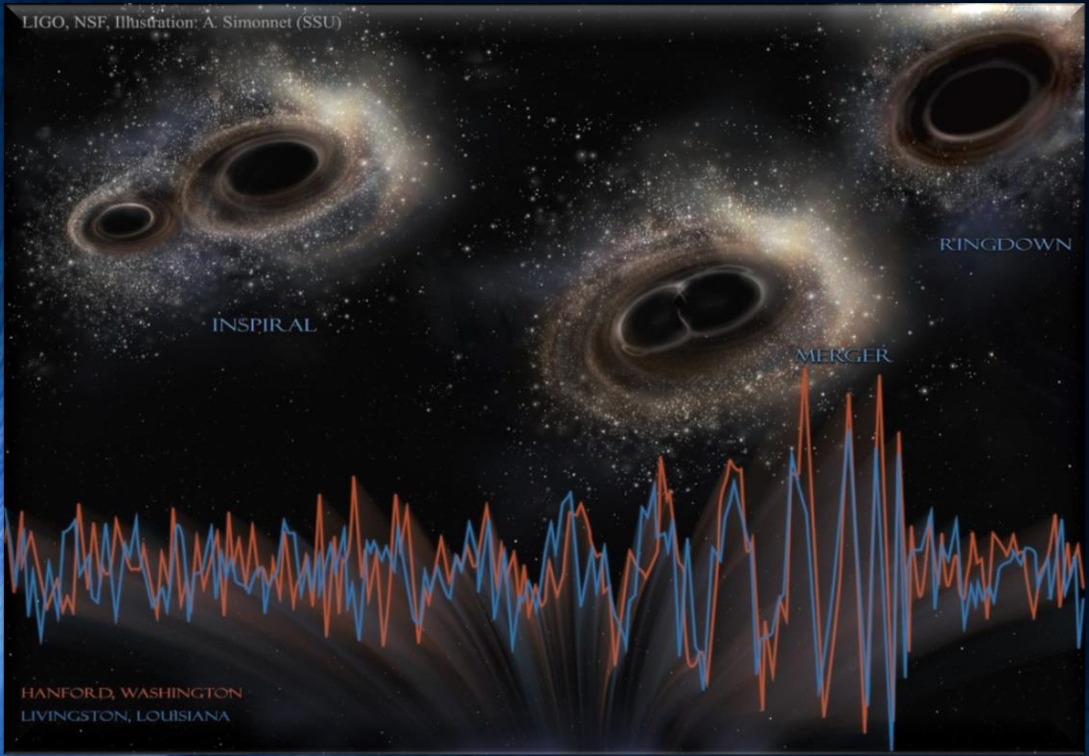

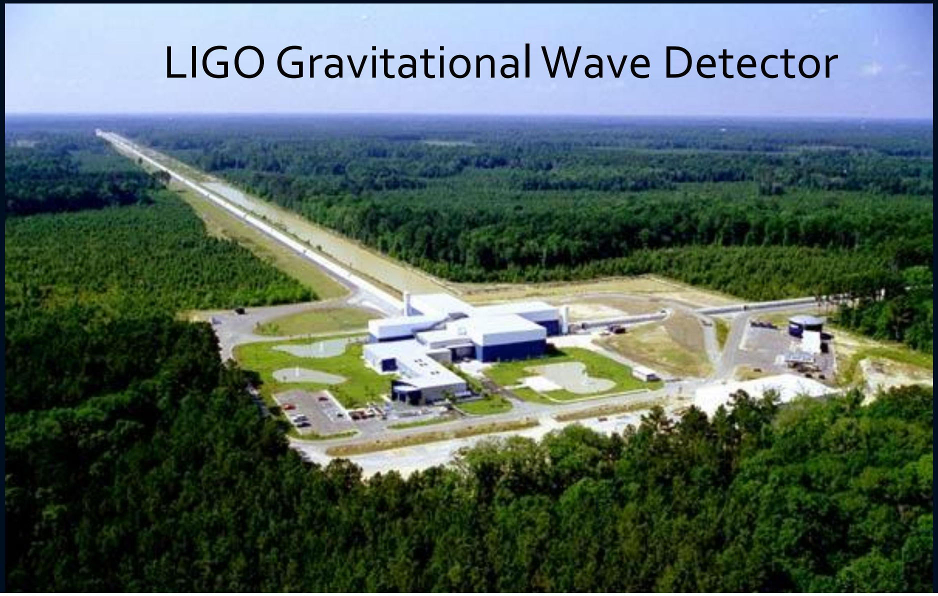

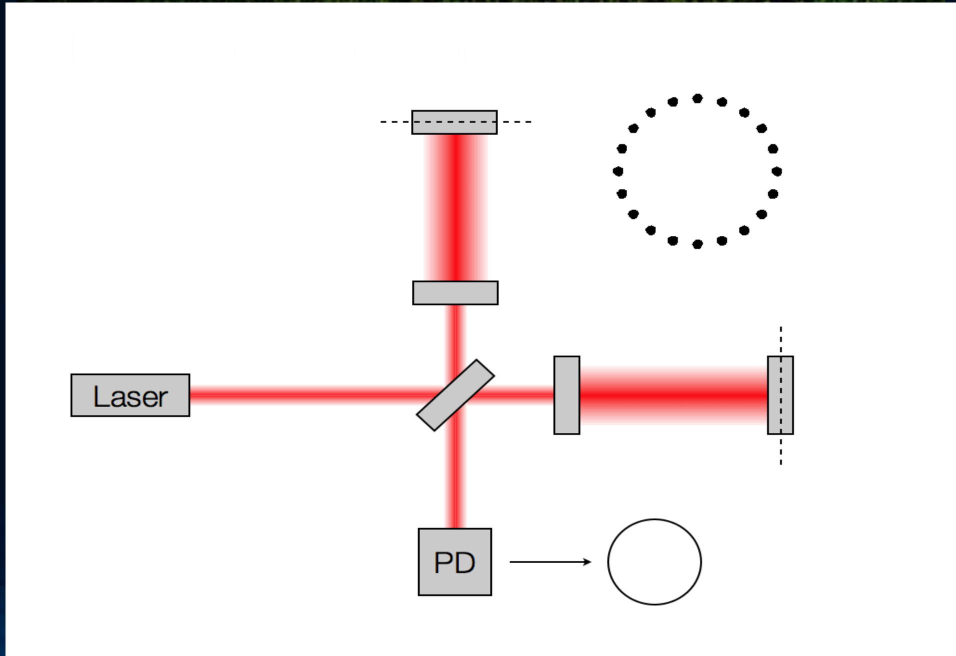

The long awaited event GW170817

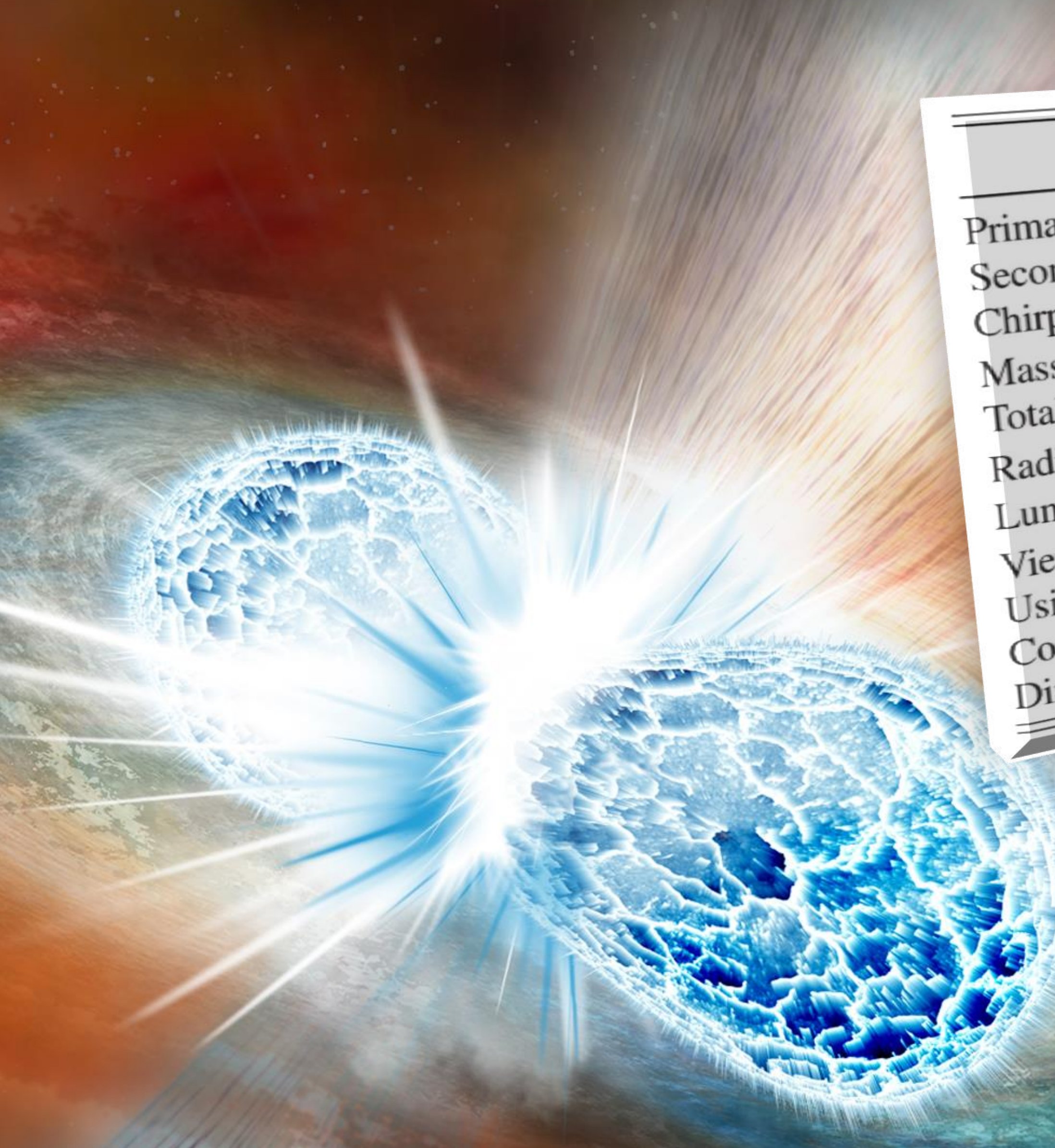

	Low-spin priors ($\lvert\chi\rvert \leq 0.05$)	High-spin priors ($\lvert\chi\rvert \leq 0.89$)
Primary mass m_1	$1.36–1.60\ M_\odot$	$1.36–2.26\ M_\odot$
Secondary mass m_2	$1.17–1.36\ M_\odot$	$0.86–1.36\ M_\odot$
Chirp mass $\mathcal{M}$	$1.188^{+0.004}_{-0.002} M_\odot$	$1.188^{+0.004}_{-0.002} M_\odot$
Mass ratio m_2/m_1	$0.7–1.0$	$0.4–1.0$
Total mass $m_{\rm tot}$	$2.74^{+0.04}_{-0.01} M_\odot$	$2.82^{+0.47}_{-0.09} M_\odot$
Radiated energy $E_{\rm rad}$	$> 0.025 M_\odot c^2$	$> 0.025 M_\odot c^2$
Luminosity distance $D_{\rm L}$	40^{+8}_{-14} Mpc	40^{+8}_{-14} Mpc
Viewing angle Θ	$\leq 55°$	$\leq 56°$
Using NGC 4993 location	$\leq 28°$	$\leq 28°$
Combined dimensionless tidal deformability $\tilde{\Lambda}$	≤ 800	≤ 700
Dimensionless tidal deformability $\Lambda(1.4 M_\odot)$	≤ 800	≤ 1400

17. August 2017

First detection of a gravitational wave from a binary neutron star merger event!

Gravitational Wave GW170817 and Gamma-Ray Emission GRB170817A

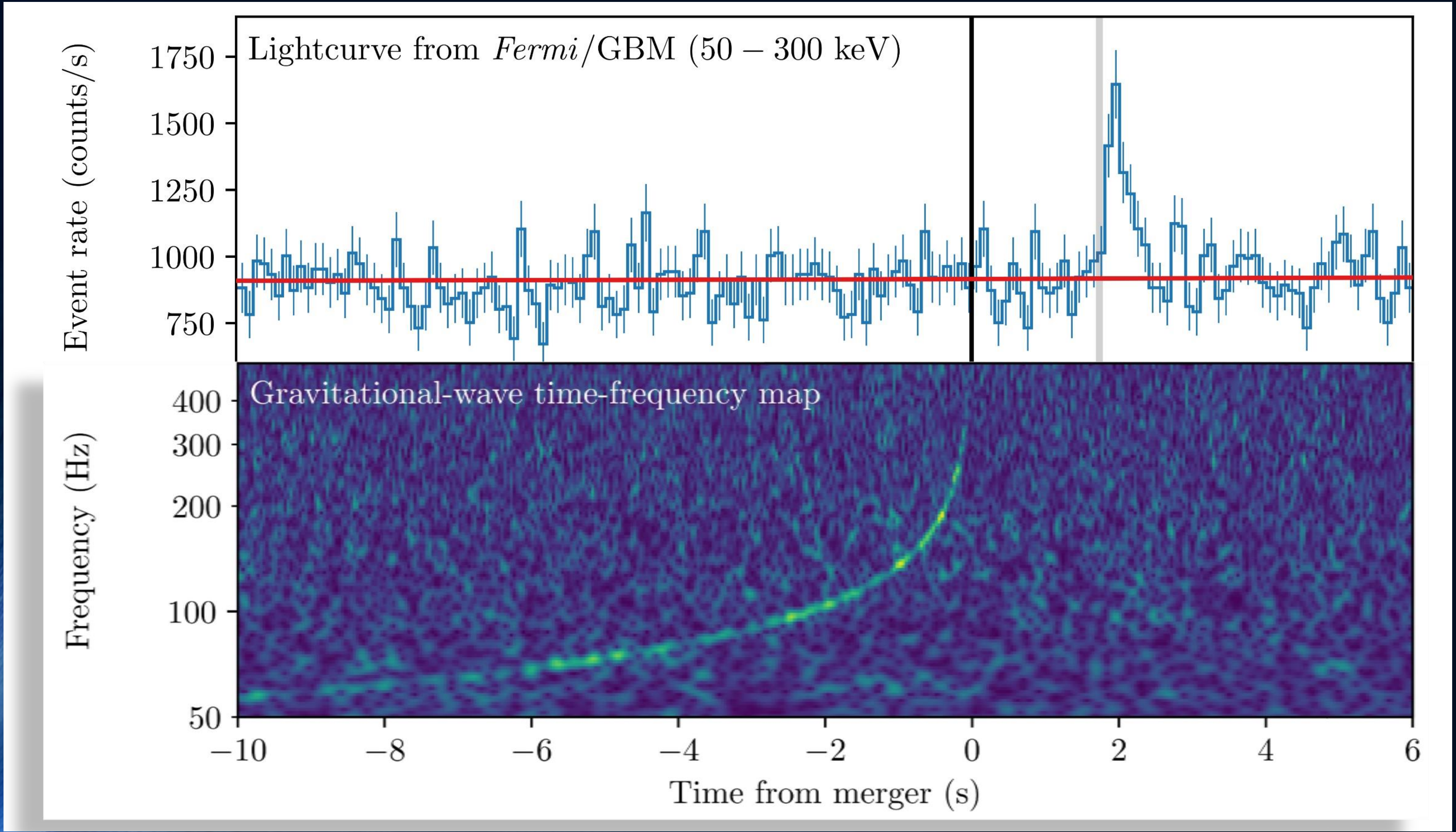

GW170817

Kilonova observed

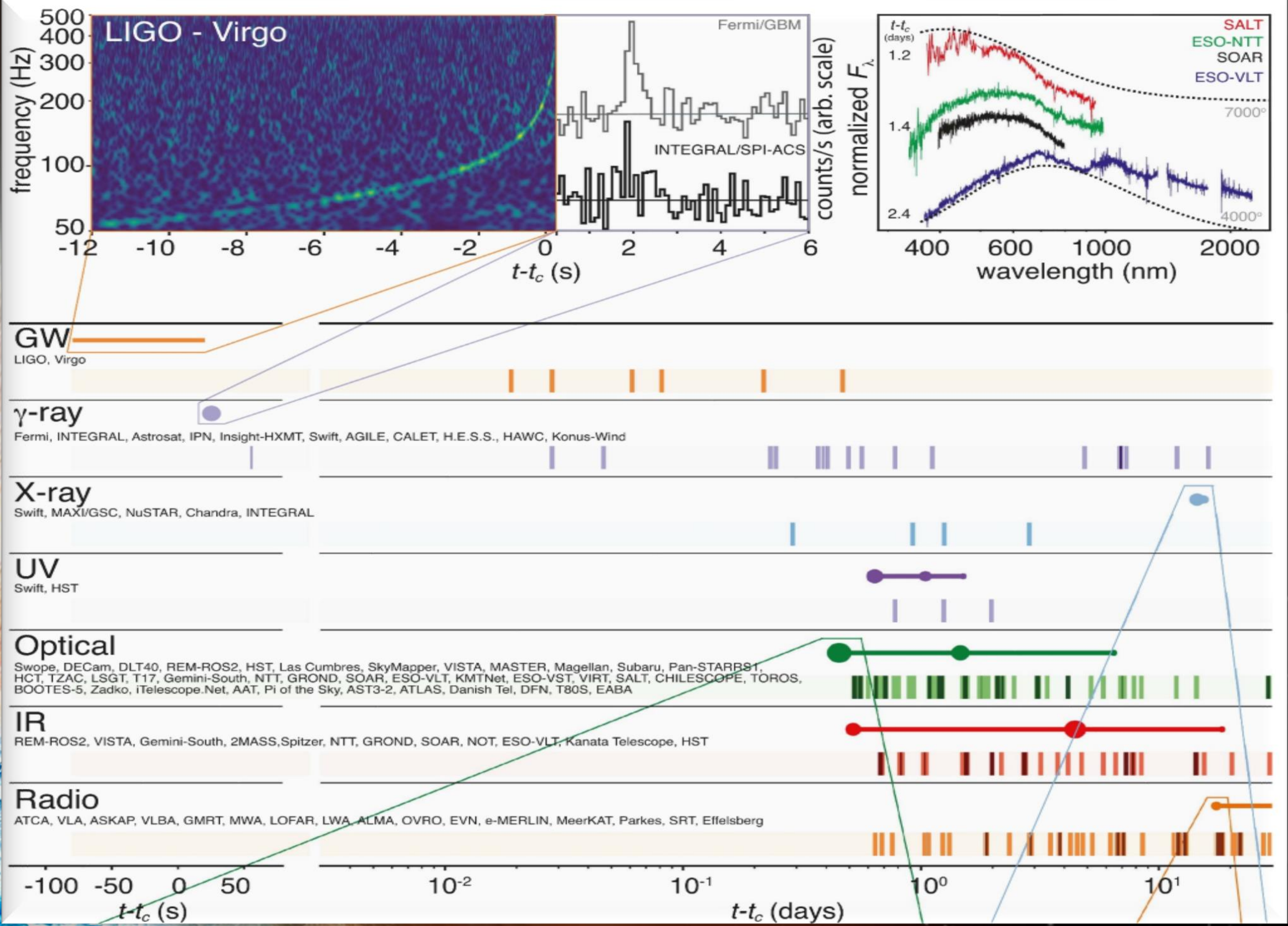

The second event: GW190425

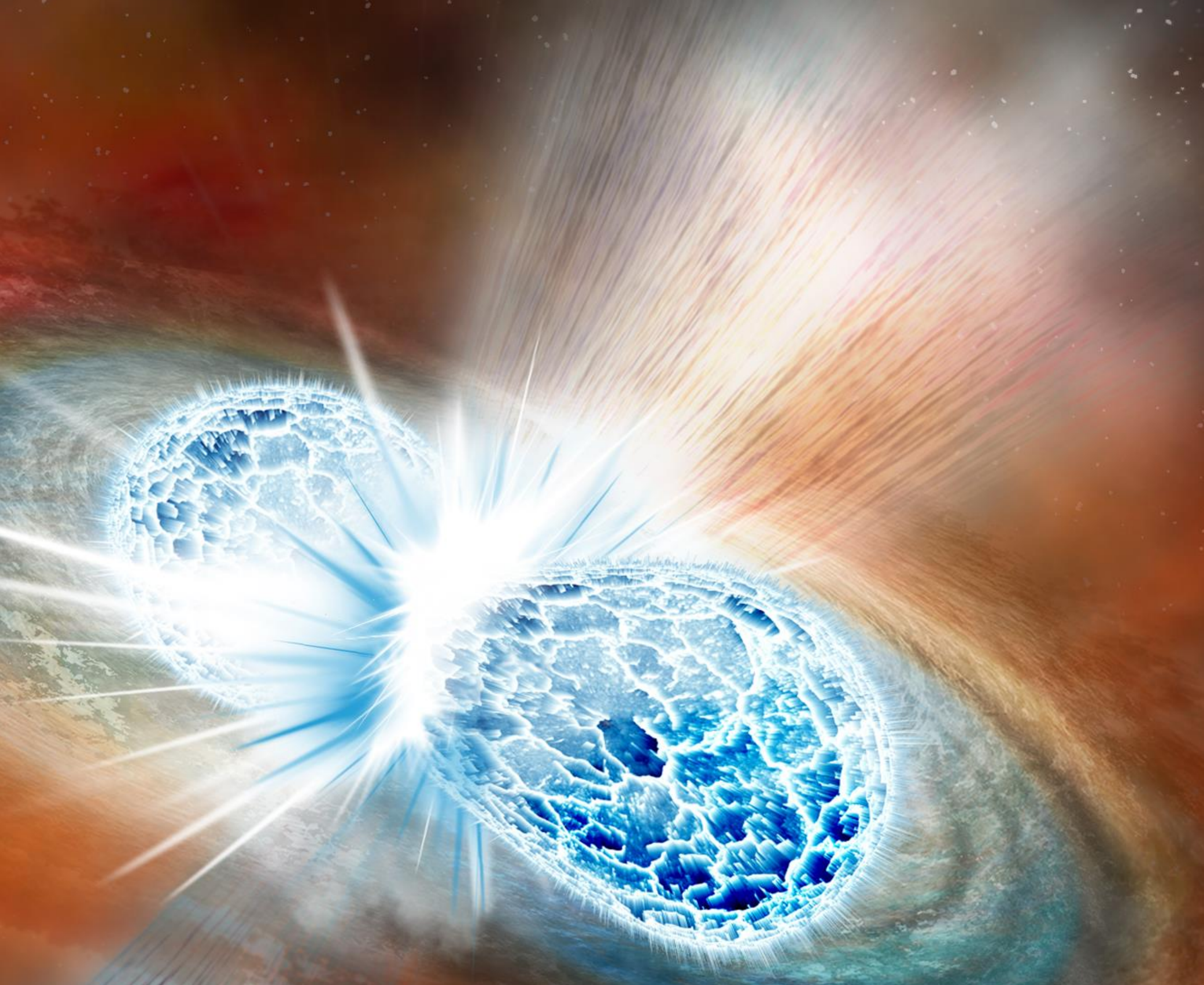

Mass ~ 3.4 $M_\odot$

19. April 2019

Second detection of a gravitational wave from a binary neutron star merger event!

Numerical Relativity and Relativistic Hydrodynamics of Binary Neutron Star Mergers

Einstein's theory of general relativity and the resulting general relativistic conservation laws for energy-momentum in connection with the rest-mass conservation are the theoretical groundings of neutron star binary mergers:

$$R_{\mu\nu} - \frac{1}{2} g_{\mu\nu} R = 8\pi T_{\mu\nu}$$

$$\nabla_\mu (\rho u^\mu) = 0\,, \qquad \nabla_\nu T^{\mu\nu} = 0\,.$$

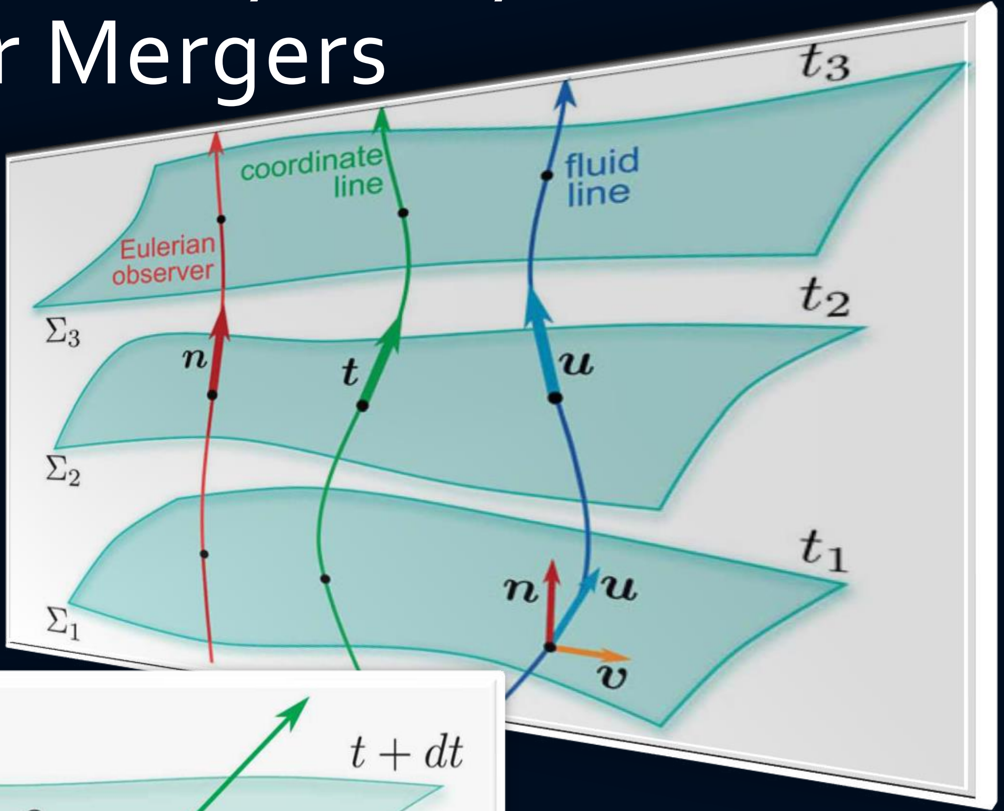

(3+1) decomposition of spacetime

$$g_{\mu\nu} = \begin{pmatrix} -\alpha^2 + \beta_i \beta^i & \beta_i \\ \beta_i & \gamma_{ij} \end{pmatrix}$$

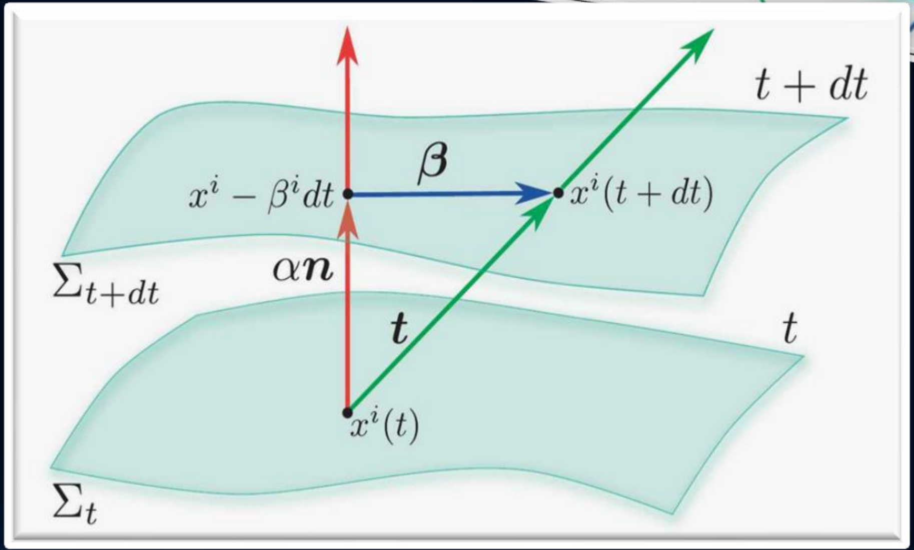

$$d\tau^2 = \alpha^2(t, x^j) dt^2 \qquad x^i_{t+dt} = x^i_t - \beta^i(t, x^j) dt$$

All figures and equations from: Luciano Rezzolla, Olindo Zanotti: Relativistic Hydrodynamics, Oxford Univ. Press, Oxford (2013)

The Einstein Equation and the EOS of Compact Stars

ART	Yang-Mills-Theories
$D_\beta v^\alpha = \partial_\beta\, v^\alpha + \Gamma^\alpha_{\sigma\beta}\, v^\sigma$	$D_{\beta a}{}^{b} = \partial_\beta\, 1_a{}^{b} + ig\, A_{\beta a}{}^{b}$
$R^\delta{}_{\mu\alpha\beta}\, v^\mu = \left[D_\alpha, D_\beta\right] v^\delta$ $R^\delta{}_{\mu\alpha\beta} = \Gamma^\delta_{\mu\alpha\vert\beta} - \Gamma^\delta_{\mu\beta\vert\alpha}$ $+\Gamma^\delta_{\nu\beta}\Gamma^\nu_{\mu\alpha} + \Gamma^\delta_{\nu\alpha}\Gamma^\nu_{\mu\beta}$	$F_{\alpha\beta a}{}^{b} = \frac{1}{ig}\left[D_{\alpha a}{}^{c}, D_{\beta c}{}^{b}\right]$ $= A_{\beta a}{}^{b}{}_{\vert\alpha} - A_{\alpha a}{}^{b}{}_{\vert\beta}$ $+\frac{1}{ig}\left[A_{\alpha a}{}^{c}, A_{\beta c}{}^{b}\right]$
$\mathcal{L}_G = R + \underbrace{\left(c_1\, R_{\mu\nu}R^{\mu\nu} + \ldots\right)}_{\equiv 0 \text{ for ART}}$	$\mathcal{L}_{YM} = \frac{1}{4} F_{\mu\nu a}{}^{b}\, F^{\mu\nu}{}_{a}{}^{b}$

QuantumCromoDynamic:

$(SU(3)_{(c)}$- Color Yang-Mills-Gauge Theory)

$$\boxed{\begin{array}{c} D_{\beta A}{}^{B} = \partial_\beta\, 1_A{}^{B} + ig\, G_{\beta A}{}^{B} \\ {}_{A,}{}^{B} = \text{red, green, blue} \end{array}}$$

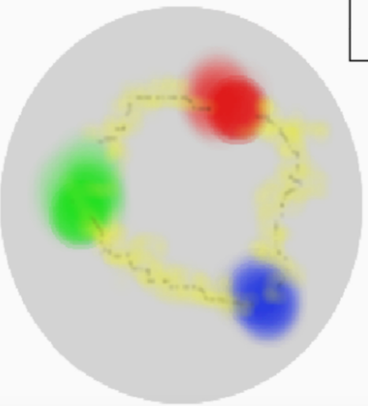

$$\psi^f_A = \begin{pmatrix} \psi^f_r \\ \psi^f_g \\ \psi^f_b \end{pmatrix}$$

Confinement

chiral symmetry, ...

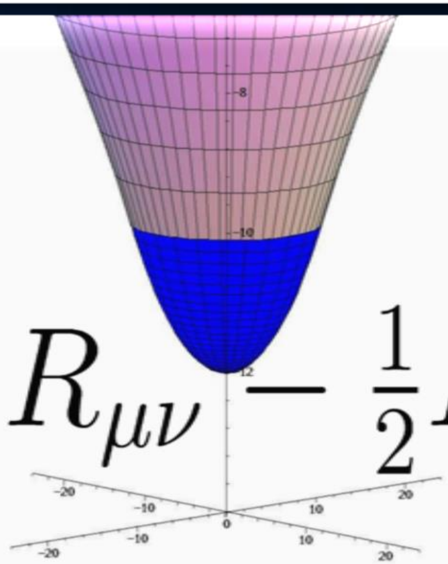

$$R_{\mu\nu} - \frac{1}{2} R\, g_{\mu\nu} = \frac{8\pi G}{c^4}\, T_{\mu\nu}$$

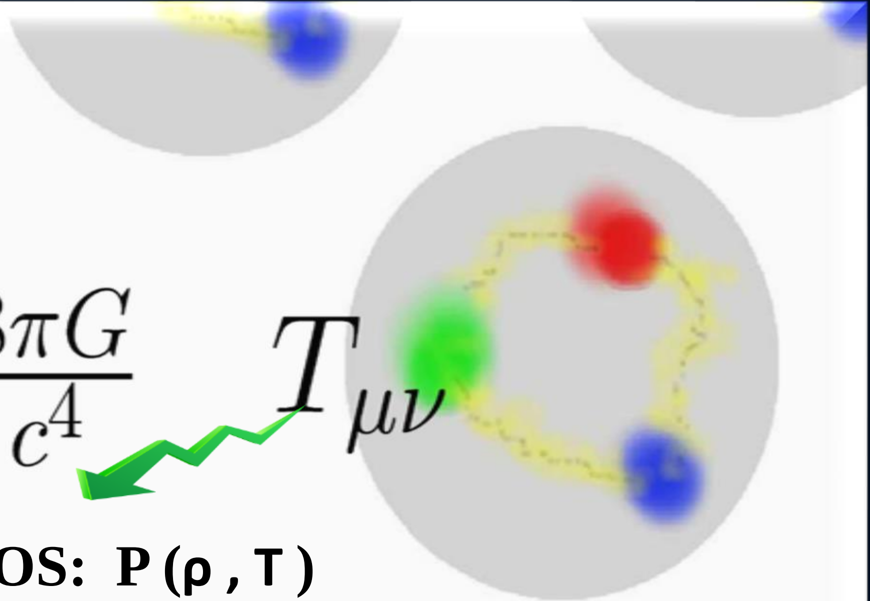

EOS: P (ρ , T)

The Hadron-Quark Phase Transition

The QCD Phase Diagram

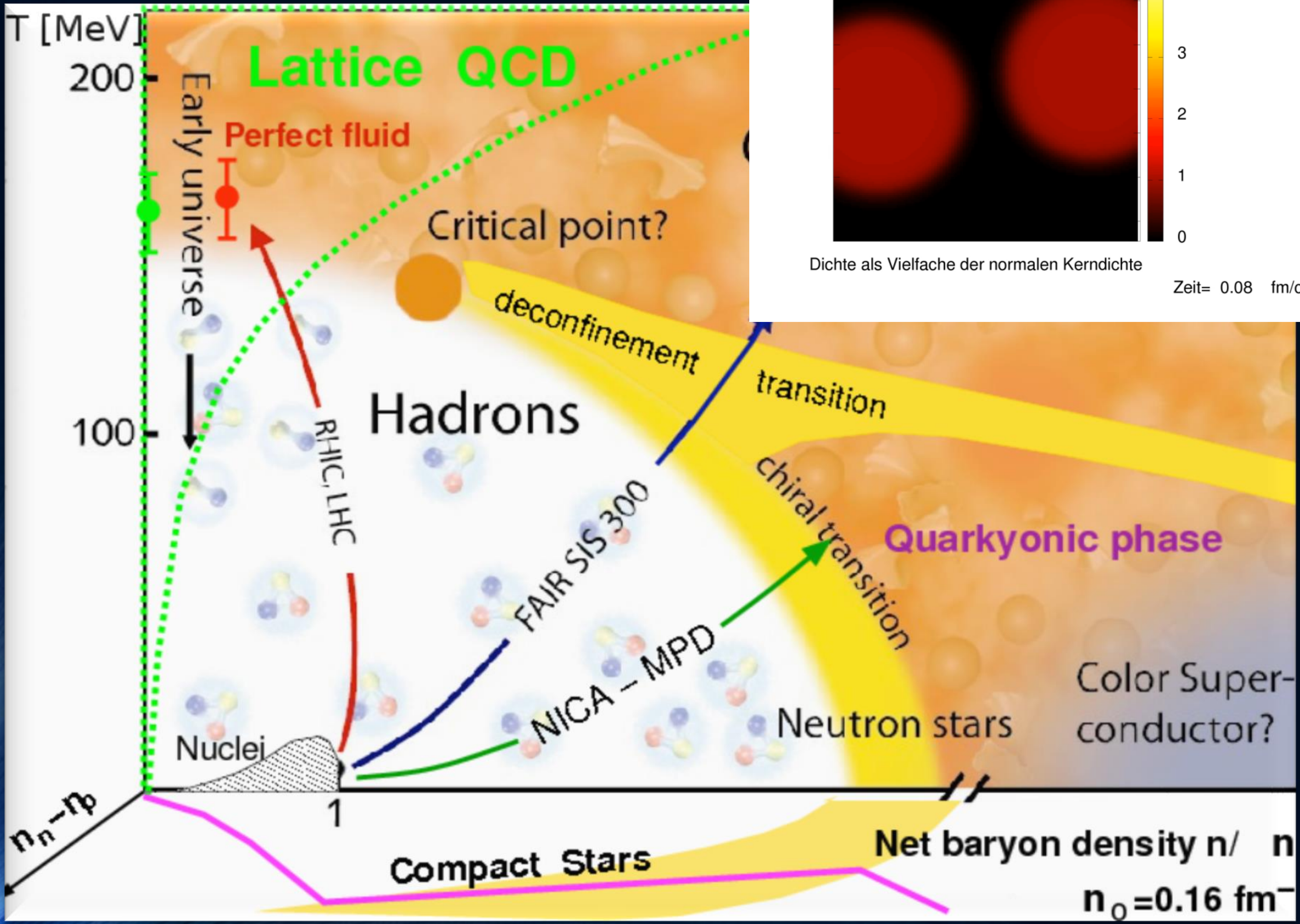

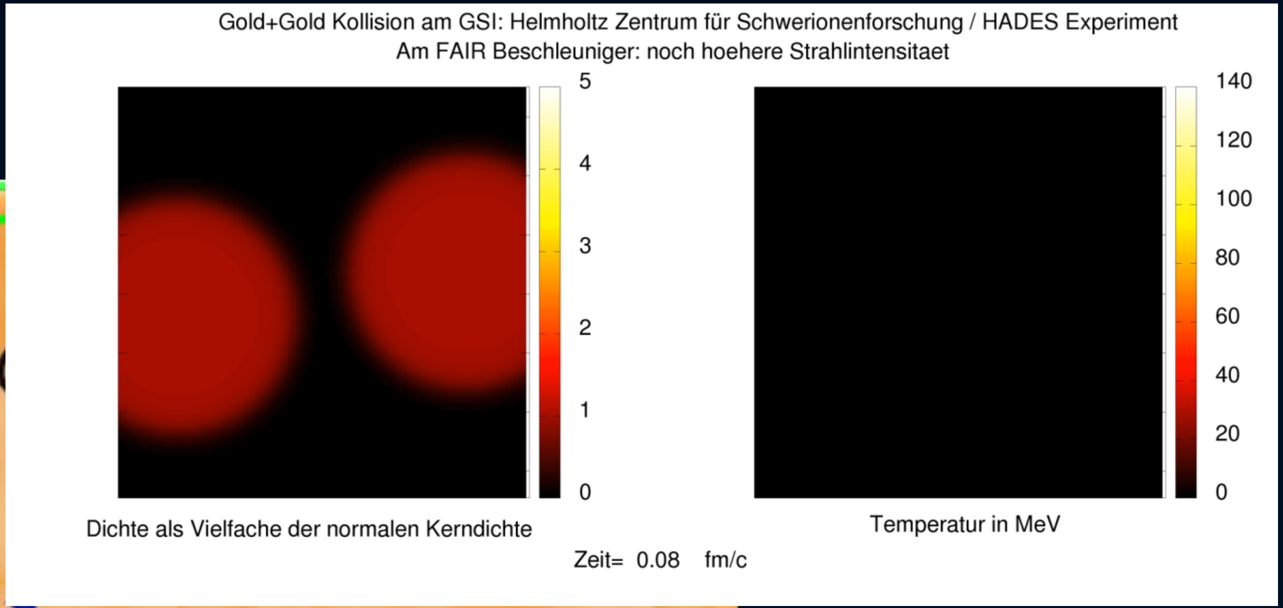

Credits:
Jan Steinheimer

Neutron

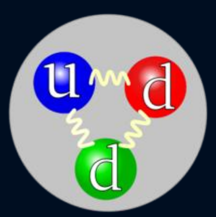

Proton

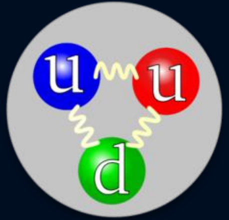

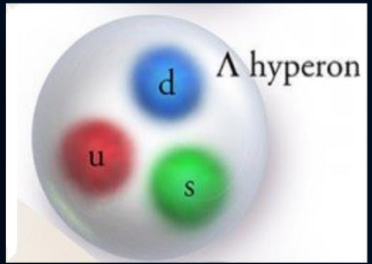

The QCD – Phase Transition and the Interior of a Hybrid Star

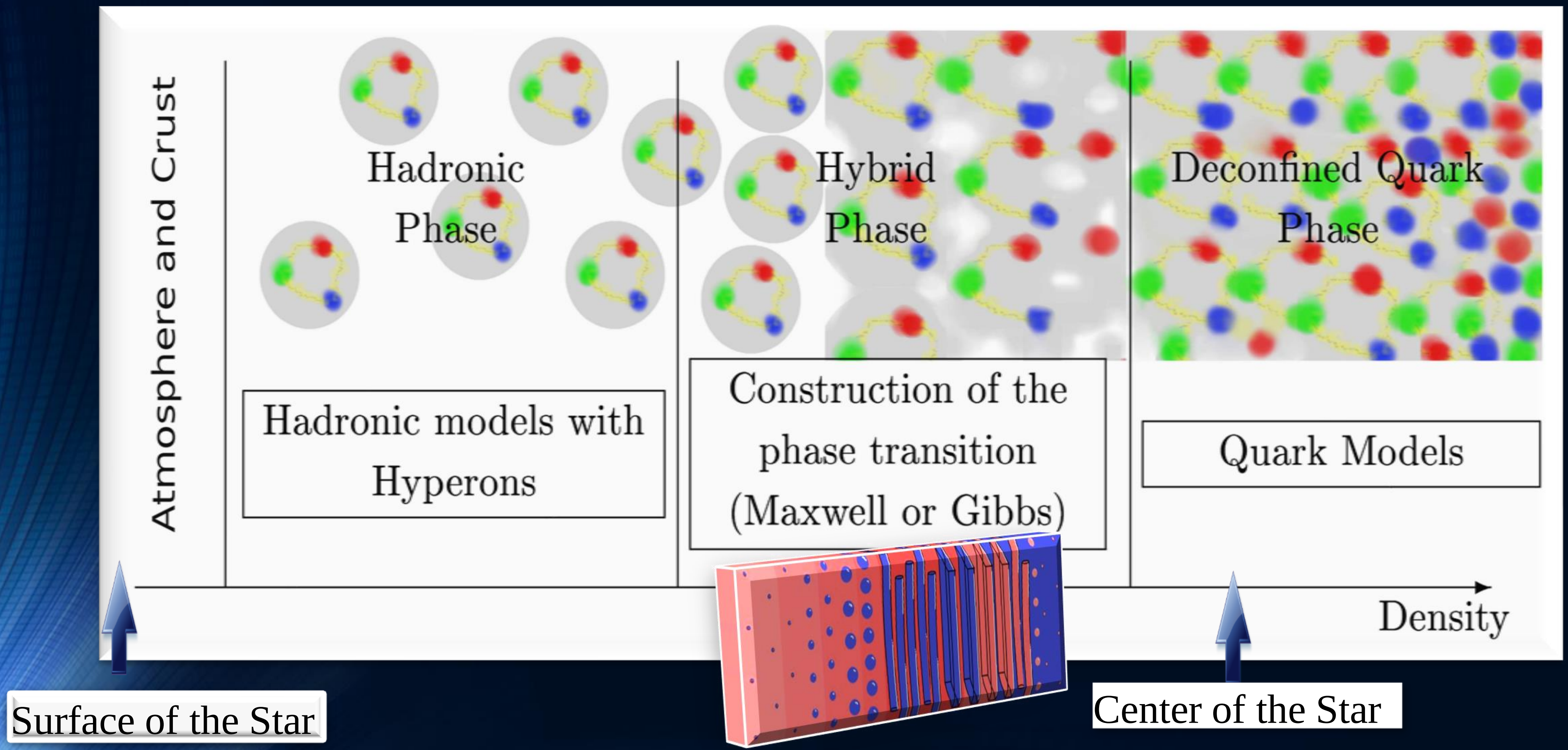

Matthias Hanauske; Doctoral Thesis:
Properties of Compact Stars within QCD-motivated Models; University Library Publication Frankfurt (2004)

Neutron Stars, Hybrid Stars, Quark Stars and Black Holes

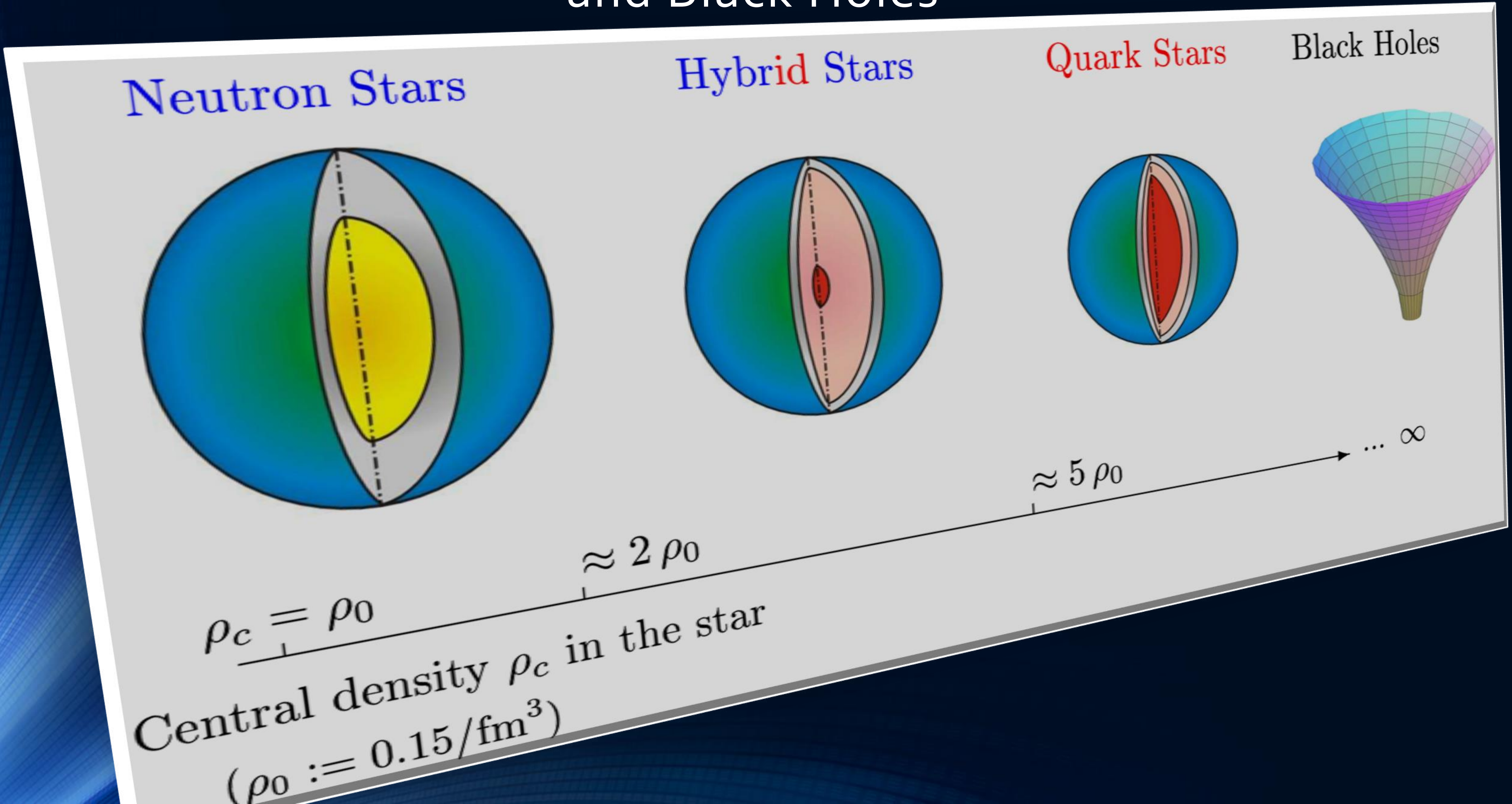

Postmerger gravitational-wave signatures of phase transitions in binary compact star mergers

Broadbrush picture

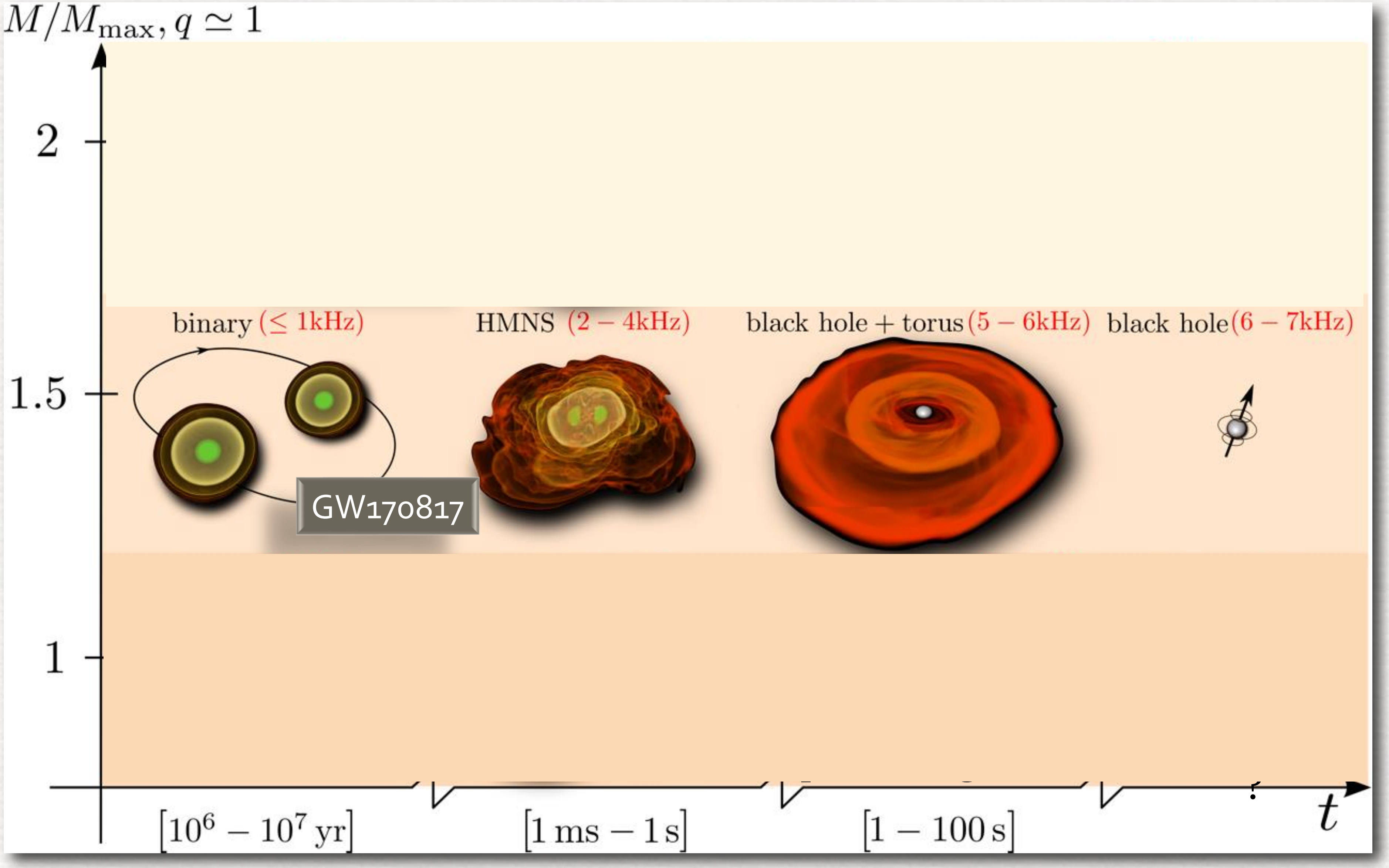

Gravitational Waves from Neutron Star Mergers

Neutron Star Collision (Simulation)

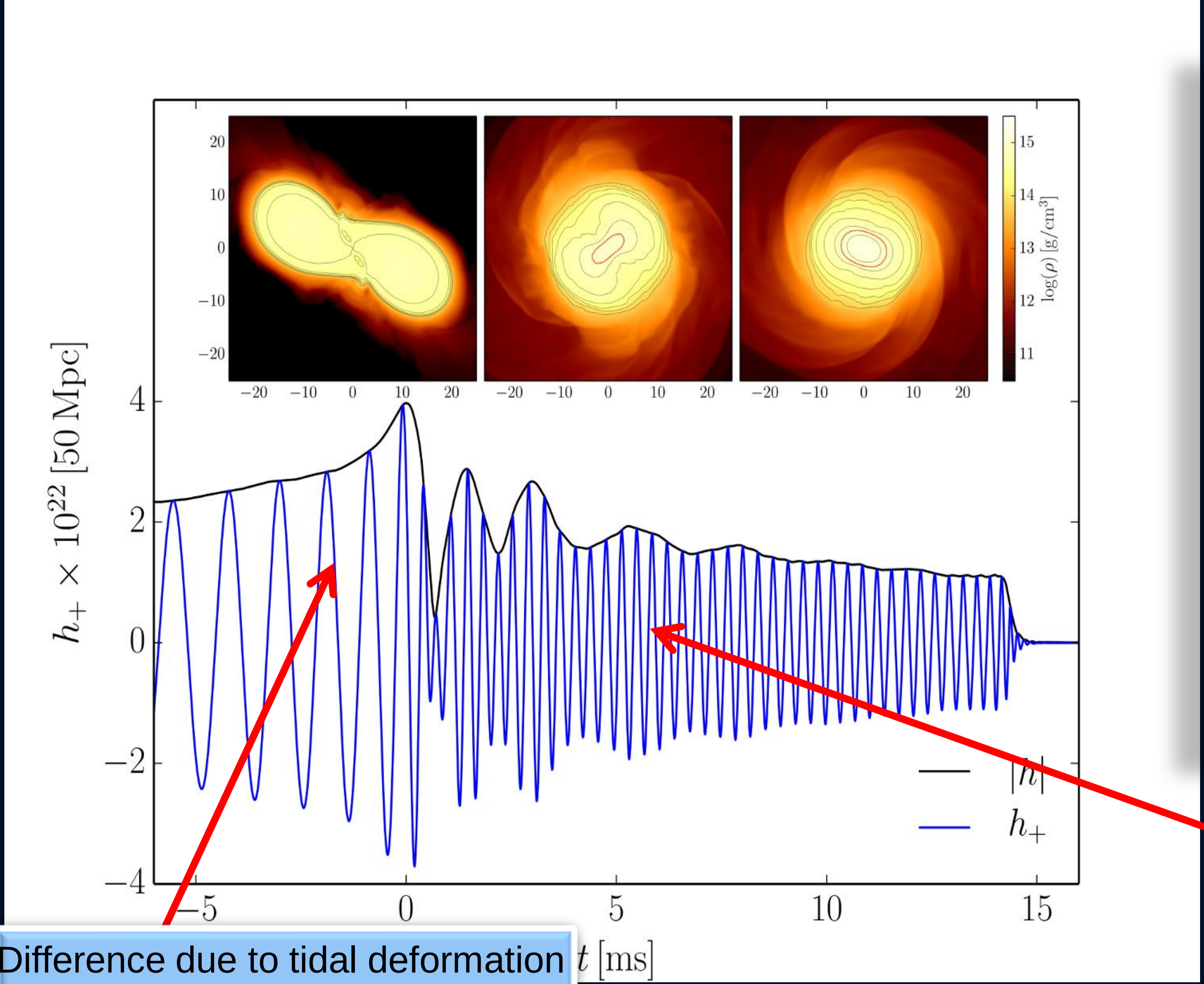

Difference due to tidal deformation in the late inspiral phase

Collision of two Black Holes
GW150914

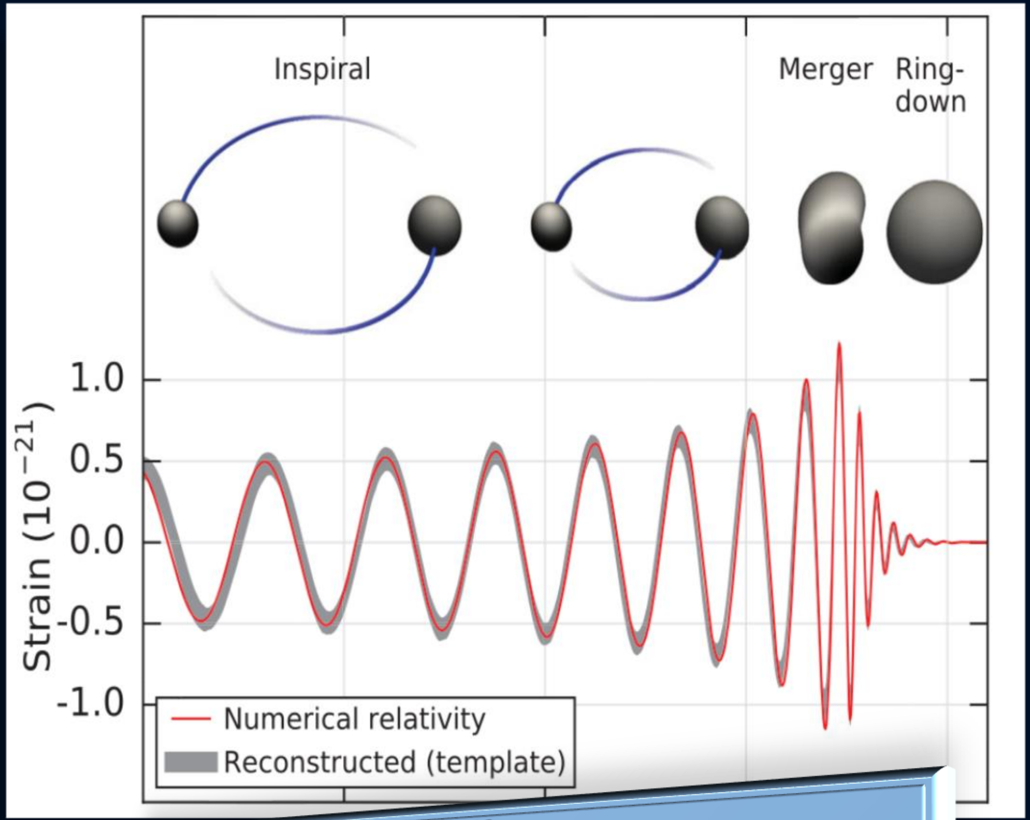

Main difference:
In binary neutron star mergers a **Post-Merger Phase** often exists

The different Phases of a Binary Compact Star Merger Event

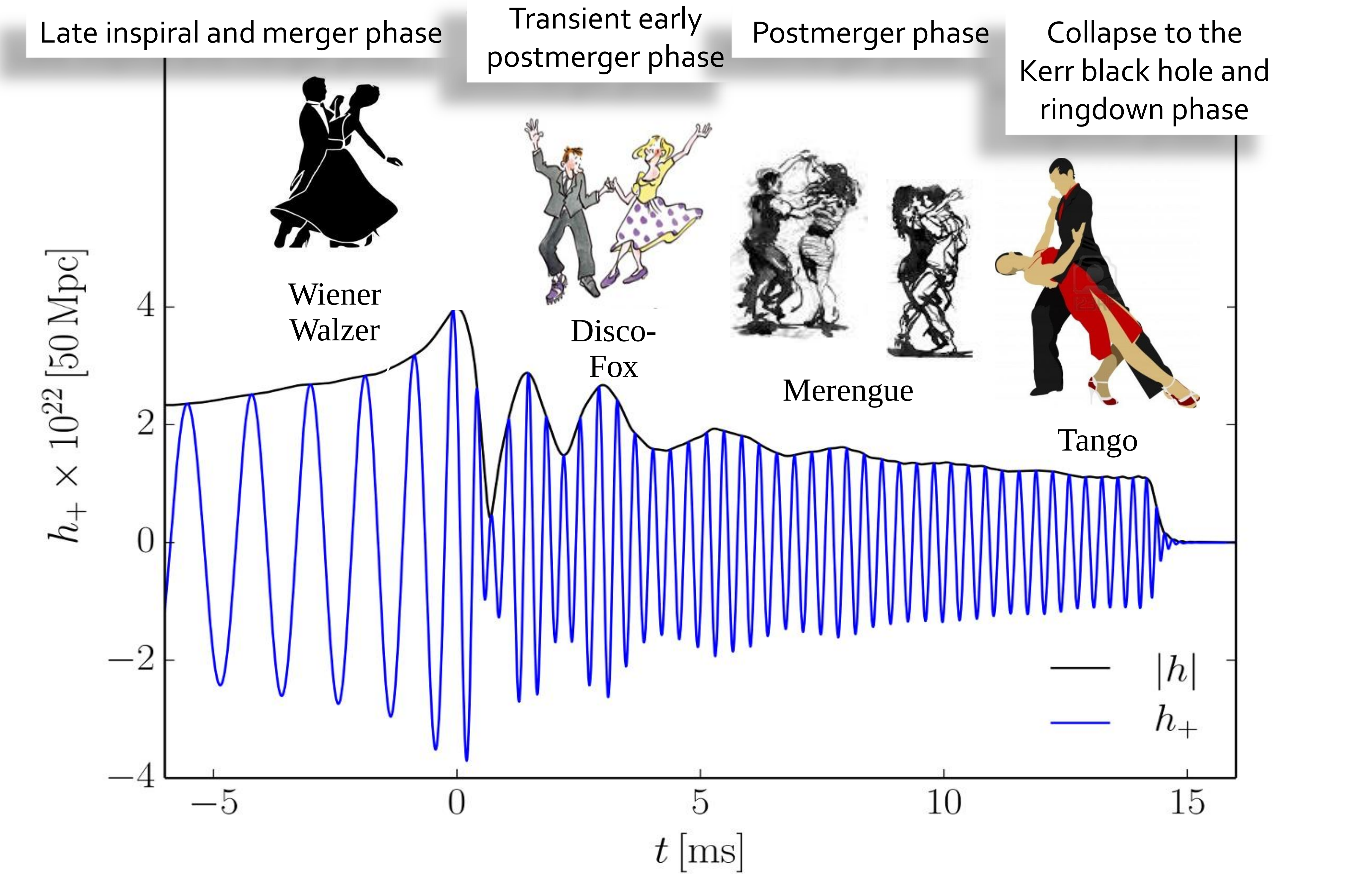

The different Phases during the Postmergerphase of the HMNS

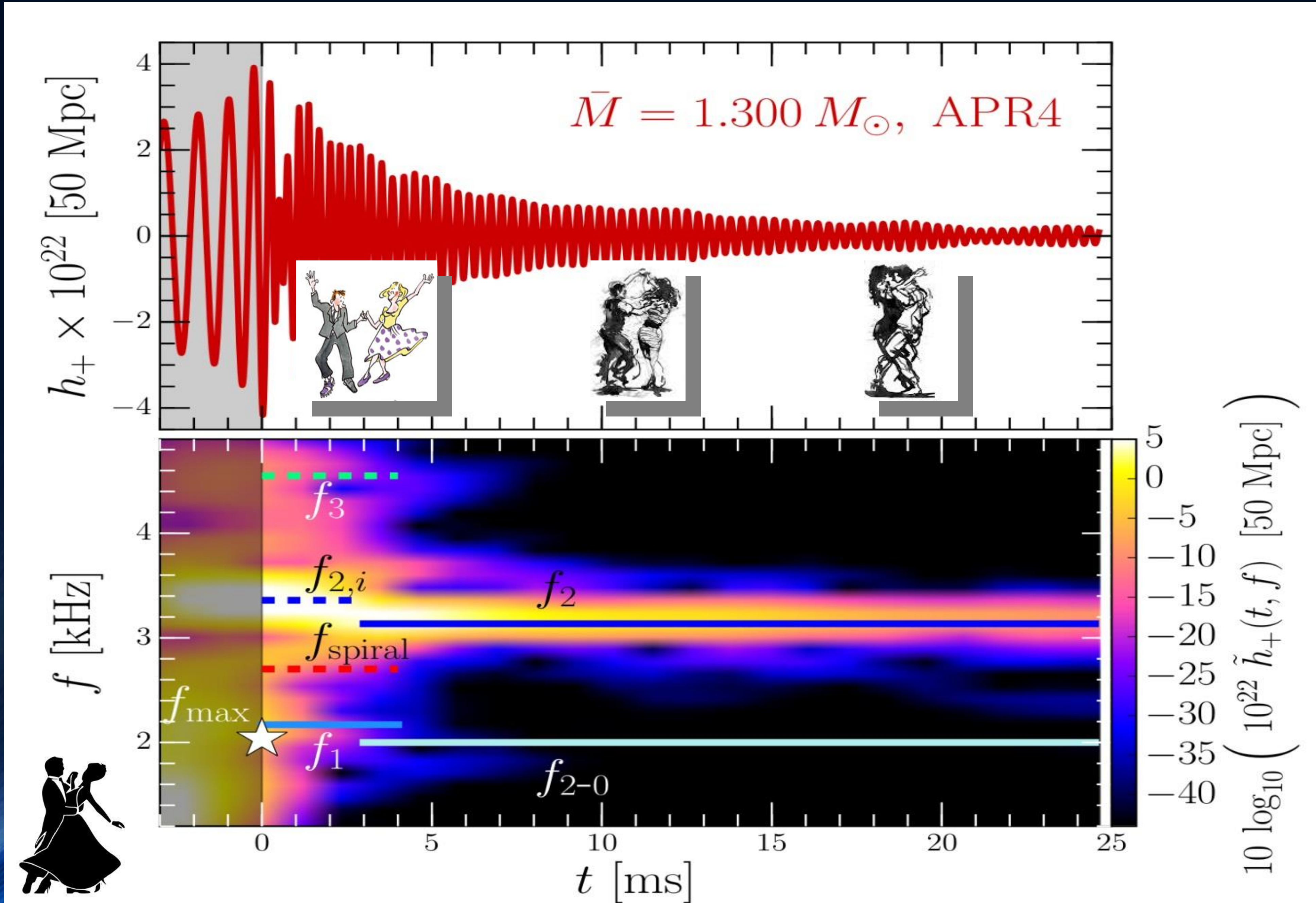

Time Evolution of the GW-Spectrum

The power spectral density profile of the post-merger emission is characterized by several distinct frequencies. Approximately 5 ms after merger, the only remaining dominant frequency is the f_2-frequency (see e.g. L.Rezzolla and K.Takami, PRD, 93(12), 124051 (2016))

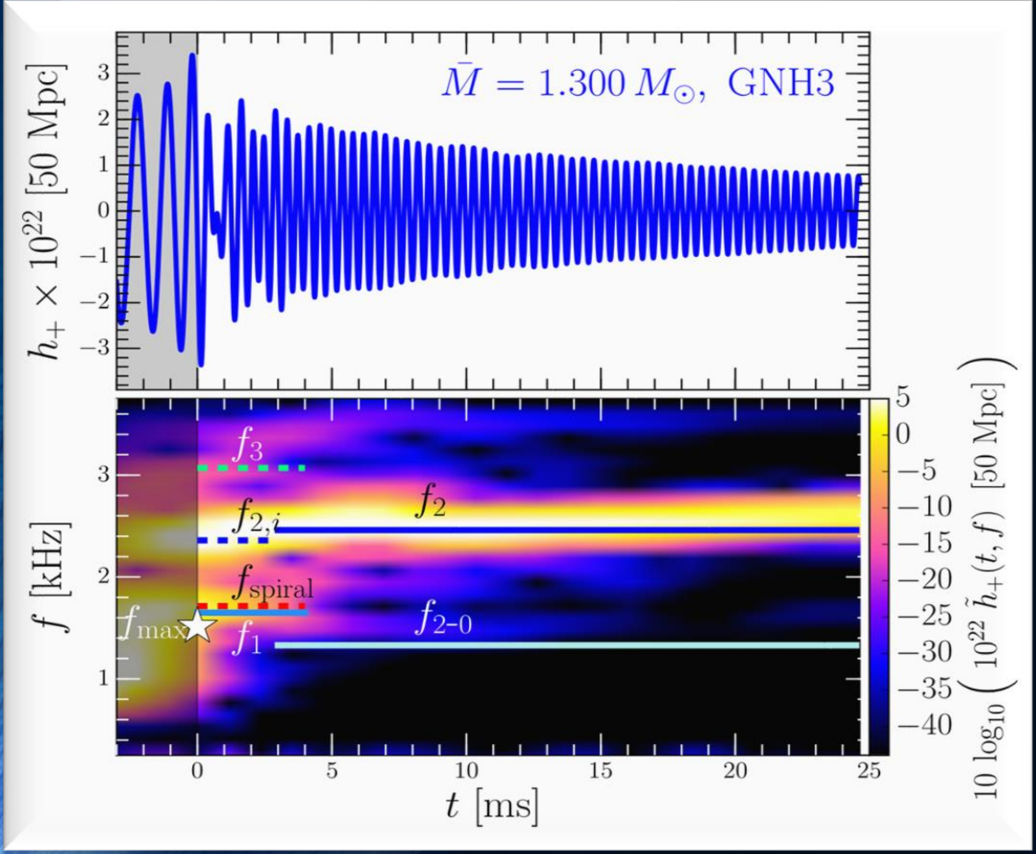

Stiff EOS

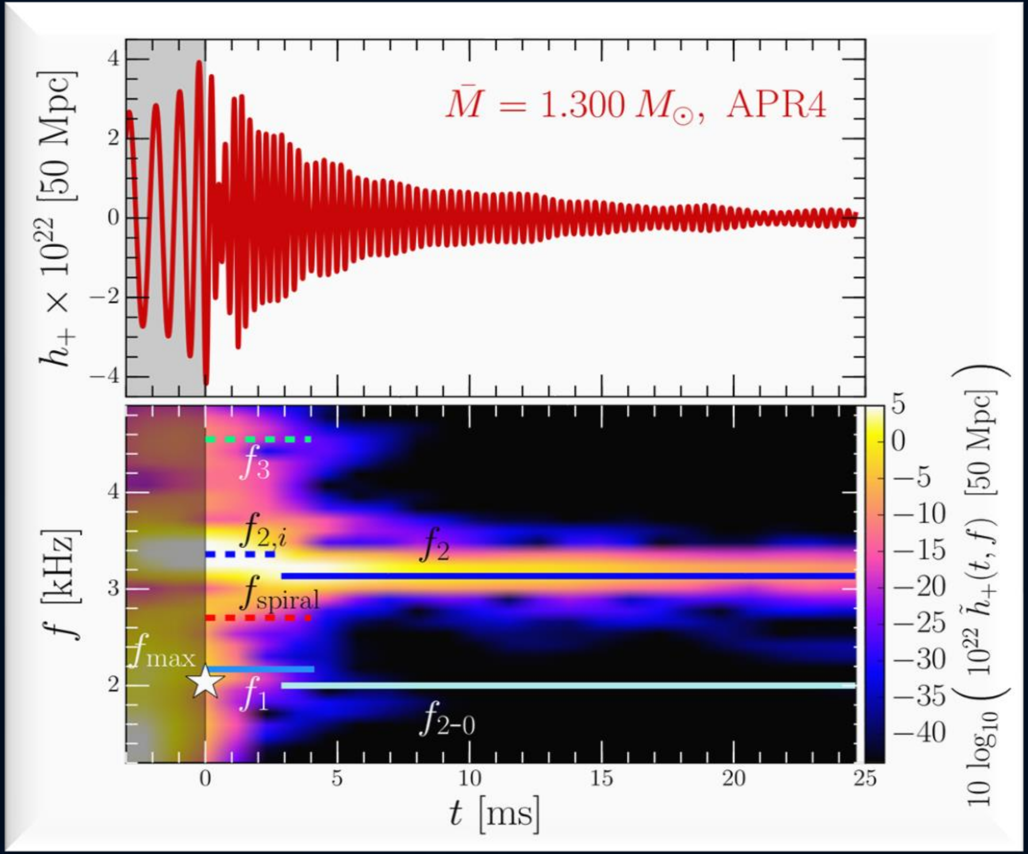

Soft EOS

Unfortunately, clow sensitivity at high gravitational wave frequencies, no post-merger signal has been found in GW170817.

But advanced detectors / next-generation detectors might be able to detect!!?

Evolution of the frequency spectrum of the emitted gravitational waves for the stiff GNH3 (left) and soft APR4 (right) EOS.

A new approach to constrain the EOS

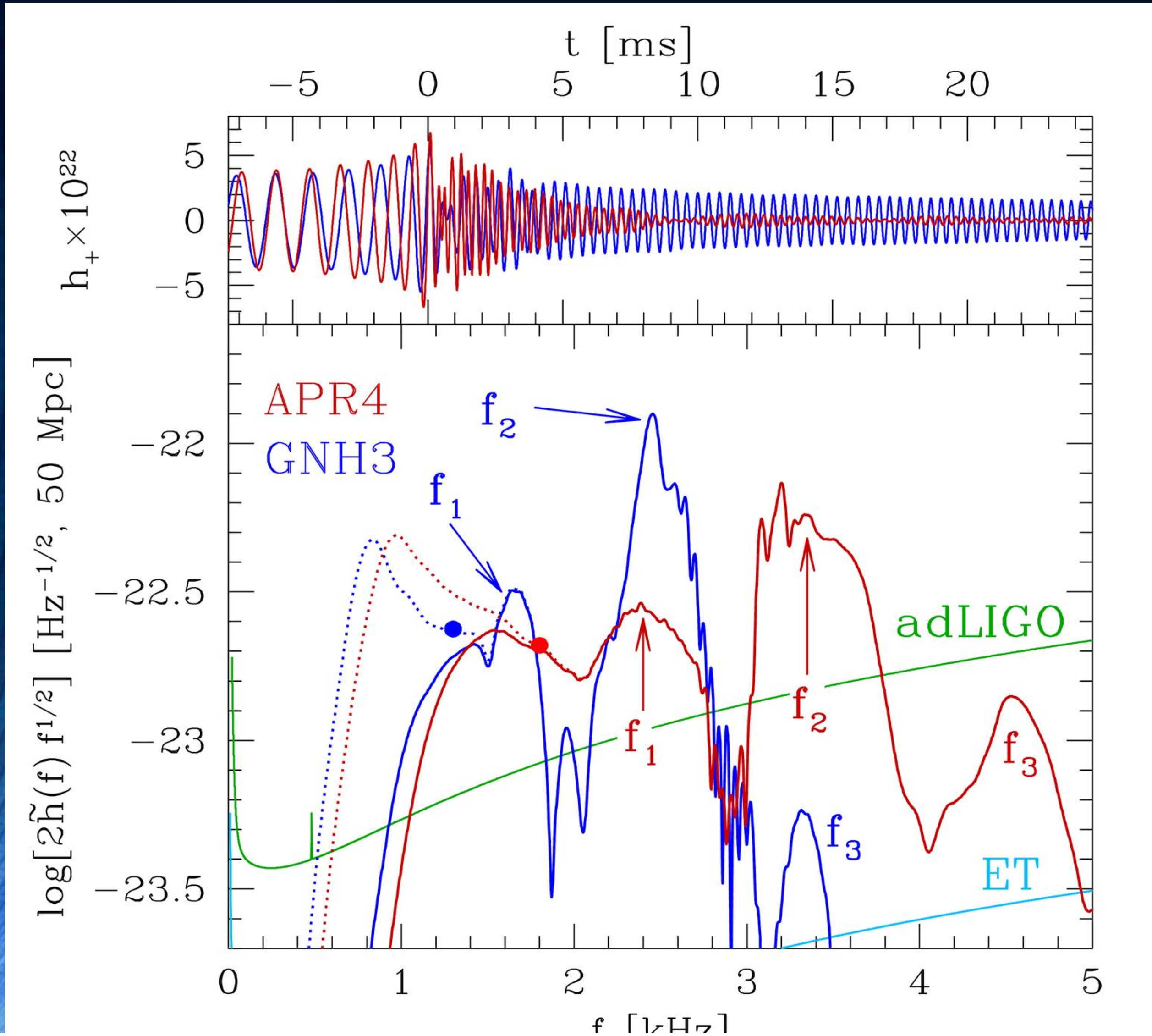

Kentaro Takami, Luciano Rezzolla, and Luca Baiotti, Physical Review D 91, 064001 (2015)

Hotokezaka, K., Kiuchi, K., Kyutoku, K., Muranushi, T., Sekiguchi, Y. I., Shibata, M., & Taniguchi, K. (2013). Physical Review D, 88(4), 044026.

Bauswein, A., & Janka, H. T. (2012). Physical review letters, 108(1), 011101.

Clark, J. A., Bauswein, A., Stergioulas, N., & Shoemaker, D. (2015). arXiv:1509.08522.

Bernuzzi, S., Dietrich, T., & Nagar, A. (2015). Physical review letters, 115(9), 091101.

Oechslin+2007, Baiotti+2008, Bauswein+ 2011, 2012, Stergioulas+ 2011, Hotokezaka+ 2013, Takami 2014, 2015, Bernuzzi 2014, 2015, Bauswein+ 2015, Clark+ 2016, Rezzolla+2016, de Pietri+ 2016, Feo+ 2017, Bose+ 2017 …

Evolution of the density in the post merger phase

ALF2-EOS: Mixed phase region starts at $3\rho_0$ (see red curve), initial NS mass: 1.35 M_{solar}

Hanauske, et.al. PRD, 96(4), 043004 (2017)

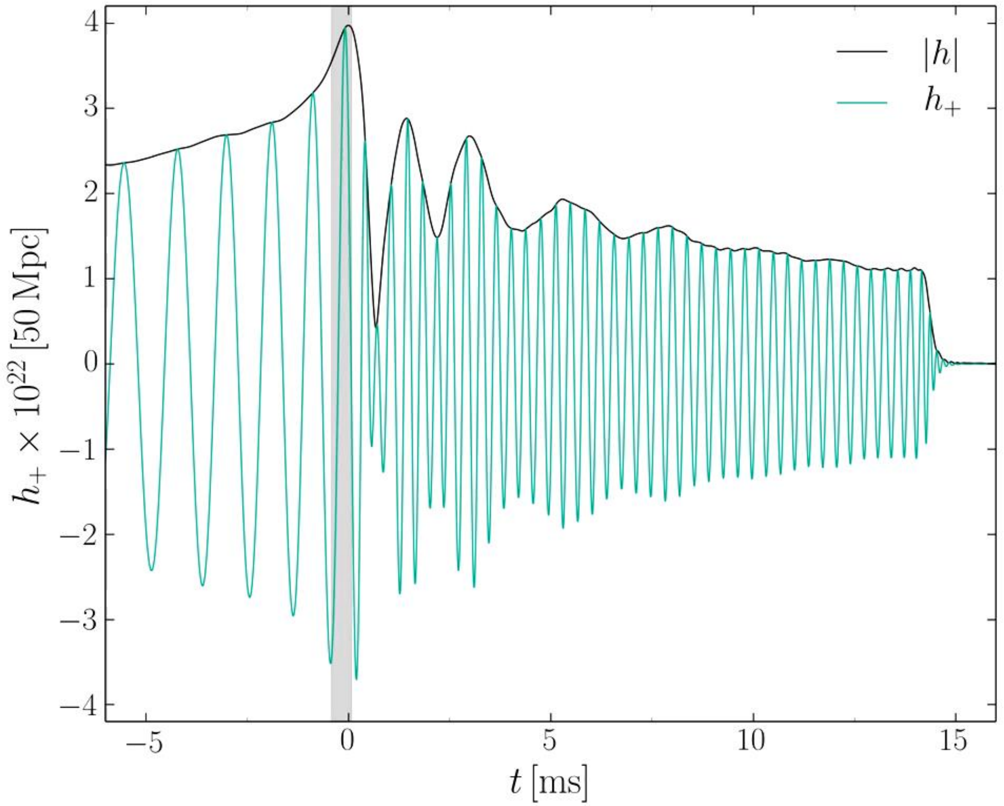

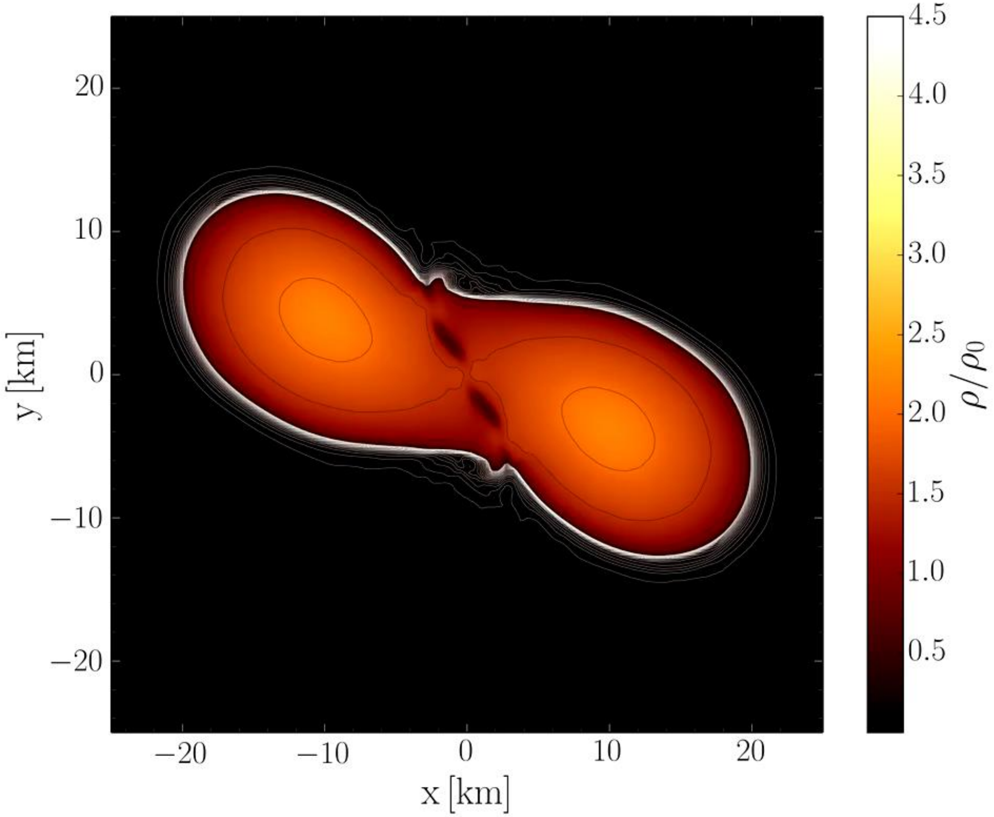

Gravitational wave amplitude at a distance of 50 Mpc

Rest mass density distribution ρ(x,y) in the equatorial plane

in units of the nuclear matter density ρ_0

Hypermassive Neutron Stars in the QCD Phase Diagram

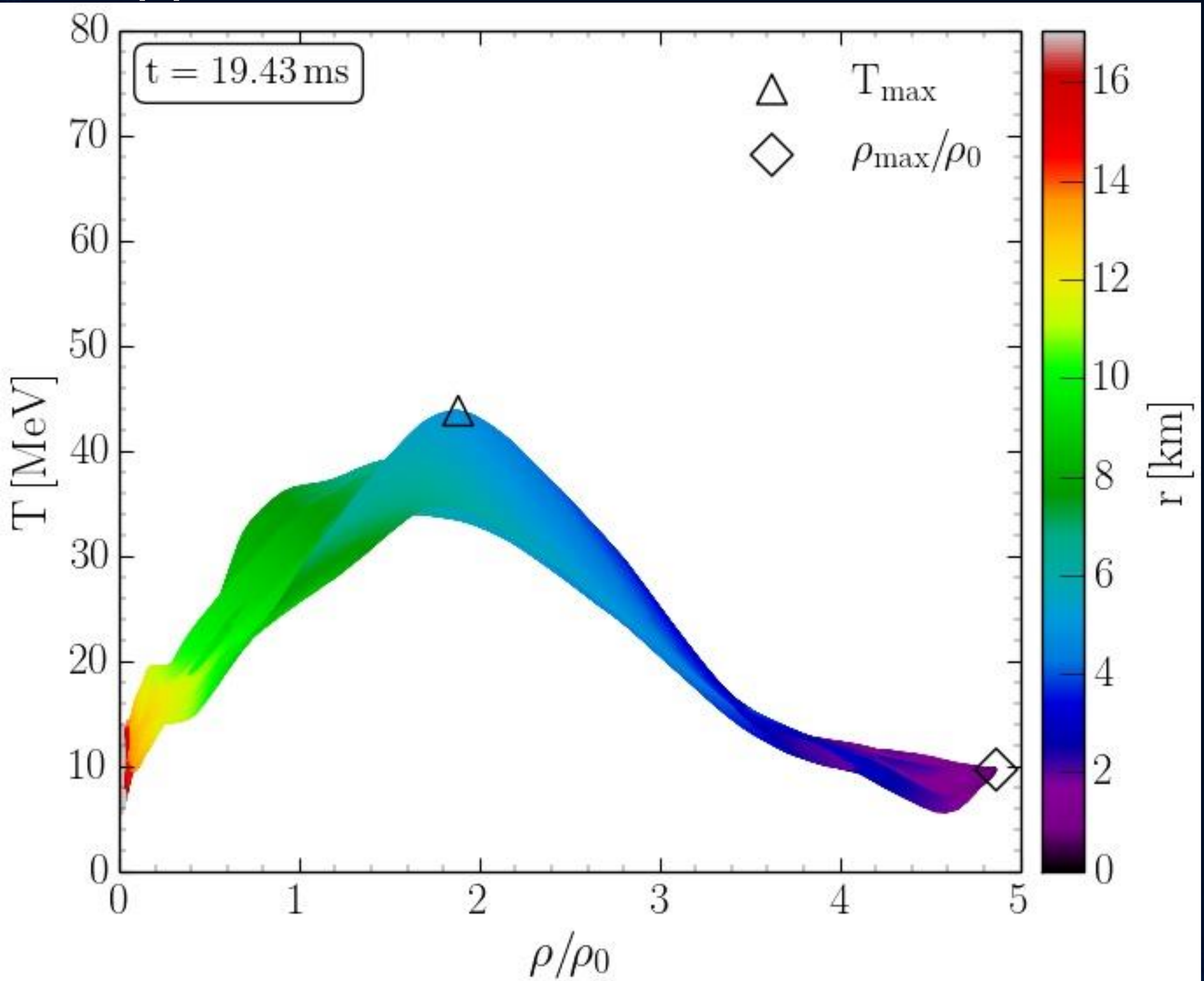

Density-temperature profiles inside the inner area of a hypermassive neutron star simulated within the LS220 EOS with a total mass of M_{total}=2.7 M_{solar} in the style of a (T-ρ) QCD phase diagram plot at t=19.43 ms after the merger.

The color-coding indicate the radial position r of the corresponding (T- ρ) fluid element measured from the origin of the simulation (x , y) = (0 , 0) on the equatorial plane at z = 0.

The open triangle marks the maximum value of the temperature while the open diamond indicates the maximum of the density.

QCD Phase Diagram: The Late Inspiral Phase

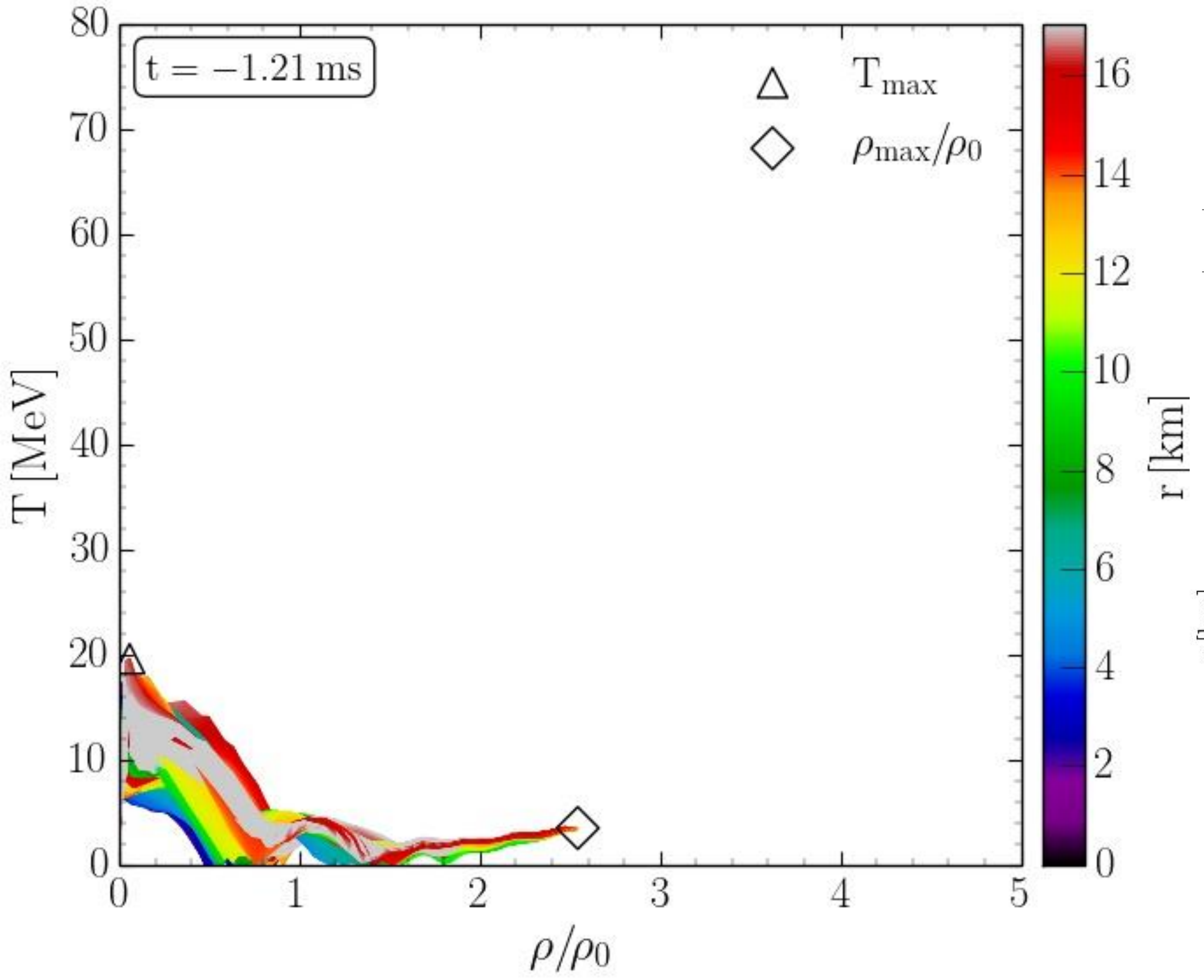

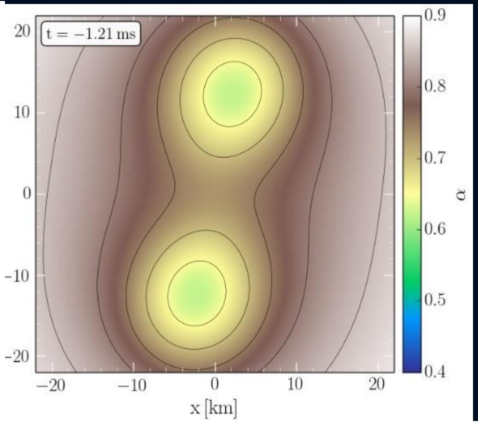

Lapse function α (left)

rest mass density ρ

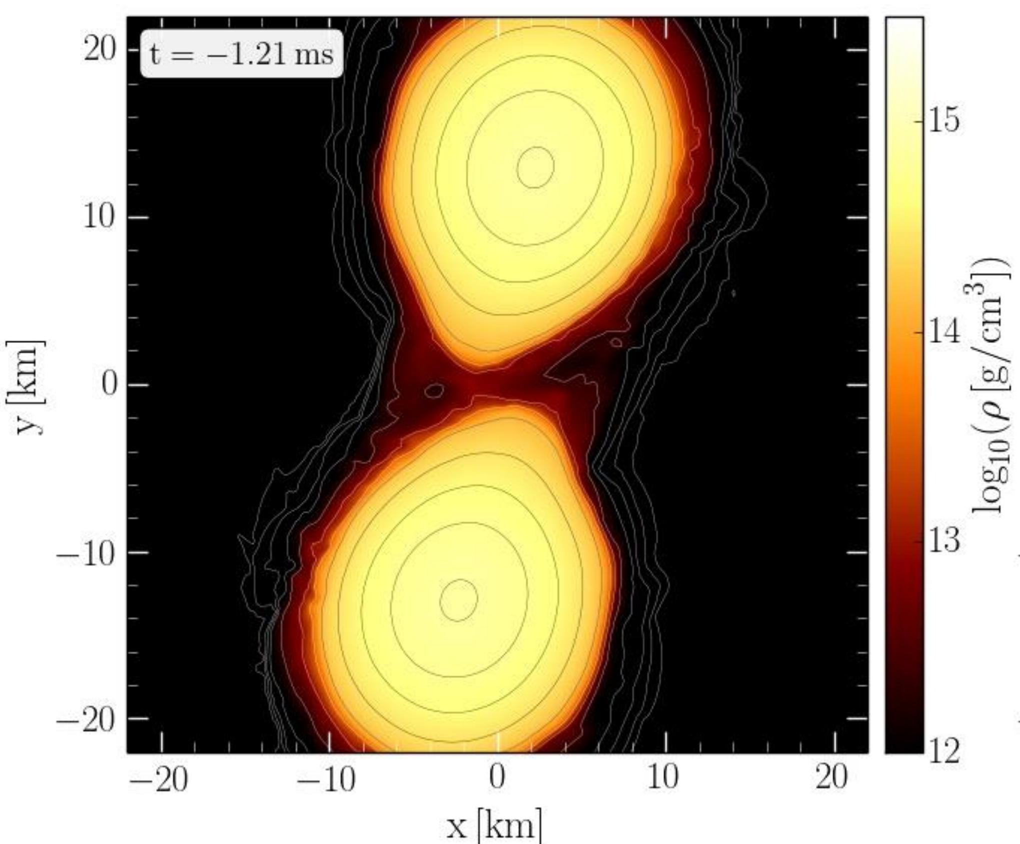

QCD Phase Diagram: The Late Inspiral Phase

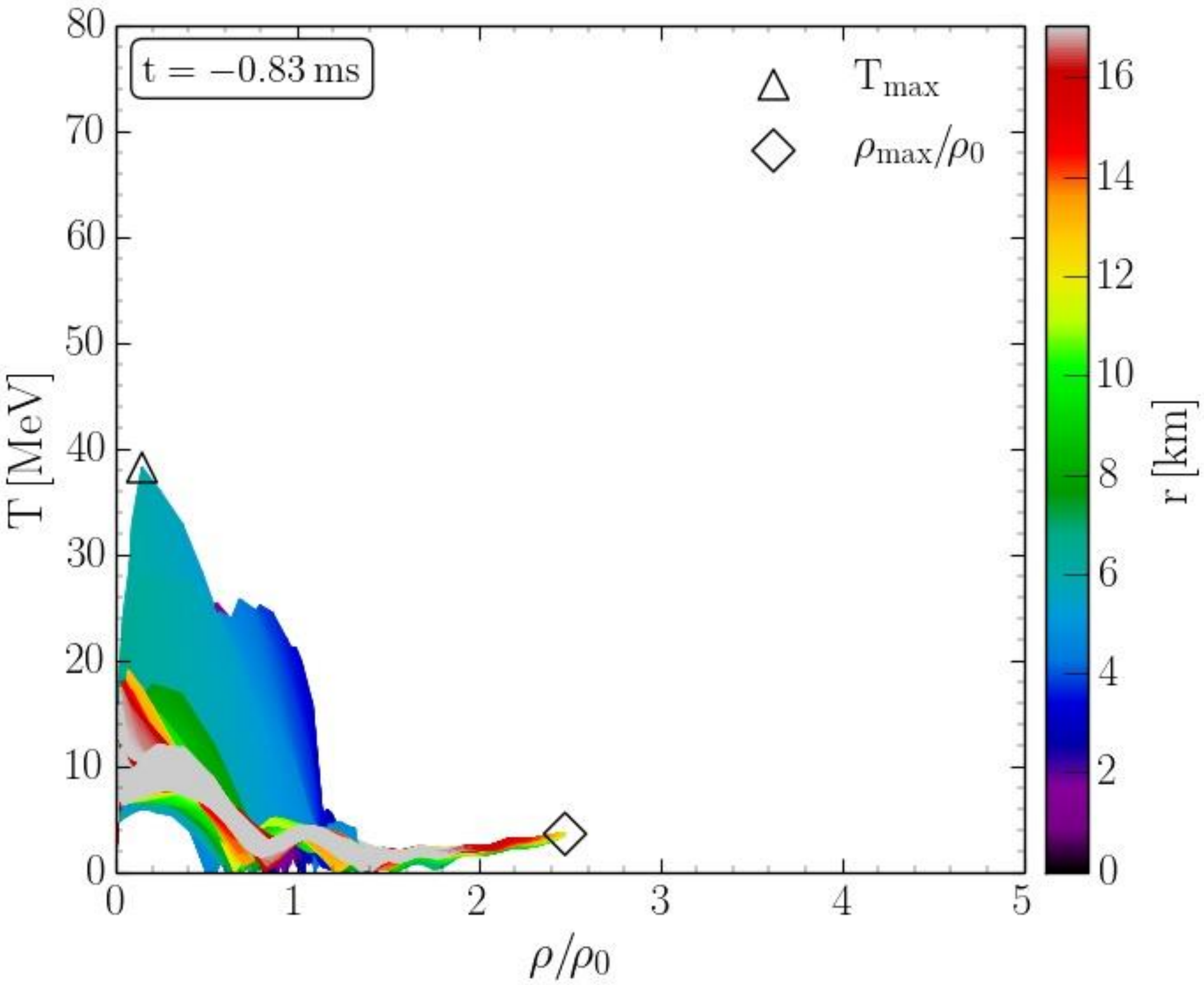

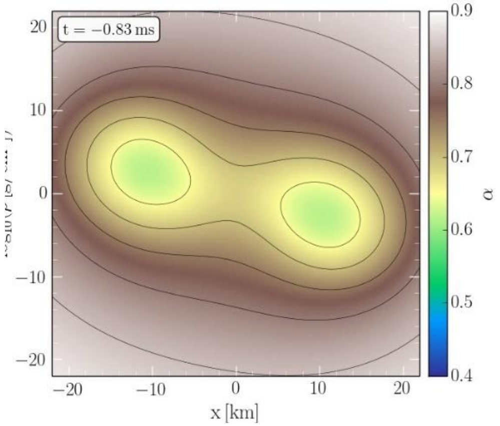

Lapse function α (left)

rest mass density ρ

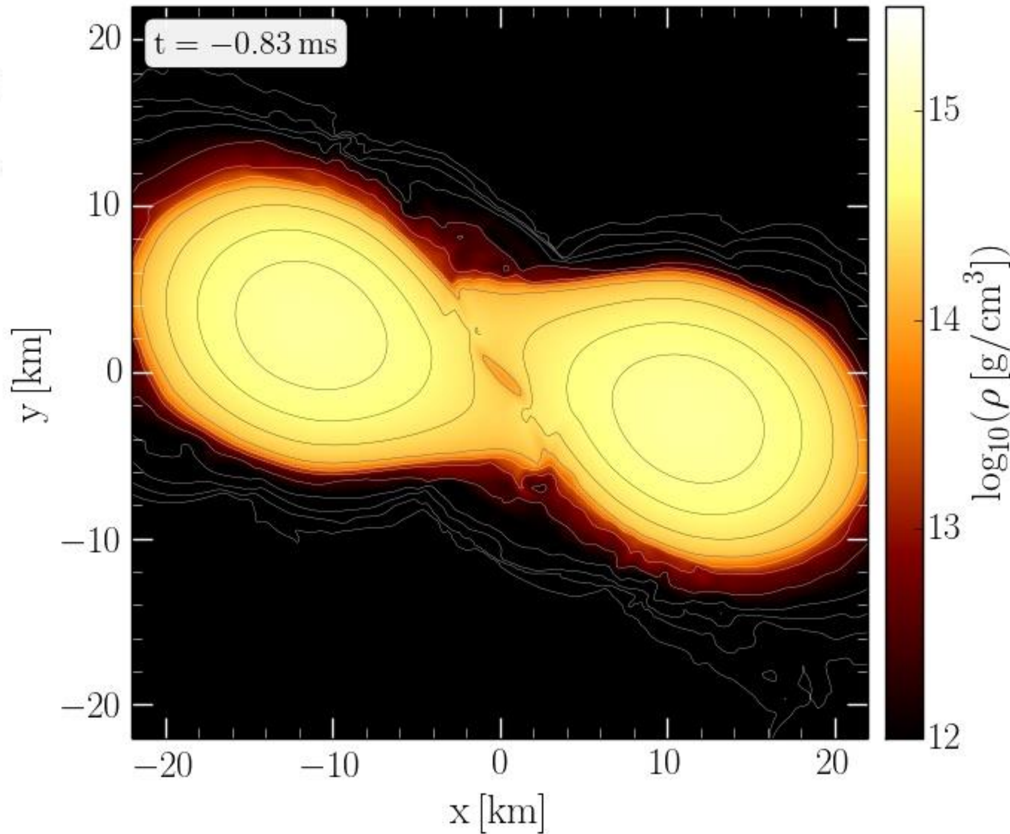

QCD Phase Diagram: The Late Inspiral Phase

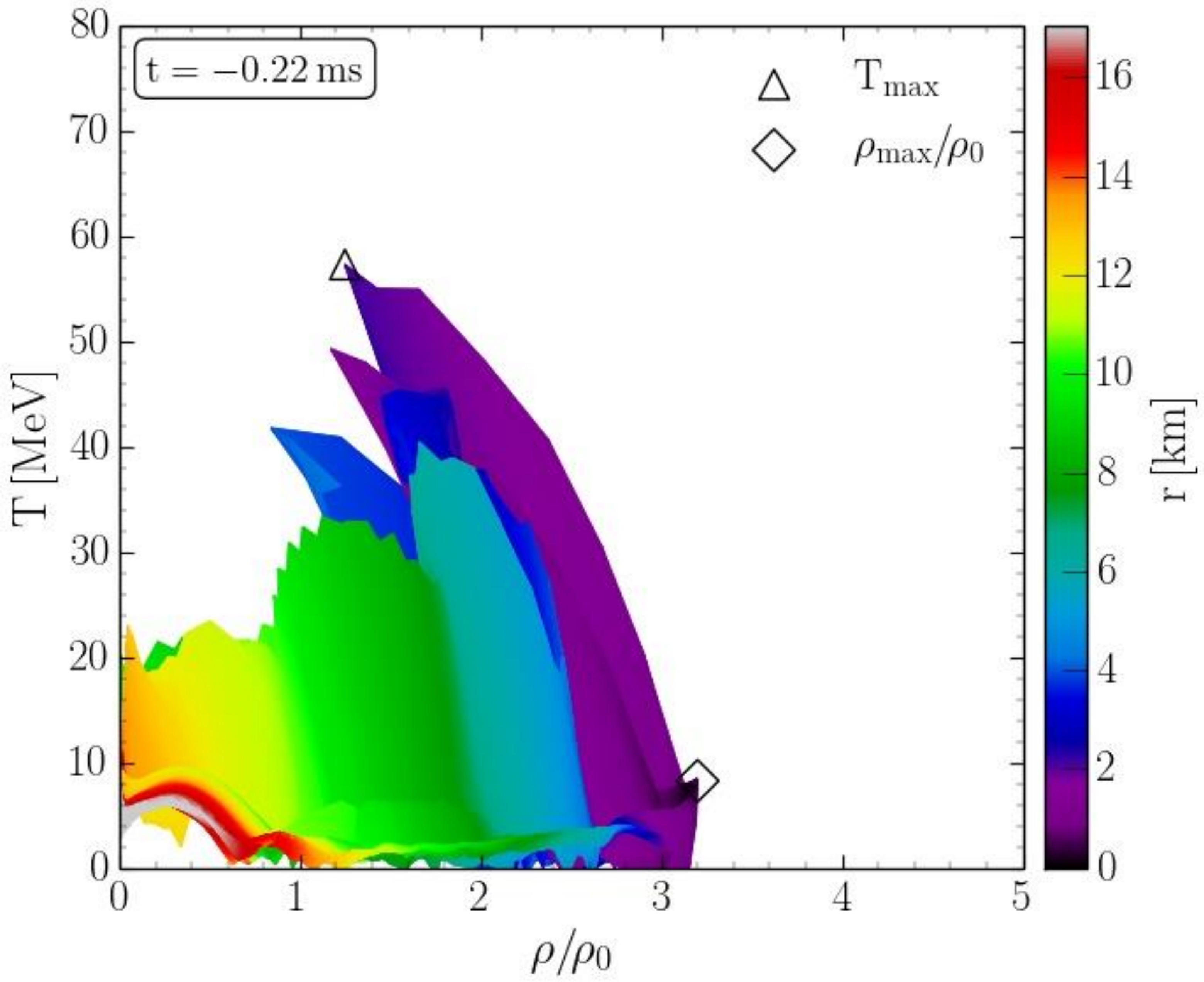

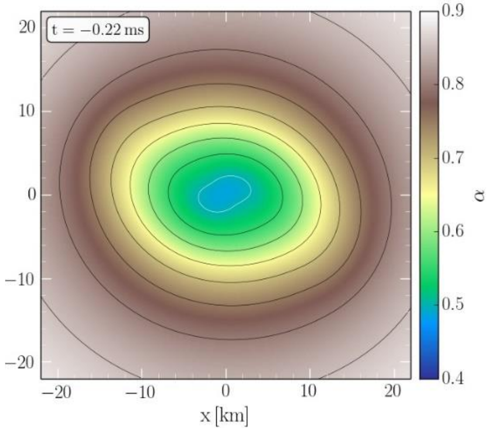

Lapse function α (left)

rest mass density ρ

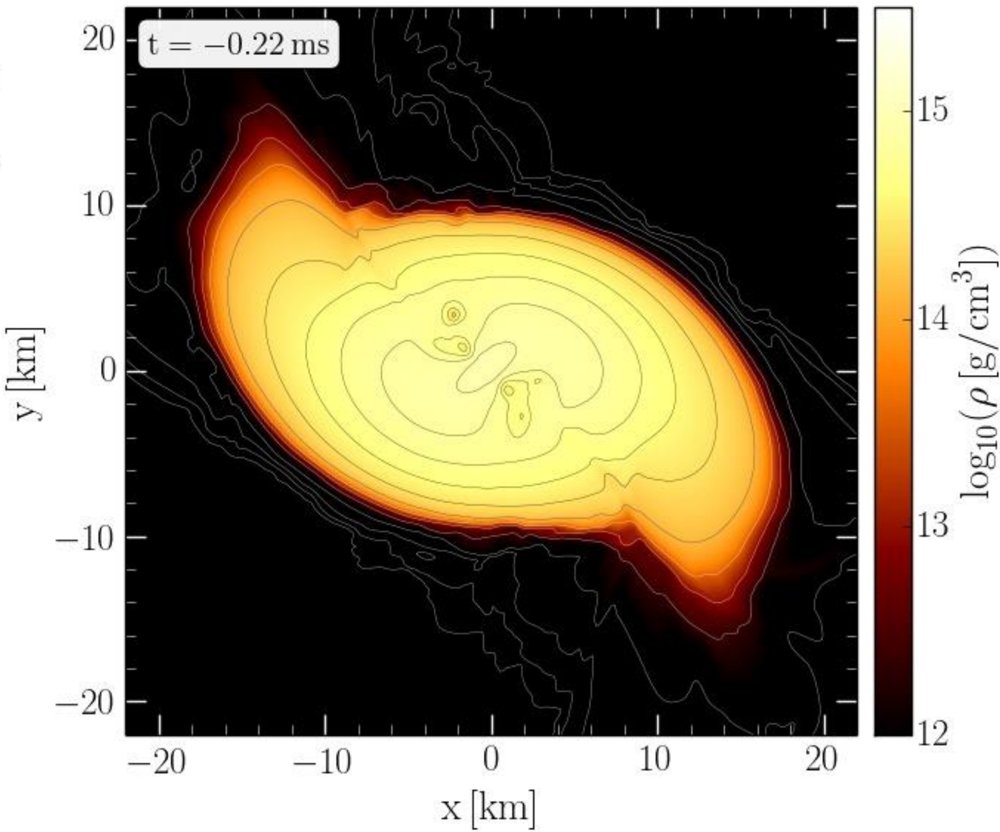

Binary Neutron Star Mergers in the QCD Phase Diagram

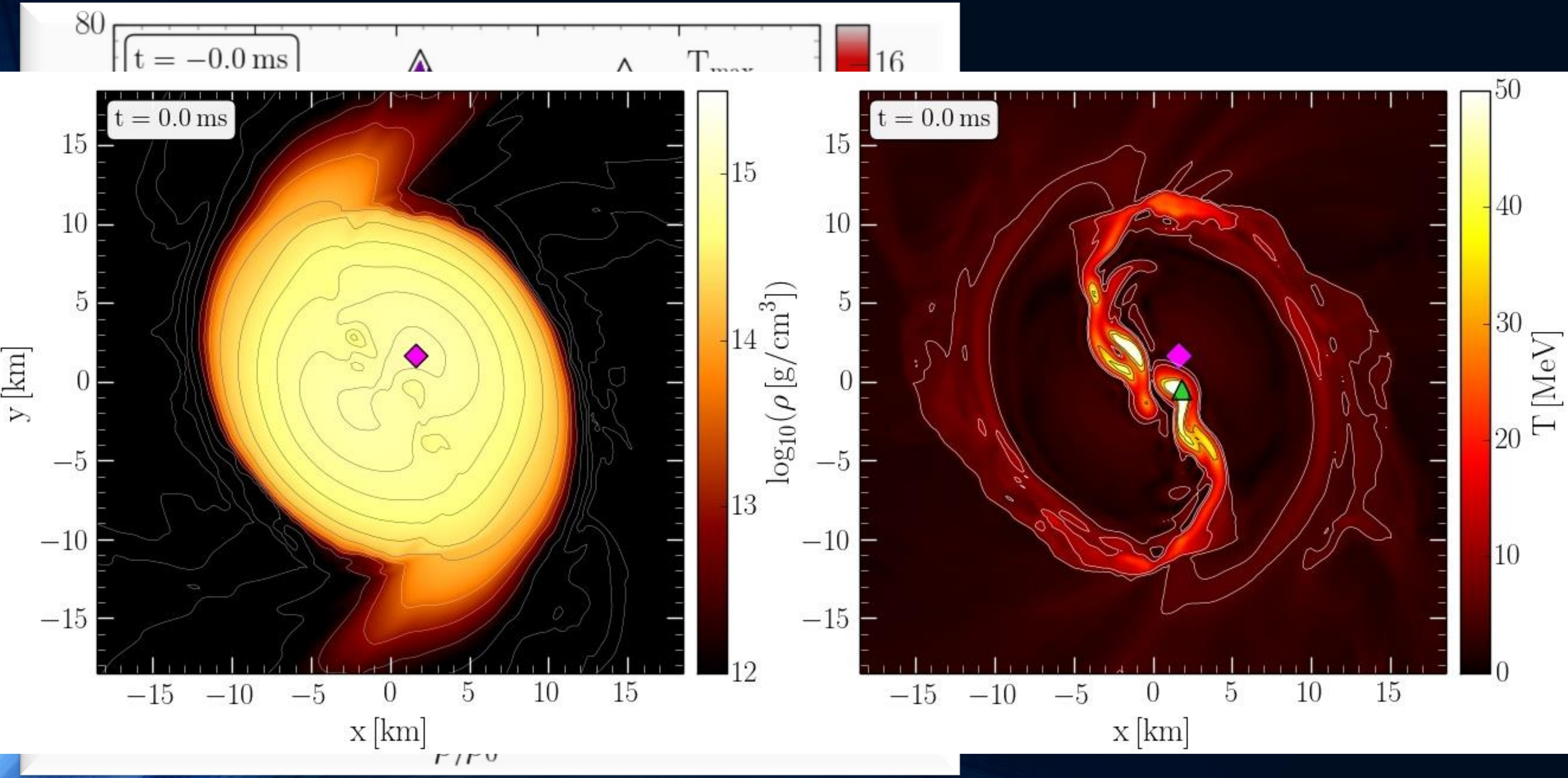

The Co-Rotating Frame

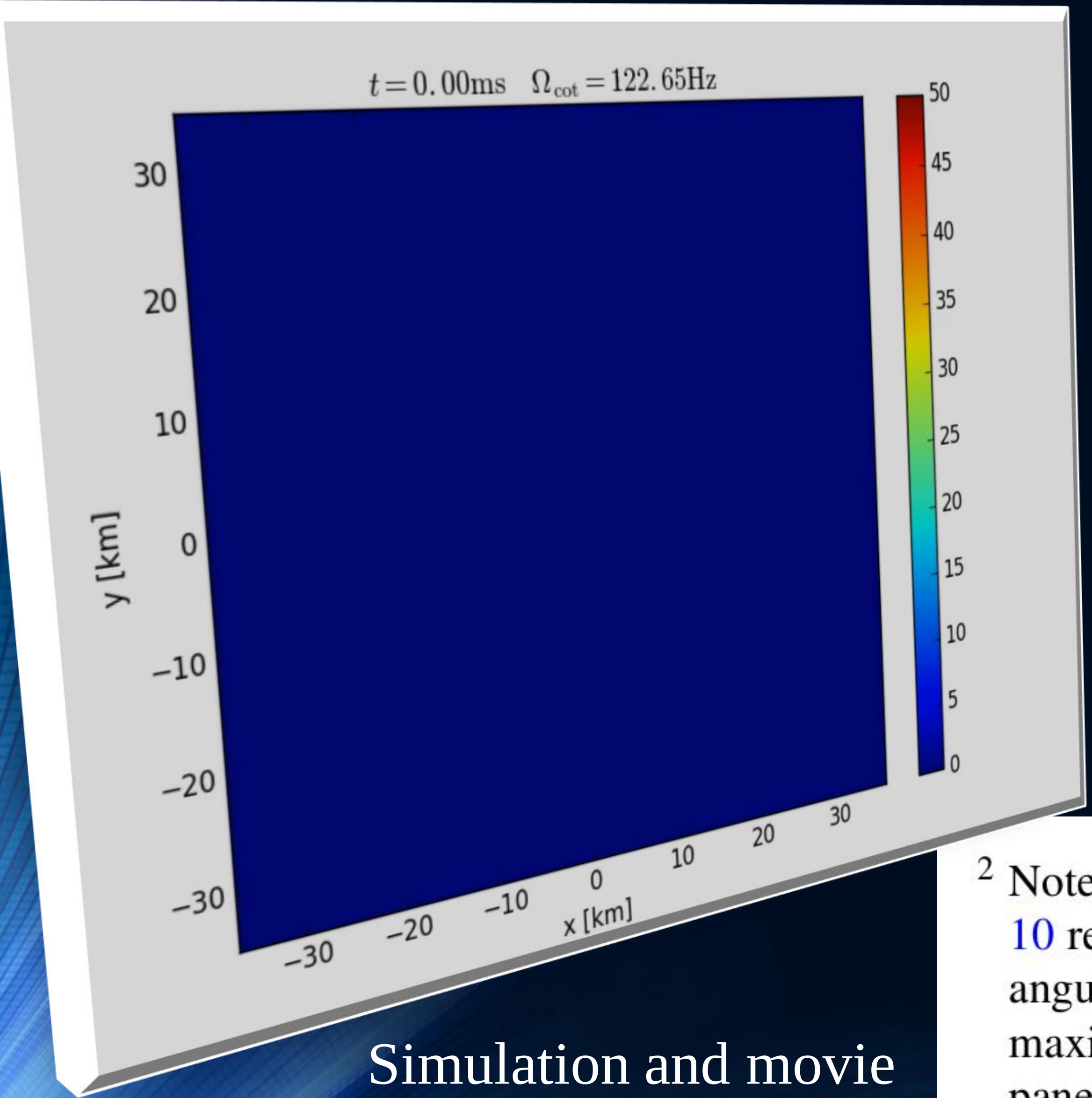

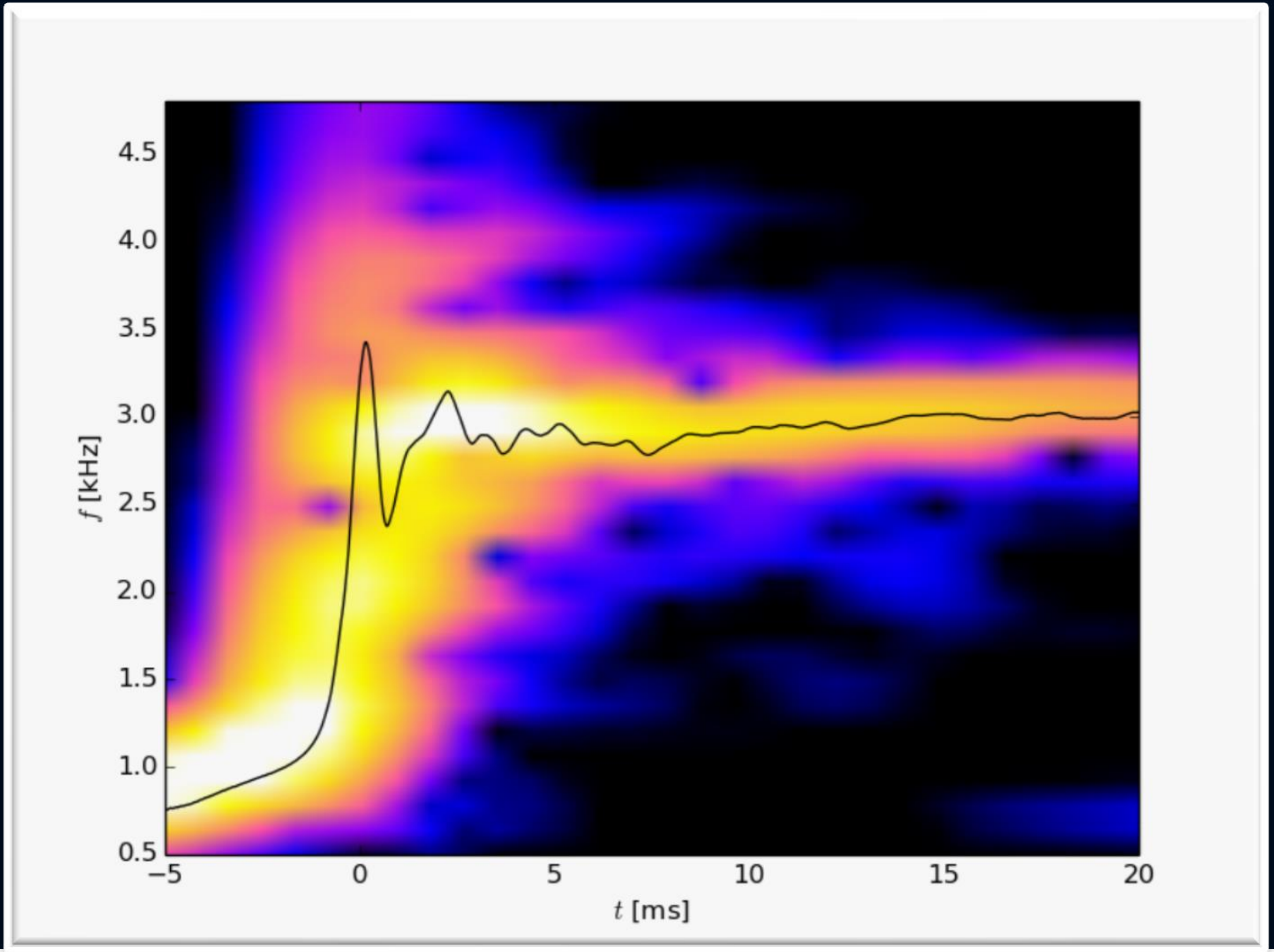

Simulation and movie has been produced by Luke Bovard

[2] Note that the angular-velocity distribution in the lower central panel of Fig. 10 refers to the corotating frame and that this frame is rotating at half the angular frequency of the emitted gravitational waves, $\Omega_{\rm GW}$. Because the maximum of the angular velocity $\Omega_{\rm max}$ is of the order of $\Omega_{\rm GW}/2$ (cf. left panel of Fig. 12), the ring structure in this panel is approximately at zero angular velocity.

Density and Temperature Evolution inside the HMNS

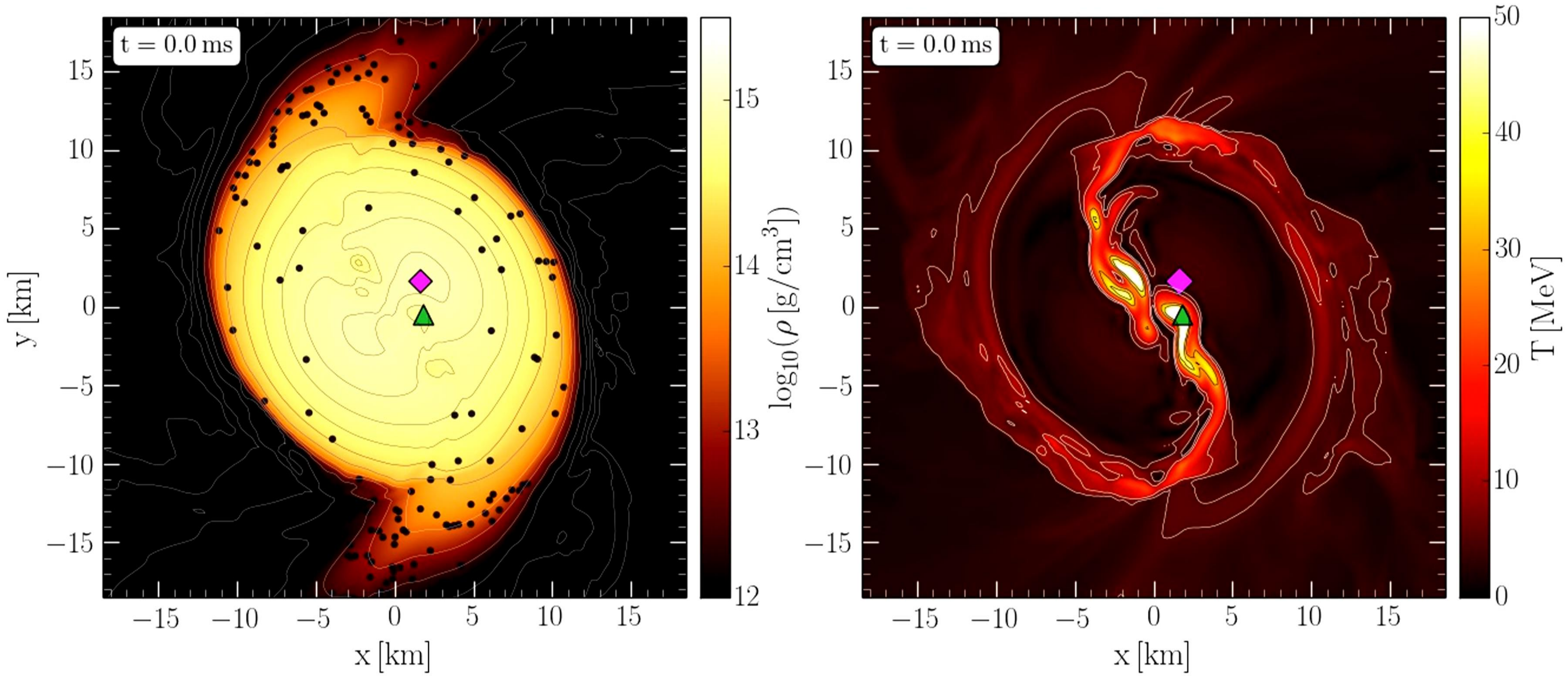

Rest mass density on the equatorial plane

Temperature on the equatorial plane

Binary Neutron Star Mergers in the QCD Phase Diagram

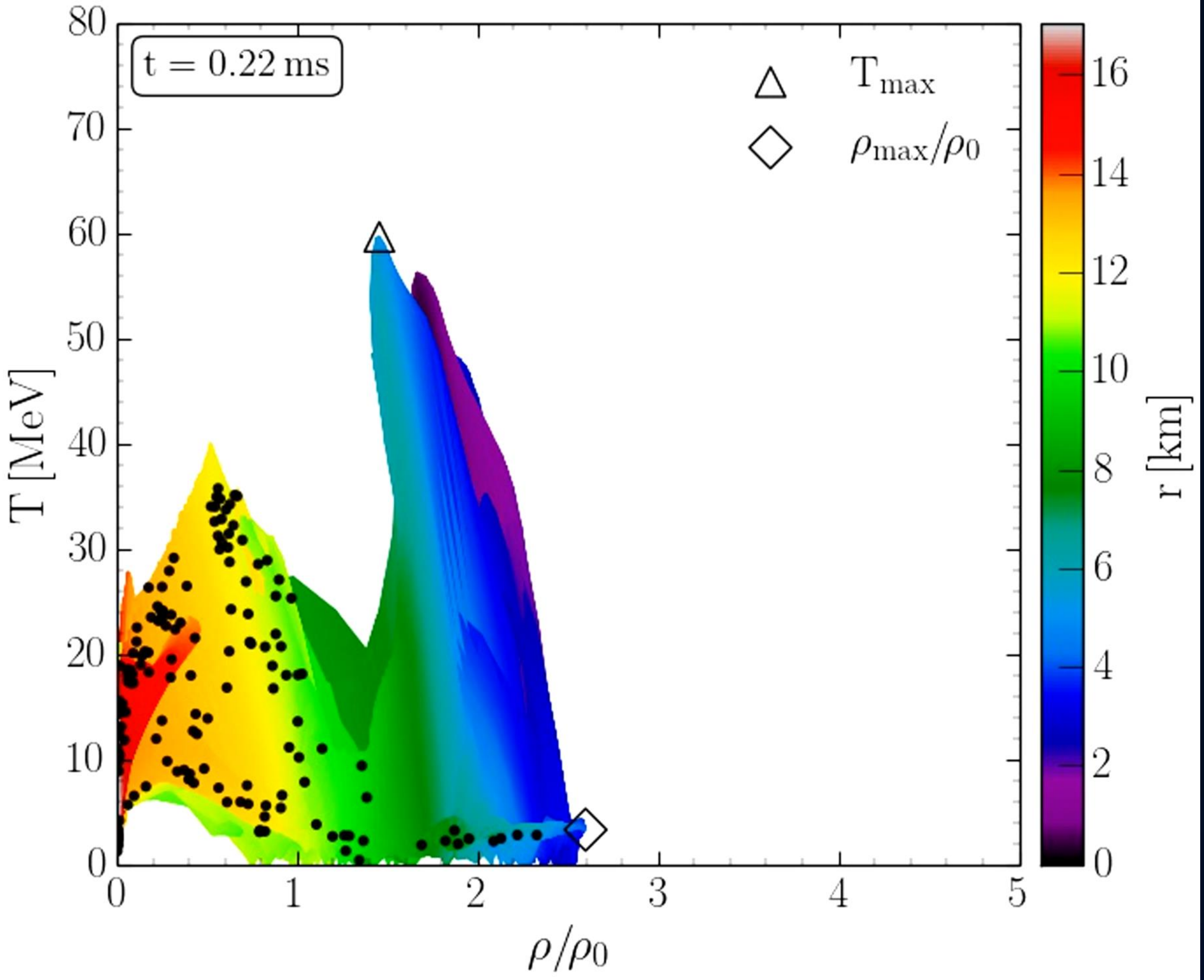

Evolution of hot and dense matter inside the inner area of a hypermassive neutron star simulated within the LS220 EOS with a total mass of M_{total}=2.7 M_{solar} in the style of a (T- ρ) QCD phase diagram plot

The color-coding indicate the radial position r of the corresponding (T- ρ) fluid element measured from the origin of the simulation (x , y) = (0 , 0) on the equatorial plane at z = 0.

The open triangle marks the maximum value of the temperature while the open diamond indicates the maximum of the density.

The Angular Velocity in the (3+1)-Split

The angular velocity Ω in the (3+1)-Split is a combination of the lapse function α , the ϕ-component of the shift vector β^ϕ and the 3-velocity v^ϕ of the fluid (spatial projection of the 4-velocity **u**):

(3+1)-decomposition of spacetime:

$$\Omega(x, y, z, t) = \frac{u^\phi}{u^t} = \alpha\, v^\phi \; - \; \beta^\phi$$

$$g_{\mu\nu} = \begin{pmatrix} -\alpha^2 + \beta_i \beta^i & \beta_i \\ \beta_i & \gamma_{ij} \end{pmatrix}$$

Angular velocity Ω

Lapse function α

Φ-component of 3-velocity v^φ

Frame-dragging β^φ

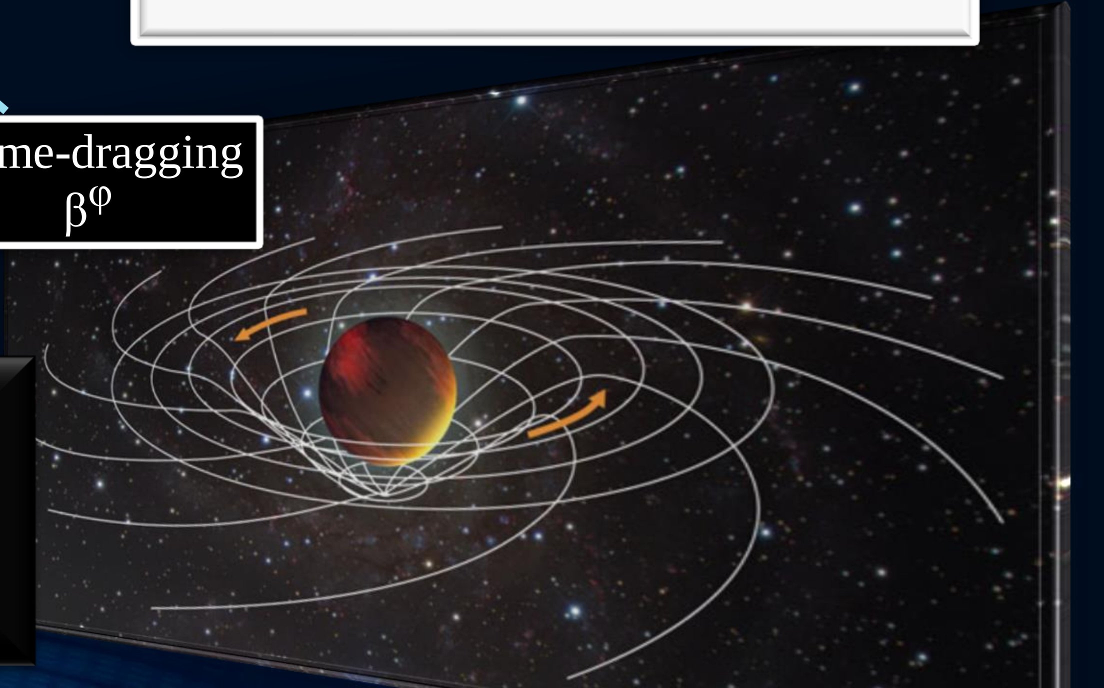

Focus: Inner core of the differentially rotating HMNS

M. Shibata, K. Taniguchi, and K. Uryu, Phys. Rev. D 71, 084021 (2005)
M. Shibata and K. Taniguchi, Phys. Rev. D 73, 064027 (2006)
F. Galeazzi, S. Yoshida and Y. Eriguchi, A&A 541, p. A156 (2012)
W. Kastaun and F. Galeazzi, Phys. Rev. D 91, p. 064027 (2015)

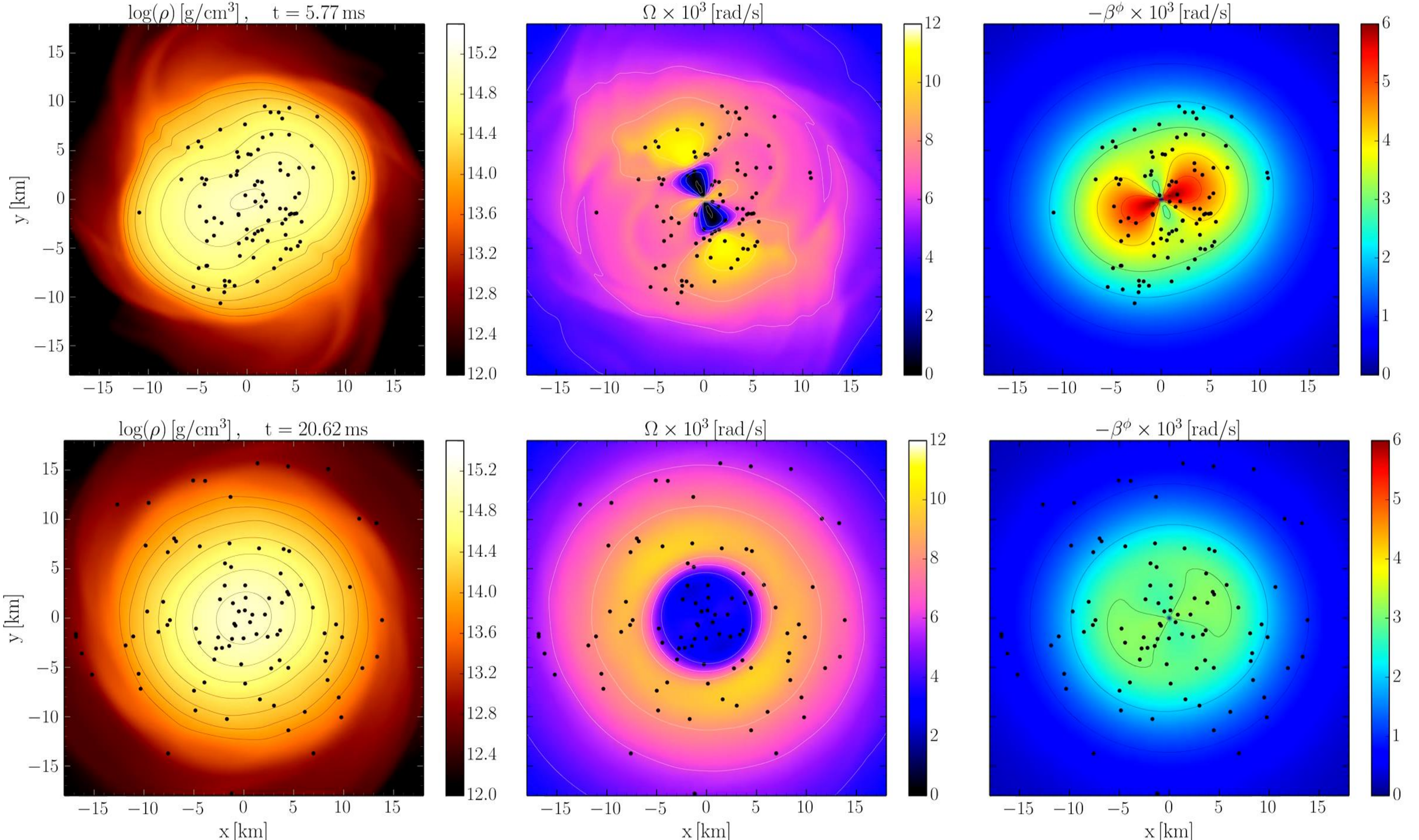

log(ρ) [g/cm³] , t = 5.77 ms
Ω × 10³ [rad/s]
−β^φ × 10³ [rad/s]
log(ρ) [g/cm³] , t = 20.62 ms
Ω × 10³ [rad/s]
−β^φ × 10³ [rad/s]
y [km]
x [km]

Time-averaged Rotation Profiles of the HMNSs

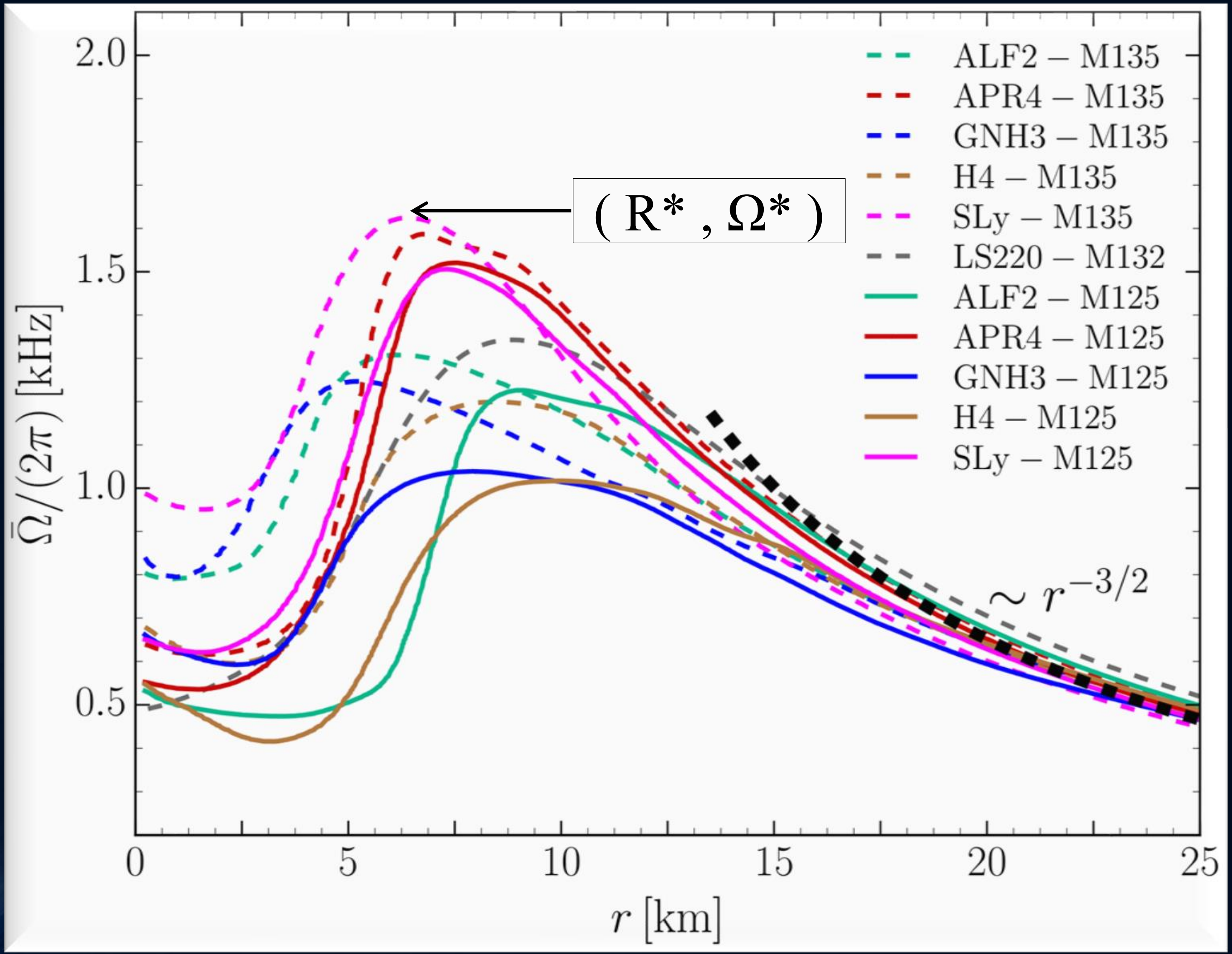

<u>Soft EoSs</u>:
Sly
APR4

<u>Stiff EoSs</u>:
GNH3
H4

Time-averaged rotation profiles for different EoS
Low mass runs (solid curves), high mass runs (dashed curves).

Hanauske, et.al. PRD, 96(4), 043004 (2017)

Temperature Angular Velocity

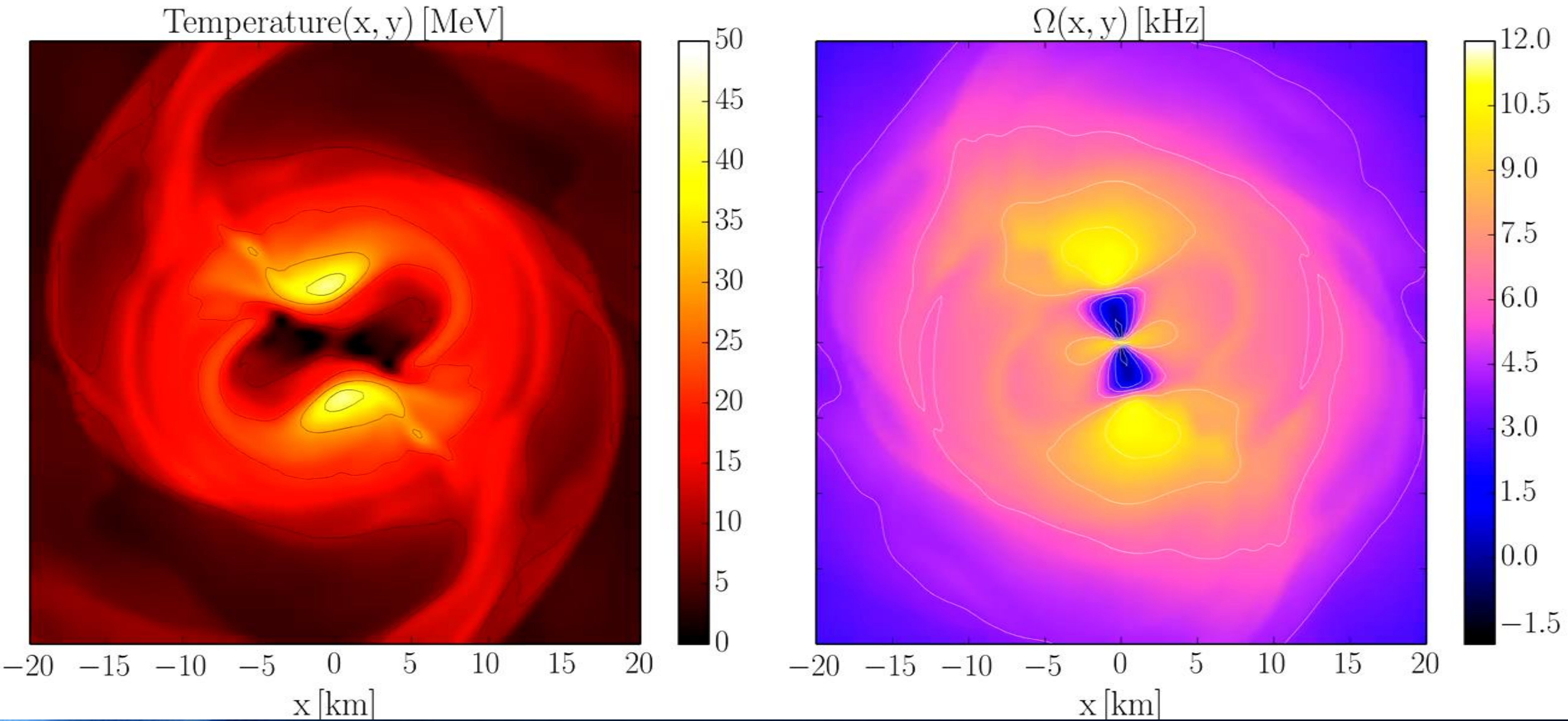

EOS: LS200 , Mass: 1.32 M_{solar} , simulation with Pi-symmetry

Postmerger gravitational-wave signatures of phase transitions in binary compact star mergers

Postmerger gravitational-wave signatures of phase transitions in binary compact star mergers

- Introduction
- Numerical general relativity of compact star mergers
- The equation of state of compact star matter and the hadron-quark phase transition
- The different phases of a binary compact star merger event
- **Gravitational-wave signatures of the hadron-quark phase transition in binary compact star mergers**
  - The inspiral and merger phase (premerger signals)
  - Hypermassive hybrid stars (HMHS) within the prompt phase transition scenario (PPT)
  - HMHS within the delayed phase transition scenario (DPT)
  - HMHS within the phase transition triggered collapse scenario (PTTC)
- Summary and Outlook

GW170817
Constraining the maximum mass and radius of neutron stars

L.Rezzolla, E.Most, L.Weih, "Using Gravitational Wave Observations and Quasi-Universal Relations to constrain the maximum Mass of Neutron Stars",The Astrophysical Journal Letters 852, L25 (2018): 2.01 +/-0.04 < M_{TOV} < 2.16 +/-0.17

Constraining M_{TOV} , see also: S.Lawrence et al. ,APJ808,186, 2015, Margalit & Metzger, The Astrophysical Journal Letters 850, L19 (2017): M_{TOV} < 2.17 (90%) Zhou, Zhou, Li, PRD 97, 083015 (2018) Ruiz, Shapiro, Tsokaros, PRD 97,021501 (2018)

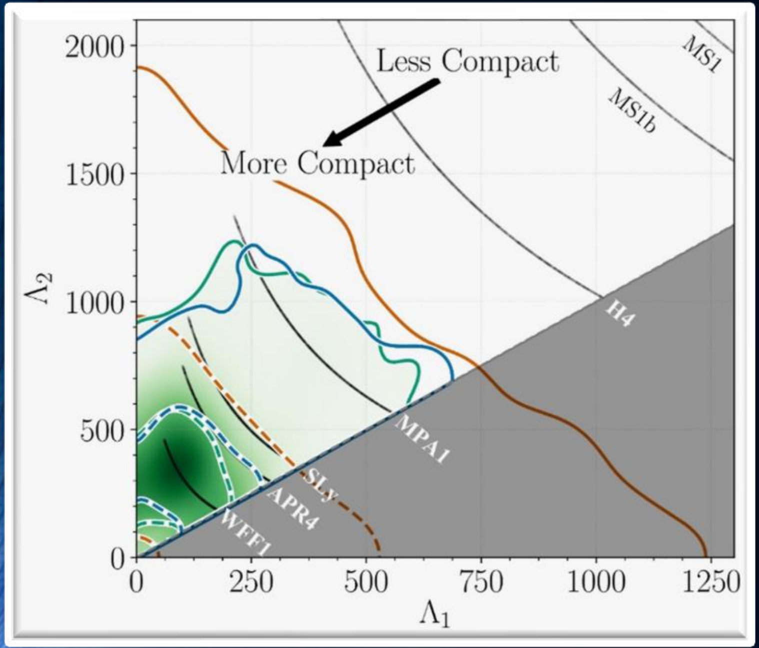

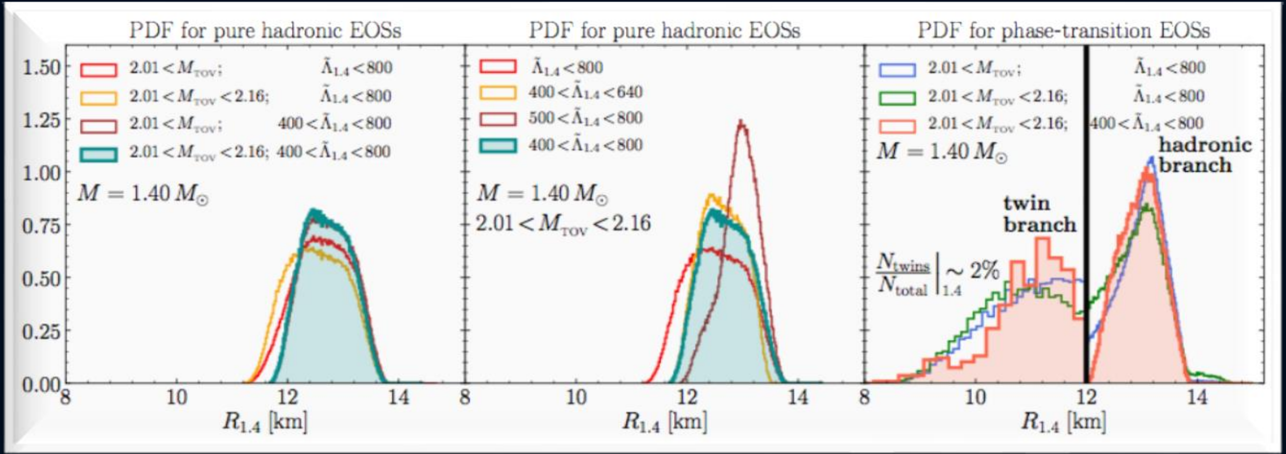

E.Most, L.Weih, L.Rezzolla, J. Schaffner-Bielich "New constraints on radii and tidal deformabilities of neutron stars from GW170817", PRL 120, 261103 (2018)

GW170817: Measurements of neutron star radii and equation of state, *The LIGO /Virgo Collaboration*, arXiv:1805.11581v1

See also: De, Finstad, Lattimer, Brown, Berger, Biwer, (2018), arXiv:1804.08583 ; Bauswein, Just, Janka, N. Stergioulas, APJL 850, L34 (2017) ; Fattoyev, Piekarewicz, Horowitz, PRL 120, 172702 (2018) ; Nandi & Char, Astrophys. J. 857, 12 (2018) ; Paschalidis, Yagi, Alvarez-Castillo, Blaschke, Sedrakian, PRD 97, 084038 ; Ruiz, Shapiro, Tsokaros, PRD 97, 021501 (2018) ; Annala, Gorda, Kurkela, Vuorinen, PRL 120, 172703 (2018) ; Raithel, Özel, Psaltis, (2018) arXiv:1803.07687

The Hadron-Quark Phase Transition and the Third Family of Compact Stars (Twin Stars)

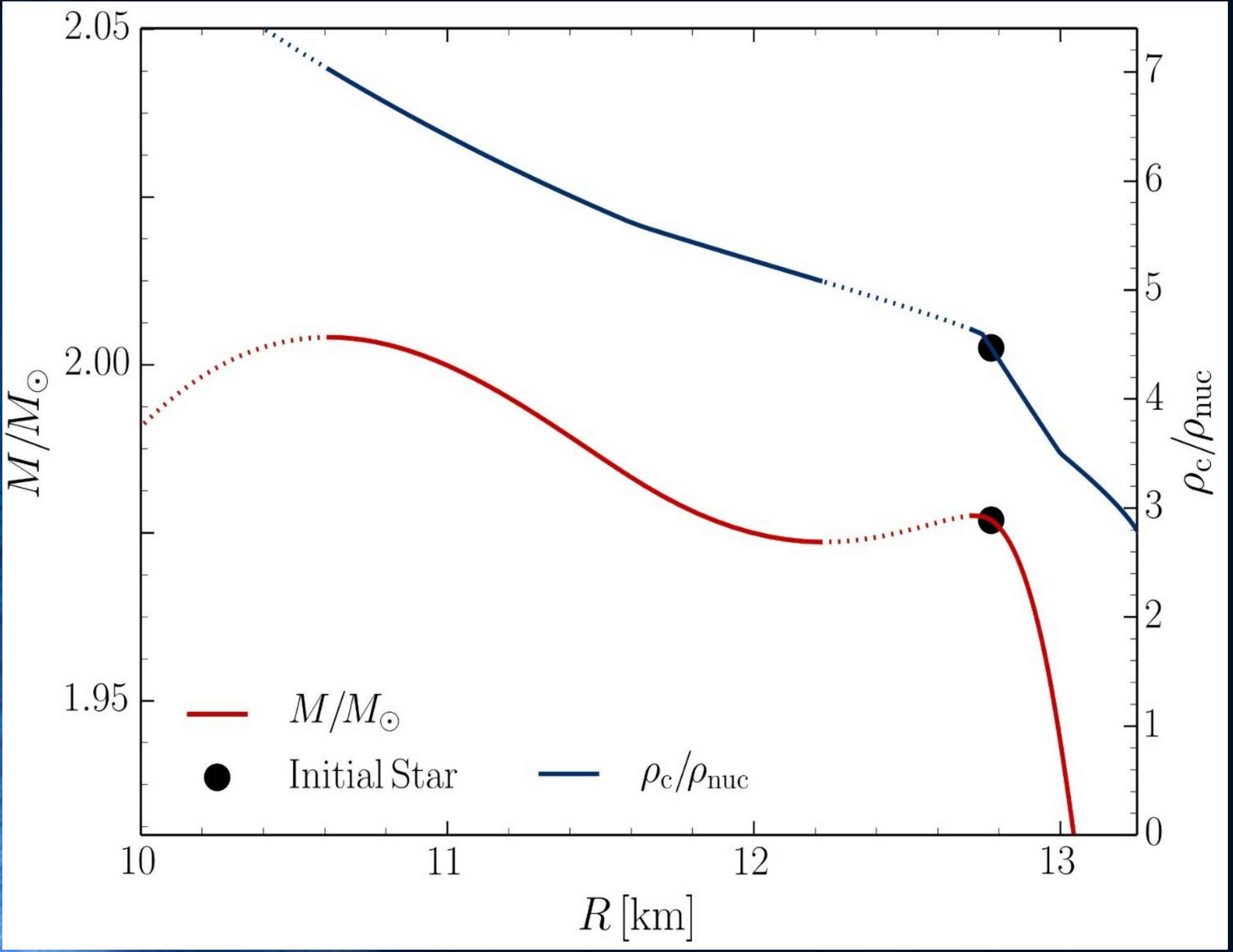

Glendenning, N. K., & Kettner, C. (1998). Nonidentical neutron star twins. Astron. Astrophys., 353(LBL-42080), L9.

Sarmistha Banik, Matthias Hanauske, Debades Bandyopadhyay and Walter Greiner, Rotating compact stars with exotic matter, Phys.Rev.D 70 (2004) p.12304

I.N. Mishustin, M. Hanauske, A. Bhattacharyya, L.M. Satarov, H. Stöcker, and W. Greiner, Catastrophic rearrangement of a compact star due to quark core formation, Physics Letters B 552 (2003) p.1-8

M.Alford and A. Sedrakian, Compact stars with sequential QCD phase transitions. Physical review letters, 119(16), 161104 (2017).

D.Alvarez-Castillo and D.Blaschke, High-mass twin stars with a multipolytrope equation of state. Physical Review C, 96(4), 045809 (2017) .

A. Ayriyan, N.-U. Bastian, D. Blaschke, H. Grigorian, K. Maslov, D. N. Voskresensky, How robust is a third family of compact stars against pasta phase effects?, arXiv:1711.03926 [nucl-th]

Constraining the hadron-quark phase transition with GW170817

Construction of the EOS with a hadron-quark phase transition

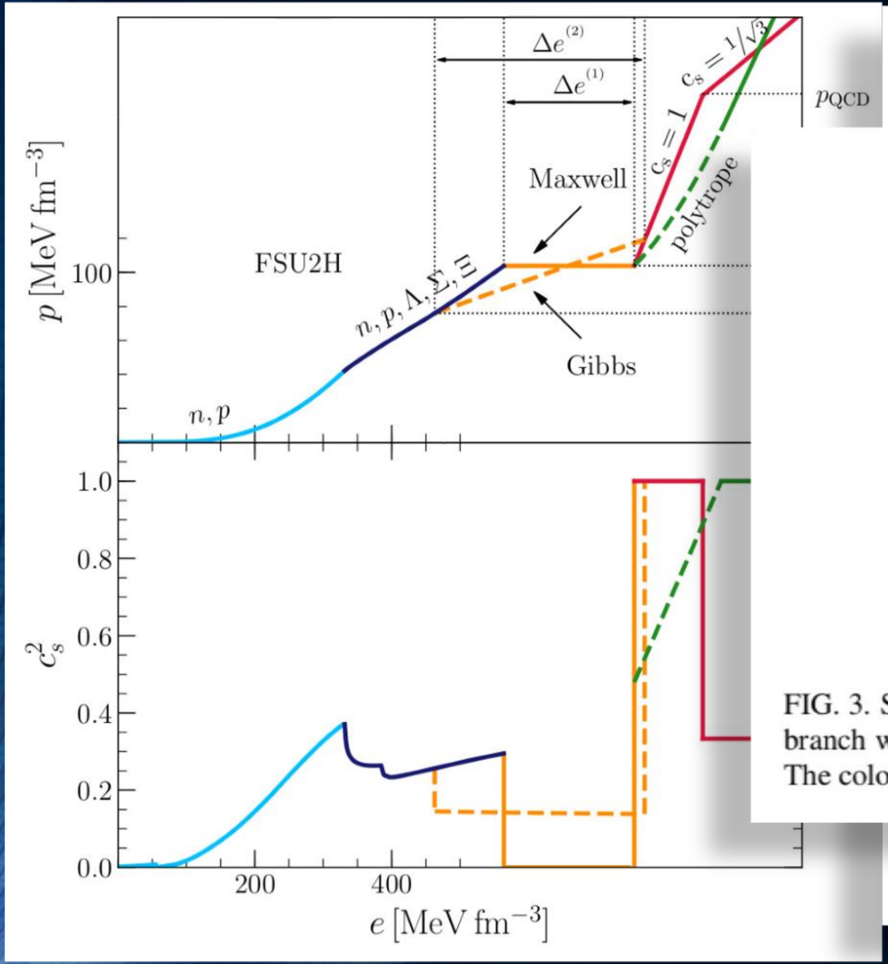

The Mass-Radius relation and the twin star property

Maxwell Construction Gibbs Construction

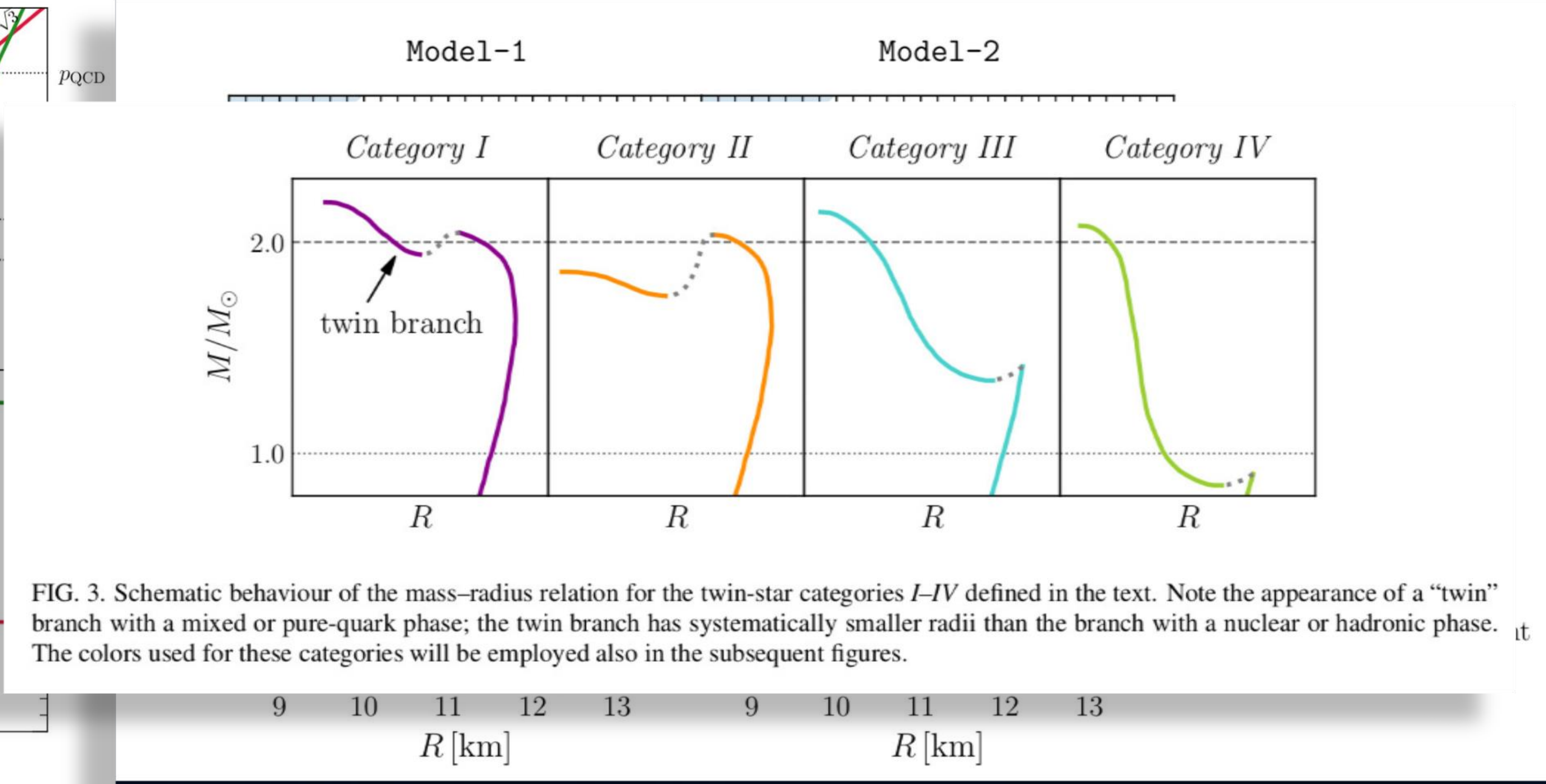

FIG. 3. Schematic behaviour of the mass–radius relation for the twin-star categories *I–IV* defined in the text. Note the appearance of a "twin" branch with a mixed or pure-quark phase; the twin branch has systematically smaller radii than the branch with a nuclear or hadronic phase. The colors used for these categories will be employed also in the subsequent figures.

G. Montana, L.Tolos, M.Hanauske and L.Rezzolla „Constraining twin stars with GW170817„, PRD 99(10), 2019

The inspiral and merger phase

Pre-merger signatures of the hadron-quark phase

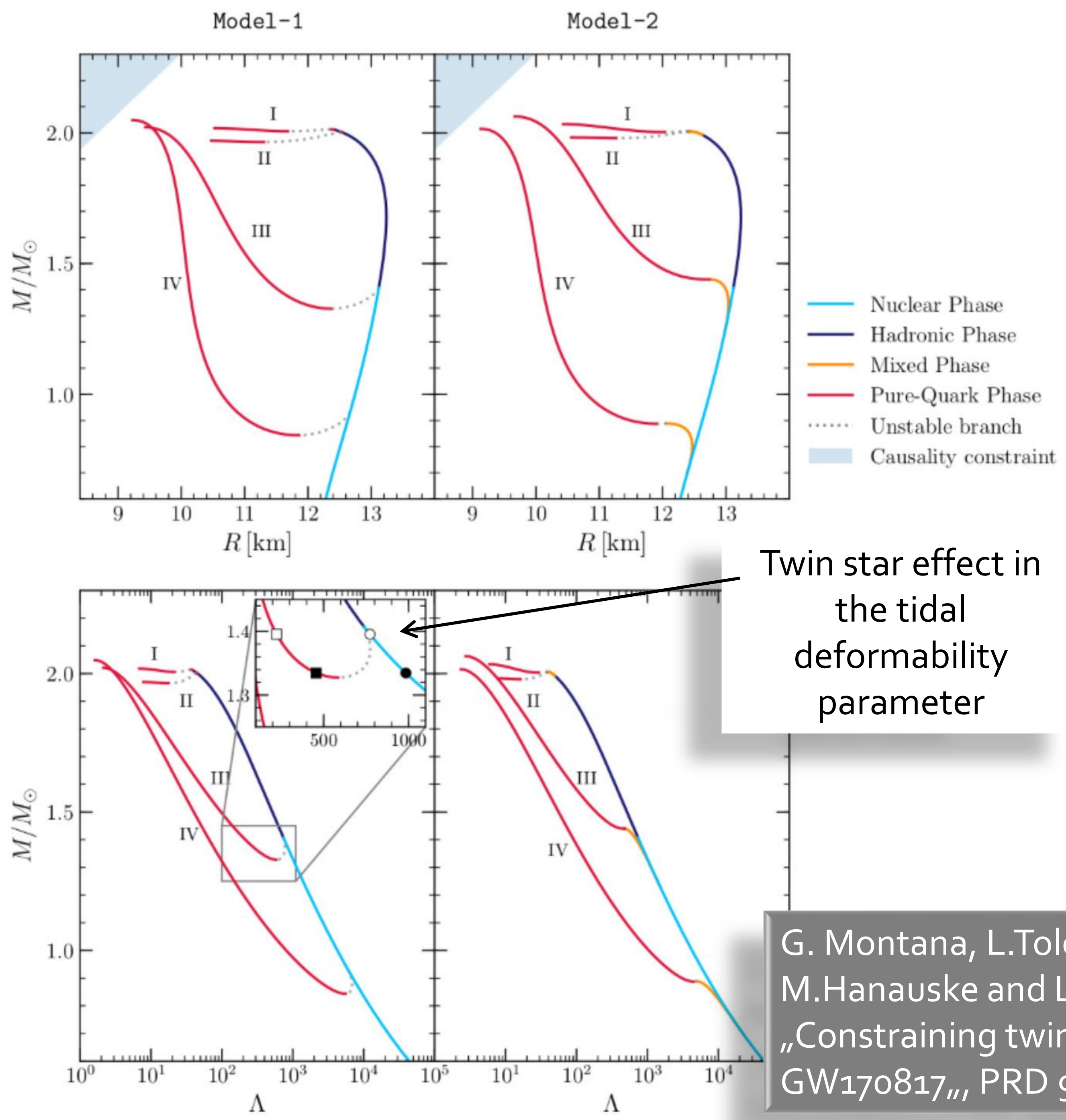

Twin star effect in the tidal deformability parameter

Reference	R_i [km]
Without a phase transition	
Bauswein et al. [42]	$10.68^{+0.15}_{-0.03} \leq R_{1.6}$
Most et al. [51]	$12.00 \leq R_{1.4} \leq 13.45$
Burgio et al. [54]	$11.8 \leq R_{1.5} \leq 13.1$
Tews et al. [55]	$11.3 \leq R_{1.4} \leq 13.6$
De et al. [56]	$8.9 \leq R_{1.4} \leq 13.2$
LIGO/Virgo [57]	$10.5 \leq R_{1.4} \leq 13.3$
With a phase transition	
Annala et al. [46]	$R_{1.4} \leq 13.6$
Most et al. [51]	$8.53 \leq R_{1.4} \leq 13.74$
Burgio et al. [54]	$R_{1.5} = 10.7$
Tews et al. [55]	$9.0 \leq R_{1.4} \leq 13.6$
This work	
NS	$R_{1.4} = 13.11$
HS Model-2	$12.9 \leq R_{1.4} \leq 13.11$
HS Model-1	$10.1 \leq R_{1.4} \leq 12.9$
l-2	$10.4 \leq R_{1.4} \leq 11.9$

...Constraints on the radius of neutron stars from ...r models without a phase transition (top), works con-... ...ssibility of a transition to quark matter (middle) and ...*ategory III* in the present work (bottom).

G. Montana, L.Tolos, M.Hanauske and L.Rezzolla „Constraining twin stars with GW170817„, PRD 99(10), 2019

Postmerger gravitational-wave signatures of phase transitions in binary compact star mergers

- Introduction
- Numerical general relativity of compact star mergers
- The equation of state of compact star matter and the hadron-quark phase transition
- The different phases of a binary compact star merger event
- **Gravitational-wave signatures of the hadron-quark phase transition in binary compact star mergers**
  - The inspiral and merger phase (premerger signals)
  - **Hypermassive hybrid stars (HMHS) within the prompt phase transition scenario (PPT)**
  - HMHS within the delayed phase transition scenario (DPT)
  - HMHS within the phase transition triggered collapse scenario (PTTC)
- Summary and Outlook

Hybrid Star Mergers with T-dependent EOS *(PRL paper 2)*

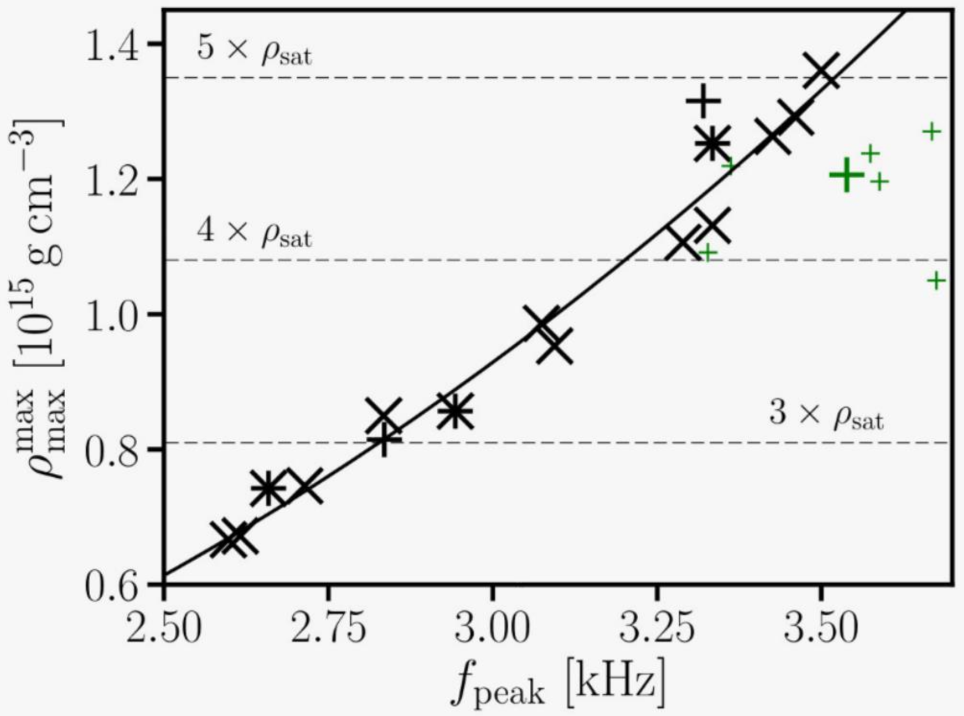

FIG. 4: Maximum rest-mass density $\rho_{\mathrm{max}}^{\mathrm{max}}$ during the first milliseconds of the postmerger phase as function of the dominant postmerger GW frequency f_{peak} for 1.35-1.35 $M_{\odot}$ mergers. Green symbols display results for DD2F-SF (big symbol for DD2F-SF-1). Asterisks indicate models with hyperons. Black plus signs display ALF2/4. Solid curve is a second order polynomial least square fit to the data excluding hybrid EOSs.

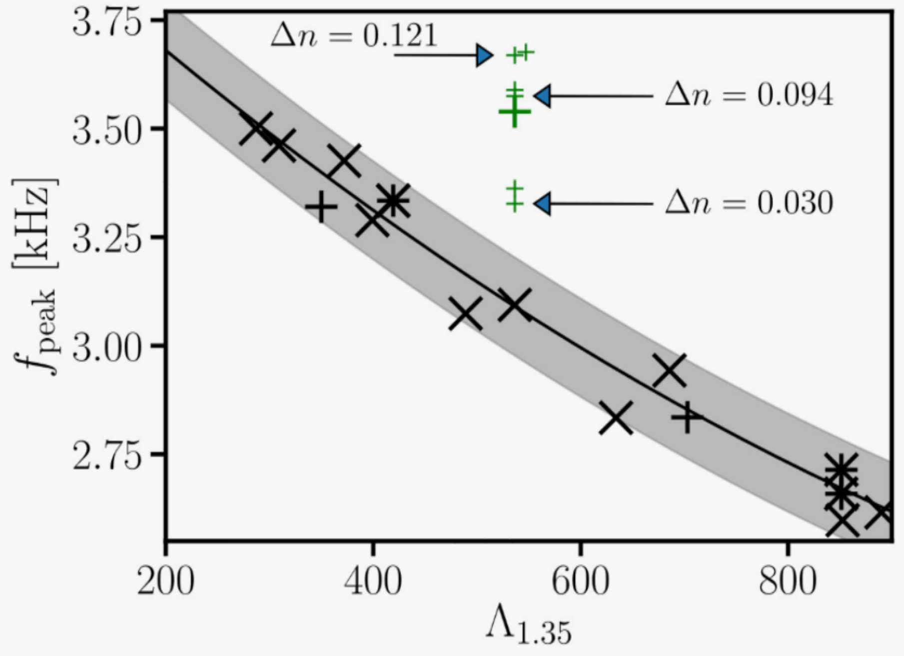

FIG. 3: Dominant postmerger GW frequency f_{peak} as function of tidal deformability Λ for 1.35-1.35 $M_{\odot}$ mergers. The DD2F-SF models with a phase transition to deconfined quark matter (green symbols) appear as clear outliers (big symbol for DD2F-SF-1). Solid curve displays the least square fit Eq. (1) for all purely hadronic EOSs (including three models with hyperons marked by asterisks). ALF2 and ALF4 are marked by black plus signs. EOSs incompatible with GW170817 are not shown. Arrows mark DD2F-SF models 3, 6 and 7, which feature differently strong density jumps Δn (in fm^{-3}) with roughly the same onset density and stiffness of quark matter.

Post-merger gravitational-wave signatures of phase transitions in binary compact star mergers

PRL 124, 171103 (2020)

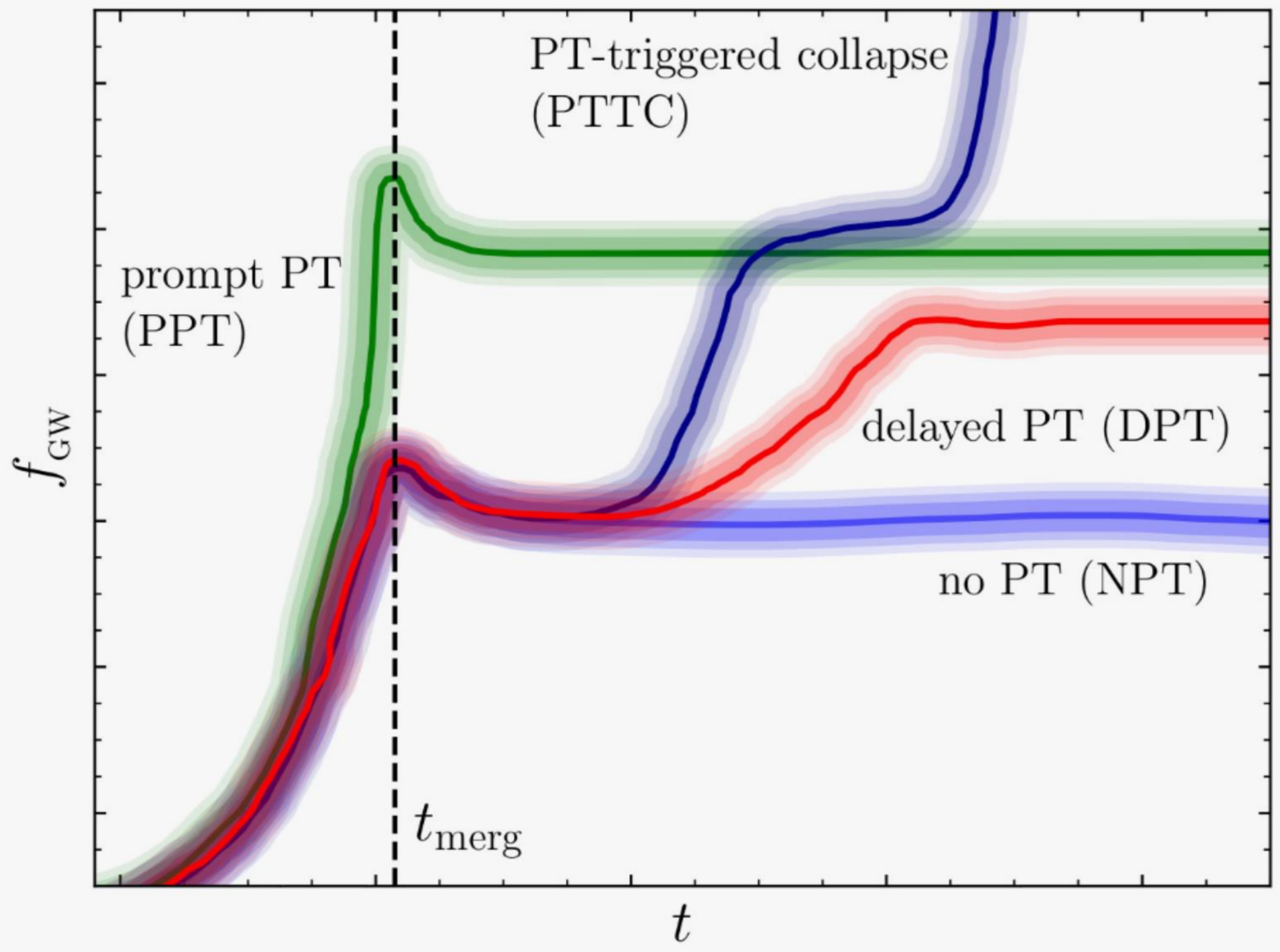

Schematic overview of the instantaneous gravitational wave frequency and how its evolution can be used to classify the different scenarios associated with a hadron-quark phase transition.

Post-merger gravit

of phase transitions in

PRL 124

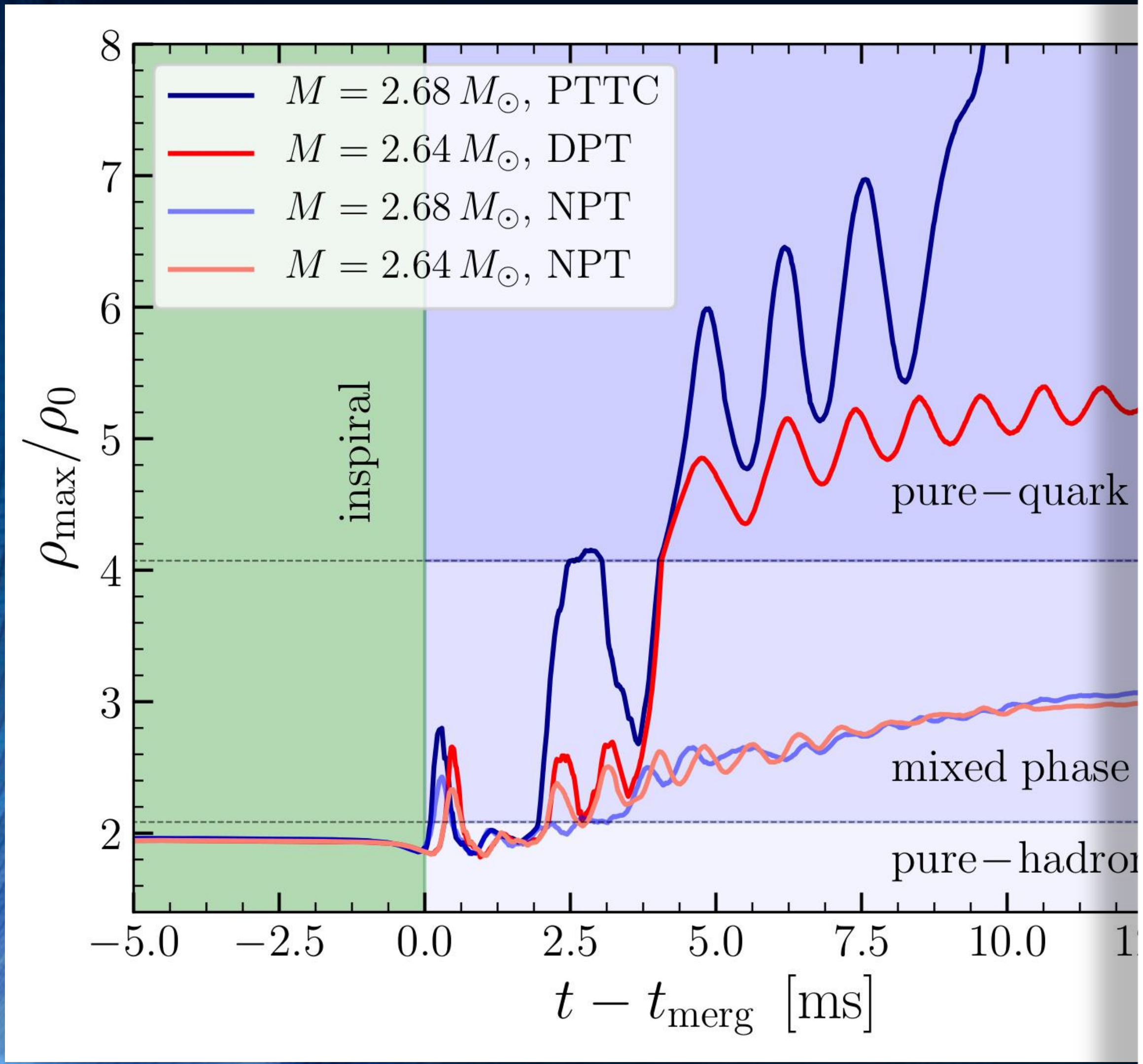

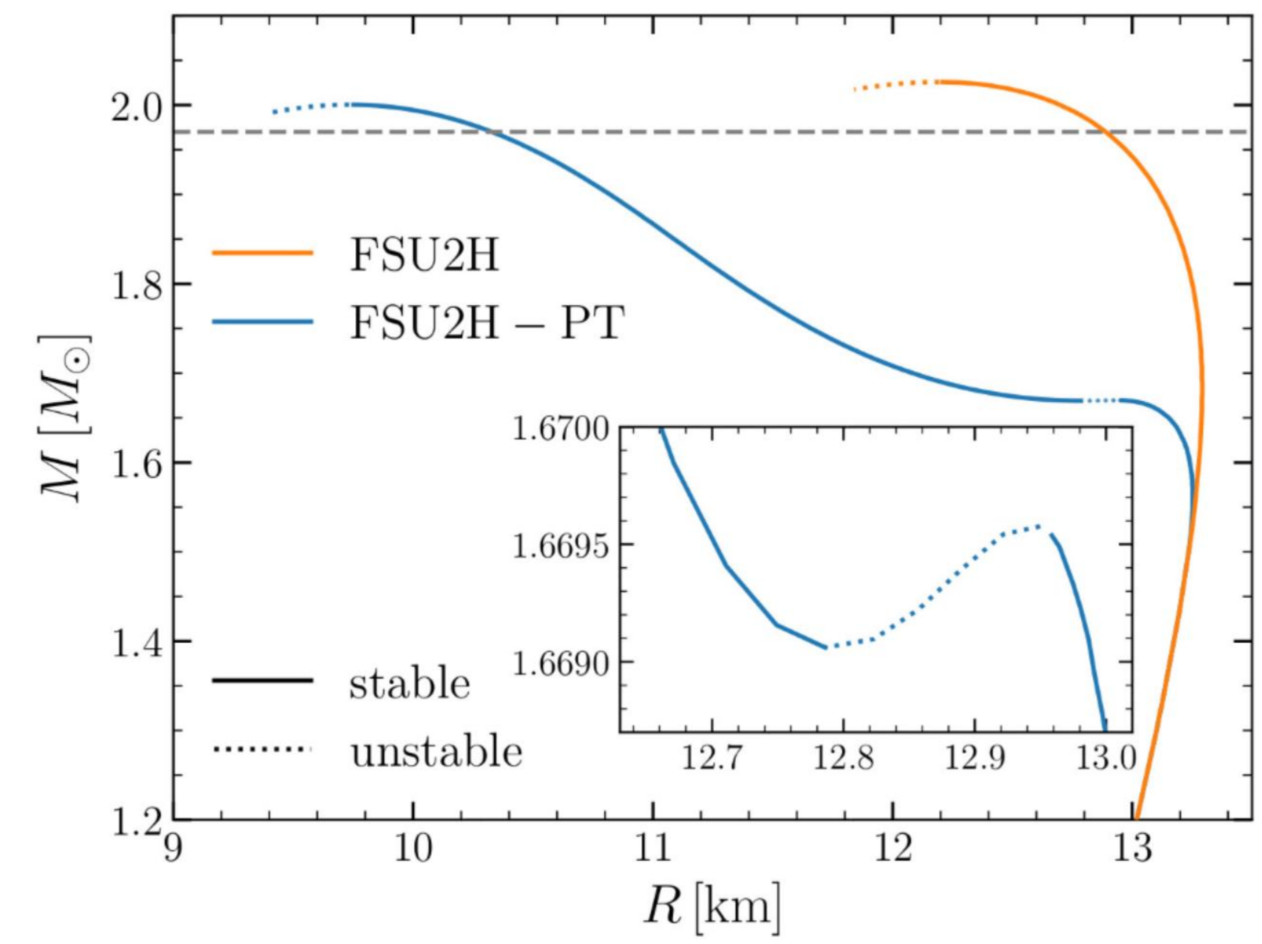

FIG. 1. Mass-radius relation for the purely hadronic EOS (FSU2H) and its modified version (FSU2H-PT). The latter shows a second stable (solid lines) branch after a small region of instability (dotted). The grey dashed line marks the limit of 1.97 $M_\odot$.

Postmerger gravitational-wave signatures of phase transitions in binary compact star mergers

- Introduction
- Numerical general relativity of compact star mergers
- The equation of state of compact star matter and the hadron-quark phase transition
- The different phases of a binary compact star merger event
- **Gravitational-wave signatures of the hadron-quark phase transition in binary compact star mergers**
  - The inspiral and merger phase (premerger signals)
  - Hypermassive hybrid stars (HMHS) within the prompt phase transition scenario (PPT)
  - **HMHS within the delayed phase transition scenario (DPT)**
  - HMHS within the phase transition triggered collapse scenario (PTTC)
- Summary and Outlook

Metastable hypermassive hybrid stars as neutron-star merger remnants

A case study

Matthias Hanauske[1,2,a], Lukas R. Weih[2], Horst Stöcker[1,2,3], and Luciano Rezzolla[2,4,5]

[1] Frankfurt Institute for Advanced Studies, Ruth-Moufang-Straße 1, 60438 Frankfurt, Germany
[2] Institut für Theoretische Physik, Max-von-Laue-Straße 1, 60438 Frankfurt, Germany
[3] GSI Helmholtzzentrum für Schwerionenforschung GmbH, 64291 Darmstadt, Germany
[4] School of Mathematics, Trinity College, Dublin 2, Ireland
[5] Helmholtz Research Academy Hesse for FAIR, Max-von-Lau

Abstract. Hypermassive hybrid stars (HMHS) are
jects that could be produced in the merger of a binar
In contrast to their purely hadronic counterparts, h
(HMNS), these highly differentially rotating objects

The delayed phase transition scenario DPT

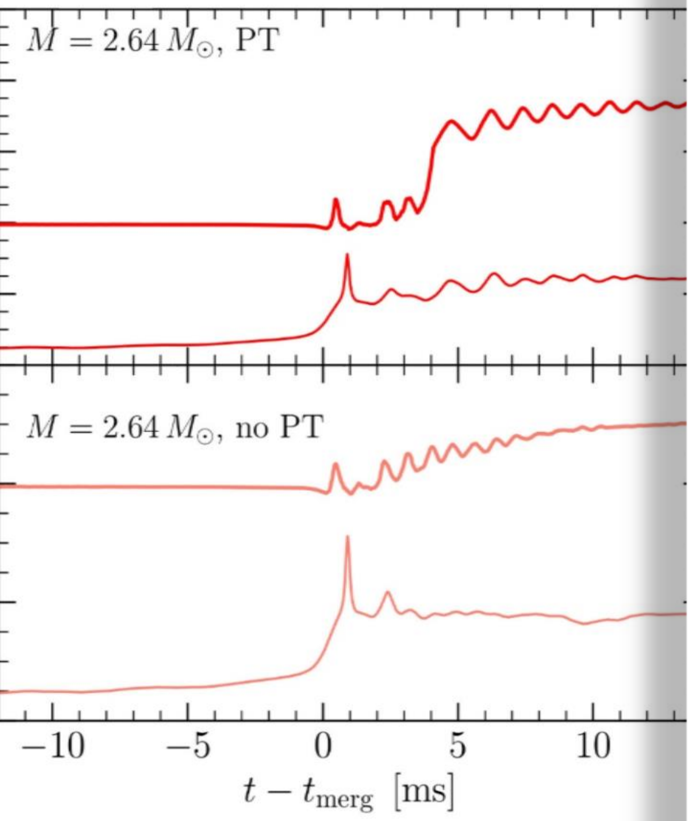

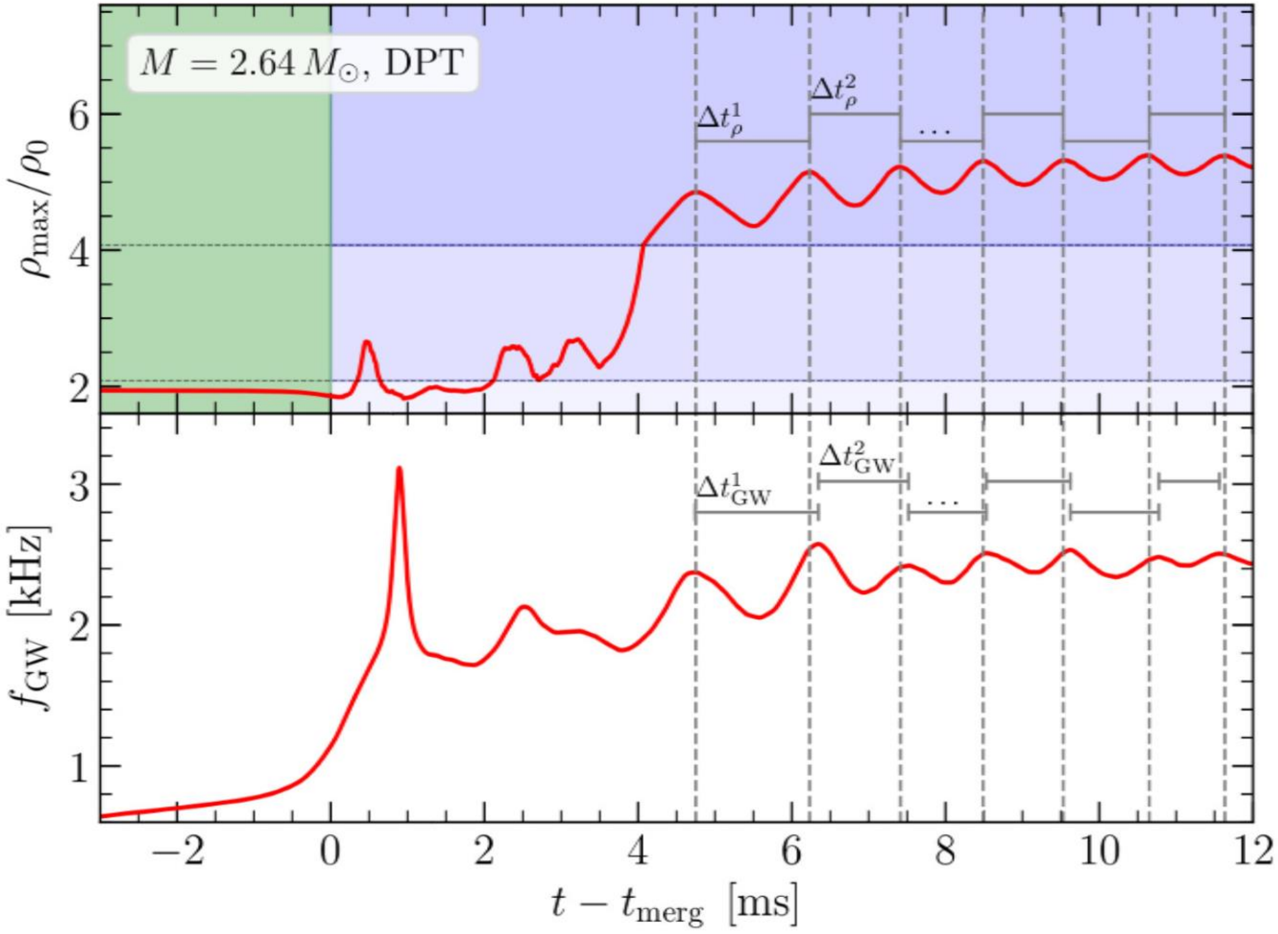

Fig. 3. *Top:* Same as Fig. 1. *Bottom:* Instantaneous GW frequency. The time intervals Δt^i_ρ and $\Delta t^i_{\rm GW}$ between consecutive peaks in the top and bottom panel, respectively, are marked by horizontal grey lines. The average difference between the two different types of peaks is less than 5%.

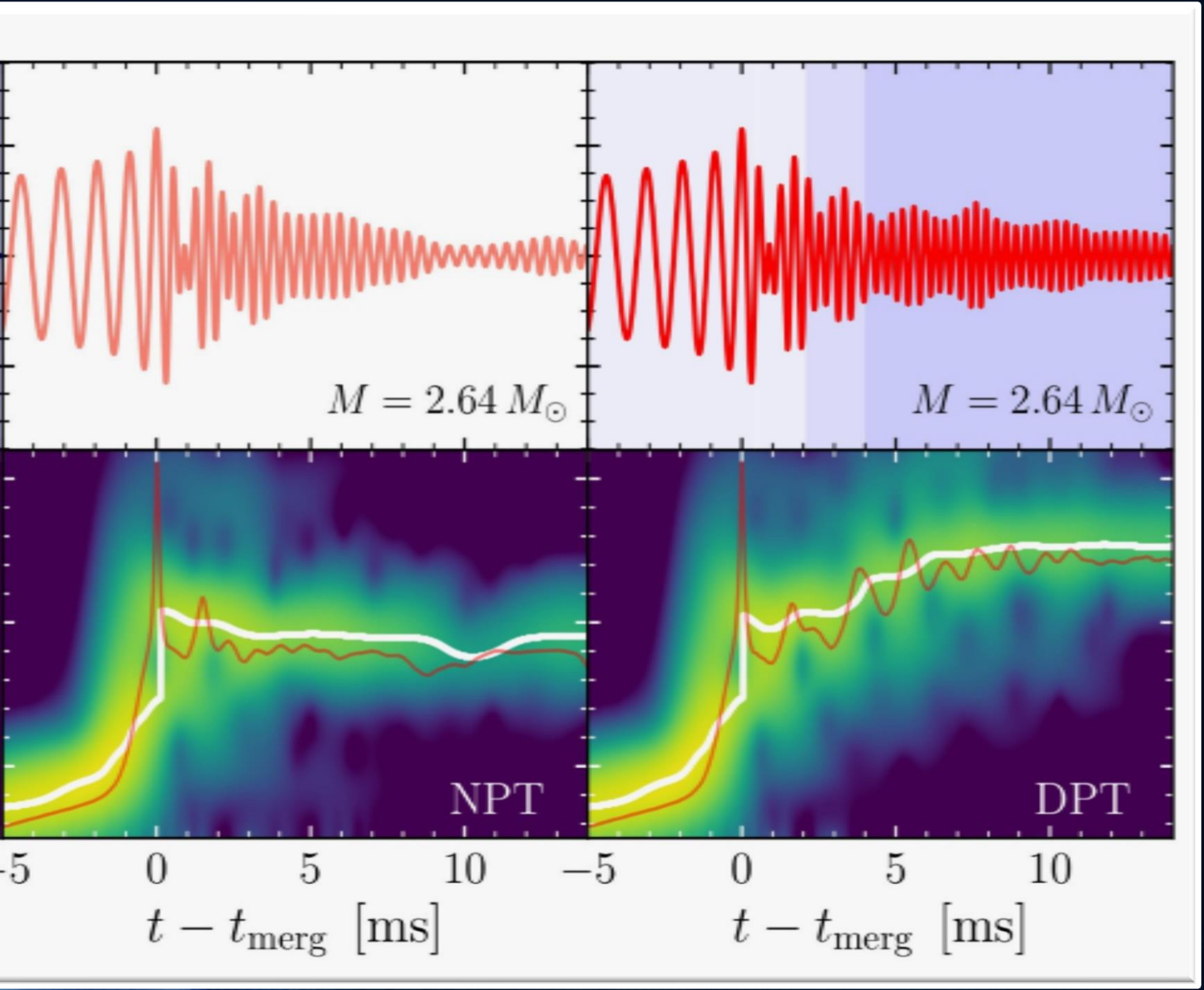

Strain h+ (top) and its spectrogram (bottom) for the binary neutron star simulation of the delayed phase transition scenario. In the top panel the different shadings mark the times when the HMNS core enters the mixed and pure quark phases.. In the bottom panels, the white lines trace the maximum of the spectrograms, while the red lines show the instantaneous gravitational-wave frequency.

Density and temperature evolution inside the HMHS

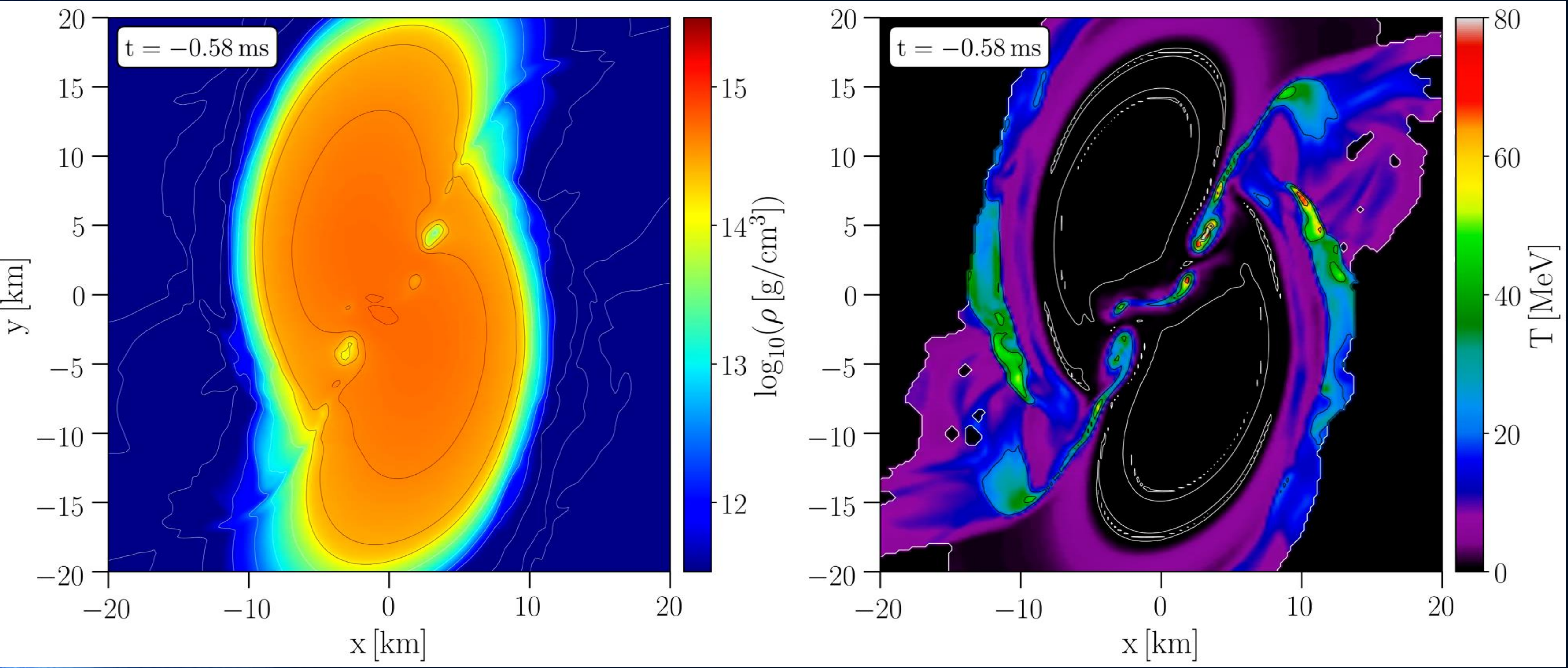

EOS: FSU2H-PT + thermal ideal fluid, Mass: 1.32 M_{solar}

Binary Neutron Star Mergers in the QCD Phase Diagram

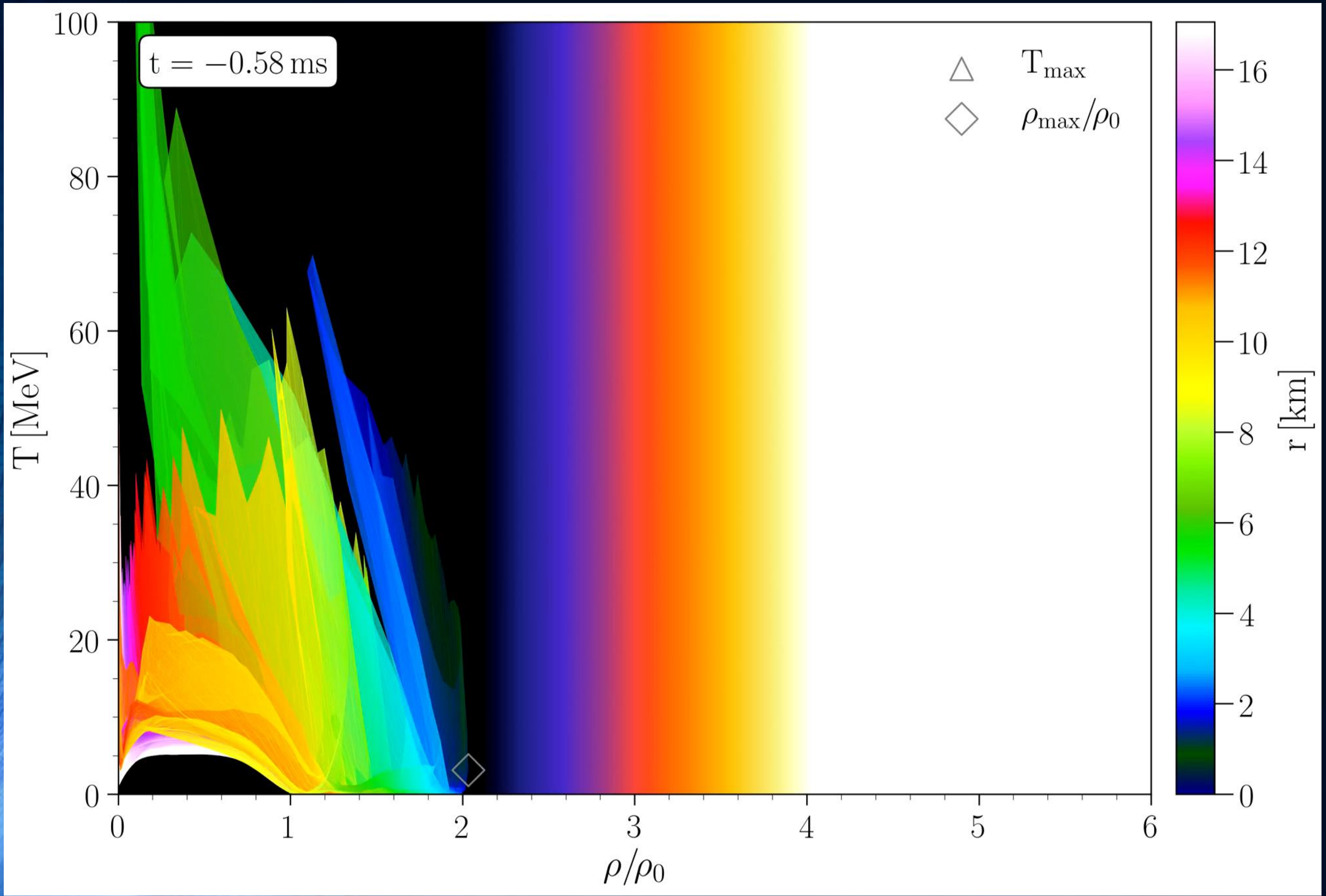

Evolution of hot and dense matter inside the inner area of a hypermassive hybrid star simulated within the (FSU2H-PT + thermal ideal fluid) EOS with a total mass of M_{total}=2.64 M_{solar} in the style of a (T- ρ) QCD phase diagram plot

The color-coding indicate the radial position r of the corresponding (T- ρ) fluid element measured from the origin of the simulation (x , y) = (0 , 0) on the equatorial plane at z = 0.

The open triangle marks the maximum value of the temperature while the open diamond indicates the maximum of the density.

These figures show the configuration of the HMHS at a time right before the collapse to the more compact star. The small asymmetry in the density profile and especially the double-core structure is amplified by the collapse resulting in a large one-sided asymmetry (i.e., an m = 1 asymmetry in a spherical-harmonics decomposition), which triggers a sizeable h21 GW strain.

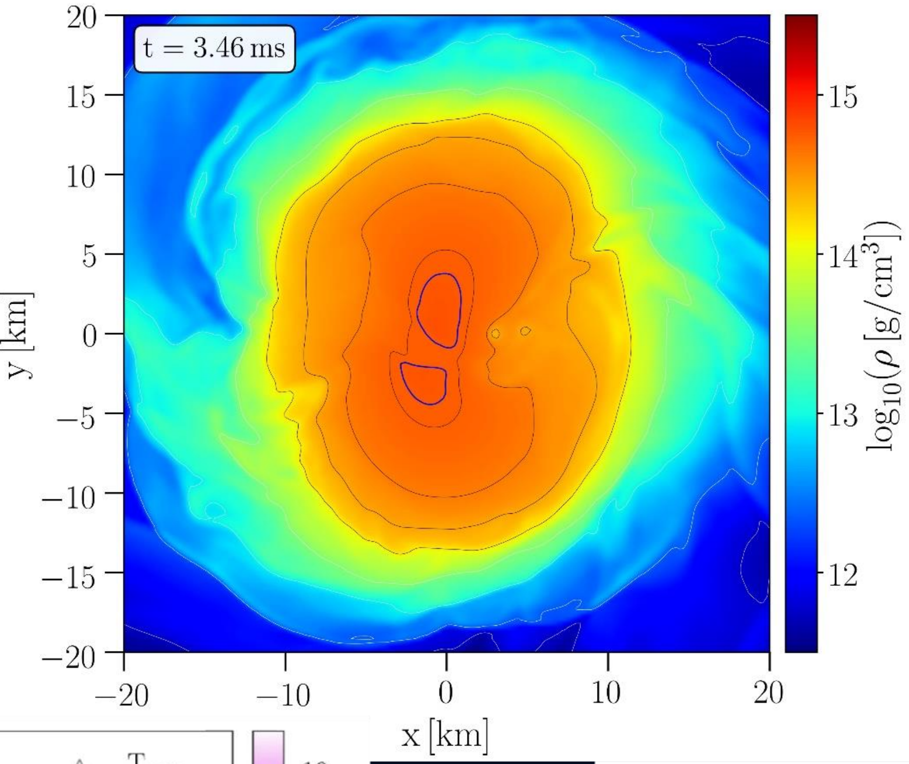

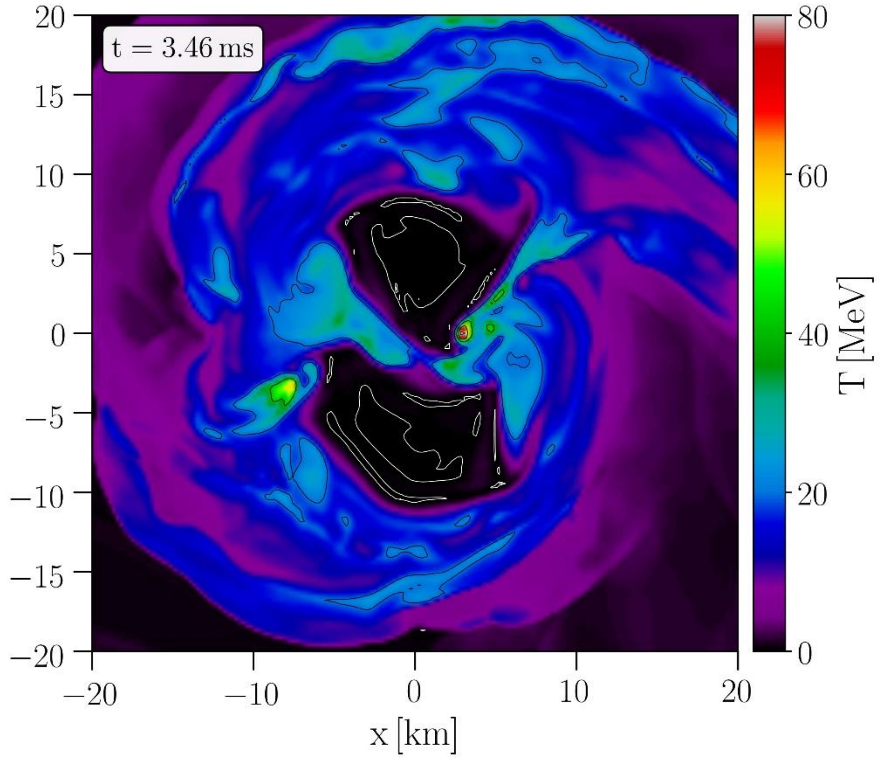

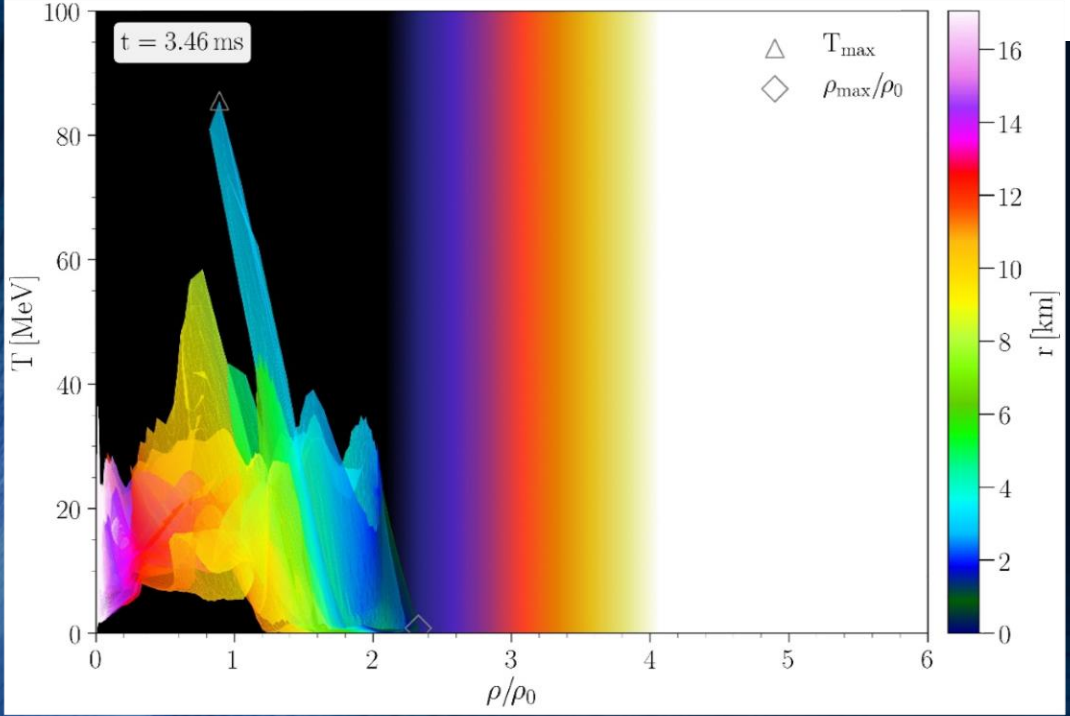

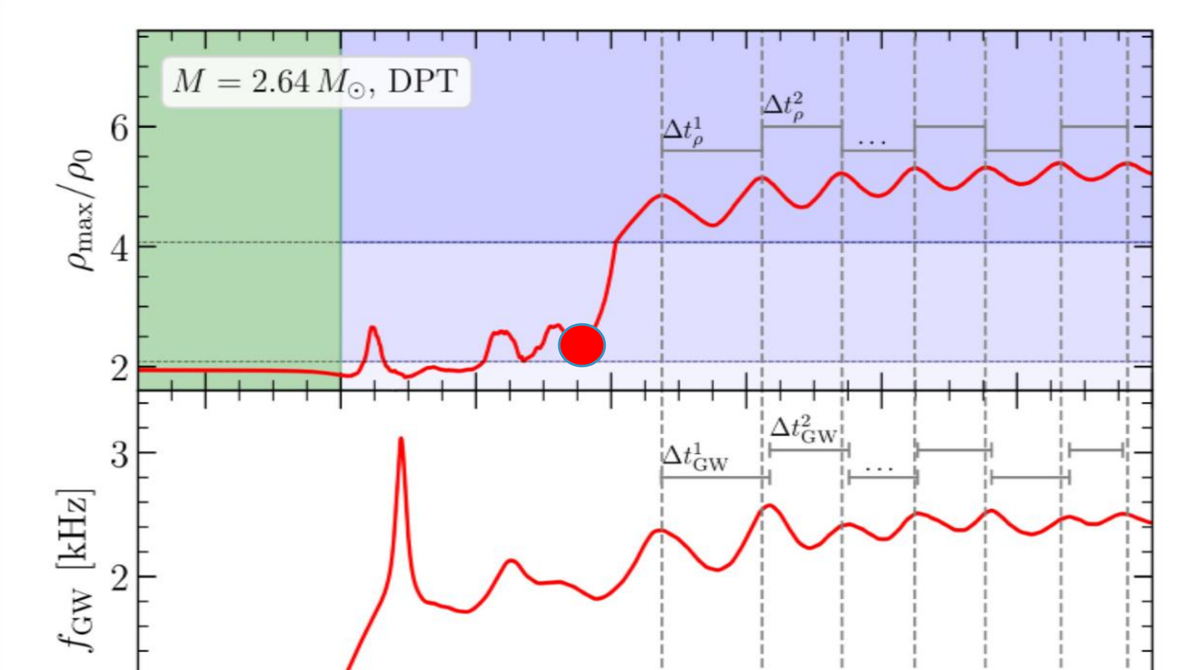

The figures correspond to a time near the first density maximum at t = 4.8ms (see red marker). The large m = 1 contribution can be seen by looking at the asymmetry of the spatial location of the quark core, which is marked with the second blue contour line. As a result of this asymmetry, the location of the two temperature are at different radial distances from the grid center.

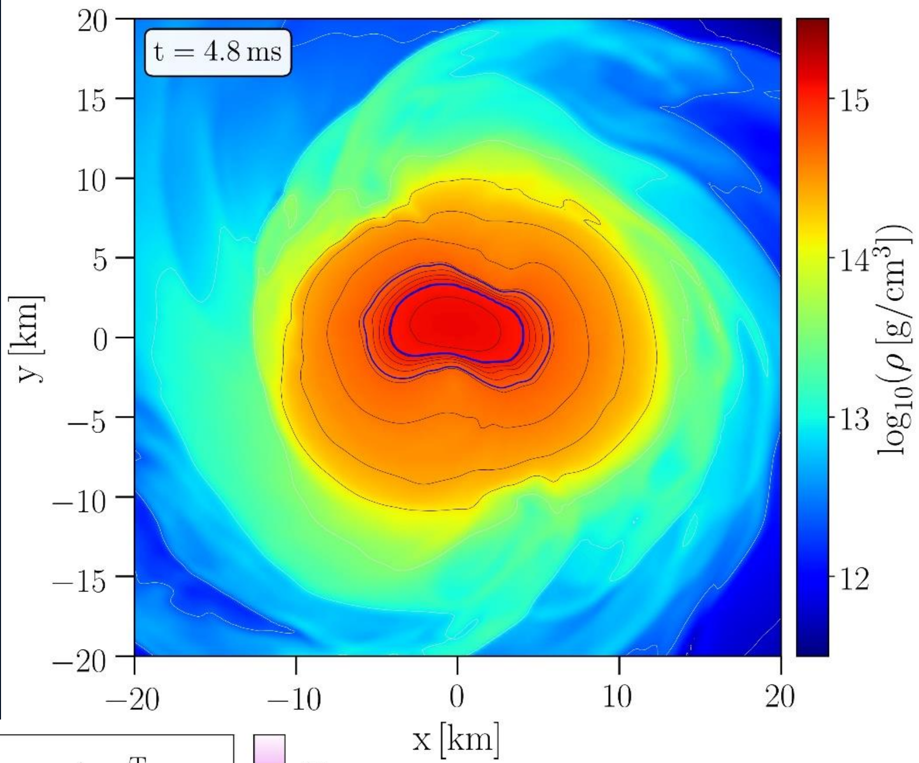

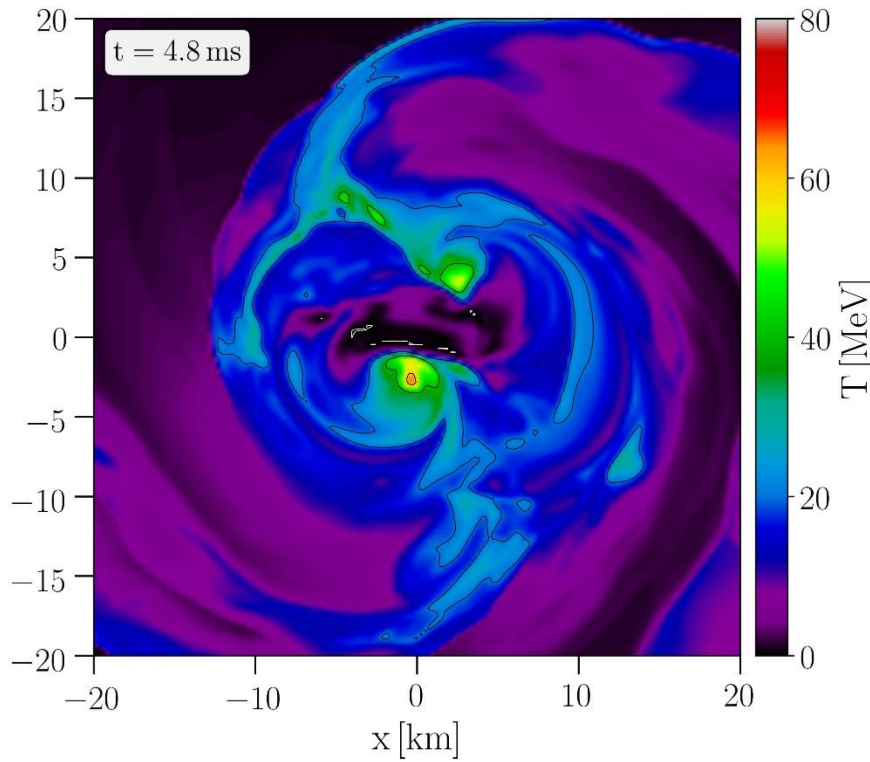

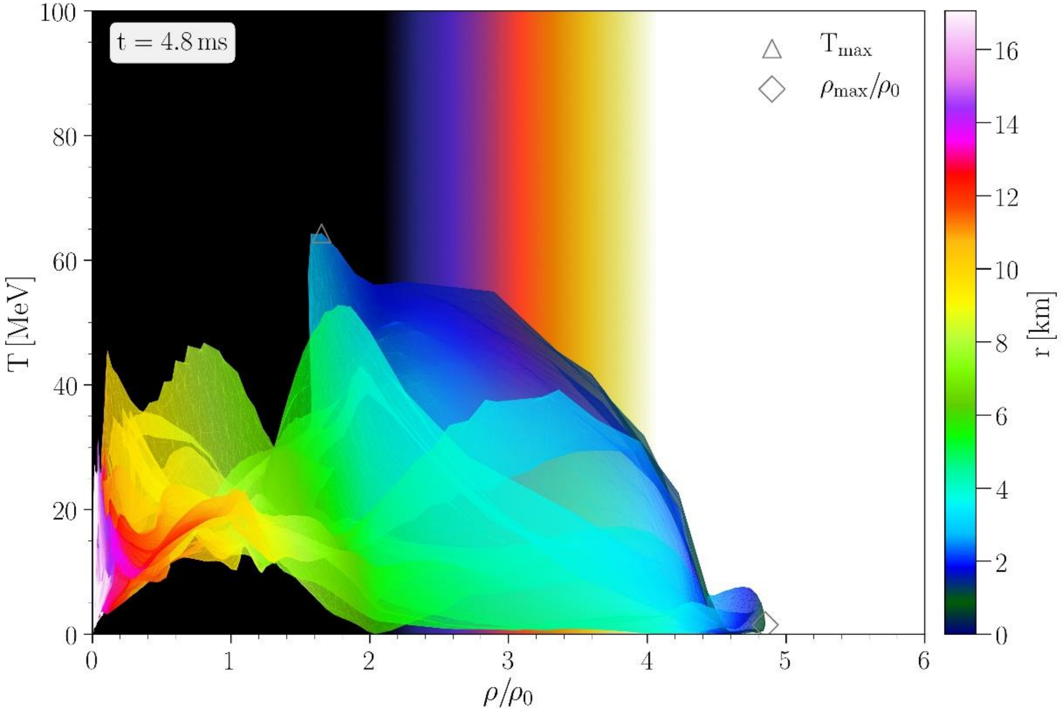

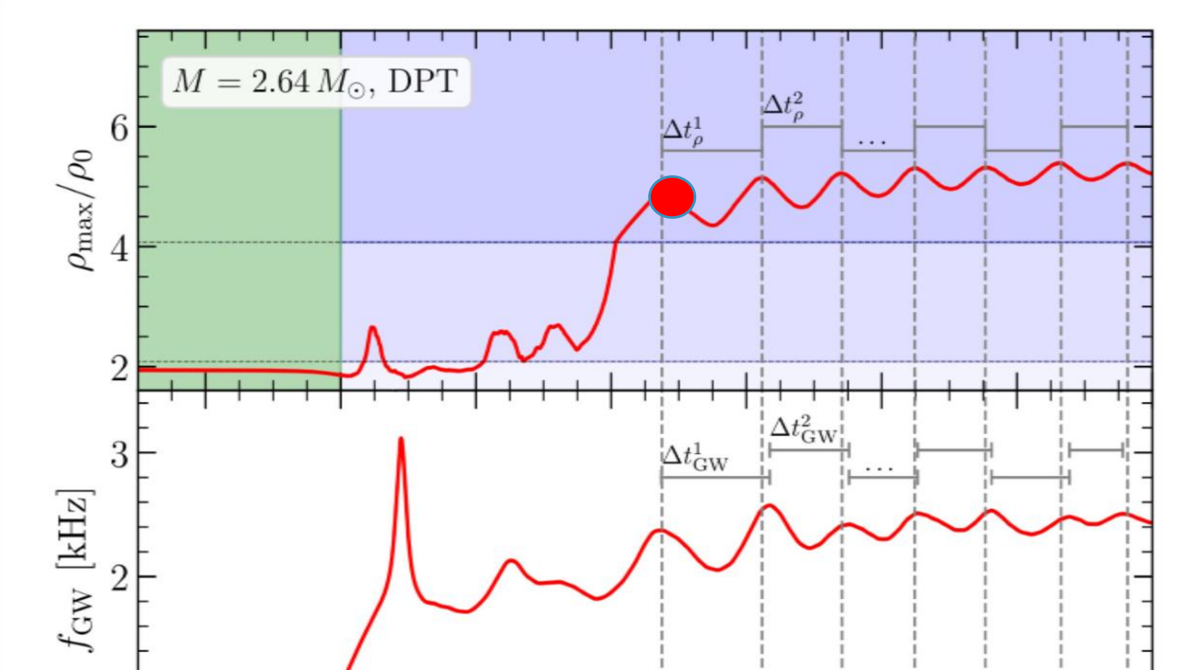

The figures correspond to a time near the first density minimum at t = 5.52ms (see red marker). The large m = 1 contribution can be seen by looking at the asymmetry of the spatial location of the quark core, which is marked with the second blue contour line. As a result of this asymmetry, the location of the two temperature are at different radial distances from the grid center.

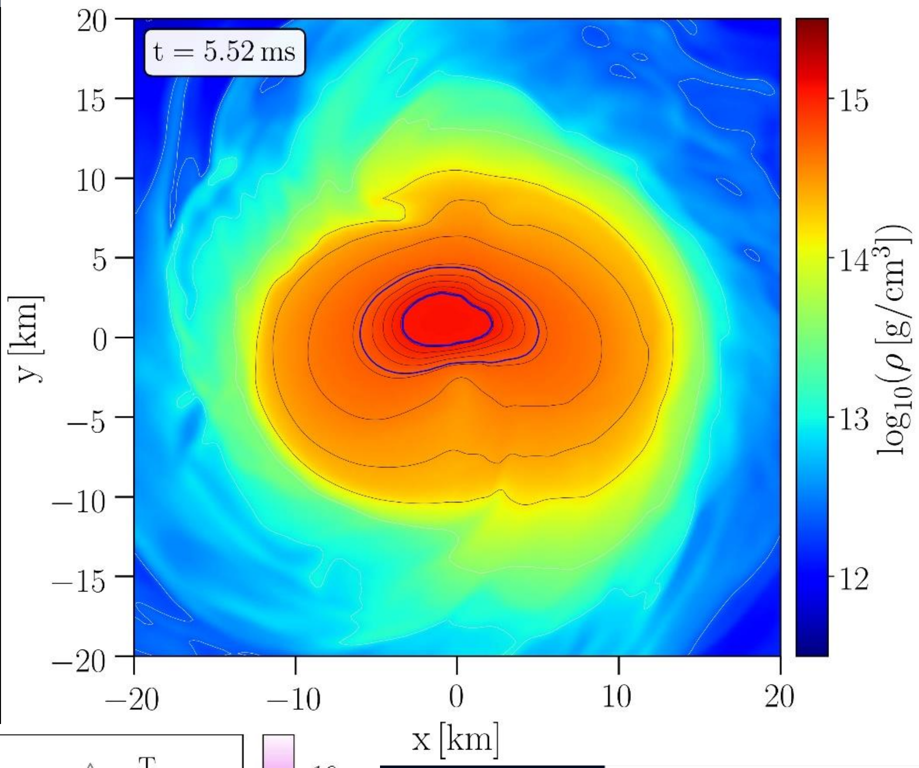

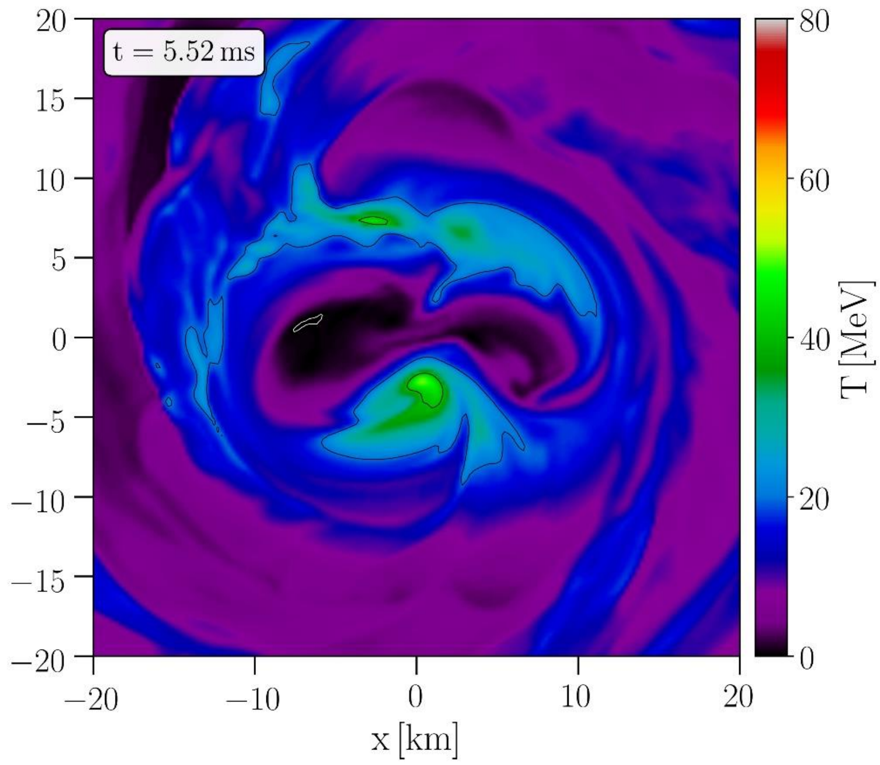

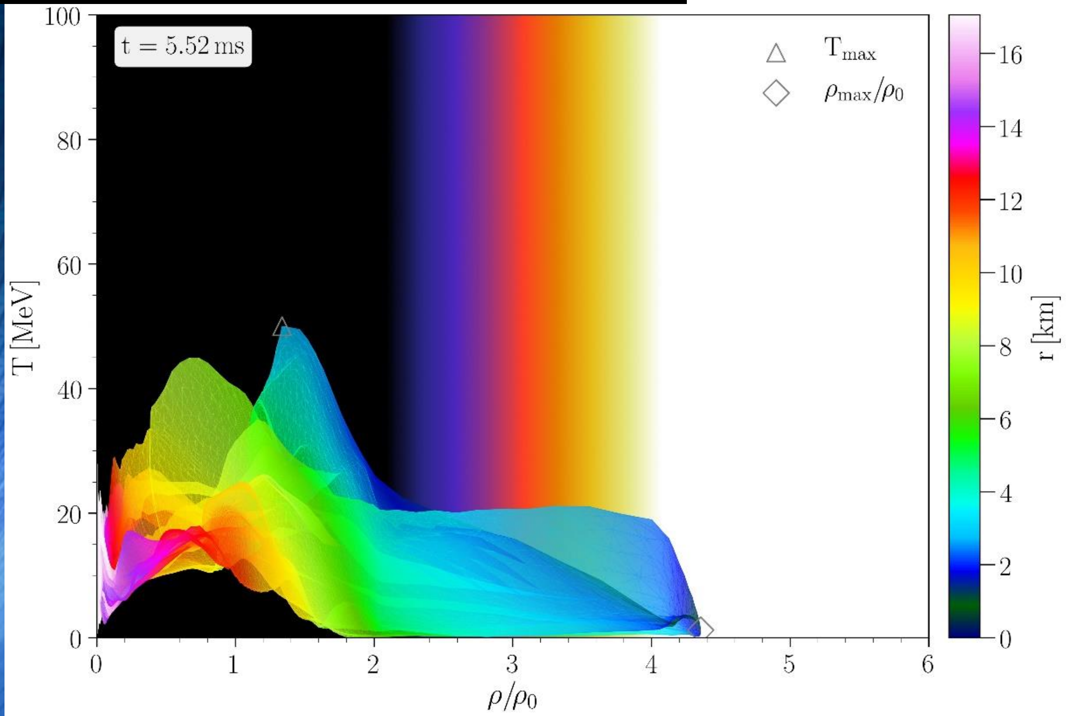

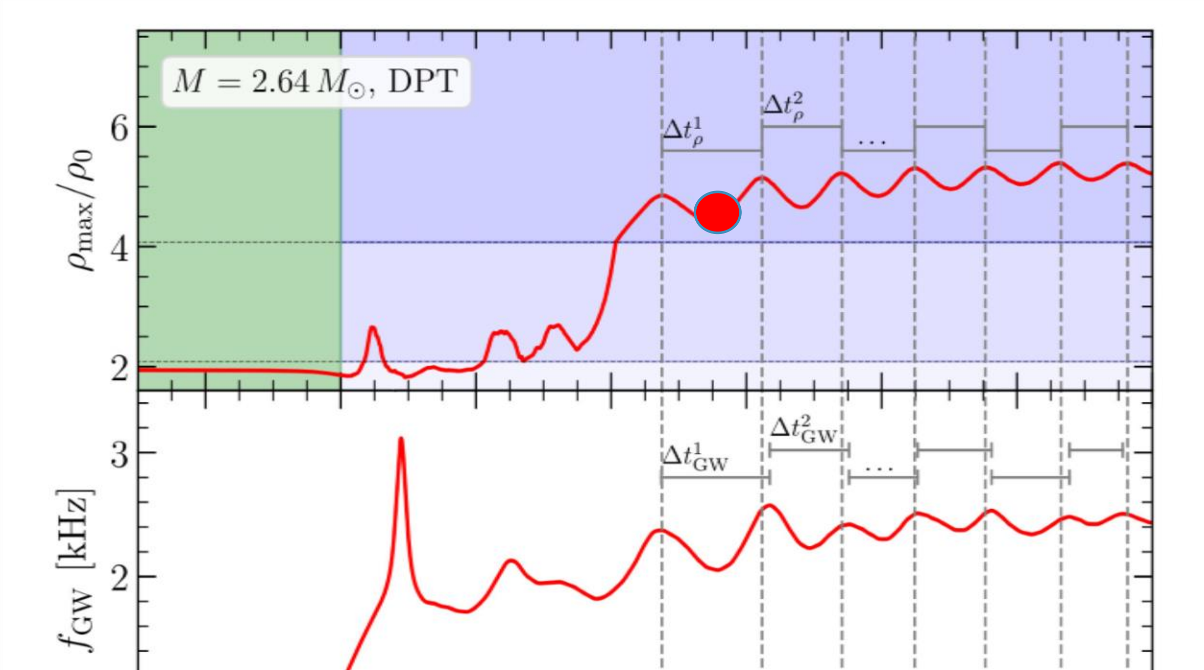

The collapse of the HMNS to the HMHS causes the system to vibrate. At the times when the maximum of the central density is reached, the pure quark core with its stiffer equation of state presses violently against the gravitational pressure and the star expands again and, as a result, its central density decreases.

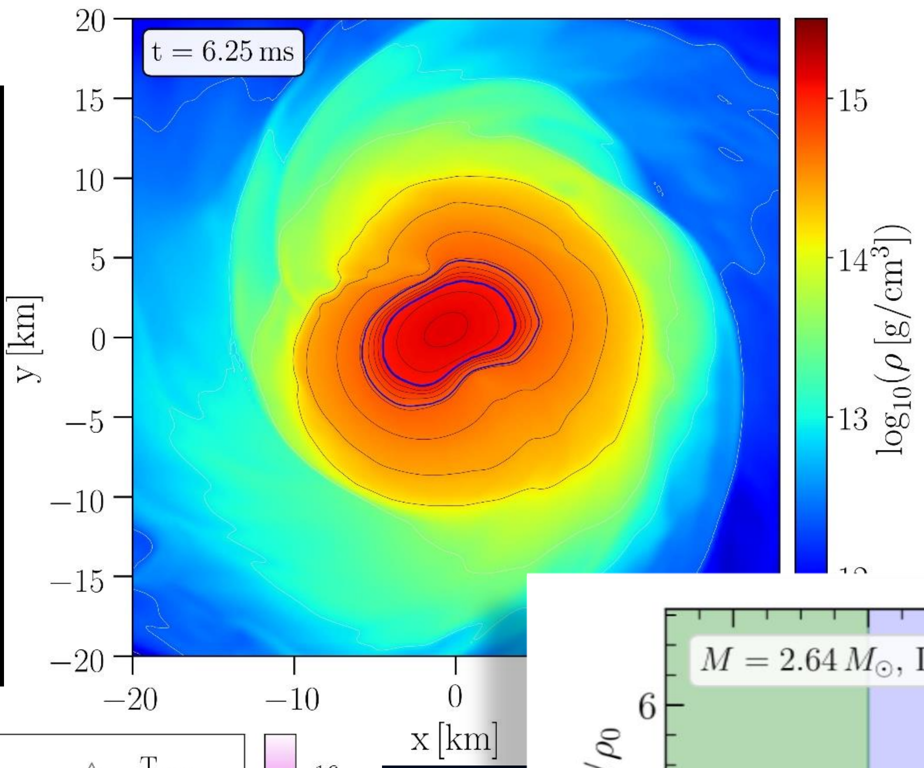

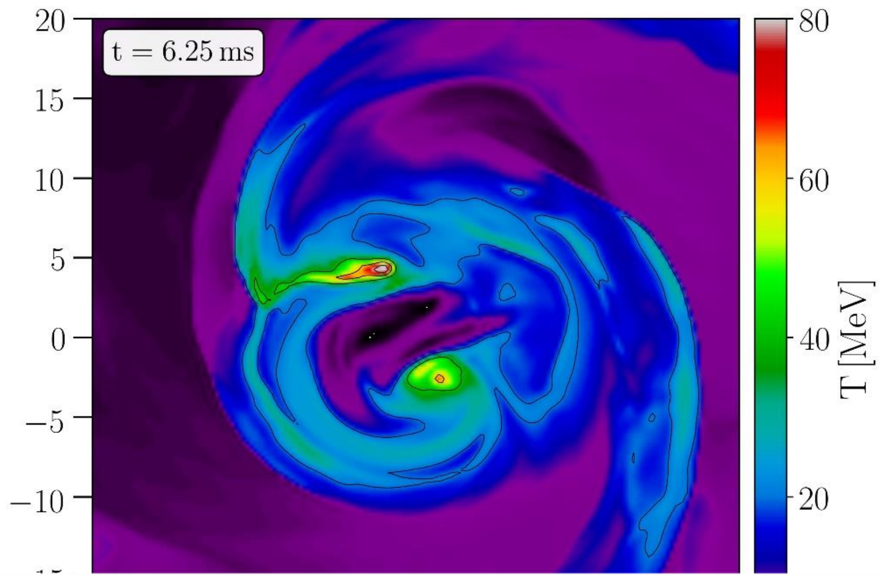

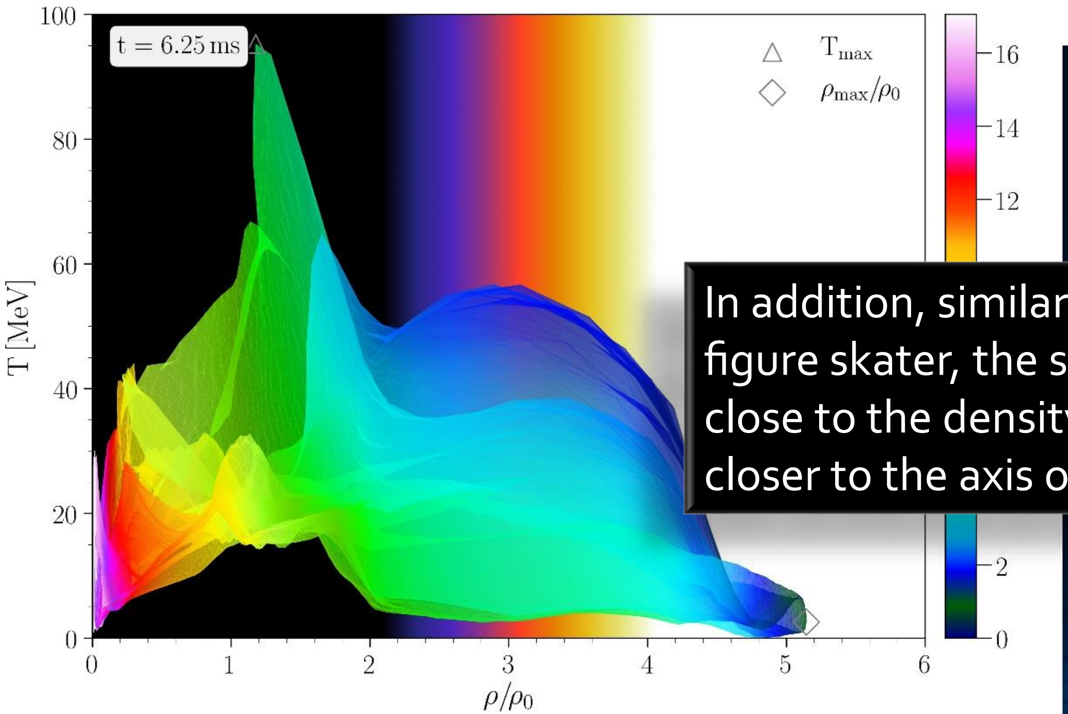

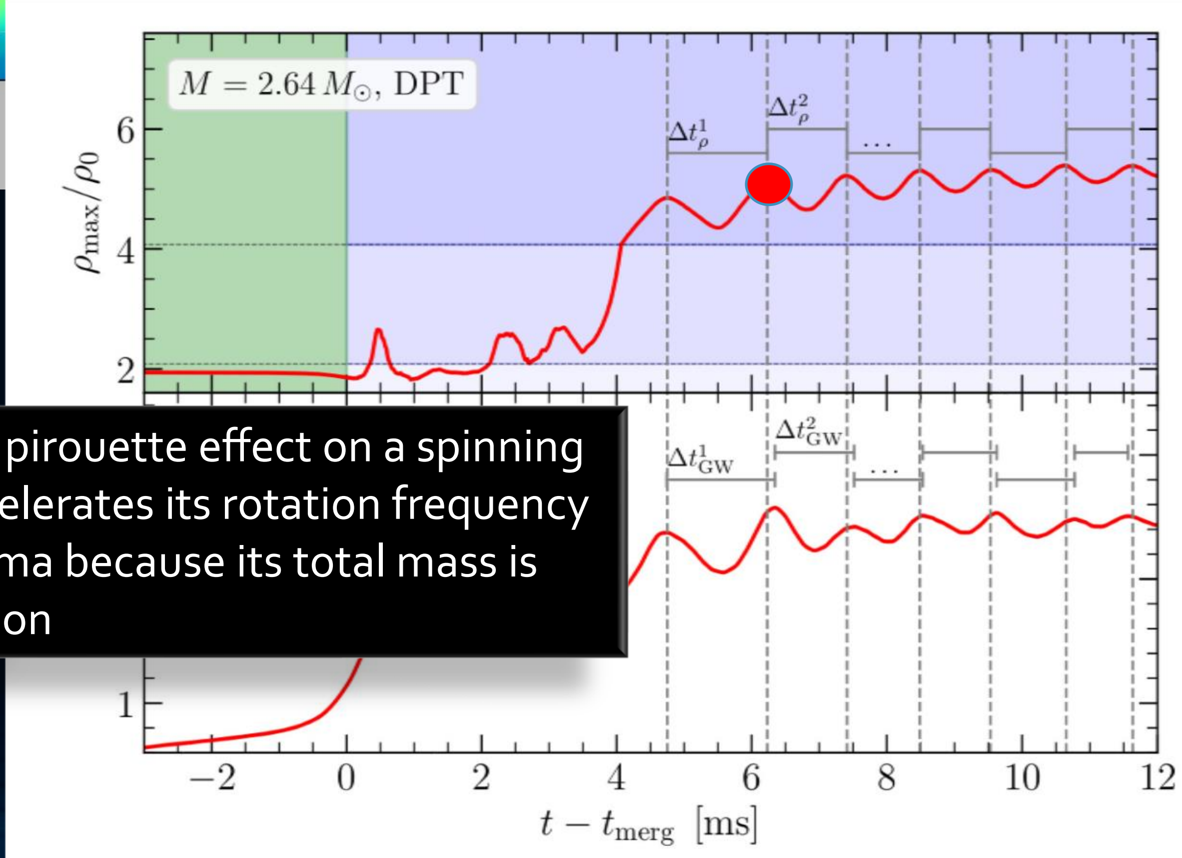

In addition, similar to the pirouette effect on a spinning figure skater, the star accelerates its rotation frequency close to the density maxima because its total mass is closer to the axis of rotation

These figures report the HMHS properties at t = 13.15ms and shows that in addition to the two temperature hot-spots, a new high temperature shell surrounding a cold core appears within the mixed phase region of the remnant . For subsequent post-merger times, the two temperature hot-spots will be smeared out to become a ring like structure on the equatorial plane

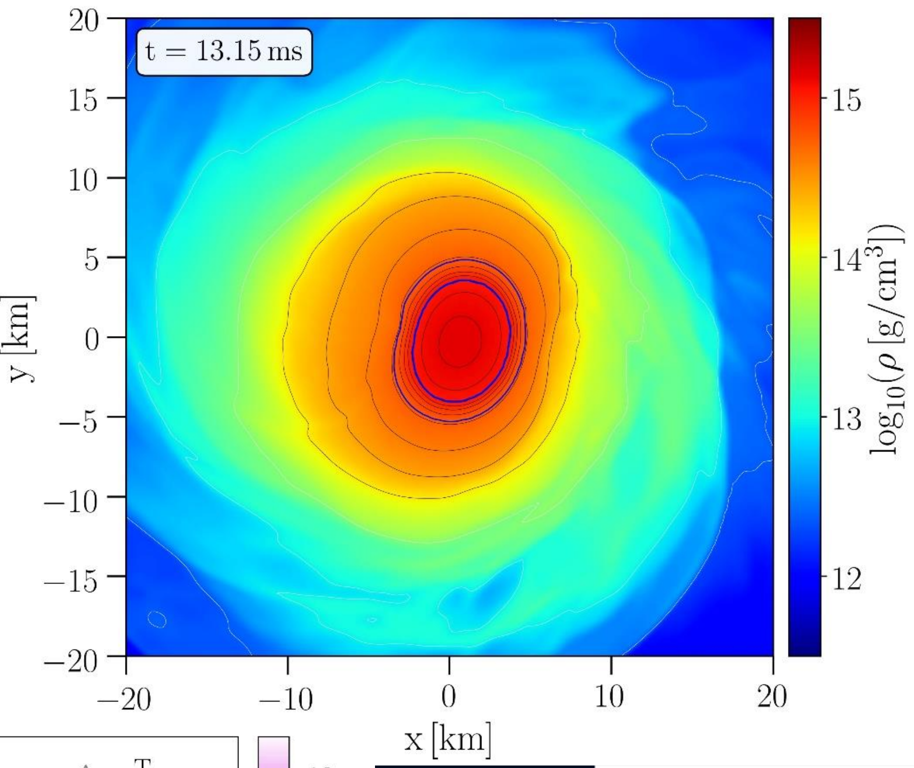

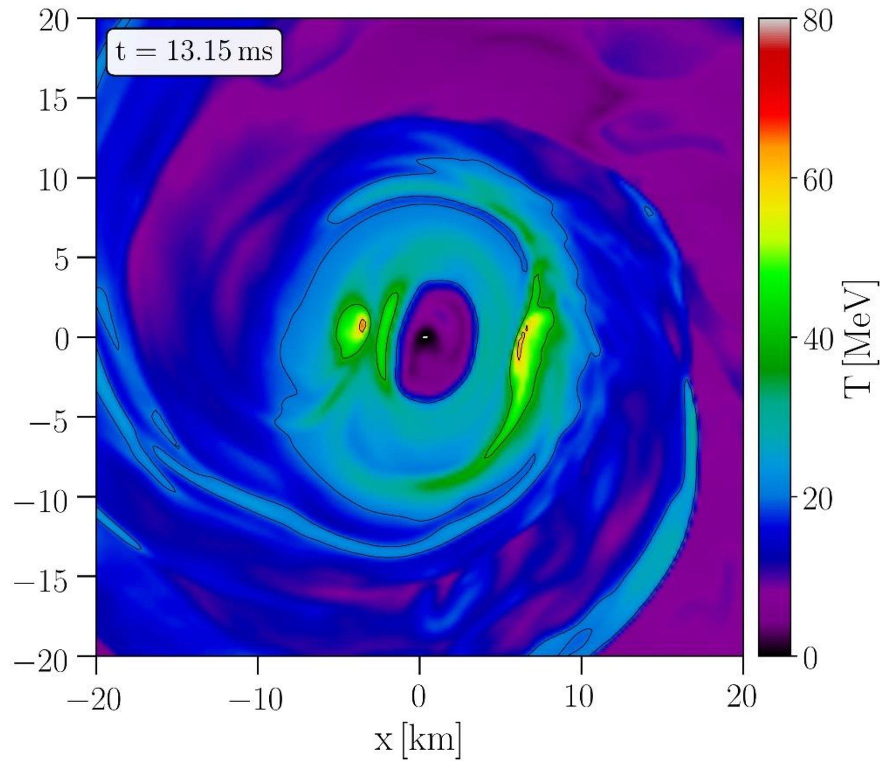

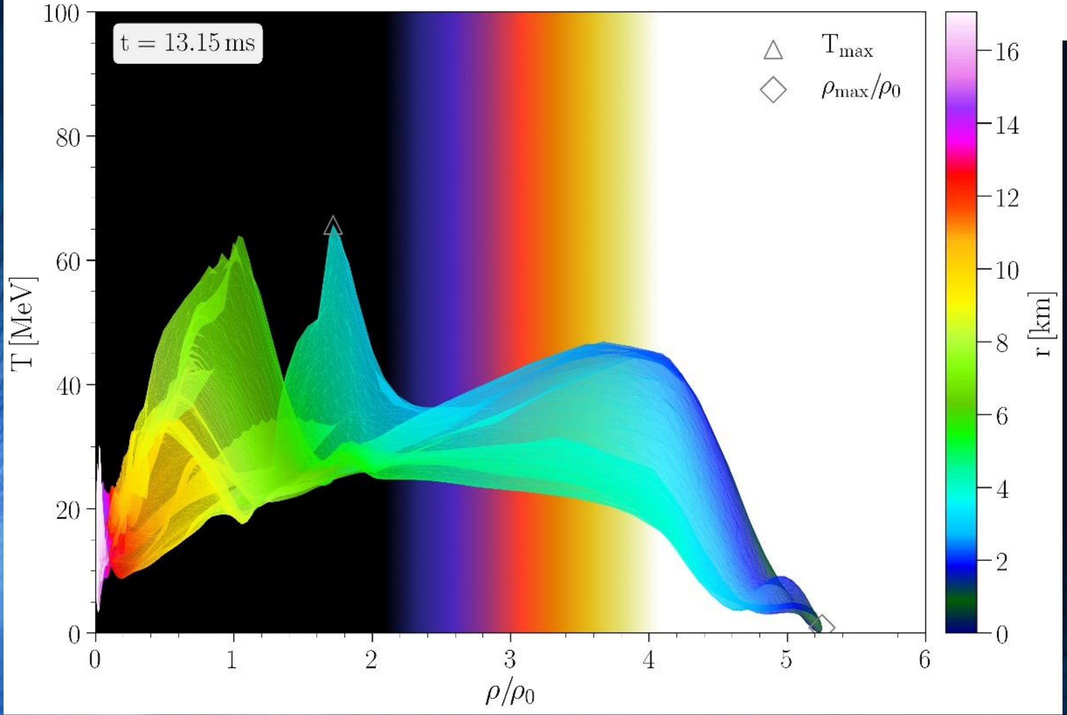

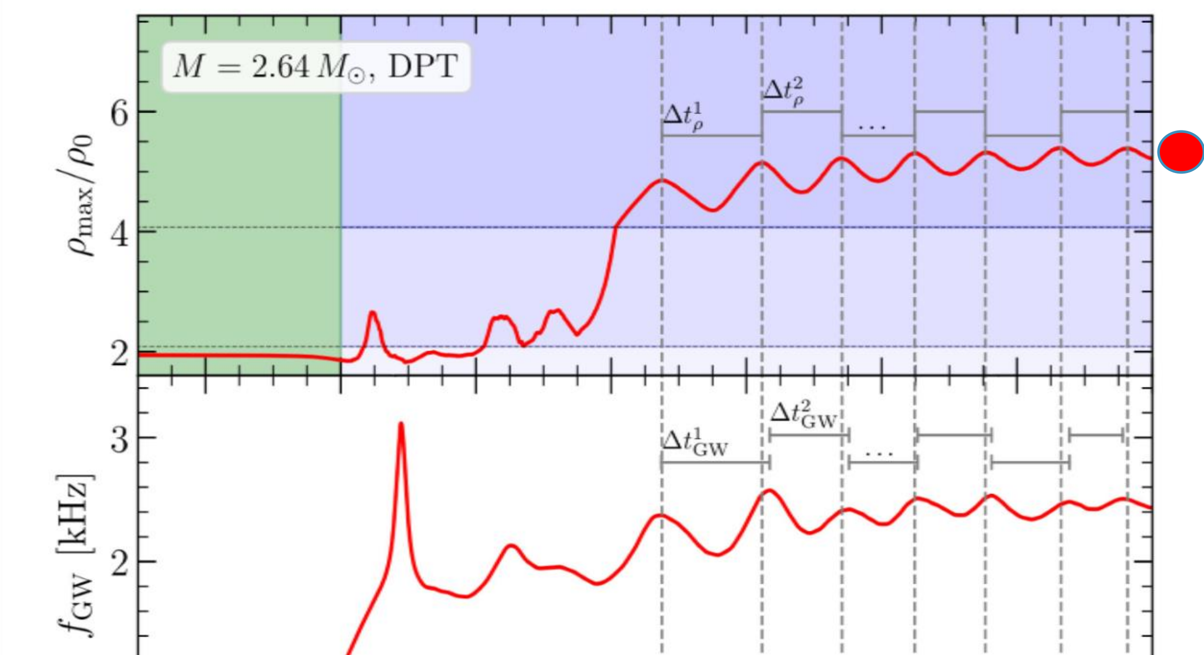

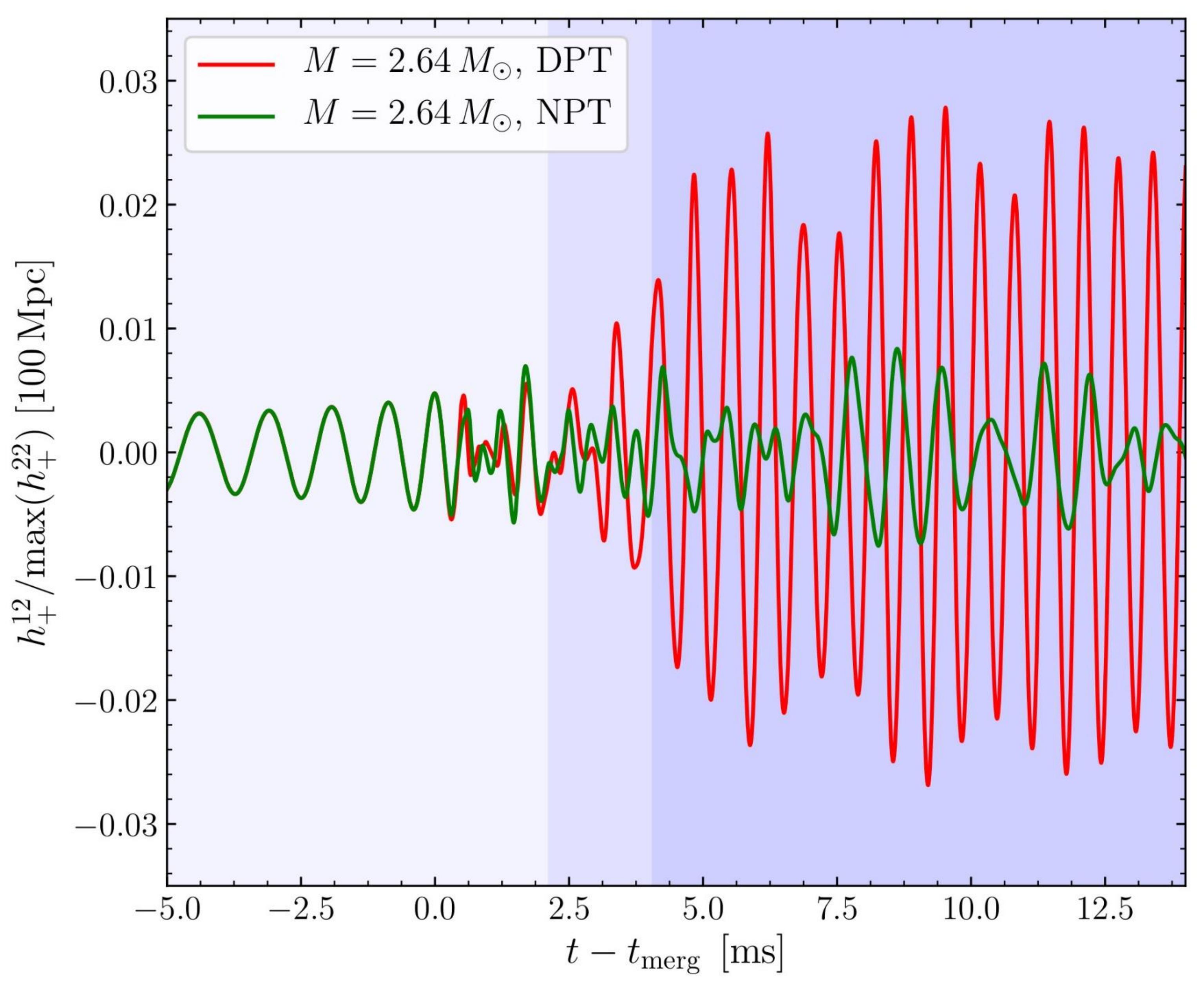

Due to the large m=1 mode of the emitted gravitational wave in the DPT case, a qualitative difference to the NPT scenario might be observable in future by focusing on the h12-gravitational wave mode during the post-merger evolution.

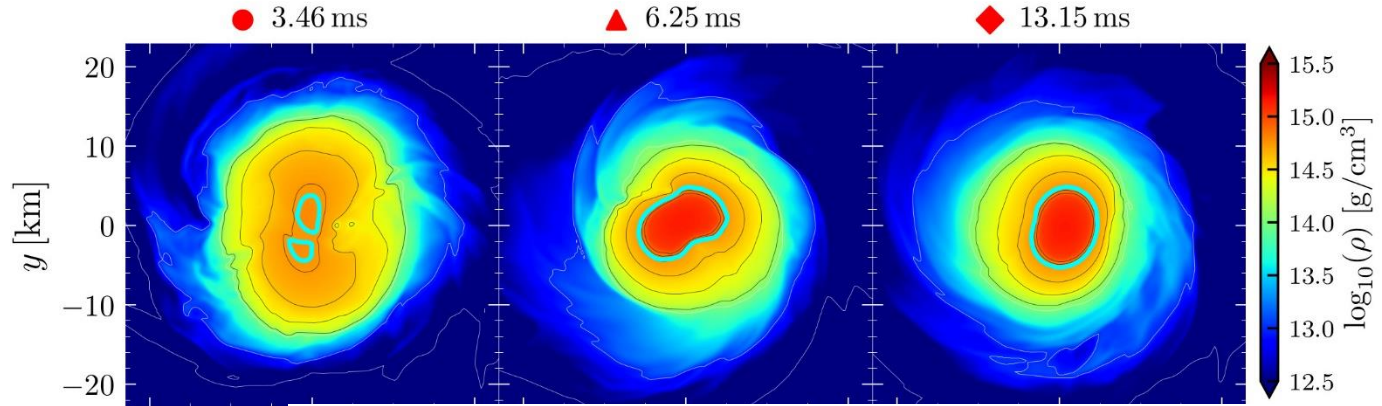

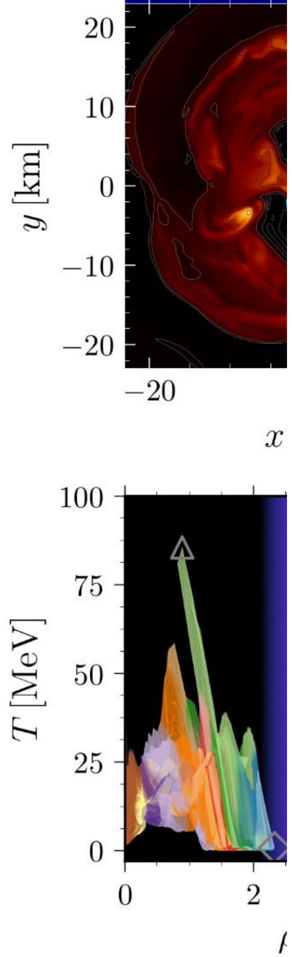

Article submitted (under review)

EPJ Special Topics on "Nuclear Astrophysics in Our Time: Supernovae, Neutron Stars and Binary Neutron Star Mergers"

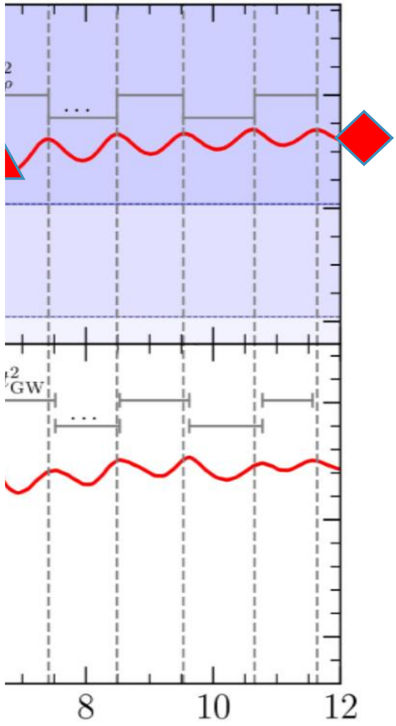

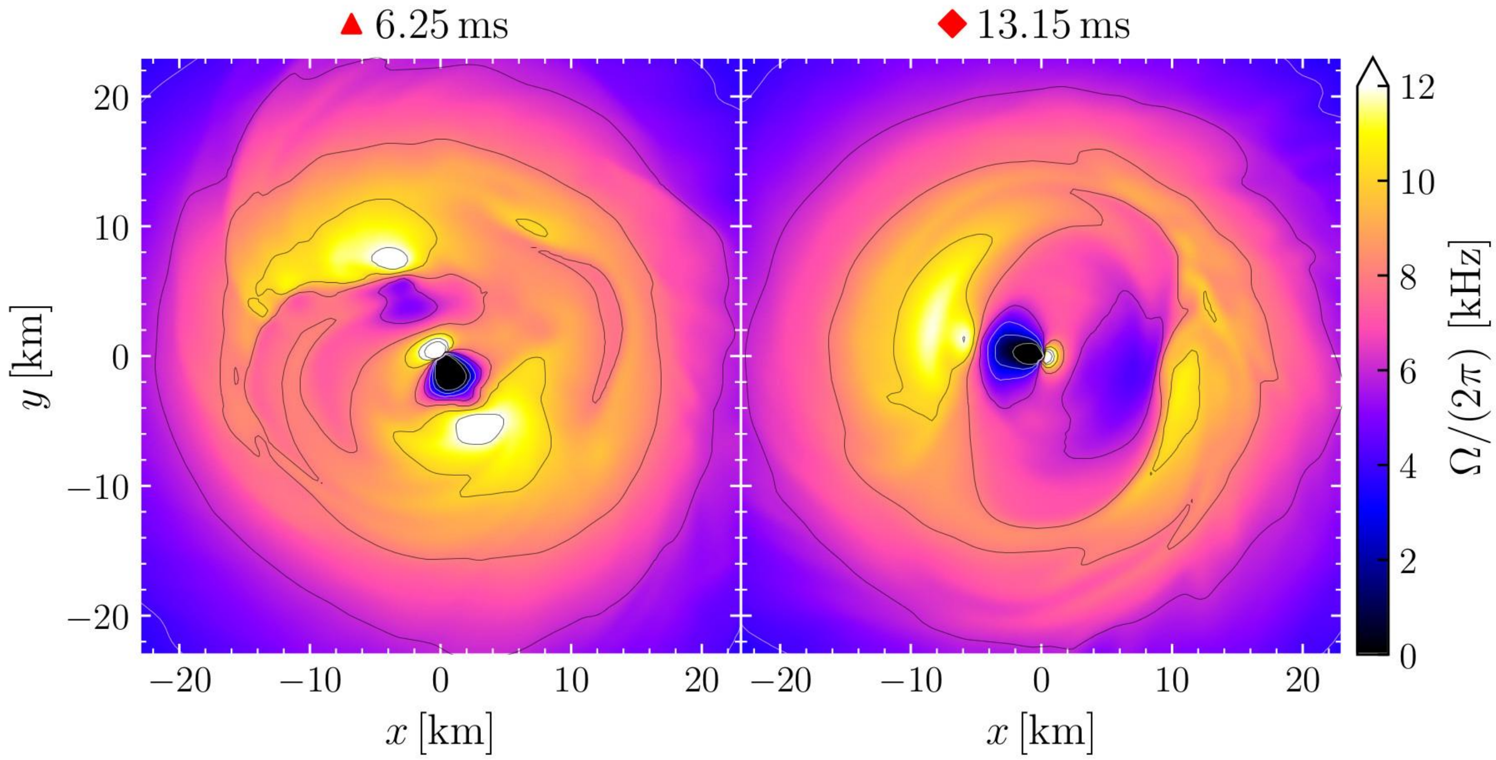

Fig. 4. Angular velocity for two representative times. Contours are drawn for $\Omega \in [0, 2, 4]$ kHz (white) and $\Omega \in [6, 8, 10, 12, 14]$ kHz (black).

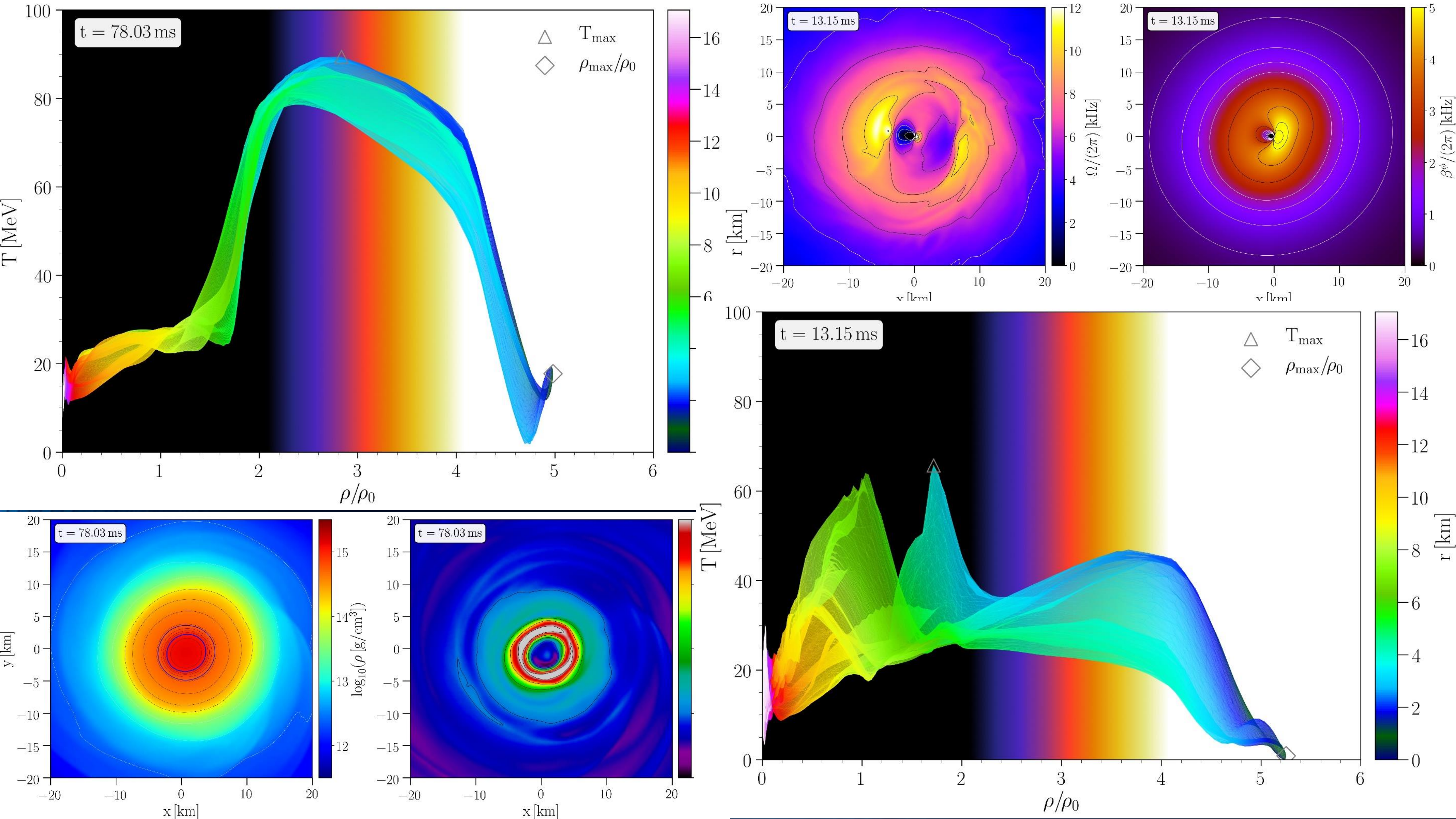

t = 78.03 ms
T_{max}
ρ_{max}/ρ_0
T [MeV]
ρ/ρ_0
t = 13.15 ms
$\Omega/(2\pi)$ [kHz]
$\beta^\phi/(2\pi)$ [kHz]
r [km]
x [km]
y [km]
$\log_{10}(\rho\,[\mathrm{g/cm^3}])$
T [MeV]
t = 13.15 ms
T_{max}
ρ_{max}/ρ_0
r [km]

How to detect the hadron-quark phase transition with gravitational waves

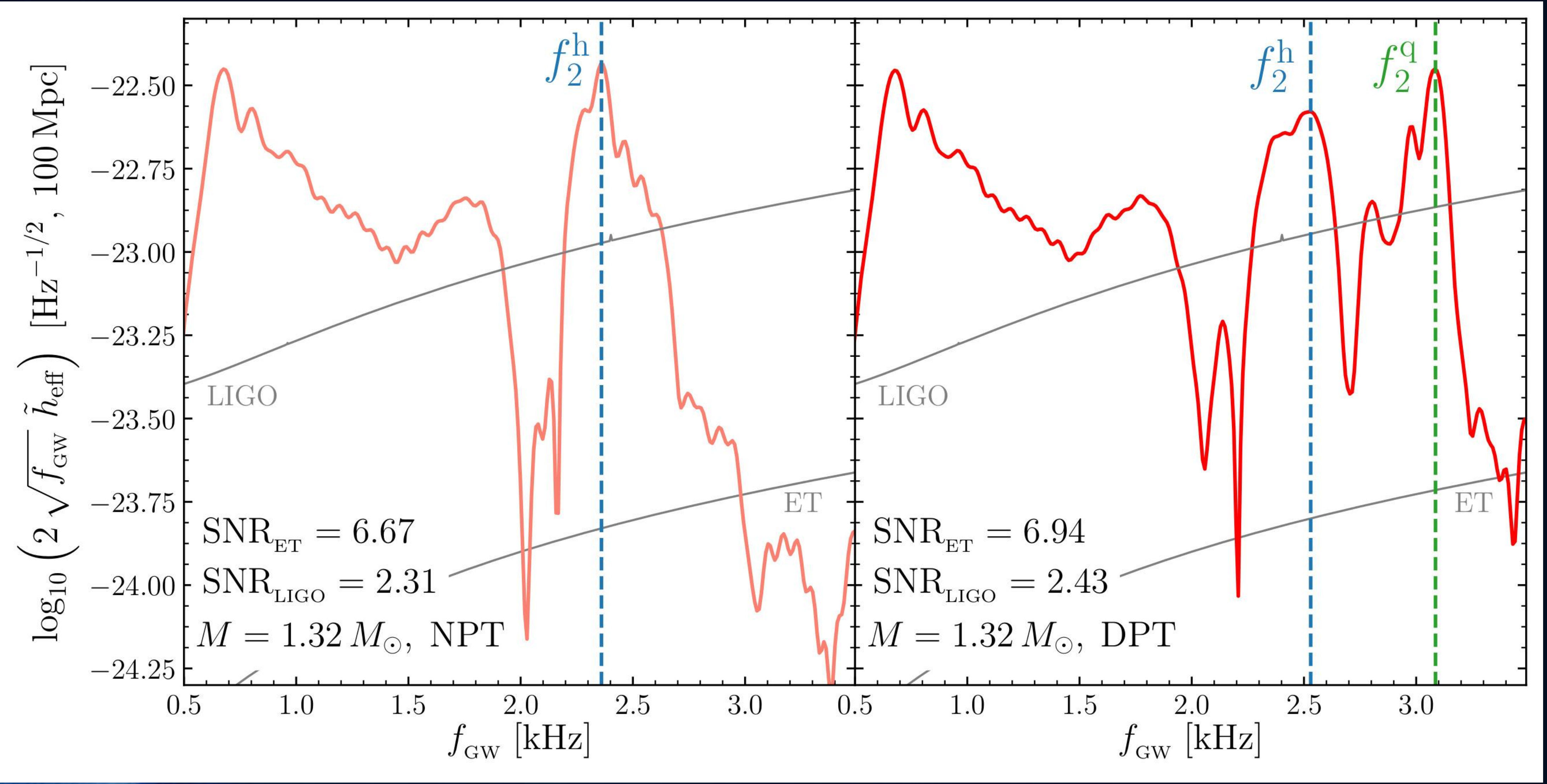

Total gravitational wave spectrum (left NPT, right DPT), PRL 124, 171103 (2020)

Postmerger gravitational-wave signatures of phase transitions in binary compact star mergers

- Introduction
- Numerical general relativity of compact star mergers
- The equation of state of compact star matter and the hadron-quark phase transition
- The different phases of a binary compact star merger event
- **Gravitational-wave signatures of the hadron-quark phase transition in binary compact star mergers**
  - The inspiral and merger phase (premerger signals)
  - Hypermassive hybrid stars (HMHS) within the prompt phase transition scenario (PPT)
  - HMHS within the delayed phase transition scenario (DPT)
  - **HMHS within the phase transition triggered collapse scenario (PTTC)**
- Summary and Outlook

HMHS within the PTTC scenario using a T-dependent EOS

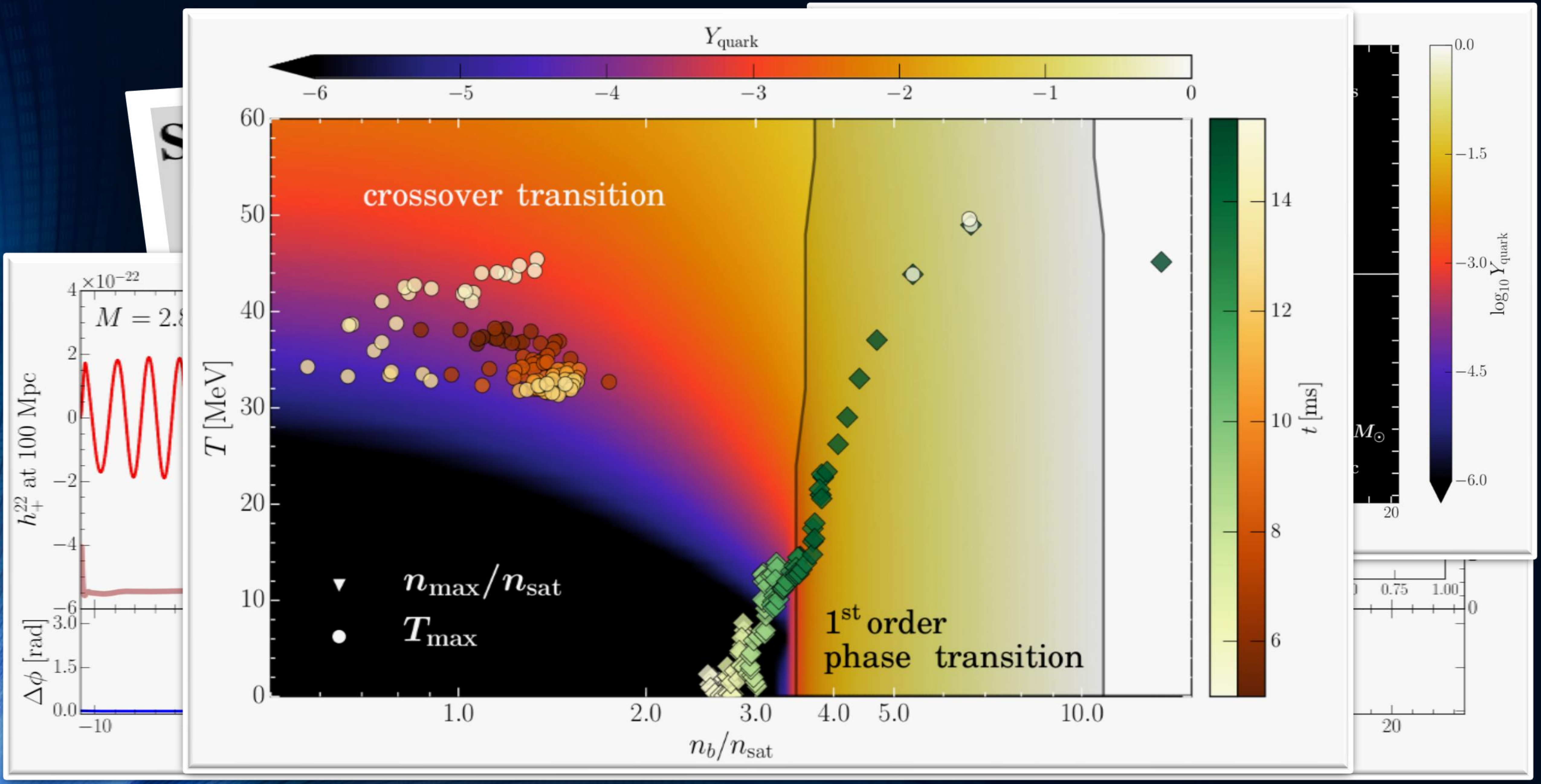

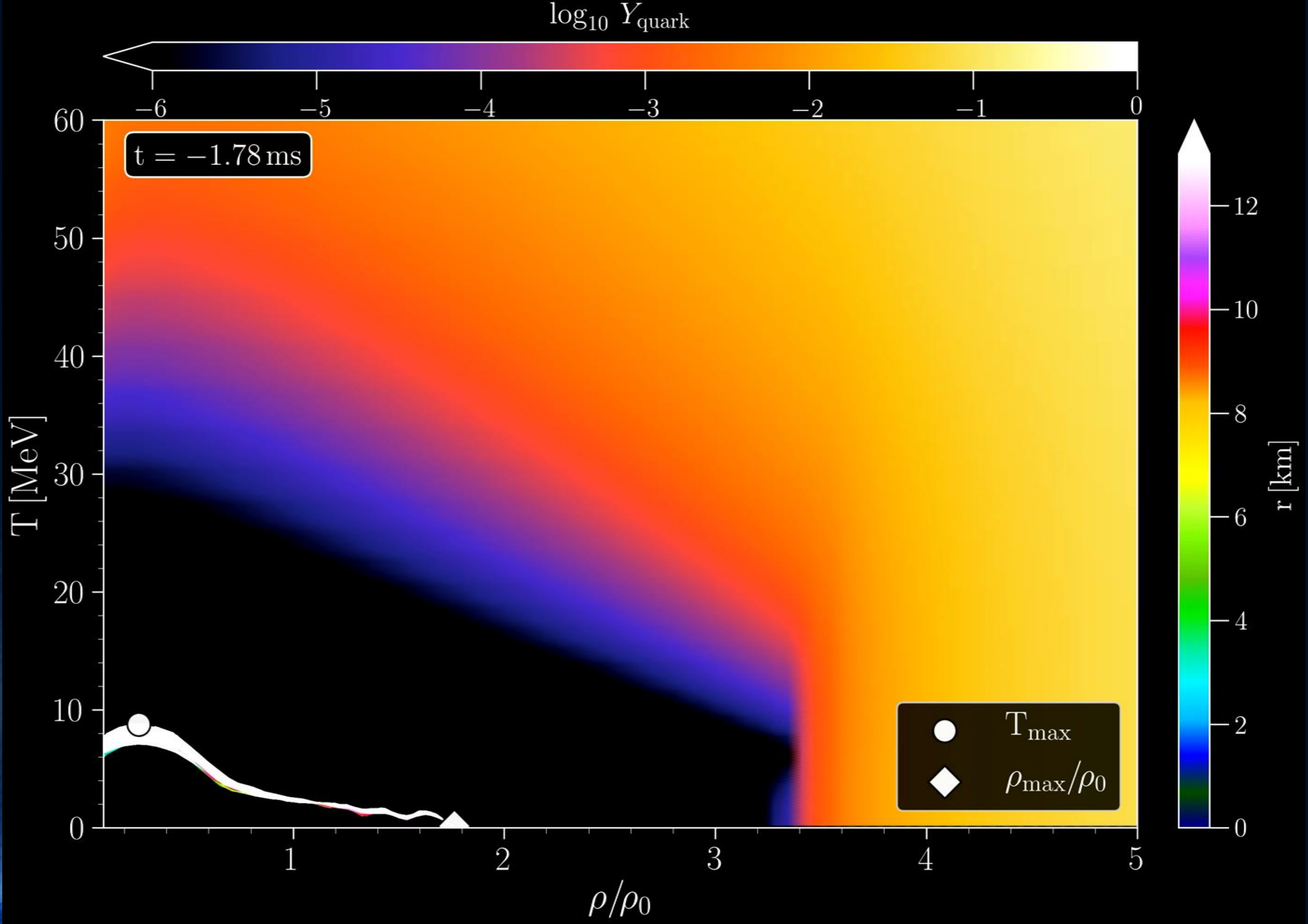

$\log_{10} Y_{\rm quark}$
−6
−5
−4
−3
−2
−1
0
$t = -1.78\,\mathrm{ms}$
T [MeV]
60
50
40
30
20
10
0
ρ/ρ_0
1
2
3
4
5
$\mathrm{T_{max}}$
$\rho_{\rm max}/\rho_0$
r [km]
12
10
8
6
4
2
0

Merger Phase

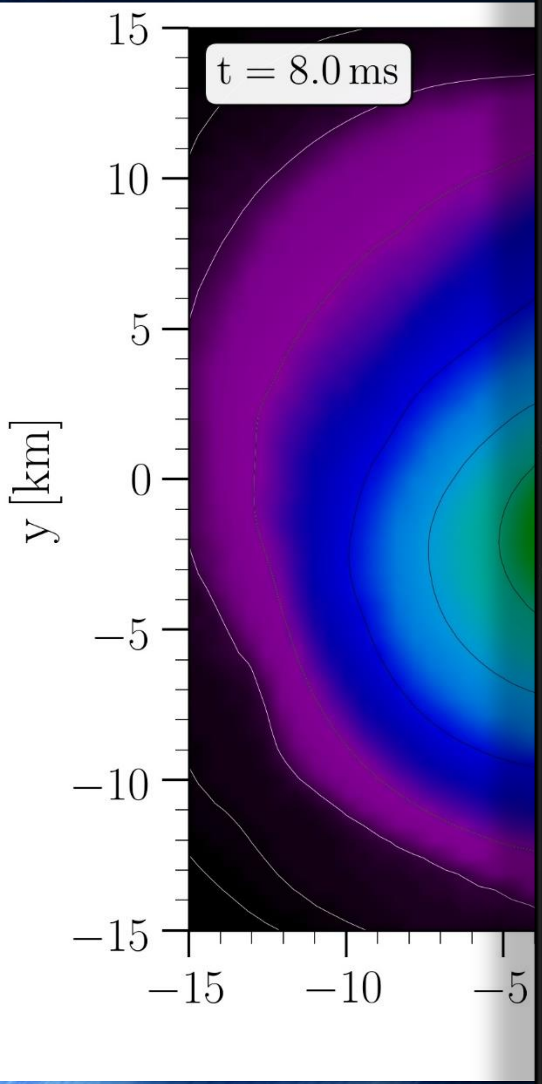

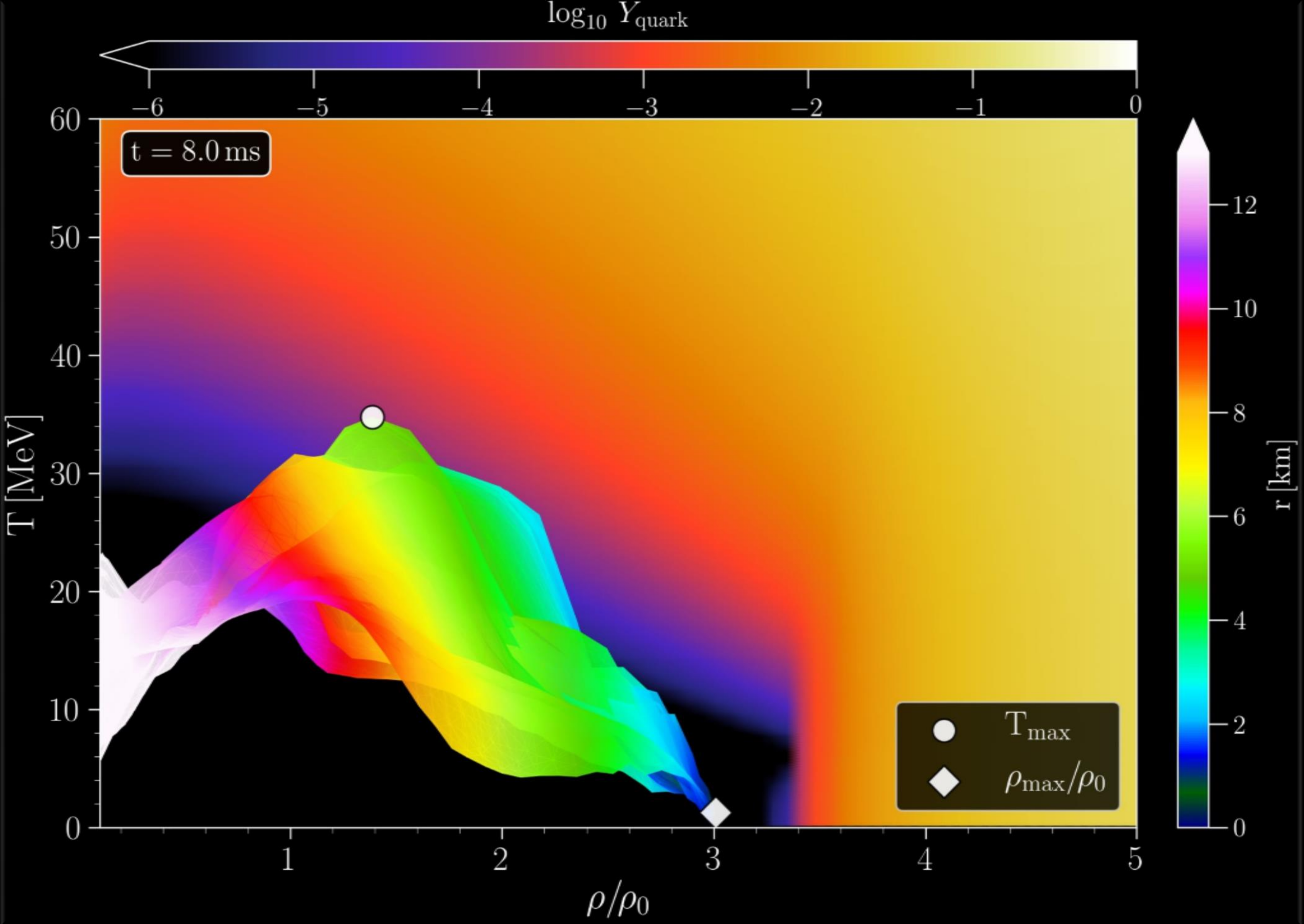

Rest mass density

Merger Phase

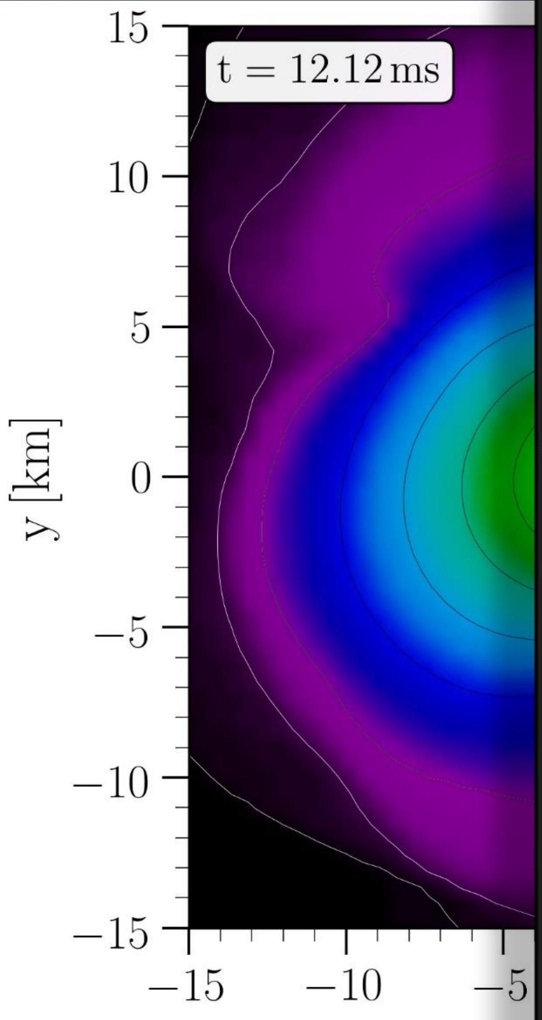

Rest mass density

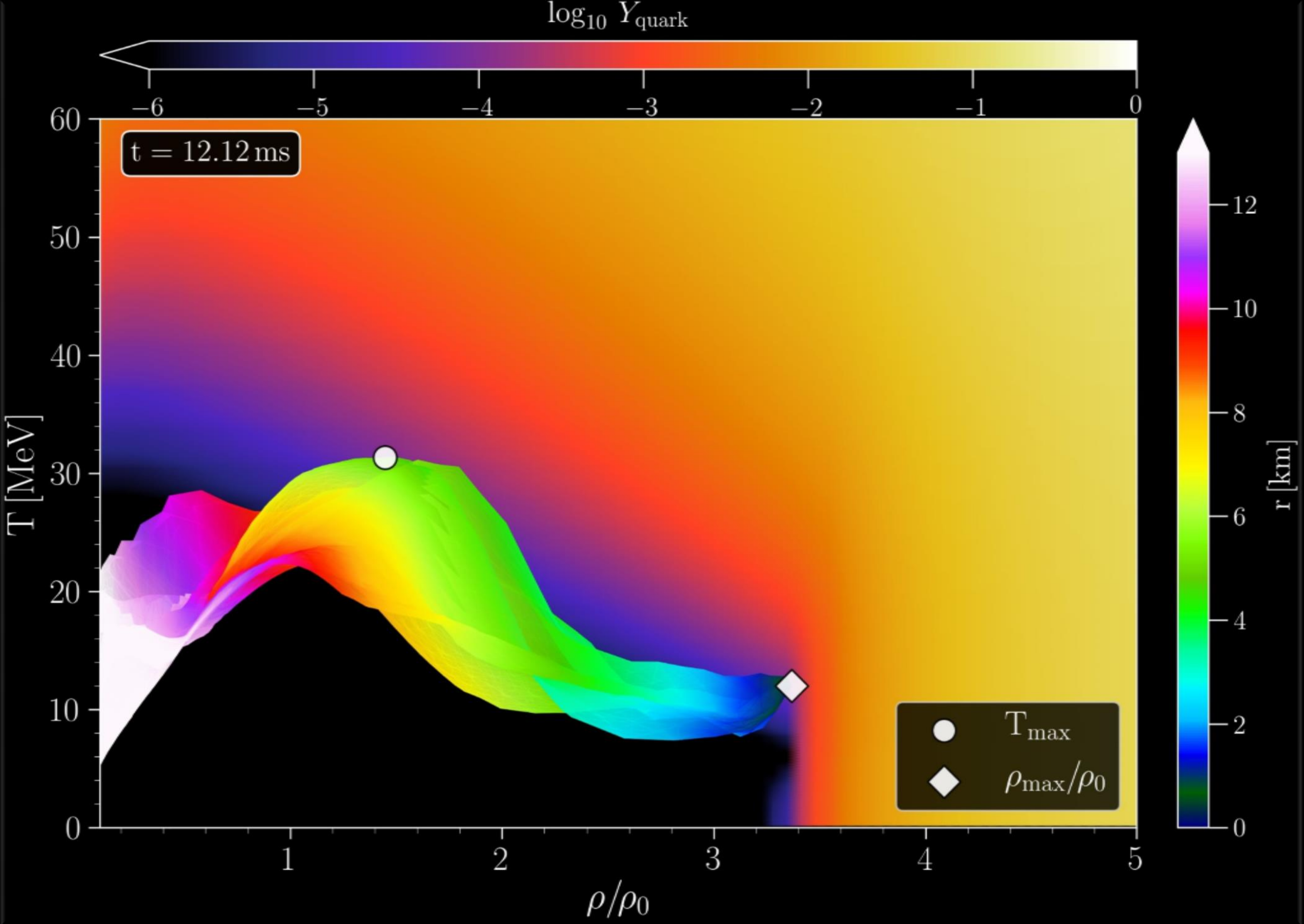

Merger Phase

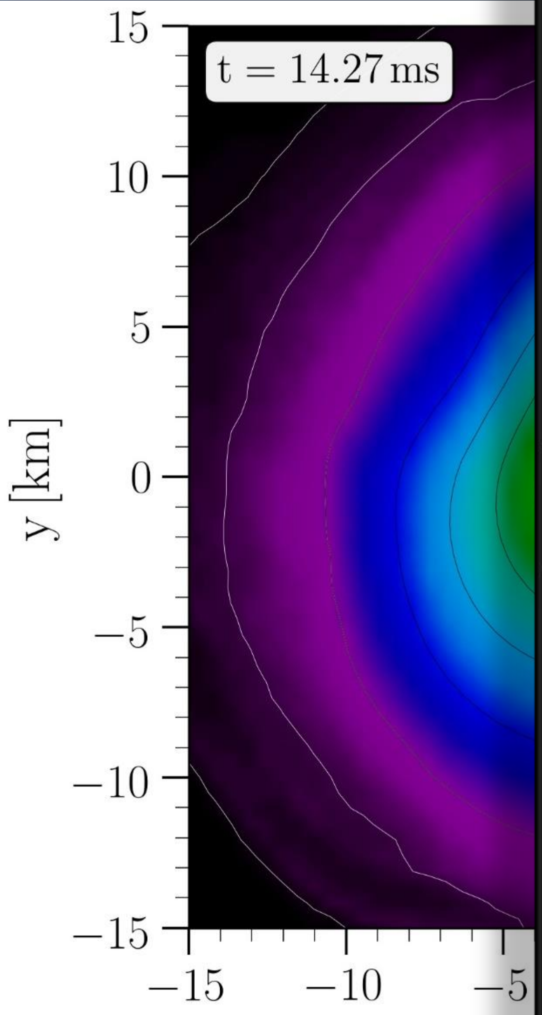

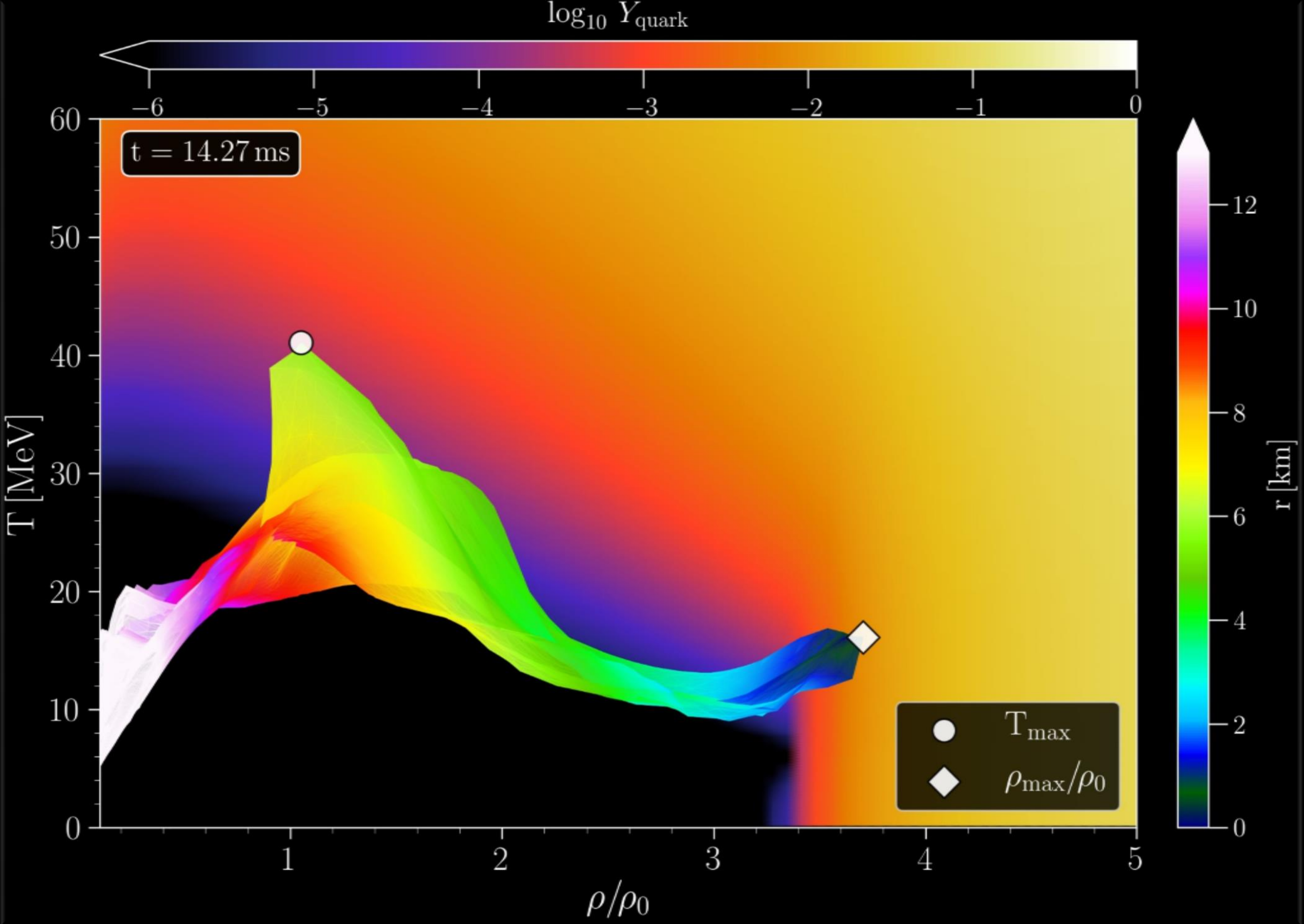

Rest mass density

Merger Phase

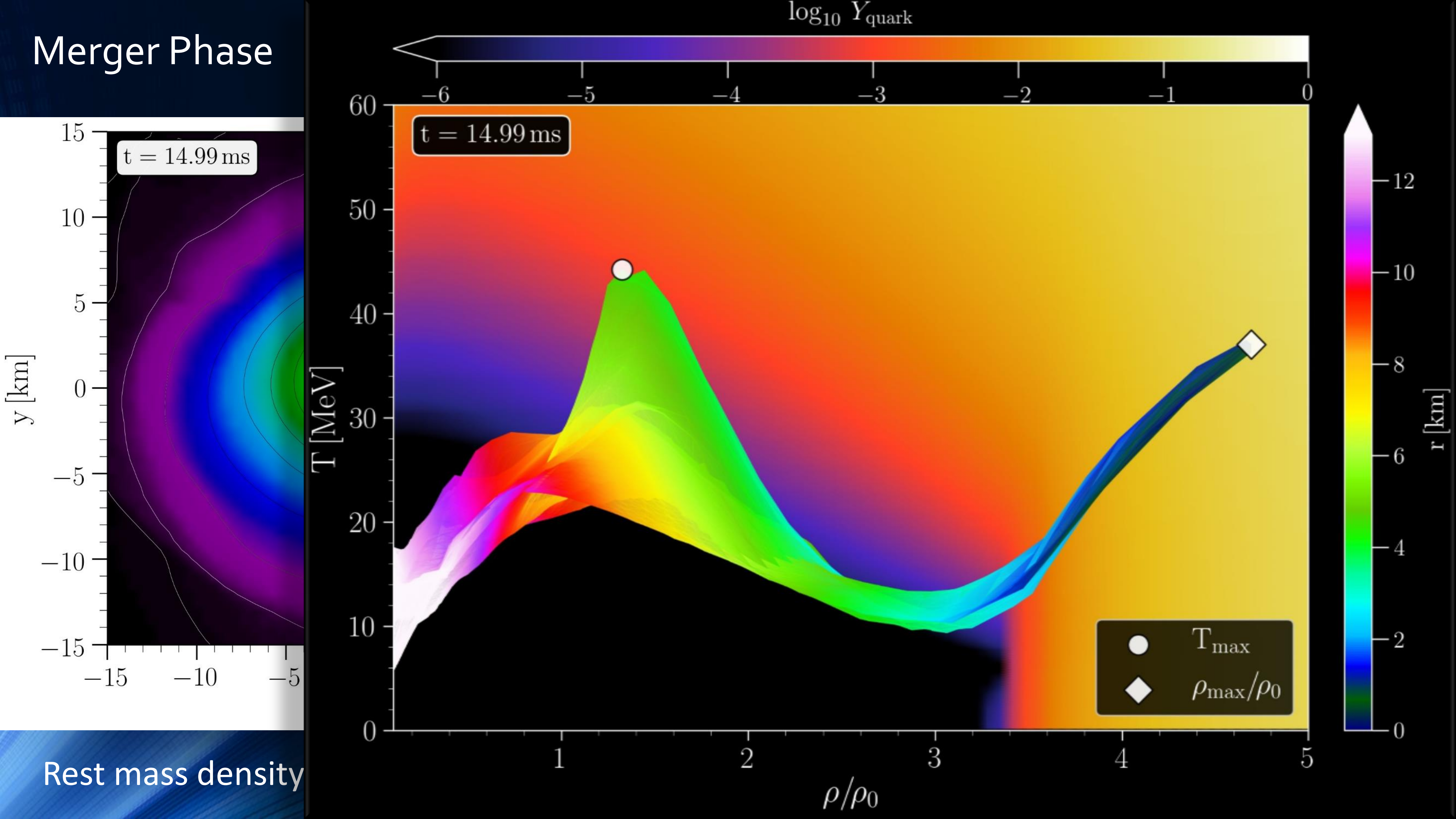

Rest mass density

Merger Phase

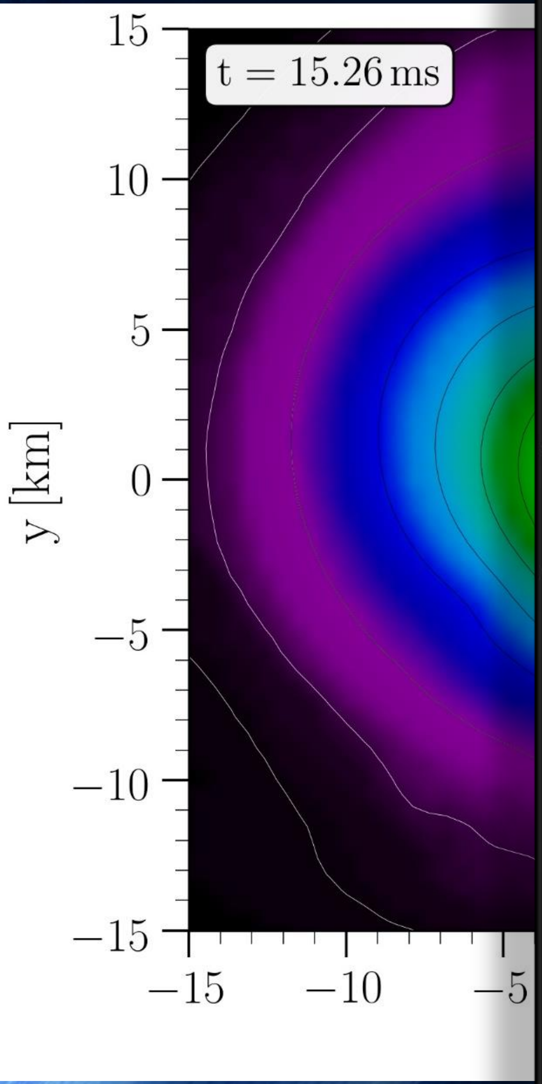

Rest mass density

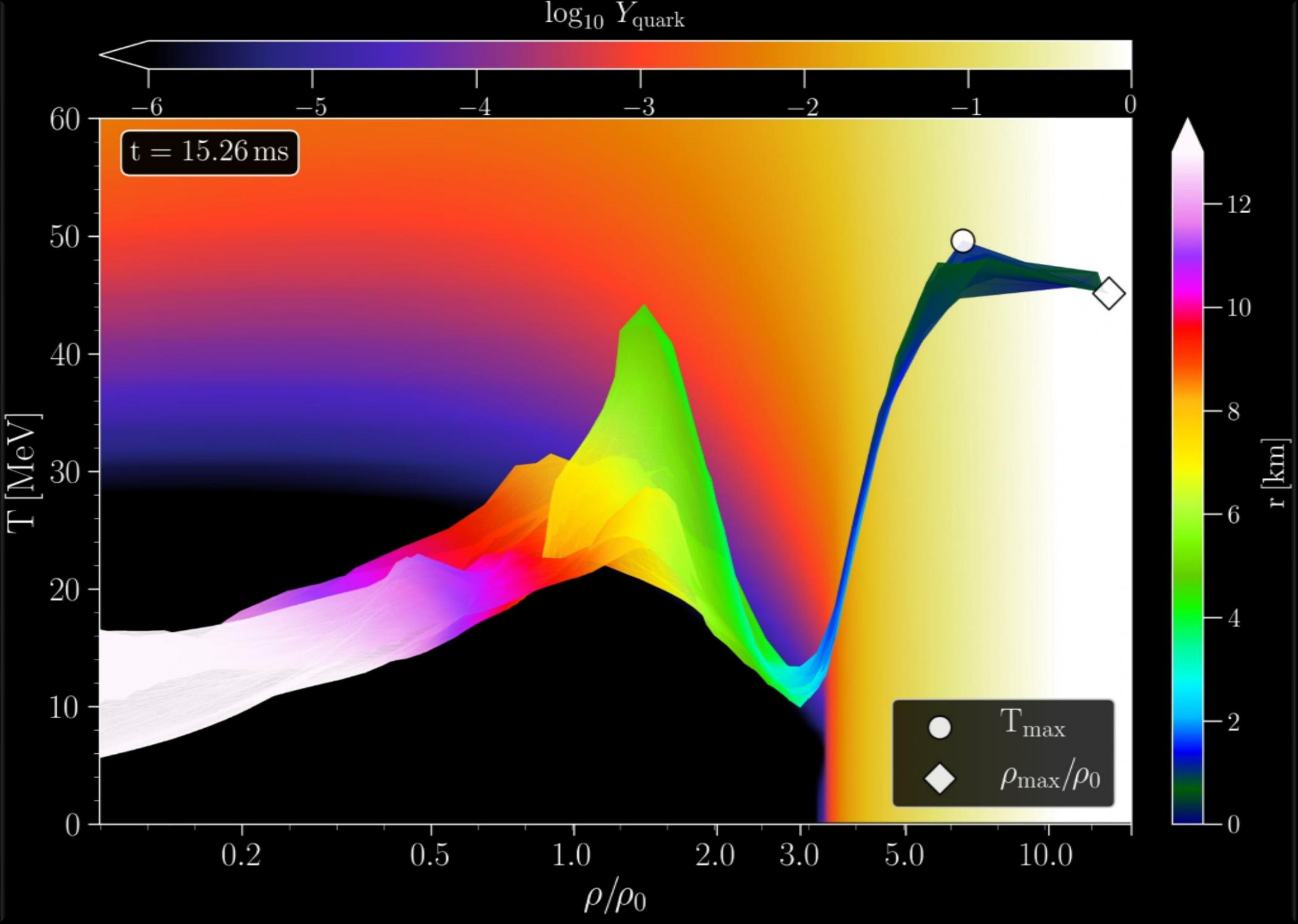

The Pelican Plot

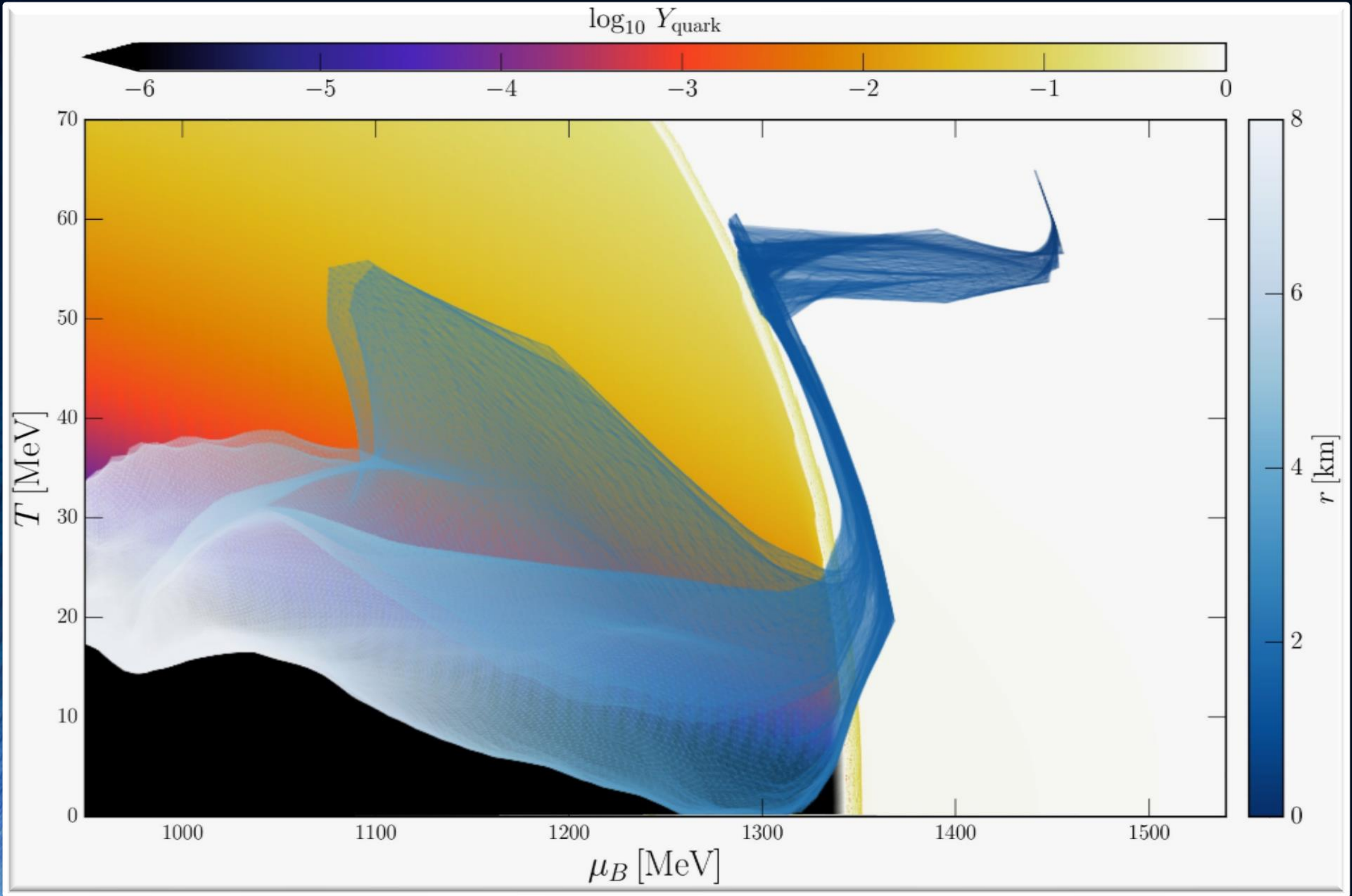

The shadowy blue image resembles the shape of a strange bird, e.g. a pelican, wherein the hot head of a pelican contains a high amount of strange quark matter, its thin neck follows the QCD phase boundary, while its hot wings (local temperature maxima) contain mostly hadronic matter at much lower densities.
The maximum tempearture and density points correspond to the head of the pelican where pure strange quark is present. Due to the stiffening of the EOS in the pure quark phase, the temperature stops rising and the high pressure in the central region pushes against the hudge gravitational force.

E.Most, J. Papenfort, V.Dexheimer, M.Hanauske, H.Stöcker and L.Rezzolla;
„On the deconfinement phase transition in neutron-star mergers„; arXiv:*1910.13893*

Postmerger gravitational-wave signatures of phase transitions in binary compact star mergers

- Introduction
- Numerical general relativity of compact star mergers
- The equation of state of compact star matter and the hadron-quark phase transition
- The different phases of a binary compact star merger event
- Gravitational-wave signatures of the hadron-quark phase transition in binary compact star mergers
  - The inspiral and merger phase (premerger signals)
  - Hypermassive hybrid stars (HMHS) within the prompt phase transition scenario (PPT)
  - HMHS within the delayed phase transition scenario (DPT)
  - HMHS within the phase transition triggered collapse scenario (PTTC)
- **Summary and Outlook**

Literature

Hanauske, Matthias, and Walter Greiner.
"Neutron star properties in a QCD-motivated model." *General Relativity and Gravitation* 33.5 (2001): 739-755.

Hanauske, Matthias. "How to detect the Quark-Gluon Plasma with Telescopes." *GSI Annual Report* (2003): 96.

Hanauske, M., Takami, K., Bovard, L., Rezzolla, L., Font, J. A., Galeazzi, F., & Stöcker, H. (2017). Rotational properties of hypermassive neutron stars from binary mergers. Physical Review D, 96(4), 043004

M. Hanauske, et.al., Connecting Relativistic Heavy Ion Collisions and Neutron Star Mergers by the Equation of State of Dense Hadron-and Quark Matter as signalled by Gravitational Waves, Journal of Physics: Conference Series, 878(1), p.012031 (2017)

Hanauske, Matthias, et al. "Gravitational waves from binary compact star mergers in the context of strange matter." *EPJ Web of Conferences*. Vol. 171. EDP Sciences, 2018.

Mark G. Alford, Luke Bovard, Matthias Hanauske, Luciano Rezzolla, and Kai Schwenzer (2018), Viscous Dissipation and Heat Conduction in Binary Neutron-Star Mergers. Phys. Rev. Lett. 120, 041101

Hanauske, Matthias, and Luke Bovard. "Neutron star mergers in the context of the hadron–quark phase transition." *Journal of Astrophysics and Astronomy* 39.4 (2018): 45.

Hanauske, Matthias, et al. "Neutron Star Mergers: Probing the EoS of Hot, Dense Matter by Gravitational Waves." *Particles* 2.1 (2019): 44-56.

Online-Lecture: General Theory of Relativity on the Computer

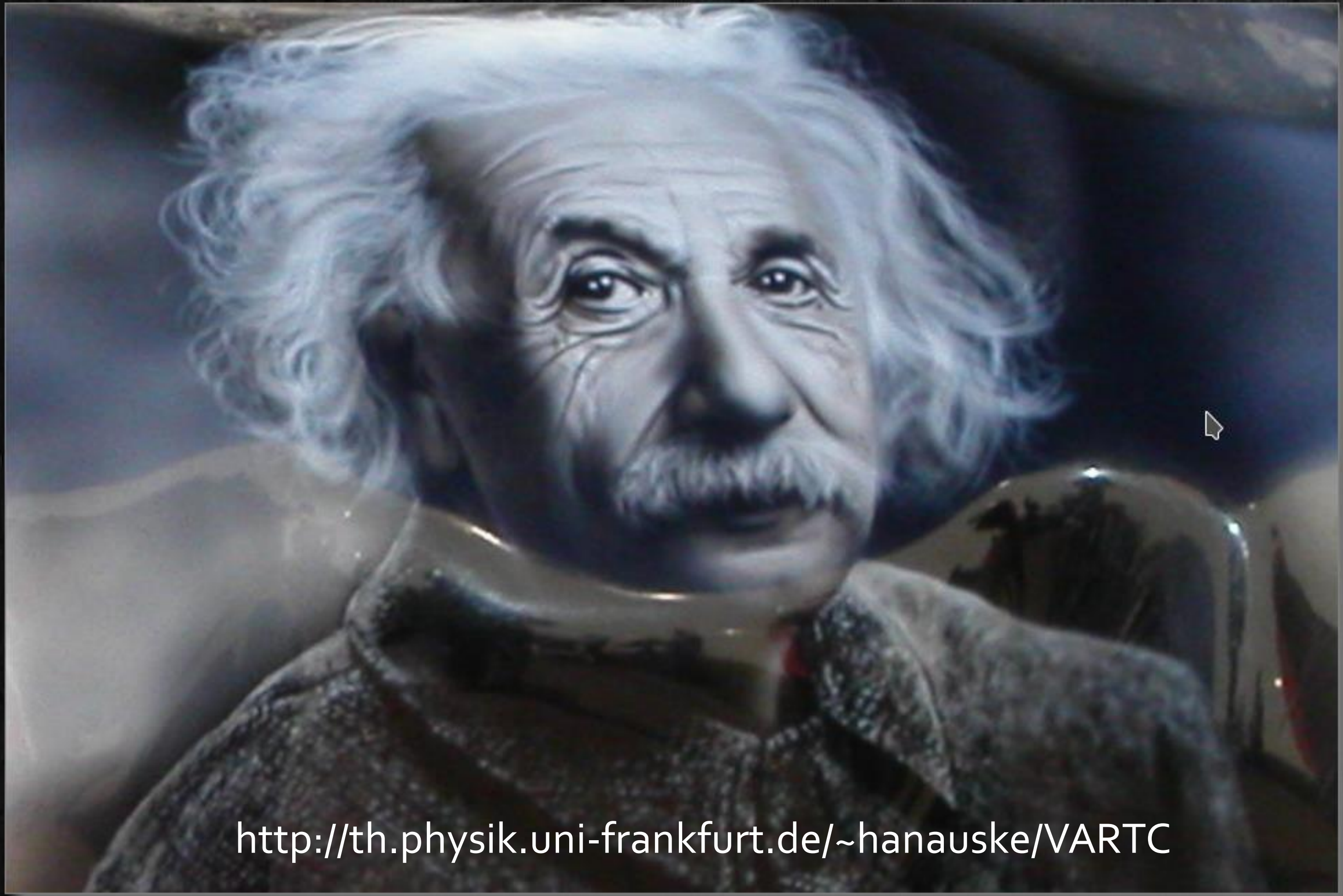

Online Vorlesungen und Zusatzmaterialien

Augrund der Corona Krise findet die Vorlesung und die freiwilligen Übungstermine in diesem Semester nur Online statt. Auf die dafür eingerichtete Internetseite gelangen Sie, wenn Sie die nebenstehende Abbildung anklicken.

Allgemeine Relativitätstheorie mit dem Computer
(General Theory of Relativity on the Computer)
Vorlesung SS 2020, Fr. 15-17.00 Uhr

Augrund der Corona Krise findet die Vorlesung und die freiwilligen Übungstermine in diesem Semester nur Online statt (näheres siehe HIER.

In dieser Vorlesung werden die mathematisch anspruchsvollen Gleichungen der Allgemeinen Relativitätstheorie (ART) in diversen Programmierumgebungen analysiert. Im ersten Teil des Kurses erlernen die Studierenden die Verwendung von Computeralgebra-Systemen (Maple und Mathematica). Die oft komplizierten und zeitaufwendigen Berechnungen der tensoriellen Gleichungen der ART können mit Hilfe dieser Programme erleichtert werden. Diverse Anwendungen der Einstein- und Geodätengleichung werden in Maple implementiert, quasi analytische Berechnungen durchgeführt und entsprechende Lösungen berechnet und visualisiert. Der zweite Teil

Physik der sozio-ökonomische...

Next Semester Lecture: Physics of Socio-Economic Systems with the Computer

Physik der sozio-ökonomischer Systeme mit dem Computer *von* Dr.phil.nat.Dr.rer.pol. Matthias Hanauske

Home Research Contact

Einführung **Teil I** **Teil II** **Teil III** ***E-Learning***

http://th.physik.uni-frankfurt.de/~hanauske/VPSOC/

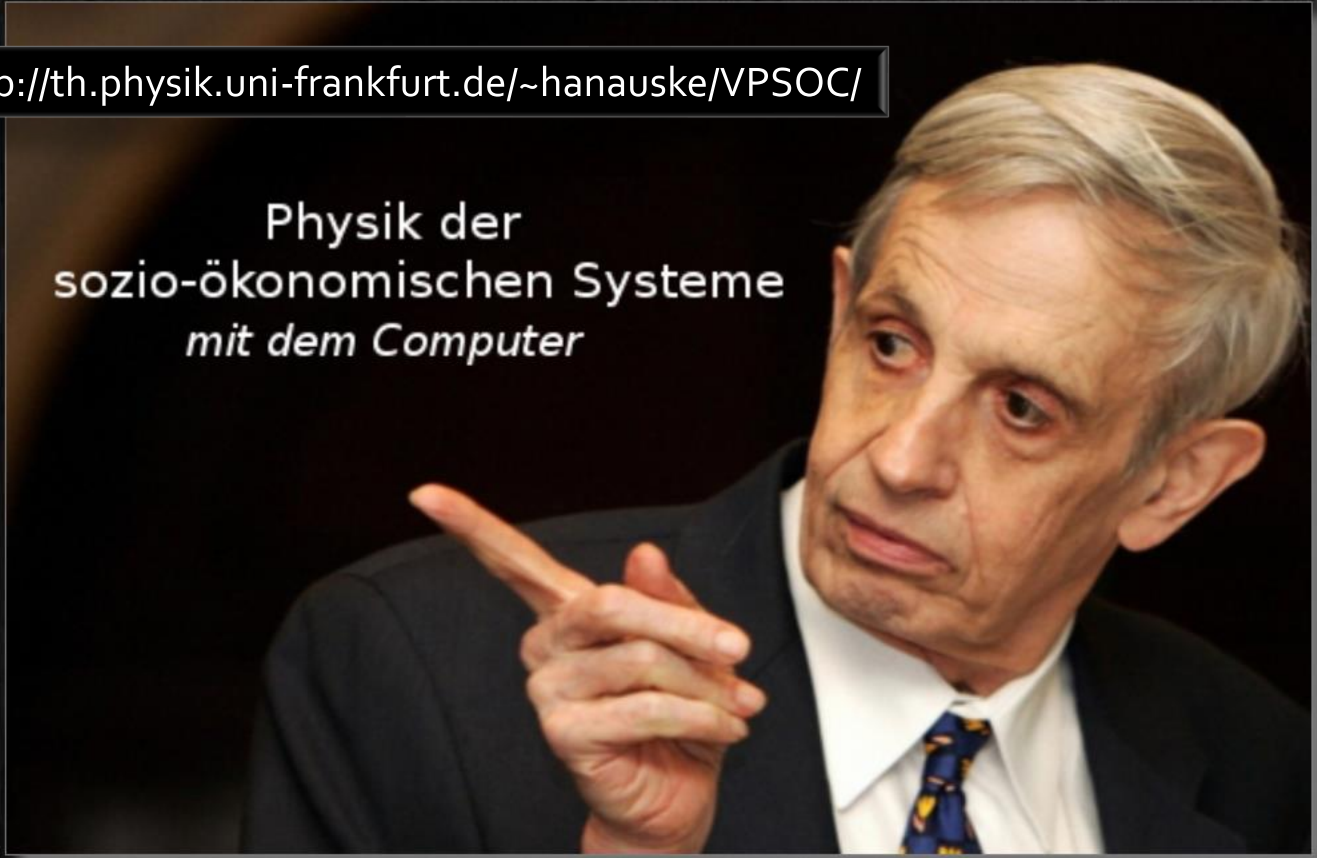

Physik sozio-ökonomischer Systeme mit dem Computer (Physics of Socio-Economic Systems with the Computer) Vorlesung WS 2017/2018, Fr. 15-17.00 Uhr, PC-Pool 01.120

Zusätzlich zur Vorlesung werden ab dem 27.10.2017 freiwillige Übungstermine eingerichtet, die jeweils freitags, eine Stunde vor der Vorlesung im PC-Pool 01.120 stattfinden (Fr. 14-15.00 Uhr).

Diese Vorlesung gibt eine Einführung in das interdisziplinäre Forschungsfeld der *Physik sozio-ökonomischer Systeme*. In sozio-ökonomischen Systemen, wie z.B. bei Finanzmärkten, sozialen Netzwerken, Verkehrssystemen oder wissenschaftliche Kooperationsnetzwerken, sind die dem System zugrunde liegenden Akteure ständigen Entscheidungssituationen ausgesetzt, wobei der Erfolg und die Auswirkung der individuell gewählten Strategie von den Entscheidungen der anderen beteiligten Akteuren abhängt. Die (evolutionäre) Spieltheorie und die Physik komplexer Netzwerke stellen die beiden Grundsäulen der theoretischen Beschreibung und mathematischen Formulierung solcher Systeme dar. Im ersten Teil des Kurses werden die grundlegenden Konzepte der Spieltheorie thematisiert und die Studierenden erlernen, unter Verwendung von Computeralgebra-Systemen (Maple und Mathematica) deren Anwendung auf diverse Spielklassen. Neben den endlichen Zweipersonen-Spielen und N-Personen-Spielen wird auch auf die evolutionäre Entwicklung ganzer Spieler-Populationen eingegangen

DEU 13:49 19.10.2017

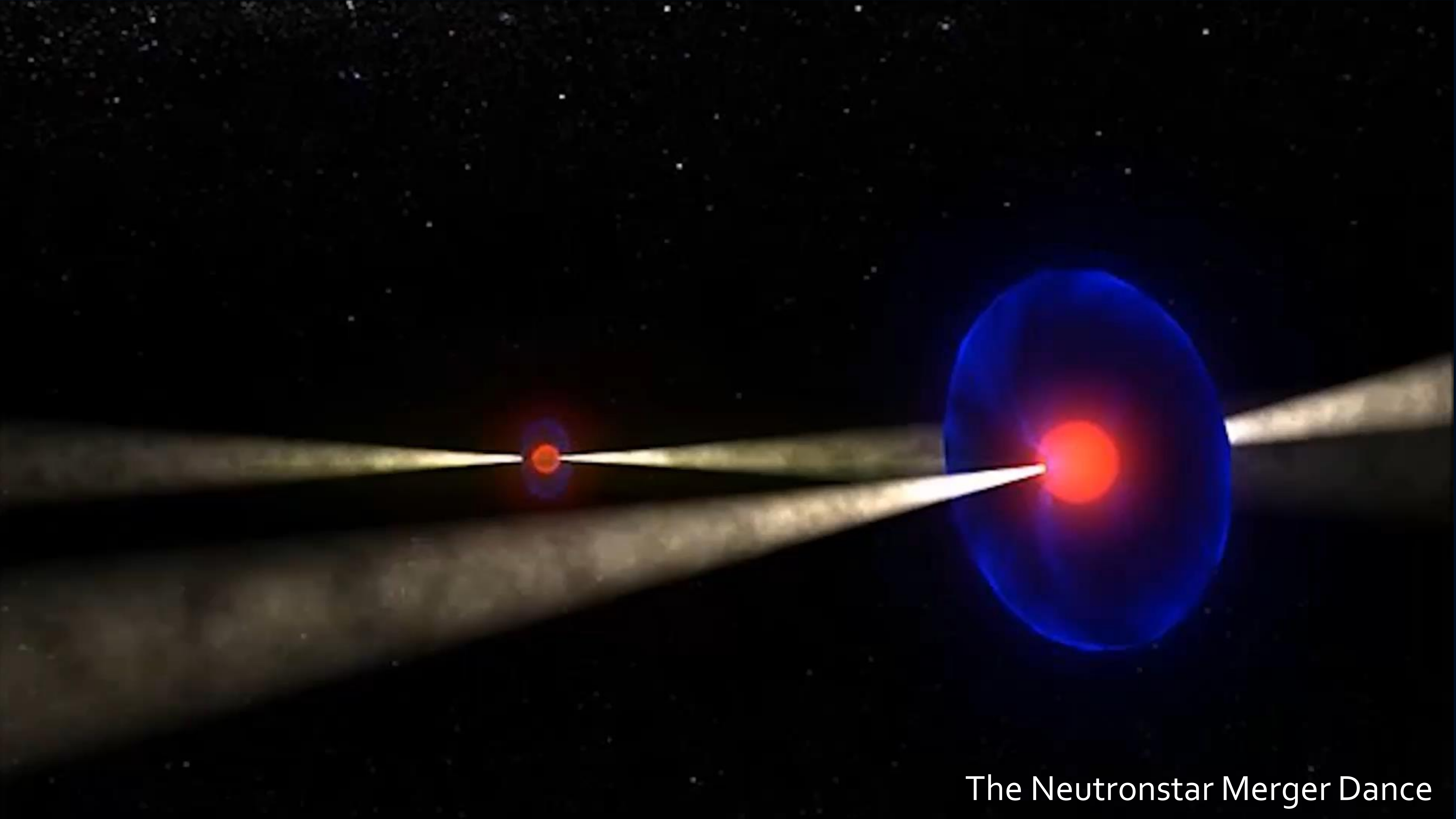

The Neutronstar Merger Dance

Credits to …

Kentaro Takami, Luke Bovard, Jose Font, Filippo Galeazzi, Jens Papenfort, Lukas Weih, Elias Most, Cosima Breu, Federico Guercilena, Natascha Wechselberger, Zekiye Simay Yilmaz, Christina Mitropoulos, Jan Steinheimer, Stefan Schramm, David Blaschke, Mark Alford, Kai Schwenzer, Antonios Nathanail, Roman Gold, Alejandro Cruz Osorio, Andreas Zacchi, Jürgen Schaffner-Bielich, Laura Tolos, Sven Köppel, Gloria Montaña, Michael Rattay, Debades Bandopadhyay,

Walter Greiner *Horst Stöcker* *Luciano Rezzolla*

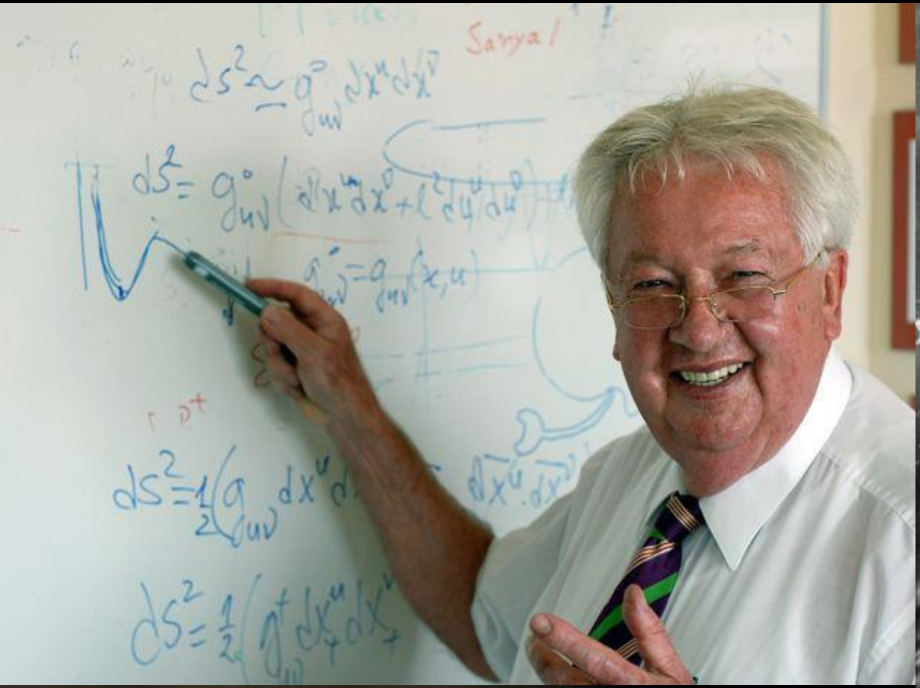

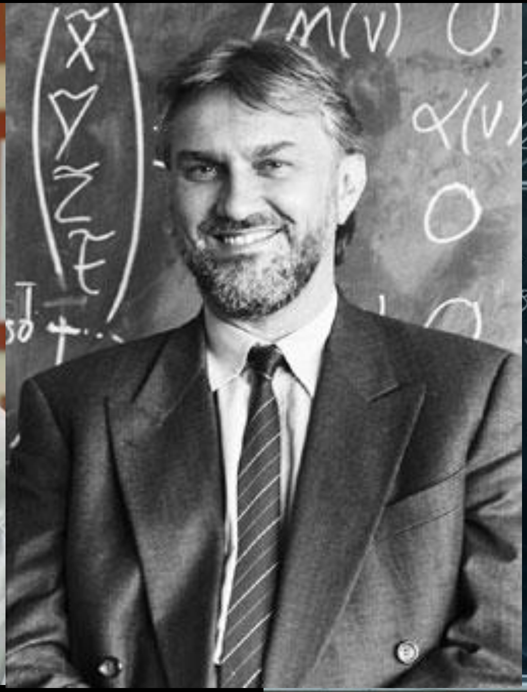

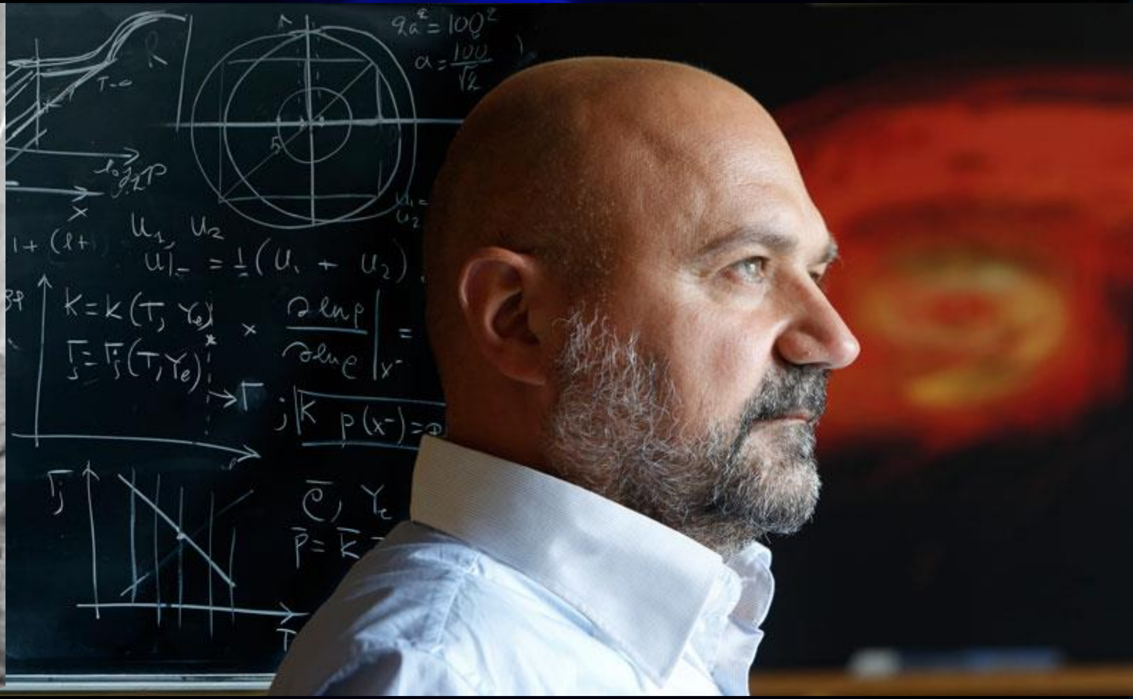

Riedberg TV, Hessisches Kompetenzzentrum für Hochleistungsrechnen und Tanzschule Wernecke

Kamera: *Pablo Rengel Lorena* Schnitt: *Luise Schulte*

Der Tanz der Neutronensterne: See today in „Deutschland Radio“

The Gibbs Construction

Hadronic and quark surface:

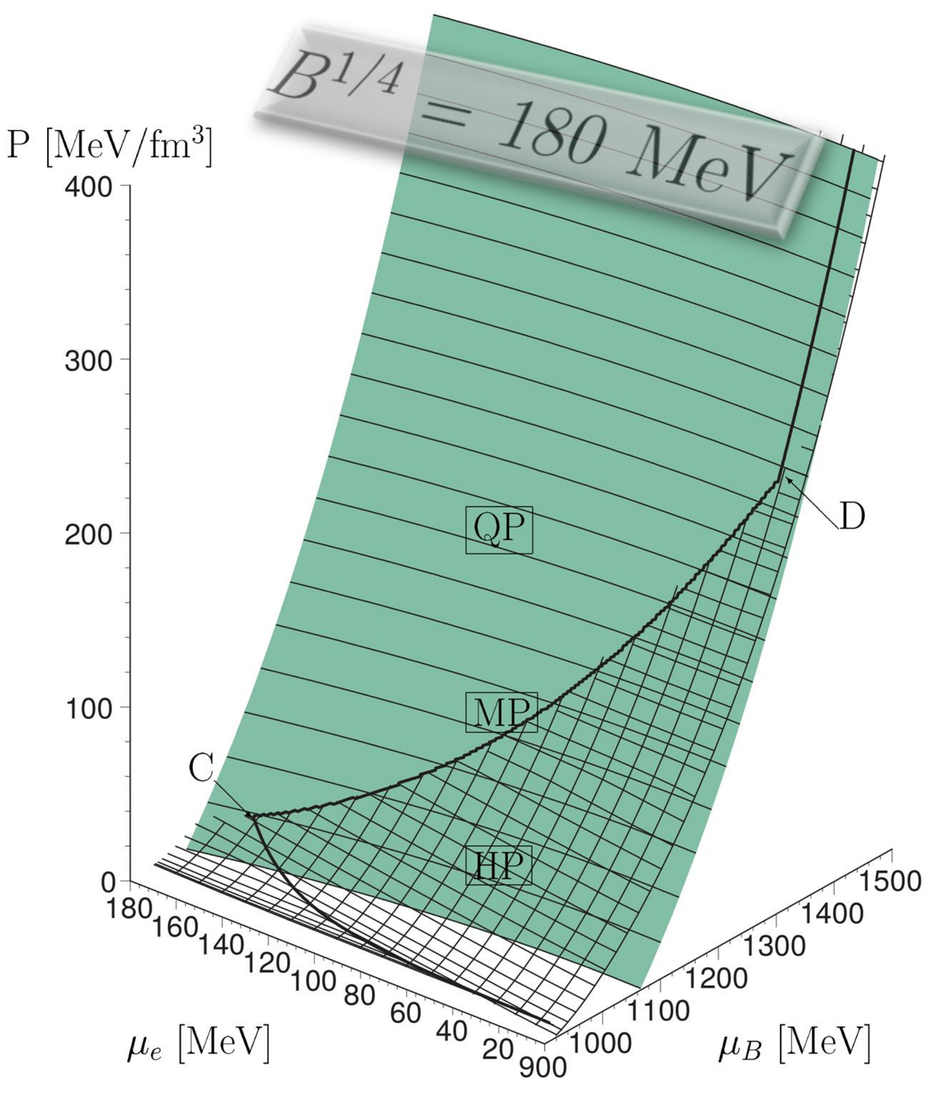

Charge neutrality condition is only globally realized

$$\rho_e := (1-\chi)\,\rho_e^H(\mu_B,\mu_e) + \chi\,\rho_e^Q(\mu_B,\mu_e) = 0\,.$$

The pressure in the mixed phase depends on two independent chemical potentials

$$\begin{aligned} P^H(\mu_B,\mu_e) \quad &= \quad P^Q(\mu_B,\mu_e)\,, \\ \mu_B = \mu_B^H \quad &= \quad \mu_B^Q\,, \\ \mu_e = \mu_e^H \quad &= \quad \mu_e^Q \end{aligned}$$

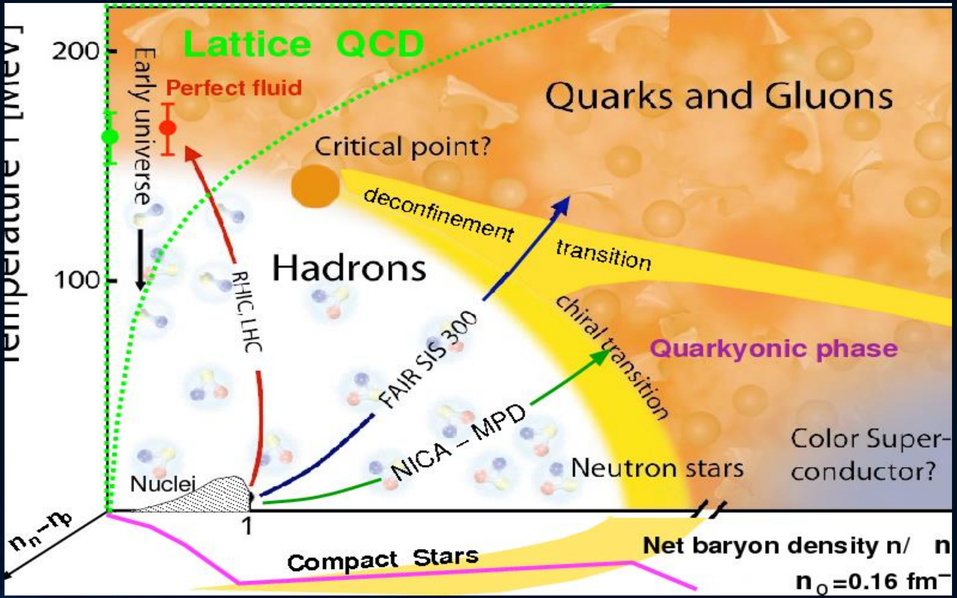

The Gibbs Construction

Hadronic and quark surface:

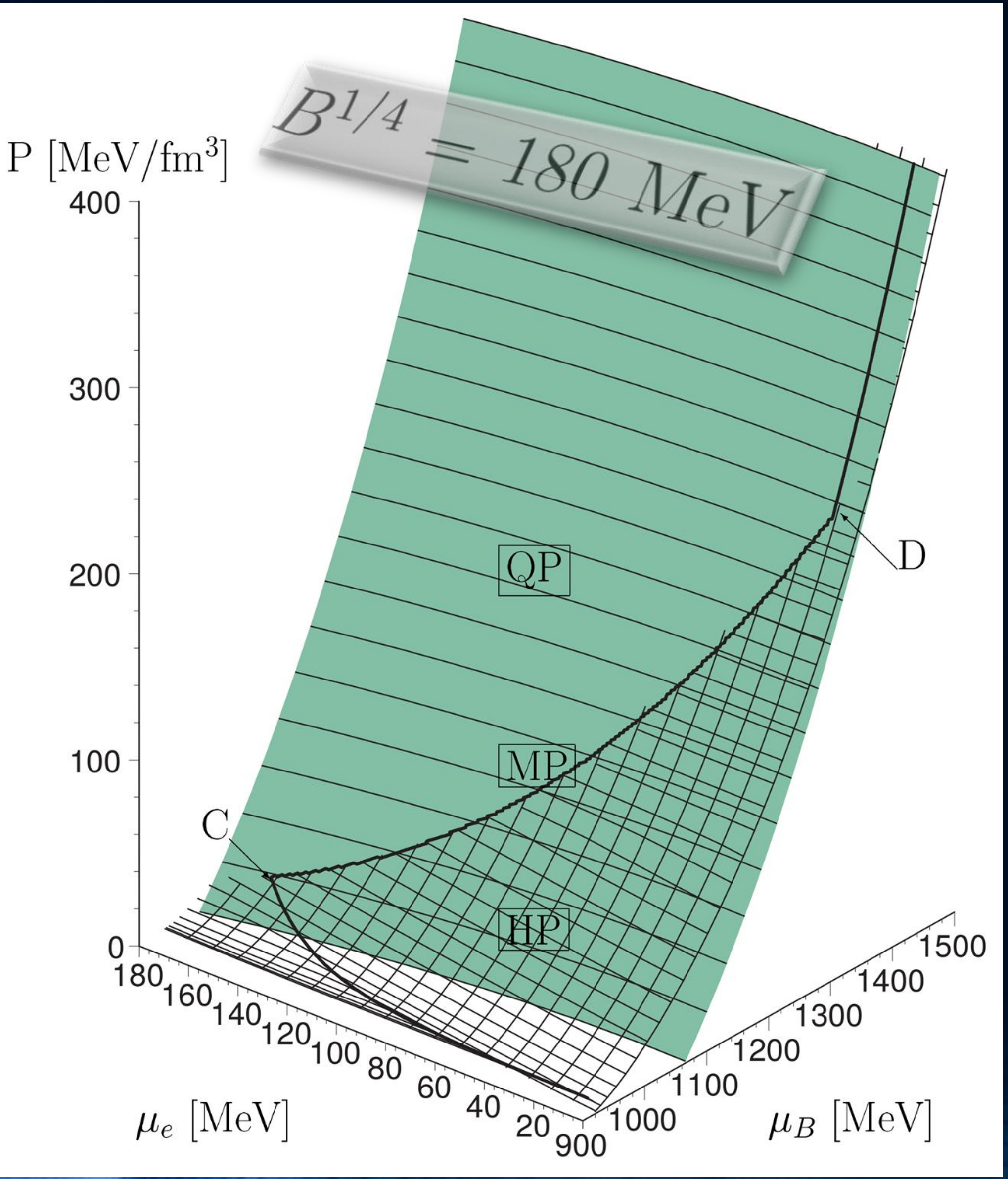

Charge neutrality condition is only globally realized

$$\rho_e := (1-\chi)\,\rho_e^H(\mu_B,\mu_e) + \chi\,\rho_e^Q(\mu_B,\mu_e) = 0\,.$$

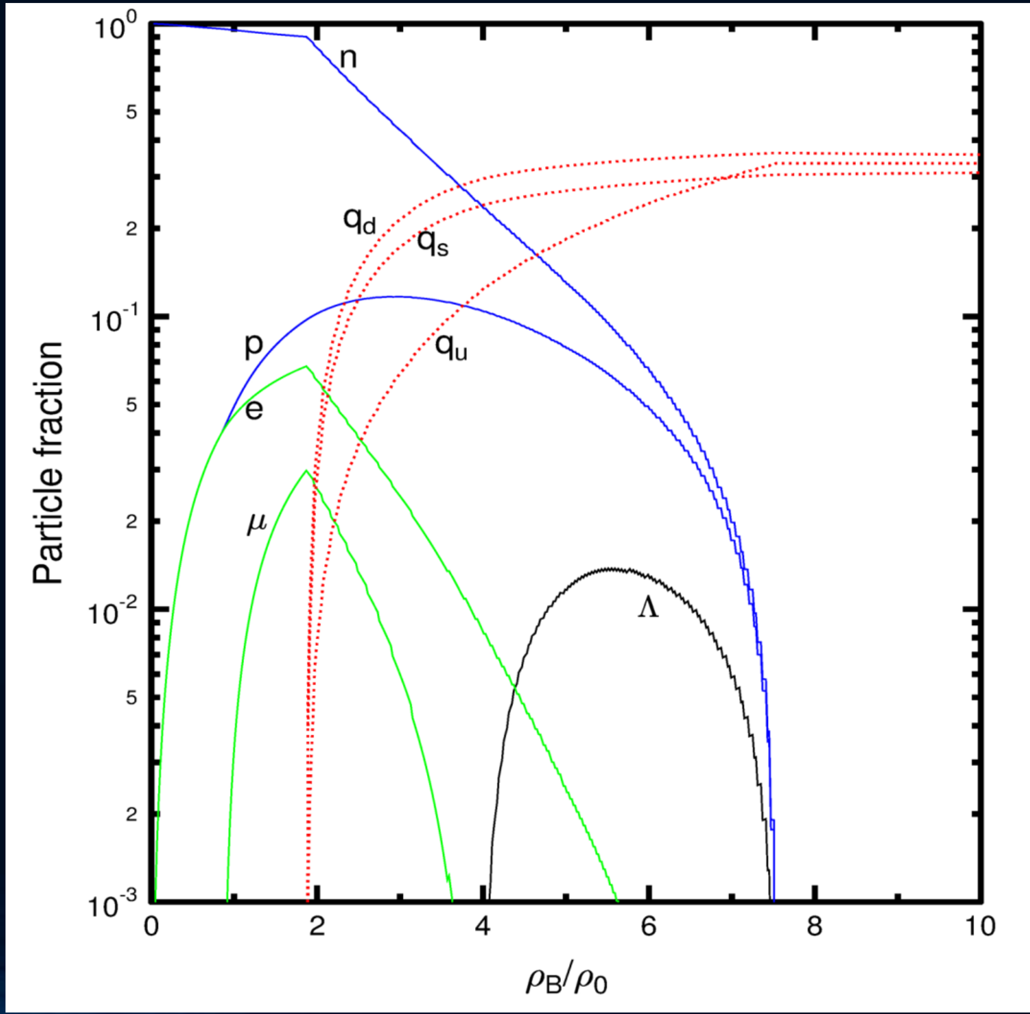

The Gibbs Construction

Hadronic and quark surface:

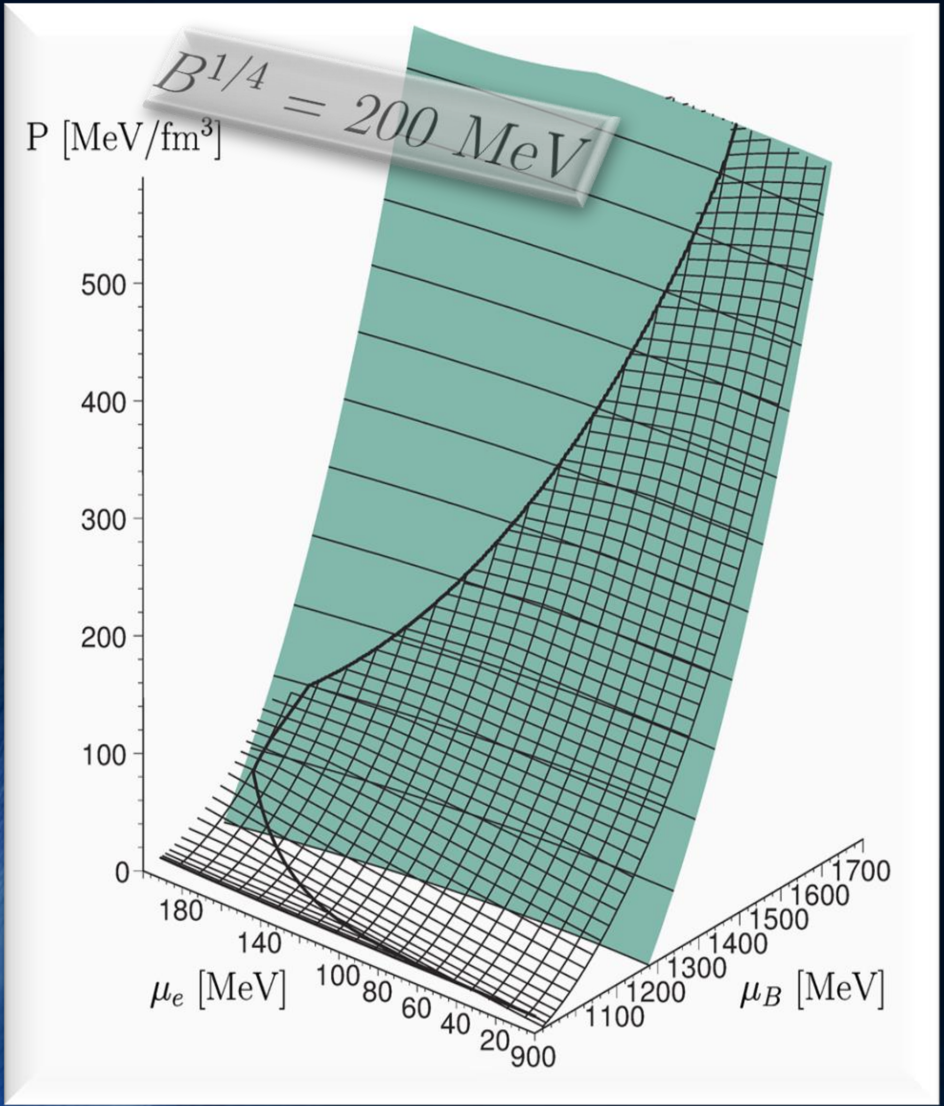

Particle composition:

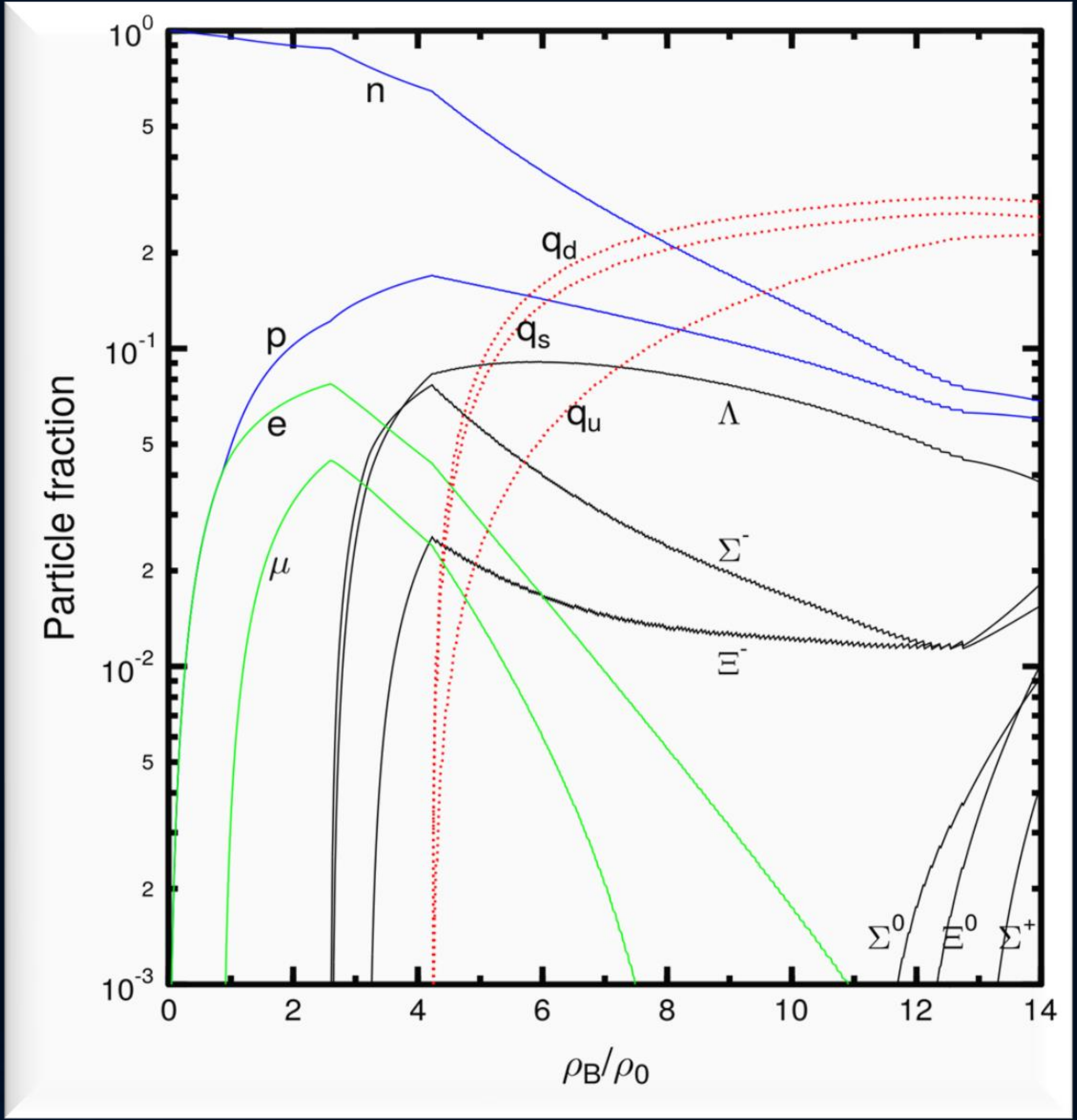

M. Hanauske, Dissertation, "Properties of Compact Stars within QCD-motivated Models"

SEARCH FOR POST-MERGER GRAVITATIONAL WAVES FROM THE REMNANT OF THE BINARYNEUTRON STAR MERGER GW170817 (see arXiv:1710.09320v1)

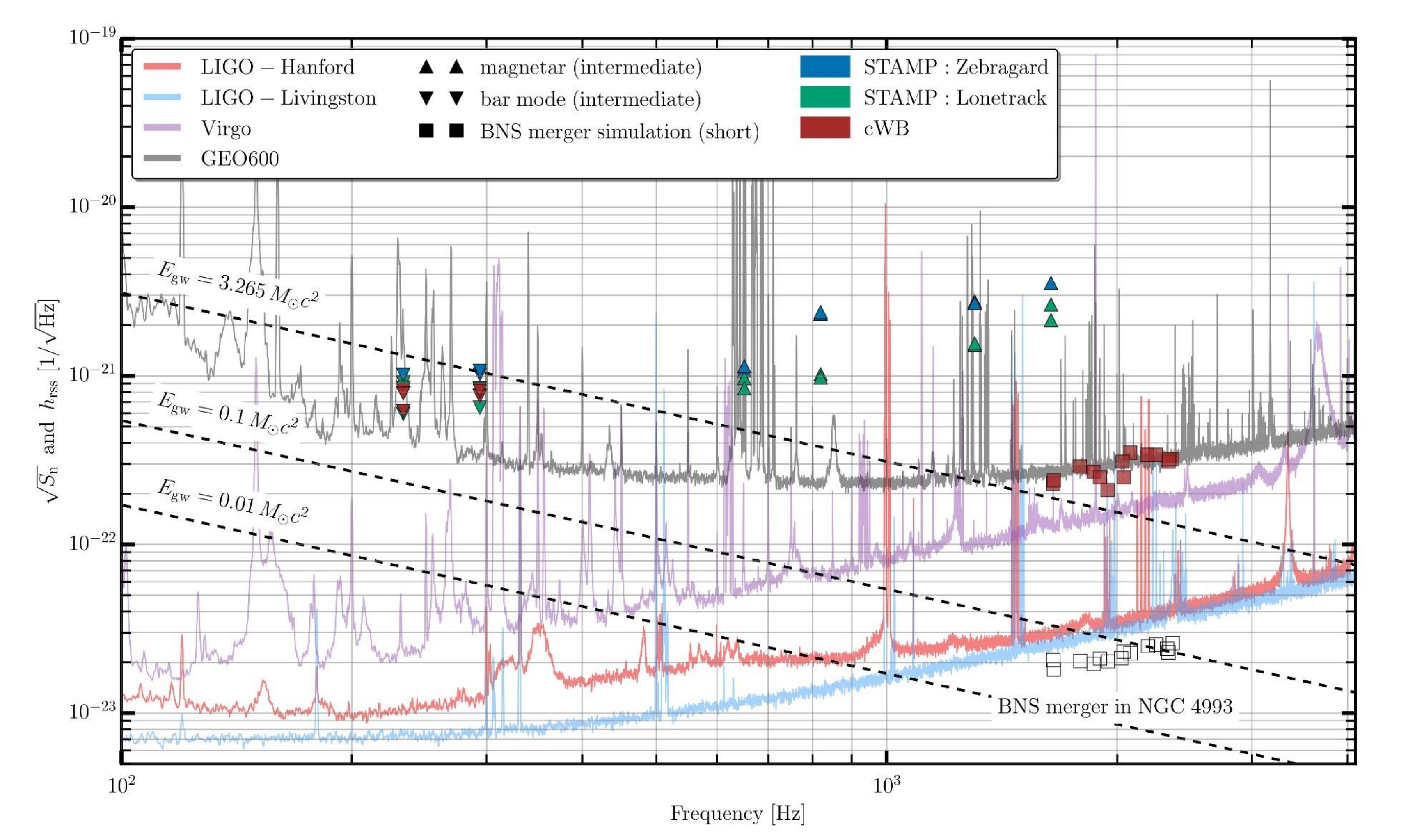

Unfortunately, due to the low sensitivity at high gravitational wave frequencies, no post-merger signal has been found in GW170817.

But, the results indicate that post-merger emission from a similar event may be detectable when advanced detectors reach design sensitivity or with next-generation detectors.

A new approach to constrain the EOS

Oechslin+2007, Baiotti+2008, Bauswein+ 2011, 2012, Stergioulas+ 2011, Hotokezaka+ 2013, Takami 2014, 2015, Bernuzzi 2014, 2015, Bauswein+ 2015, Clark+ 2016, LR+2016, de Pietri+ 2016, Feo+ 2017, Bose+ 2017 …

merger frequency

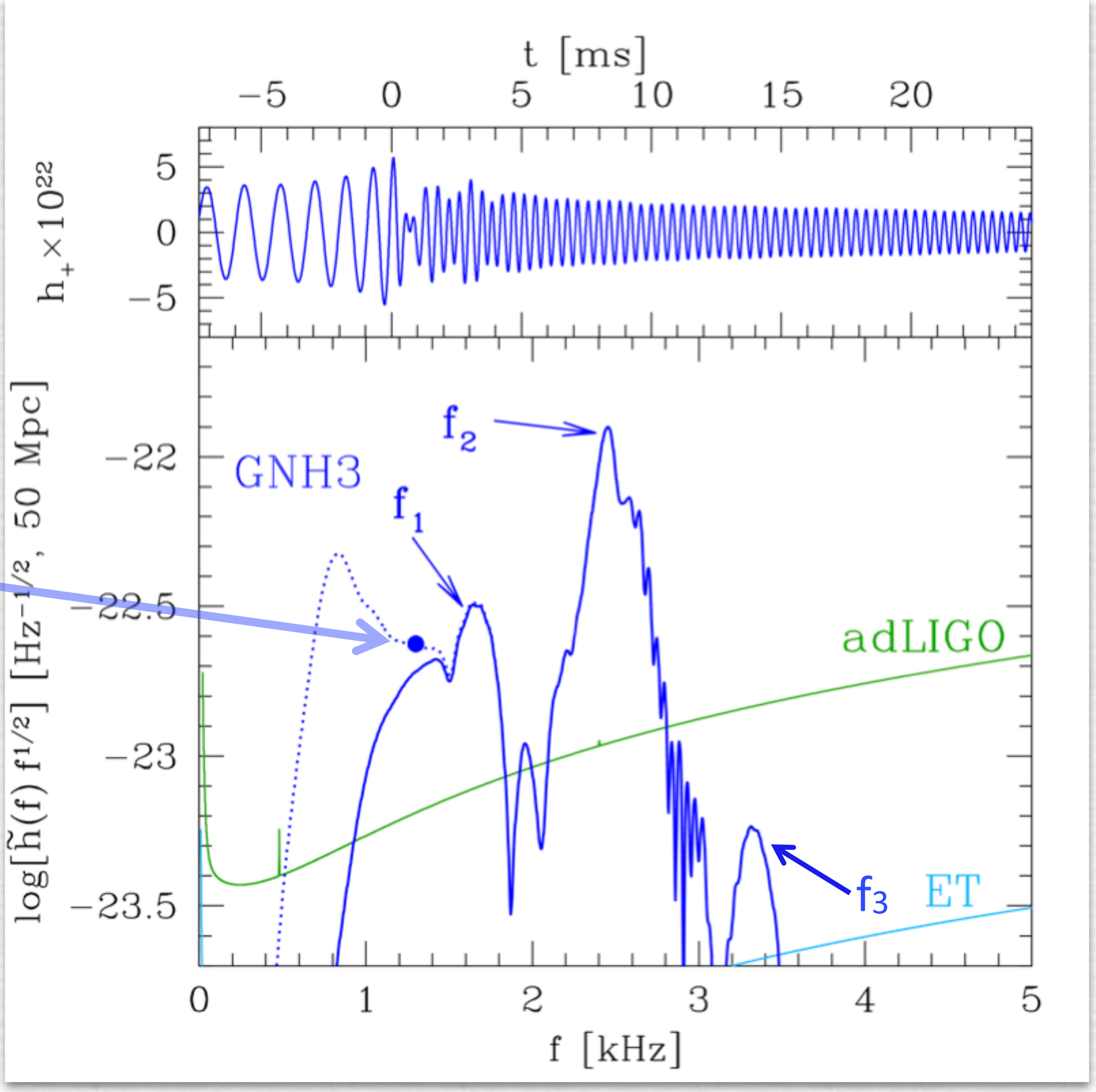

Slide from Luciano Rezzolla

A spectroscopic approach to the EOS

Oechslin+2007, Baiotti+2008, Bauswein+ 2011, 2012, Stergioulas+ 2011, Hotokezaka+ 2013, Takami 2014, 2015, Bernuzzi 2014, 2015, Bauswein+ 2015, Clark+ 2016, LR+2016, de Pietri+ 2016, Feo+ 2017, Bose+ 2017 …

merger frequency

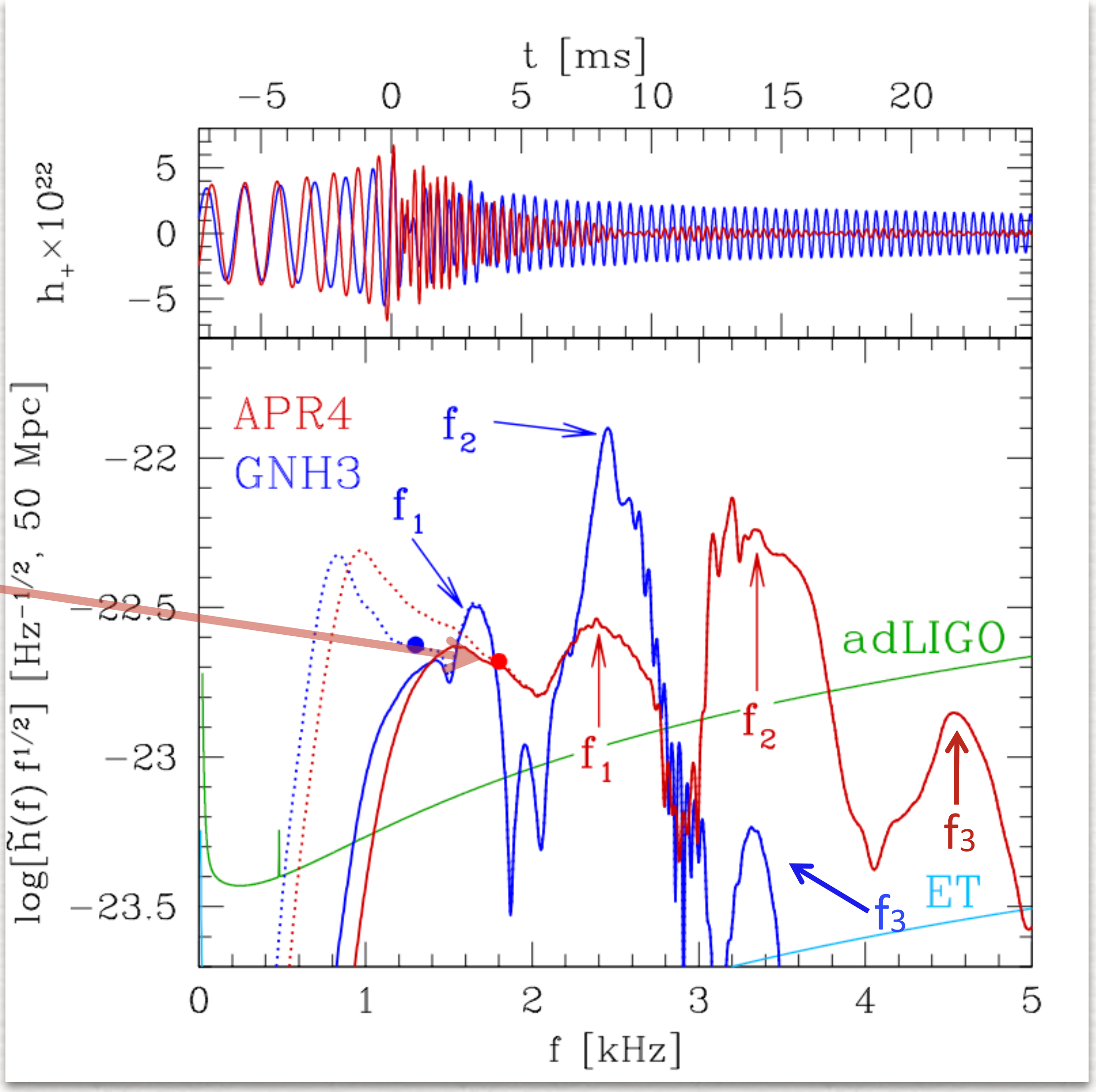

Slide from Luciano Rezzolla

Evolution of Tracer-particles tracking individual fluid elements in the equatorial plane of the HMNS at post-merger times

Mark G. Alford, Luke Bovard, Matthias Hanauske, Luciano Rezzolla, and Kai Schwenzer (2018) Viscous Dissipation and Heat Conduction in Binary Neutron-Star Mergers. Phys. Rev. Lett. 120, 041101

Different rotational behaviour of the quark-gluon-plasma produced in non-central ultra-relativistic heavy ion collisions
L. Adamczyk et.al., "Global Lambda-hyperon polarization in nuclear collisions: evidence for the most vortical fluid", Nature 548, 2017

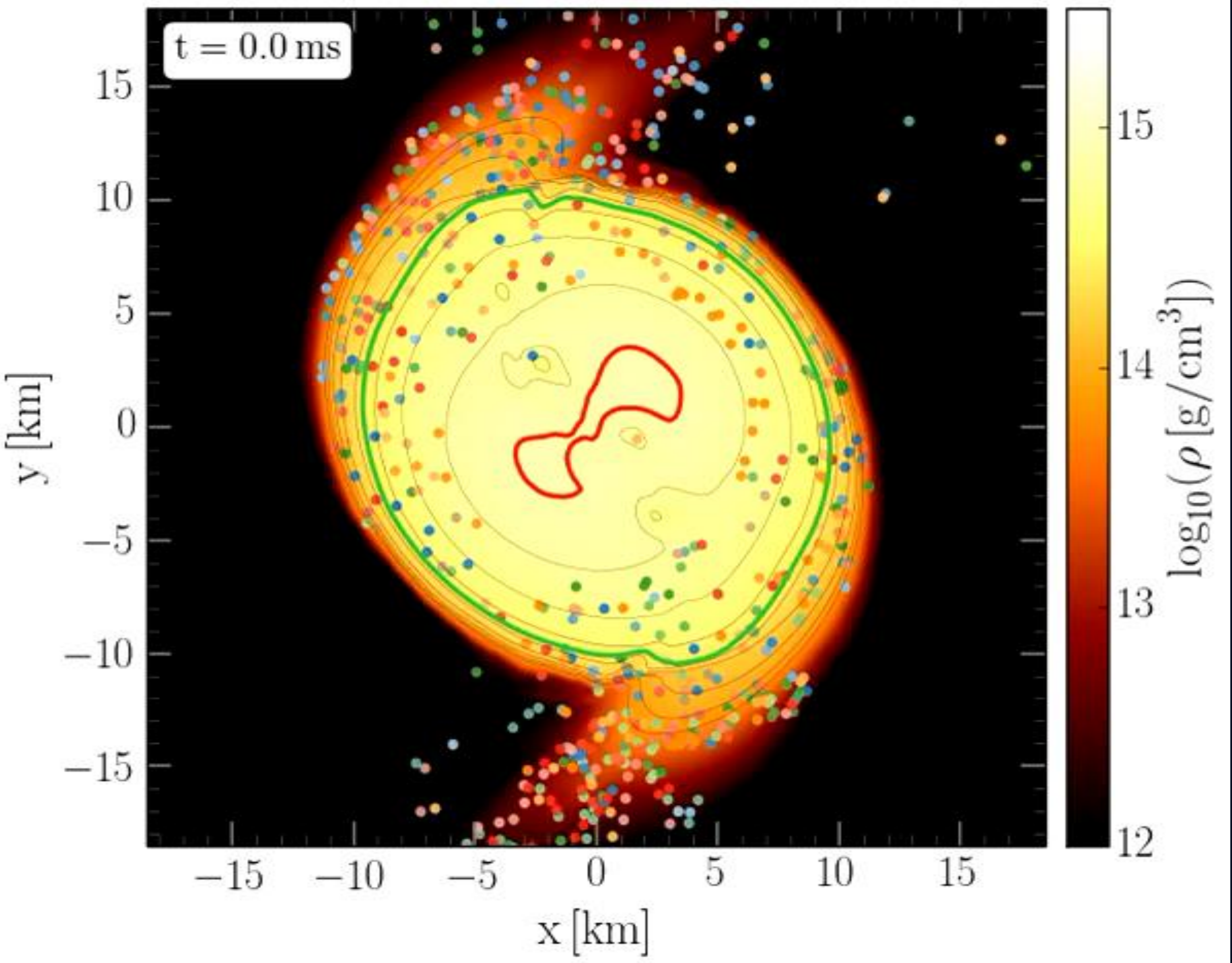

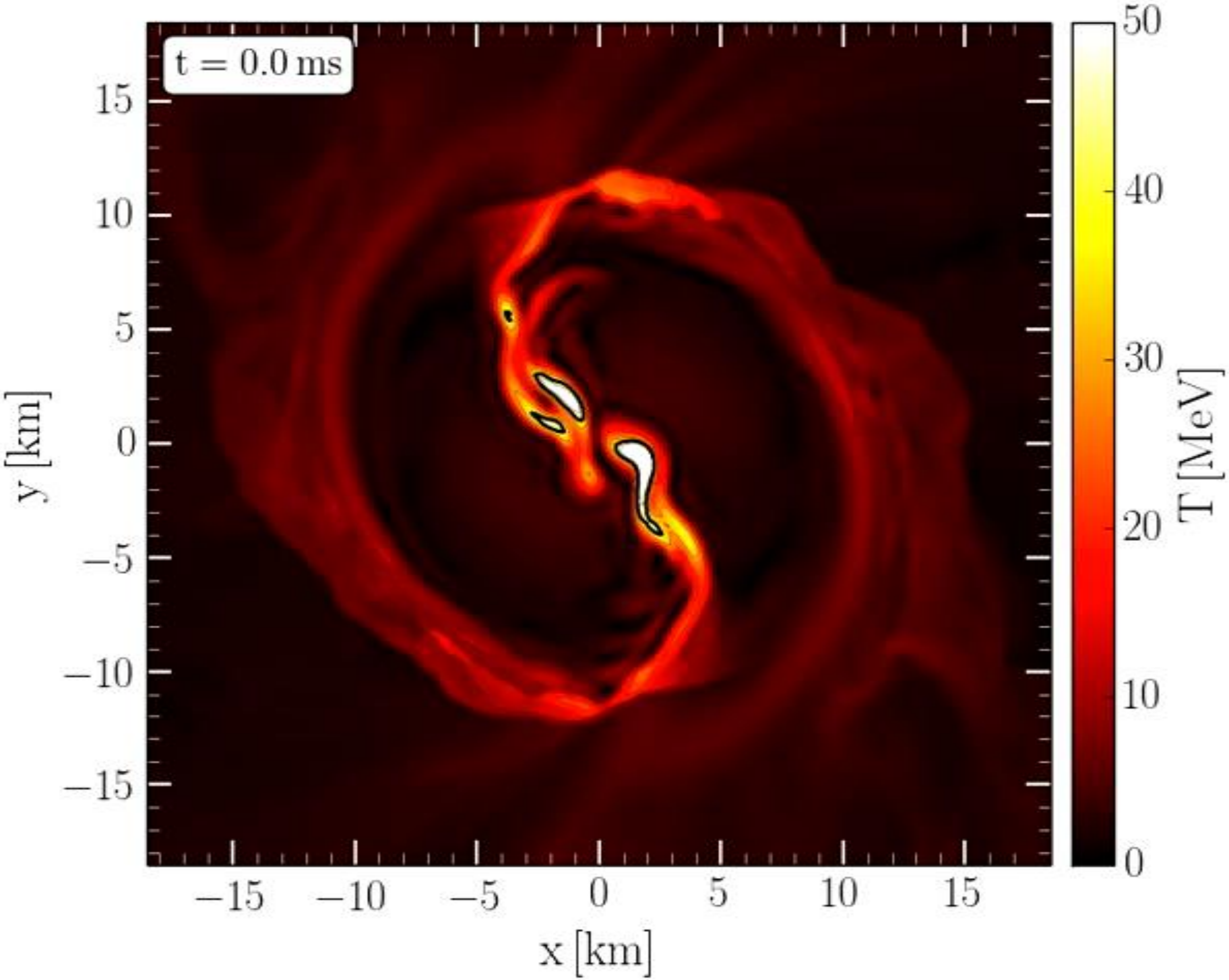

Evolution of the Temperature in the post merger phase

Hanauske, M., Takami, K., Bovard, L., Rezzolla, L., Font, J. A., Galeazzi, F., & Stöcker, H. (2017). Rotational properties of hypermassive neutron stars from binary mergers. Physical Review D, 96(4), 043004

Kastaun, W., Ciolfi, R., Endrizzi, A., & Giacomazzo, B. (2017). Structure of stable binary neutron star merger remnants: Role of initial spin. Physical Review D, 96(4), 043019

M. Hanauske, et.al., Connecting Relativistic Heavy Ion Collisions and Neutron Star Mergers by the Equation of State of Dense Hadron-and Quark Matter as signalled by Gravitational Waves, Journal of Physics: Conference Series, 878(1), p.012031 (2017)

GW170817: Constraining the maximum mass of Neutron Stars

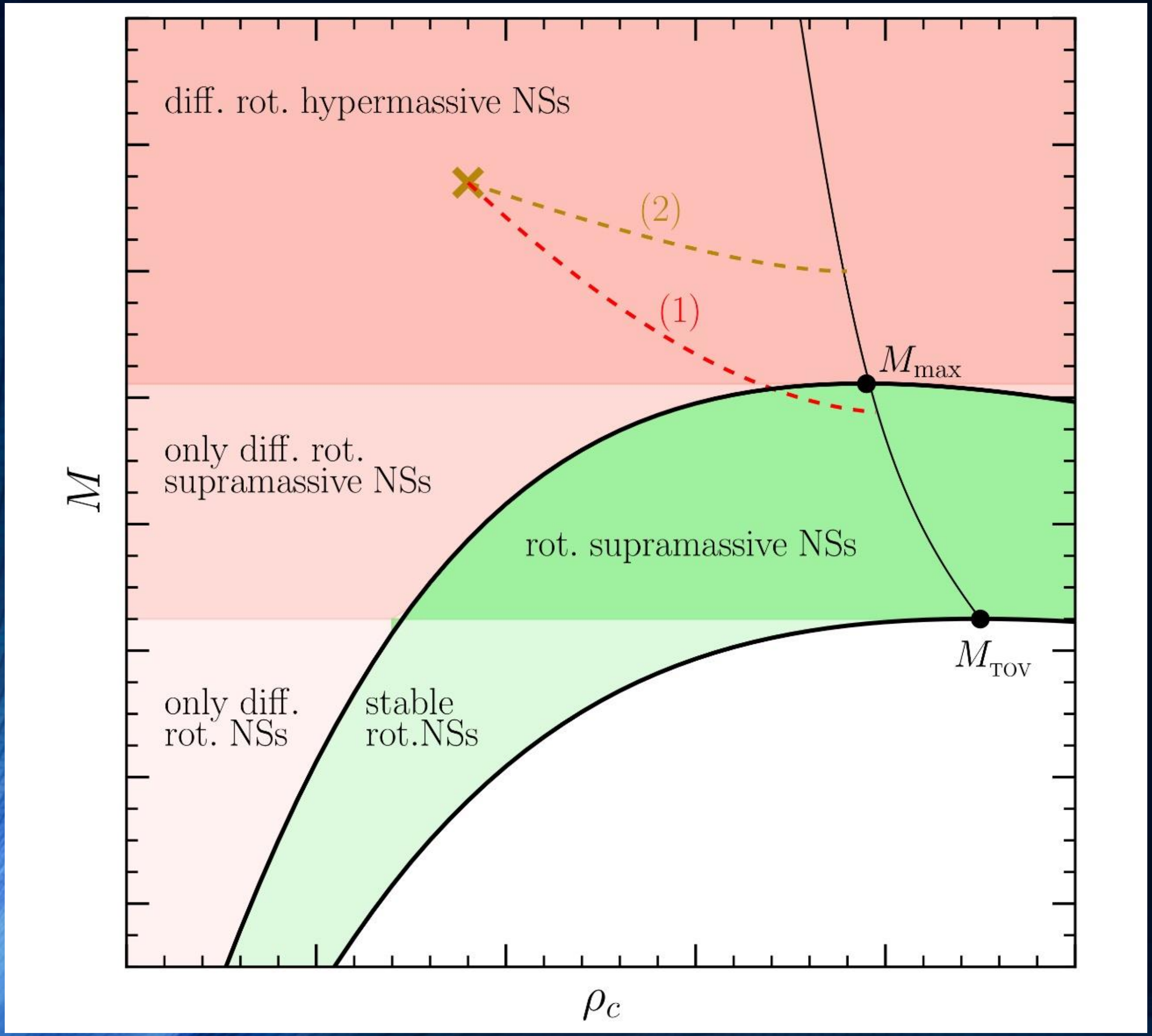

The highly differentially rotating hypermassive/supramassive neutron star will spin down and redistribute its angular momentum (e.g. due to viscosity effects, magnetic braking). After ~1 second it will cross the stability line as a uniformly rotating supramassive neutron star (close to M_{max}) and collapse to a black hole. Parts of the ejected matter will fall back into the black hole producing the gamma-ray burst.

L.Rezzolla, E.Most, L.Weih, "Using Gravitational Wave Observations and Quasi-Universal Relations to constrain the maximum Mass of Neutron Stars",The Astrophysical Journal Letters 852, L25 (2018): $2.01 \pm 0.04 < M_{TOV} < 2.16 \pm 0.17$

See also: S.Lawrence et al. ,APJ808,186, 2015
Margalit & Metzger, The Astrophysical Journal Letters 850, L19 (2017): $M_{TOV} < 2.17$ (90%)
Zhou, Zhou, Li, PRD 97, 083015 (2018)
Ruiz, Shapiro, Tsokaros, PRD 97,021501 (2018)

GW170817: Tidal Deformability Restrictions on the Equation of State (EOS) (for high and low spin assumption)

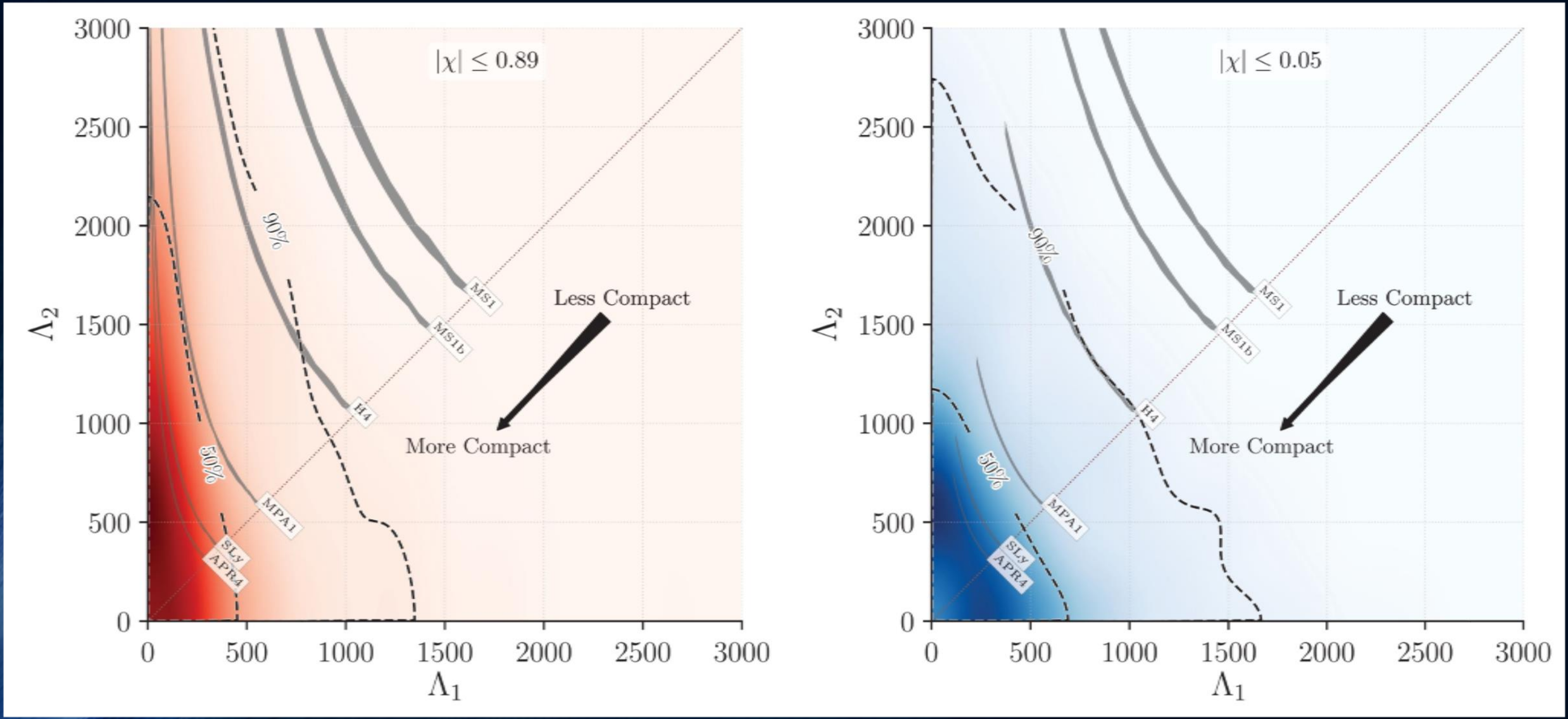

GW170817: Constraining the Neutron Star Radius and EOS

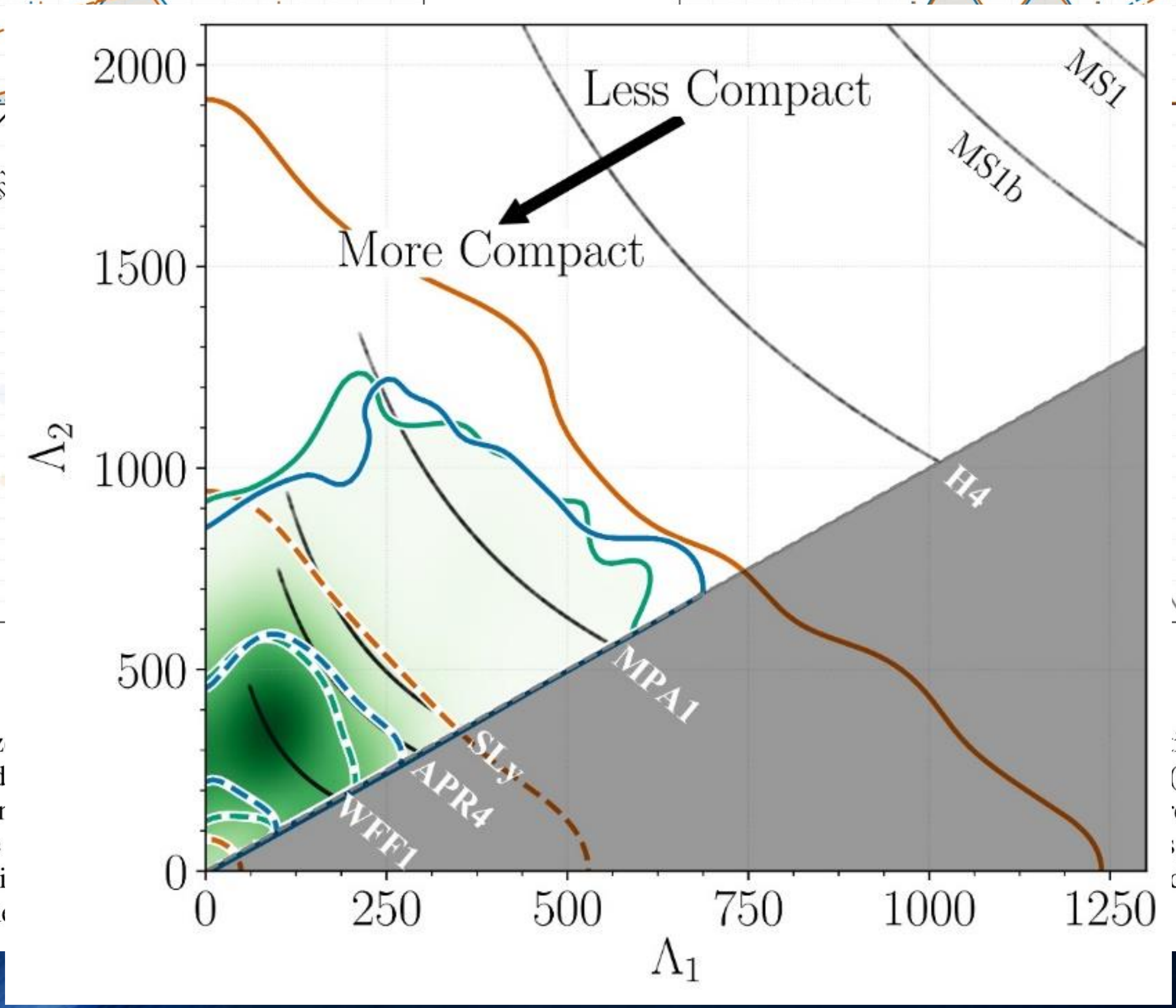

FIG. 3. Marginaliz
and a parametrized
posterior correspon
the top left denote
used for the posteri
of the 90% credibl

ions (left panel)
(bottom orange)
ey. The lines in
, solid lines are
d for the bounds

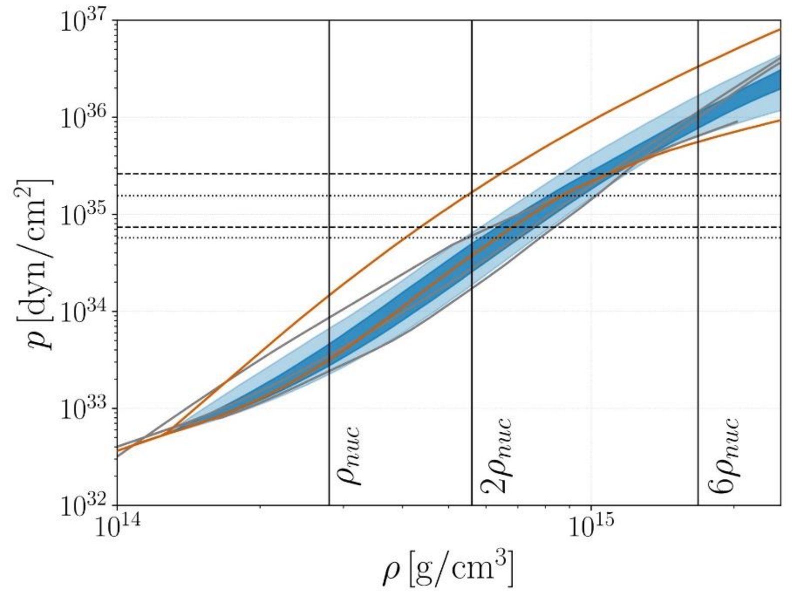

FIG. 2. Marginalized posterior (blue) and prior (orange) for the pressure p as a function of the rest-mass density ρ of the NS interior using the spectral EOS parametrization and imposing a lower limit on the maximum NS mass supported by the EOS of $1.97\,M_\odot$. The dark (light) blue shaded region corresponds to the 50% (90%) posterior credible level and the orange lines show the 90% prior credible interval. Horizontal lines denote the 90% credible interval for the central pressure of the heavier (dashed) and the lighter (dotted) binary components. Vertical lines correspond to once, twice, and six times the nuclear saturation density. Overplotted in grey are representative EOS models [121, 122, 124], using data taken from [19]; from top to bottom at $2\rho_{\rm nuc}$ we show H4, APR4, and WFF1.

GW170817: Measurements of neutron star radii and equation of state, *The LIGO /Virgo Collaboration*, arXiv:1805.11581v1

GW170817: … us

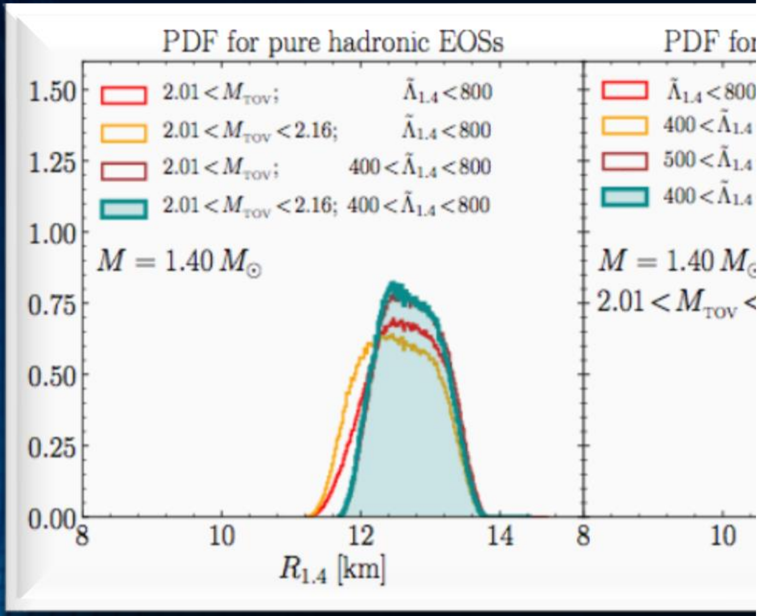

$$12.00 < R_{1.4}/\mathrm{km} < 13.45$$

$$8.53 < R_{1.4}/\mathrm{km} < 13.74 \quad \bar{R}$$

Reference	R_i [km]
Without a phase transition	
Bauswein et al. [42]	$10.68^{+0.15}_{-0.03} \leq R_{1.6}$
Most et al. [51]	$12.00 \leq R_{1.4} \leq 13.45$
Burgio et al. [54]	$11.8 \leq R_{1.5} \leq 13.1$
Tews et al. [55]	$11.3 \leq R_{1.4} \leq 13.6$
De et al. [56]	$8.9 \leq R_{1.4} \leq 13.2$
LIGO/Virgo [57]	$10.5 \leq R_{1.4} \leq 13.3$
With a phase transition	
Annala et al. [46]	$R_{1.4} \leq 13.6$
Most et al. [51]	$8.53 \leq R_{1.4} \leq 13.74$
Burgio et al. [54]	$R_{1.5} = 10.7$
Tews et al. [55]	$9.0 \leq R_{1.4} \leq 13.6$
This work	
NS	$R_{1.4} = 13.11$
HS `Model-2`	$12.9 \leq R_{1.4} \leq 13.11$
$\mathrm{HS_T}$ `Model-1`	$10.1 \leq R_{1.4} \leq 12.9$
$\mathrm{HS_T}$ `Model-2`	$10.4 \leq R_{1.4} \leq 11.9$

TABLE II. Constraints on the radius of neutron stars from GW170817 for models without a phase transition (top), works considering the possibility of a transition to quark matter (middle) and for EOSs of *Category III* in the present work (bottom).

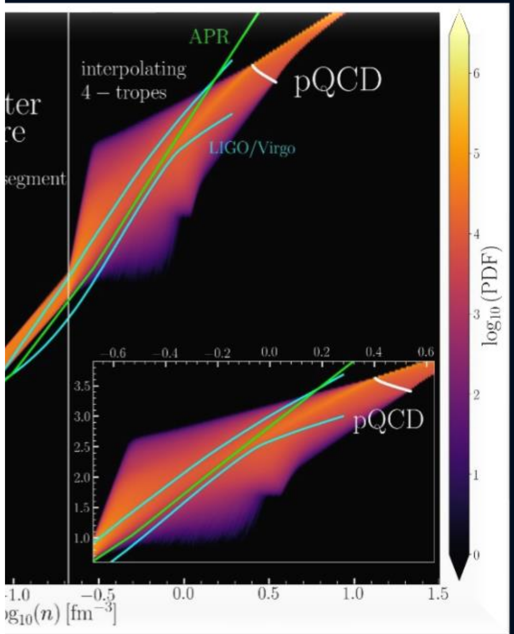

t, L.Weih, L.Rezzolla, J.
fner-Bielich "New
aints on radii and tidal
mabilities of neutron
rom GW170817",
1803.00549,
pted in PRL)

See also: De, Finstad, Lattimer, Brown, Berger, Biwe … v, Piekarewicz, Horowitz, PRL 120, 172702 (2018) ; Nandi & Char, Astrophys. J. 857, 12 (201 … ros, PRD 97, 021501 (2018) ; Annala, Gorda, Kurkela, Vuorinen, PRL 120, 172703 (201 …

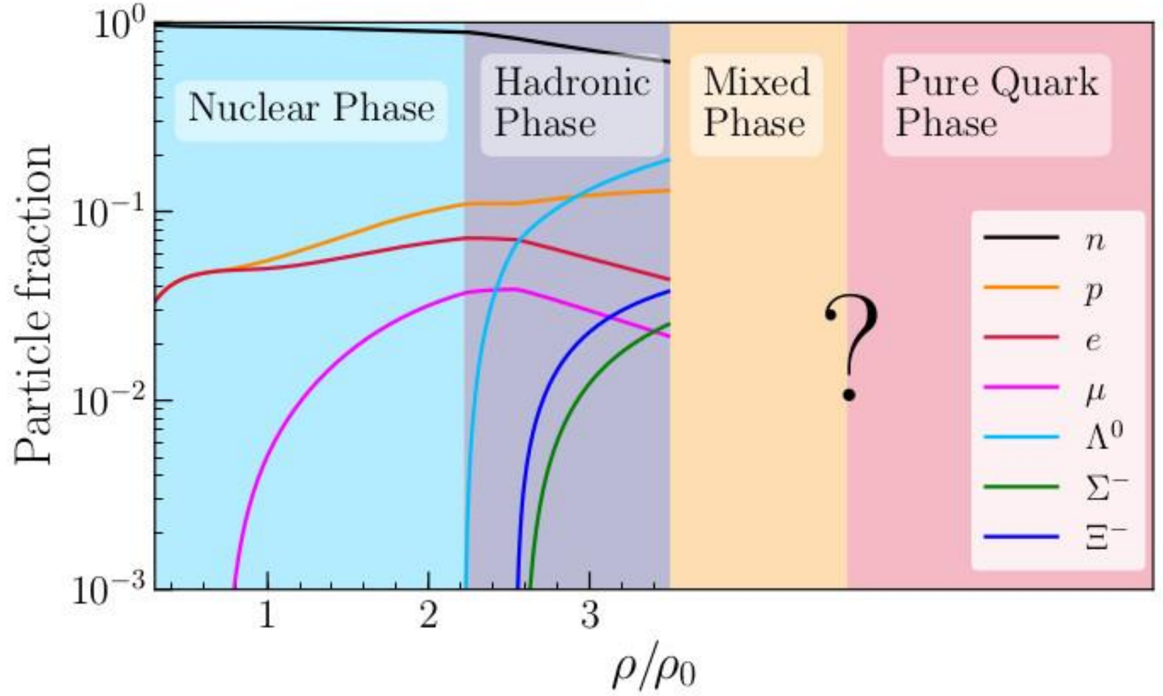

FIG. 1. Particle fractions as functions of the baryonic density for the FSU2H model [69, 70] up to the point where the HQPT is implemented, giving rise to a phase of deconfined quark matter which can be separated from the nuclear (or hadronic) phase by a mixed phase of hadrons and quarks. We note that the actual fractions of nucleons/hyperons and quarks u, d, s in the mixed and quark phases cannot be determined with the parametrizations used in this work.

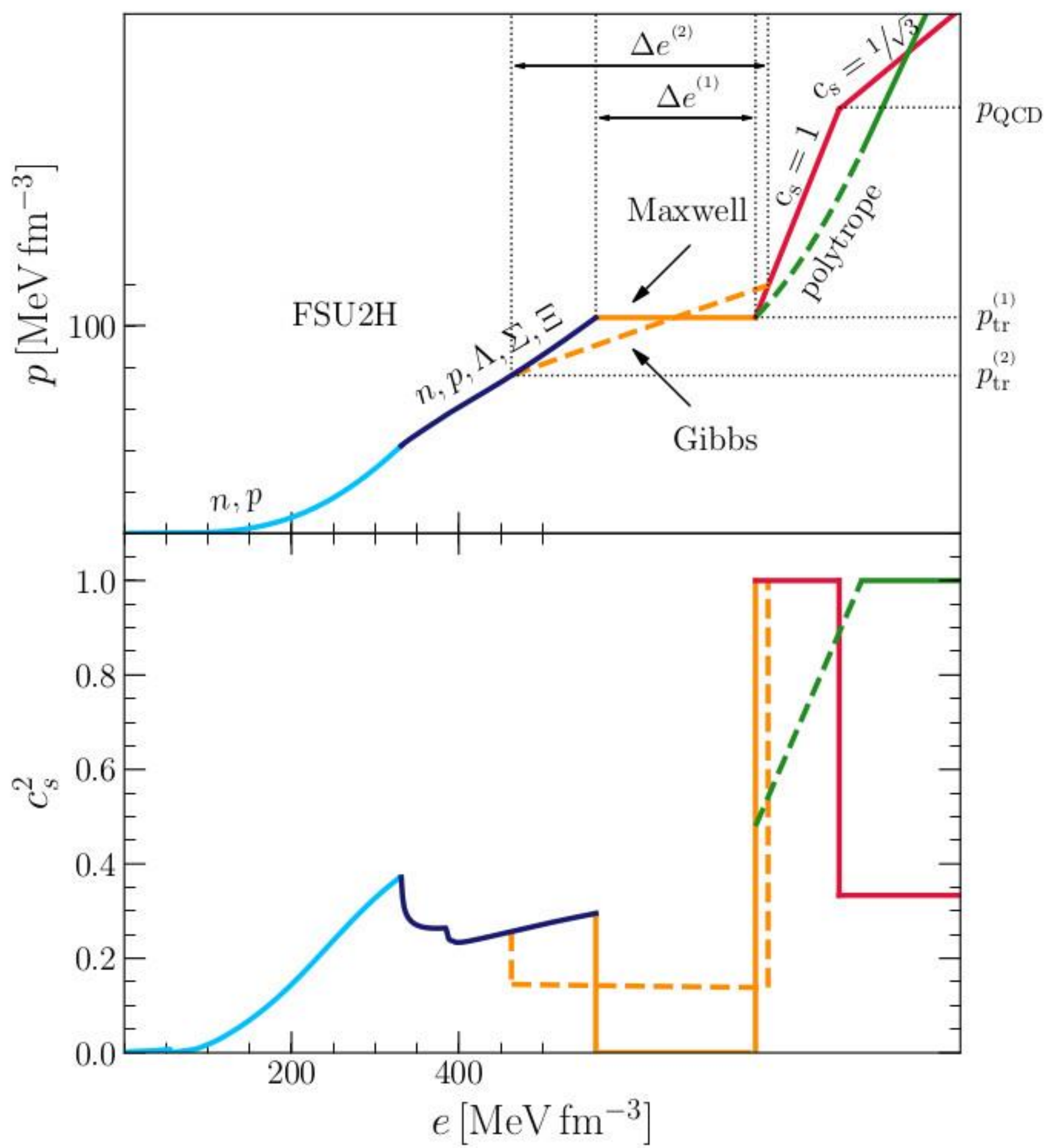

Mass-Radius Relations for Twin-Star EOSs

The mass and radius of a single, non-rotating and spherically symmetric neutron star can be easily calculated by solving the static TOV equation numerically for a given EOS.

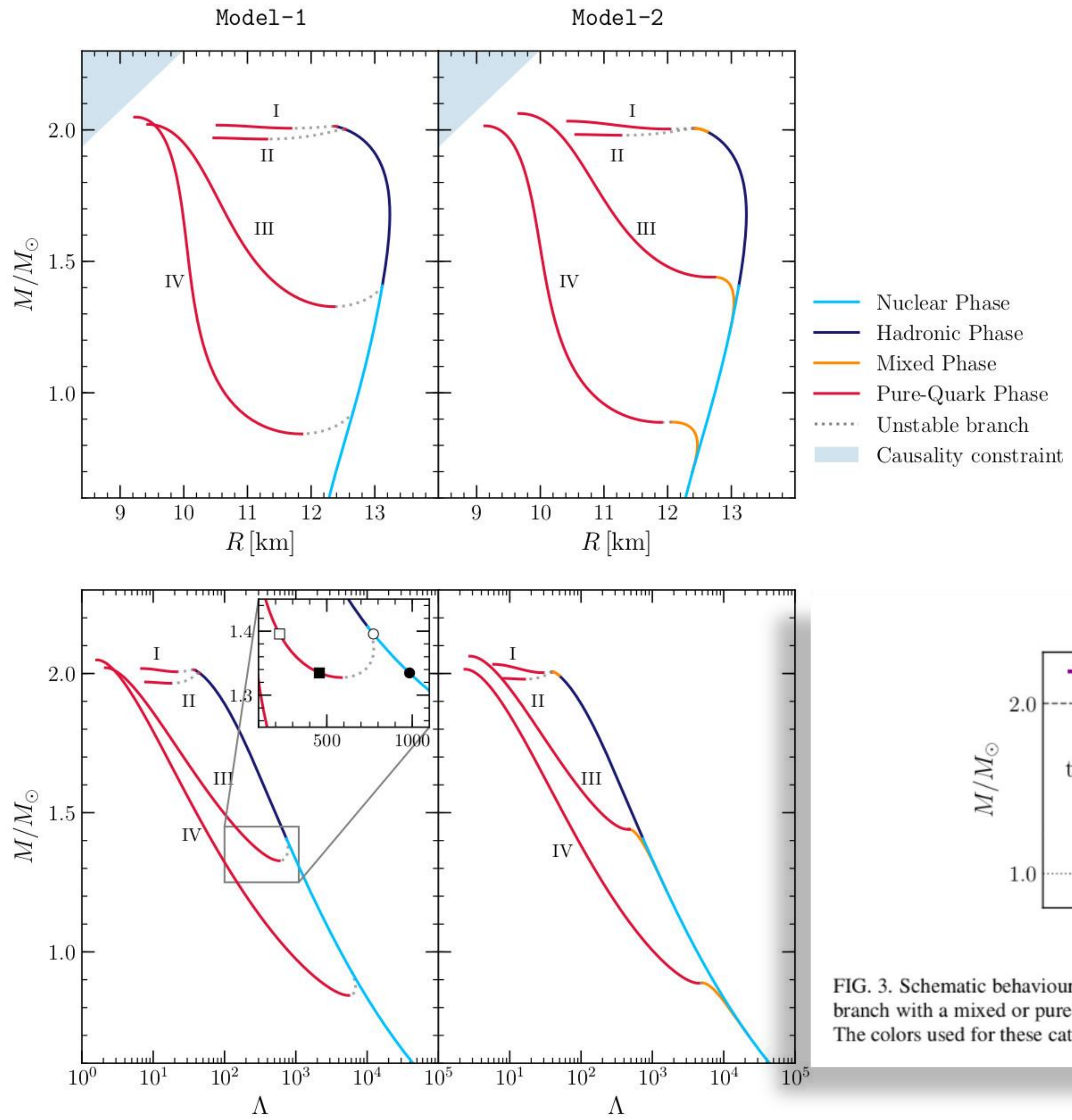

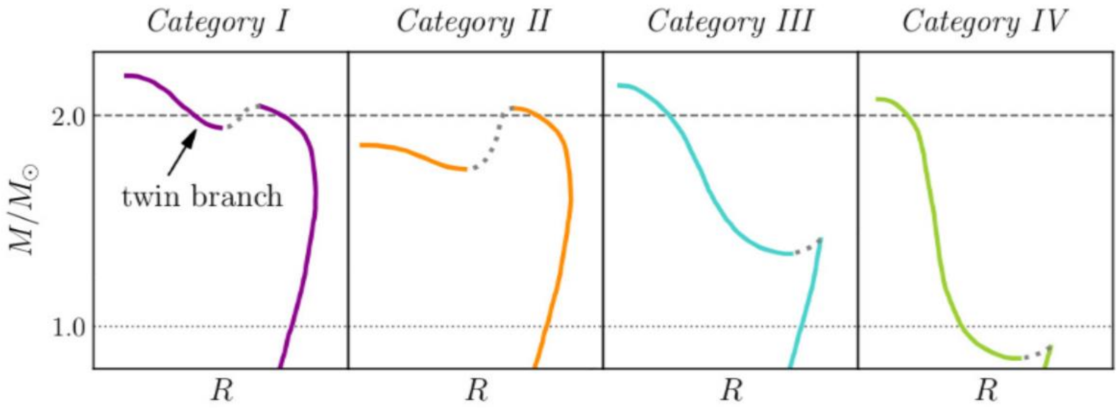

FIG. 3. Schematic behaviour of the mass–radius relation for the twin-star categories *I–IV* defined in the text. Note the appearance of a "twin" branch with a mixed or pure-quark phase; the twin branch has systematically smaller radii than the branch with a nuclear or hadronic phase. The colors used for these categories will be employed also in the subsequent figures.

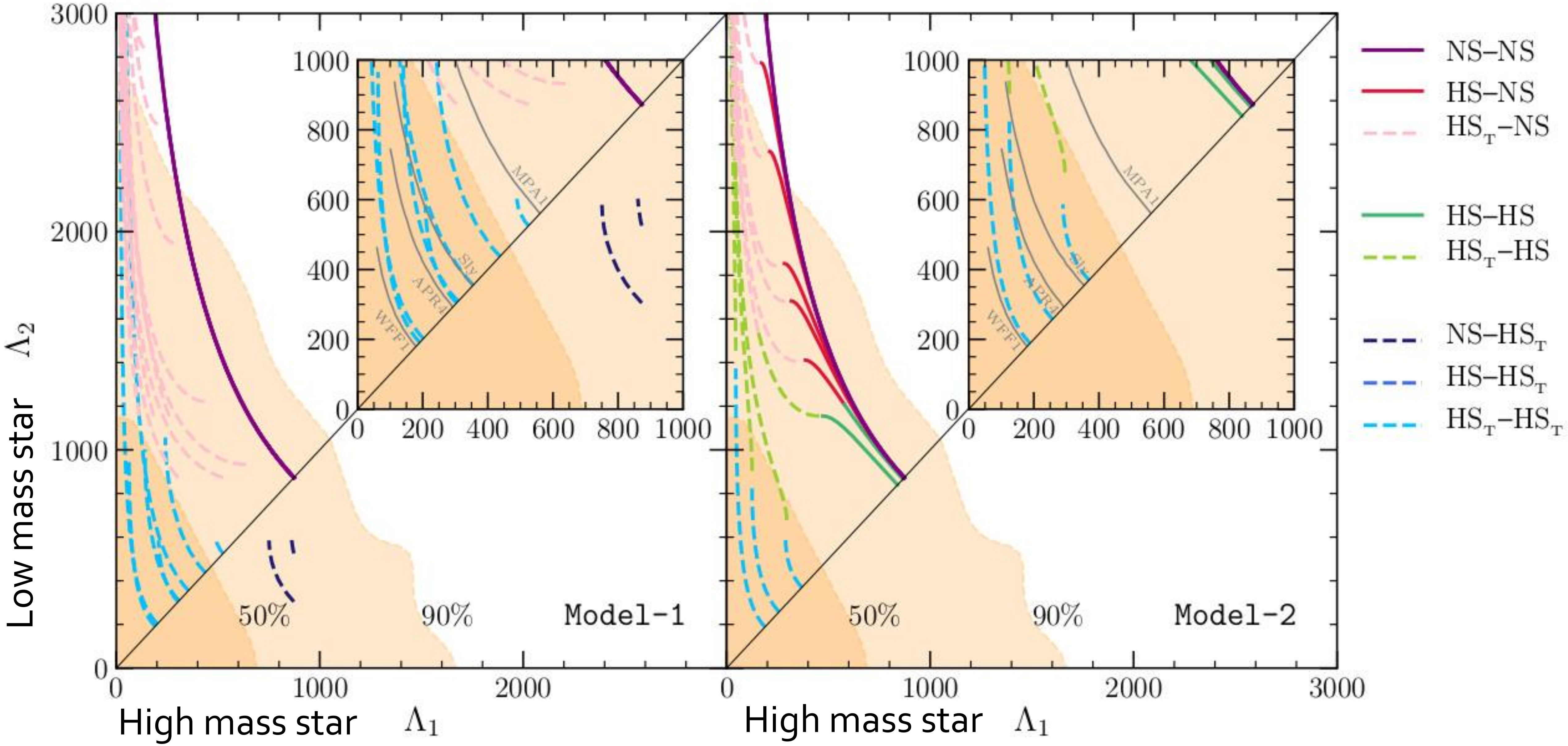

In a binary hybrid star merger the two masses of the individual stars can be different (q<1). As a result, the tidal deformability and the stars composition can be different. In this plot the total mass of the binary system has been fixed to the measured chirp mass of GW170817 (M=1.188 Msolar) and the different curve show results for EOSs of Category III.

Constraining the global parameters of the phase transition with GW170817

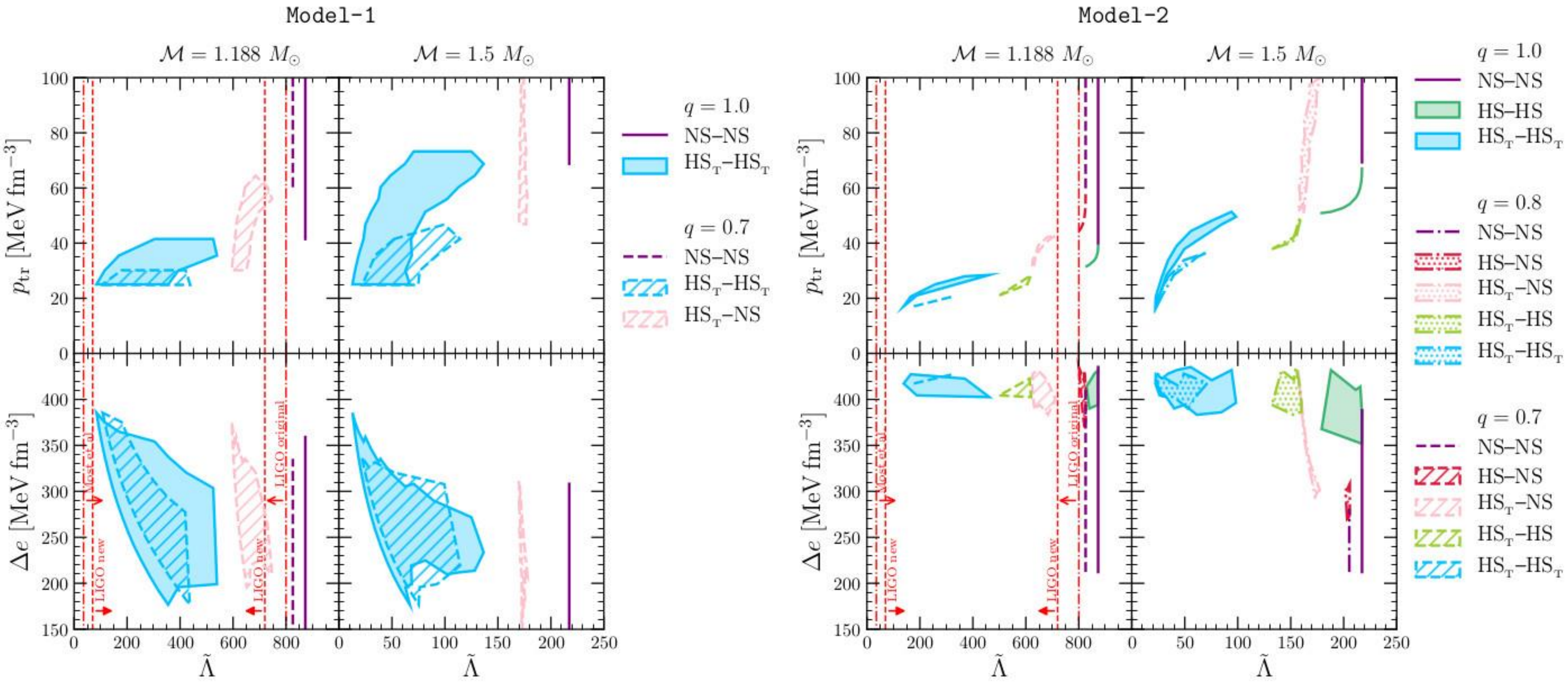

Binary Hybrid Star Mergers and the QCD Phase Diagram

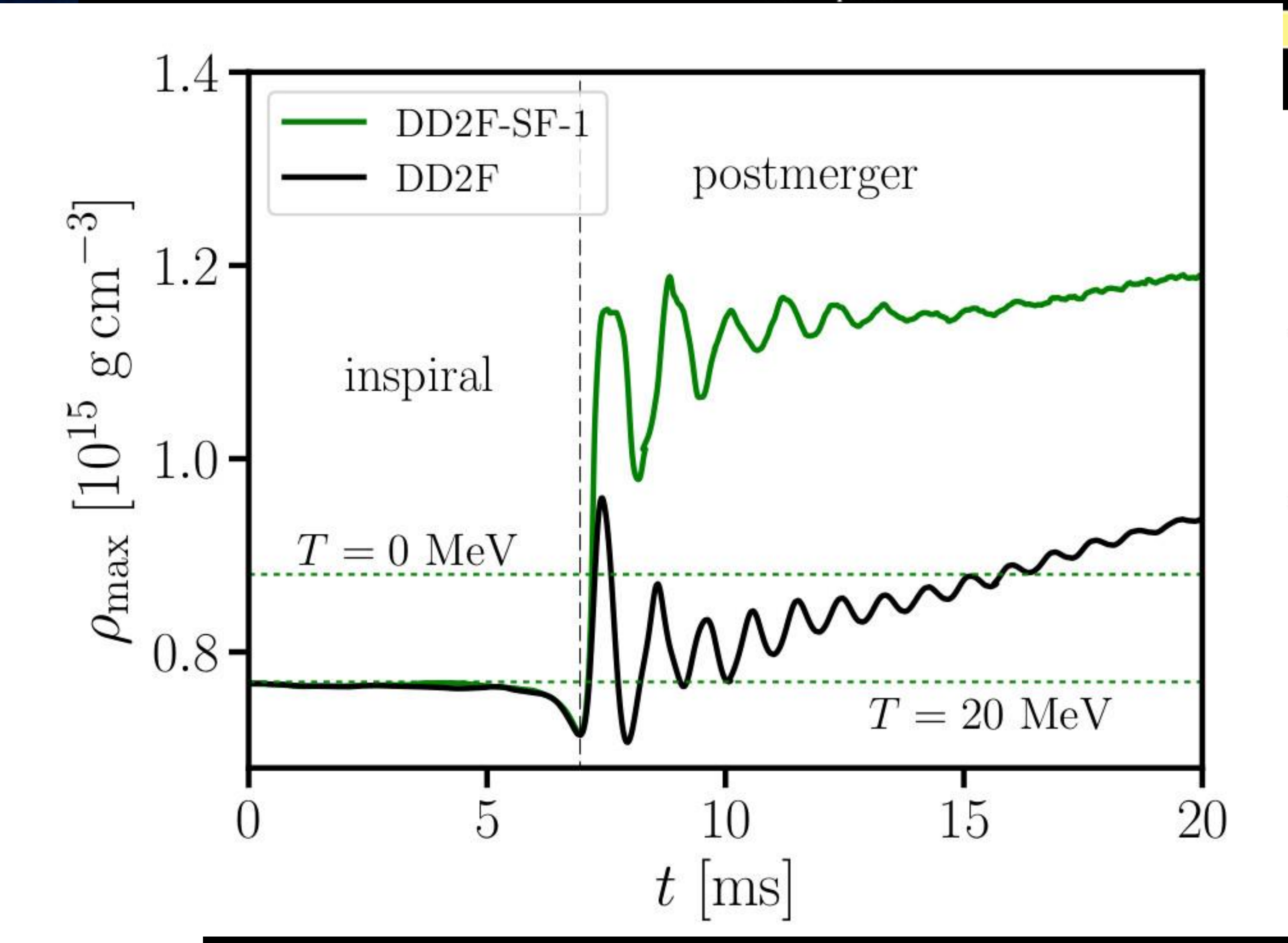

Hot and dense matter inside the inner area of a hypermassive

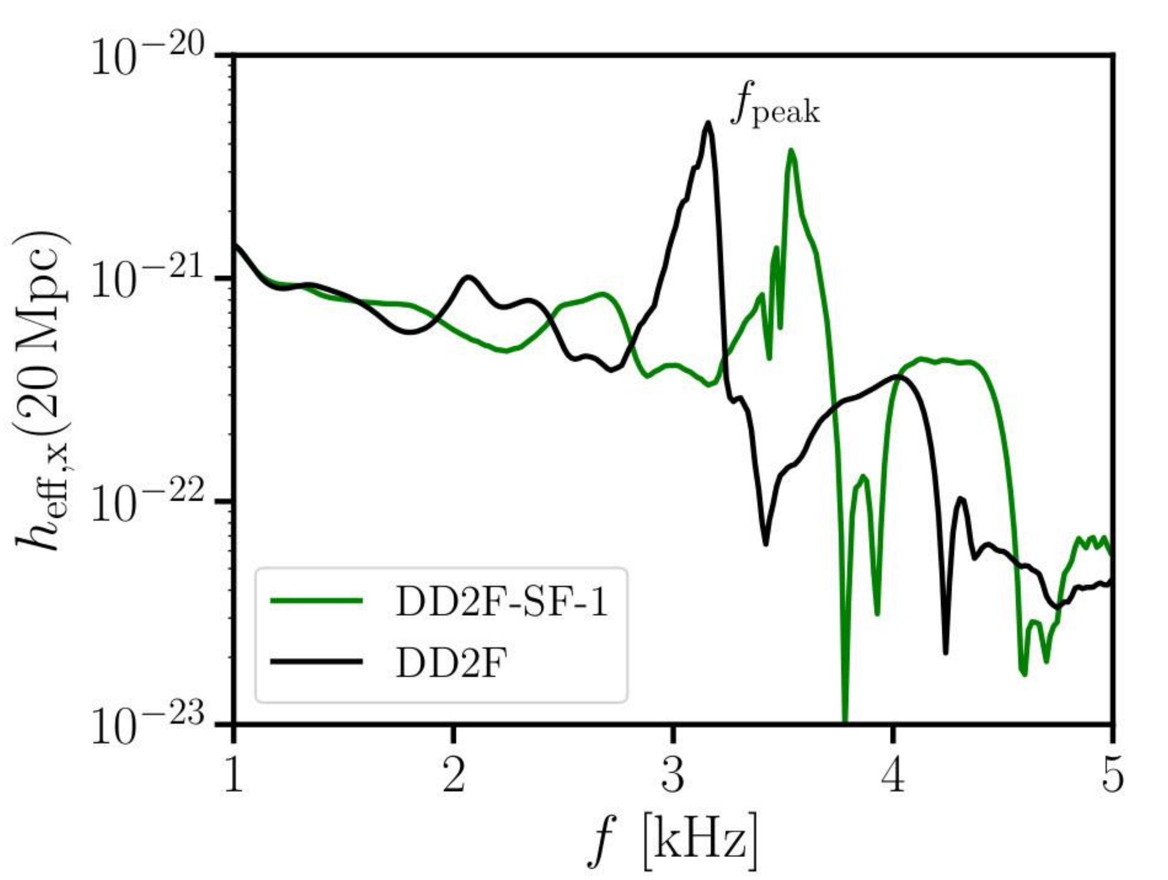

A.Bauswein, N.U.F. Bastian, D.B.Blaschke, K.Chatziioannou, J.A.Clark, T.Fischer and M.Oertel
„Identifying a first-order transition in neutron star mergers through gravitational waves“, PRL 2019

E.R.Most, L.J.Papenfort, V.Dexheimer, M.Hanauske, S.Schramm, H.Stöcker and L.Rezzolla
„Signatures of quark-hadron phase transitions in general-relativistic neutron-star mergers„, PRL 2019

Post-merger gravitational-wave signatures of phase transitions in binary compact star mergers

PRL 124, 171103 (2020)

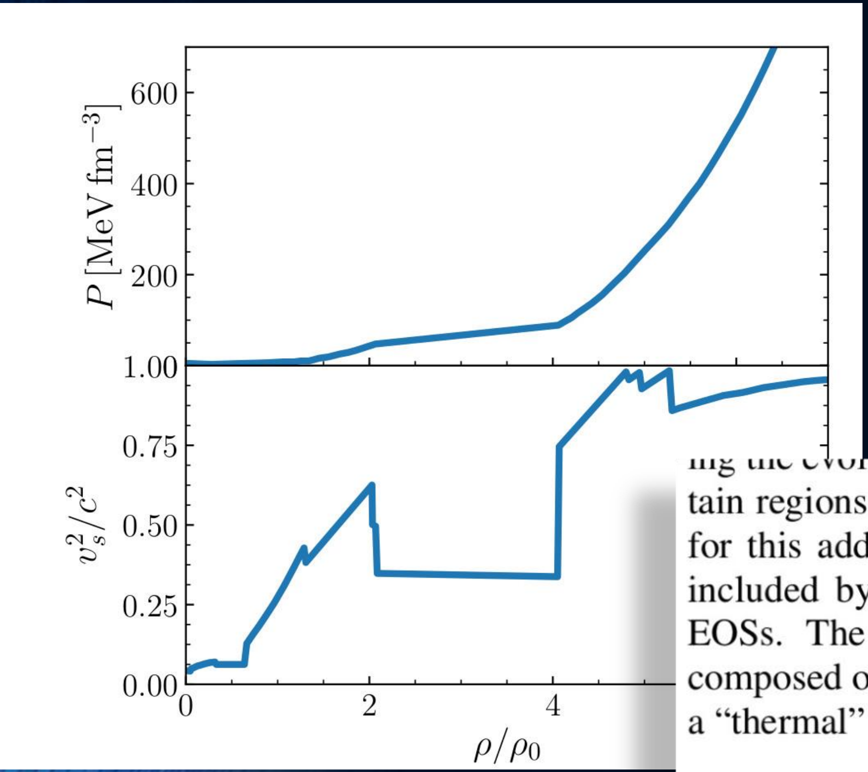

Cold EOS: FSU2H-PT

To account for additional shock heating during the merger and post-merger phase, thermal effects are included by adding a "thermal" ideal-fluid component ($p_{\rm th} = \rho\epsilon_{\rm th}\,(\Gamma_{\rm th} - 1)$) to the cold EOS where ρ is the rest-mass density, and $\Gamma_{\rm th} = 1.75$. The effective temperature obtained within this ideal-gas approach can be roughly approximated as $T = (m_{\rm n} p_{\rm th})/(k_{\rm B}\rho)$, where $m_{\rm n}$ is the nucleonic mass and $k_{\rm B}$ the Boltzmann constant. It should be stressed that the estimated temperature within this simple approximation only accounts for contributions of the ideal gas of neutrons and protons (mass differences have been neglected). Especially at the low-density regions of the outer crust of the hybrid star (which is composed of gas of leptons and nuclei at high values of electron fraction Y_e), the underlying temperature estimates deduced from the thermal pressure should be decreased by a factor $(1 + Y_e)$ and account … pressure [see Eq. (2) in [26]]. Finally, the thermal … s not account for any contribution resulting from a … r transition and, as a result, the structure of the phase … om that resulting from fully temperature-dependent

ing the evolution, shocks will increase the temperature in certain regions of the collapsing and oscillating star. To account for this additional shock heating, the thermal effects where included by adding an ideal-fluid component to the "cold" EOSs. The pressure p and the specific internal energy ϵ are composed of the "cold" part ($p_{\rm c}$) which includes a HQPT and a "thermal" ideal-fluid component $p_{\rm th}$ [117]

$$p = p_{\rm c} + p_{\rm th}\,, \quad \epsilon = \epsilon_{\rm c} + \epsilon_{\rm th}\,, \quad p_{\rm th} = \frac{k_B}{m_N}\,\rho T\,, \qquad (3)$$

where p and ϵ are the pressure and specific internal energy, respectively. The "thermal" part of the EOS is given by

$$p_{\rm th} = \rho\,\epsilon_{\rm th}\,(\Gamma_{\rm th} - 1)\,, \qquad \epsilon_{\rm th} = \epsilon - \epsilon_{\rm c}\,, \qquad (4)$$

where $\Gamma_{\rm th} = 1.75$.

arXiv:1912.09340v1

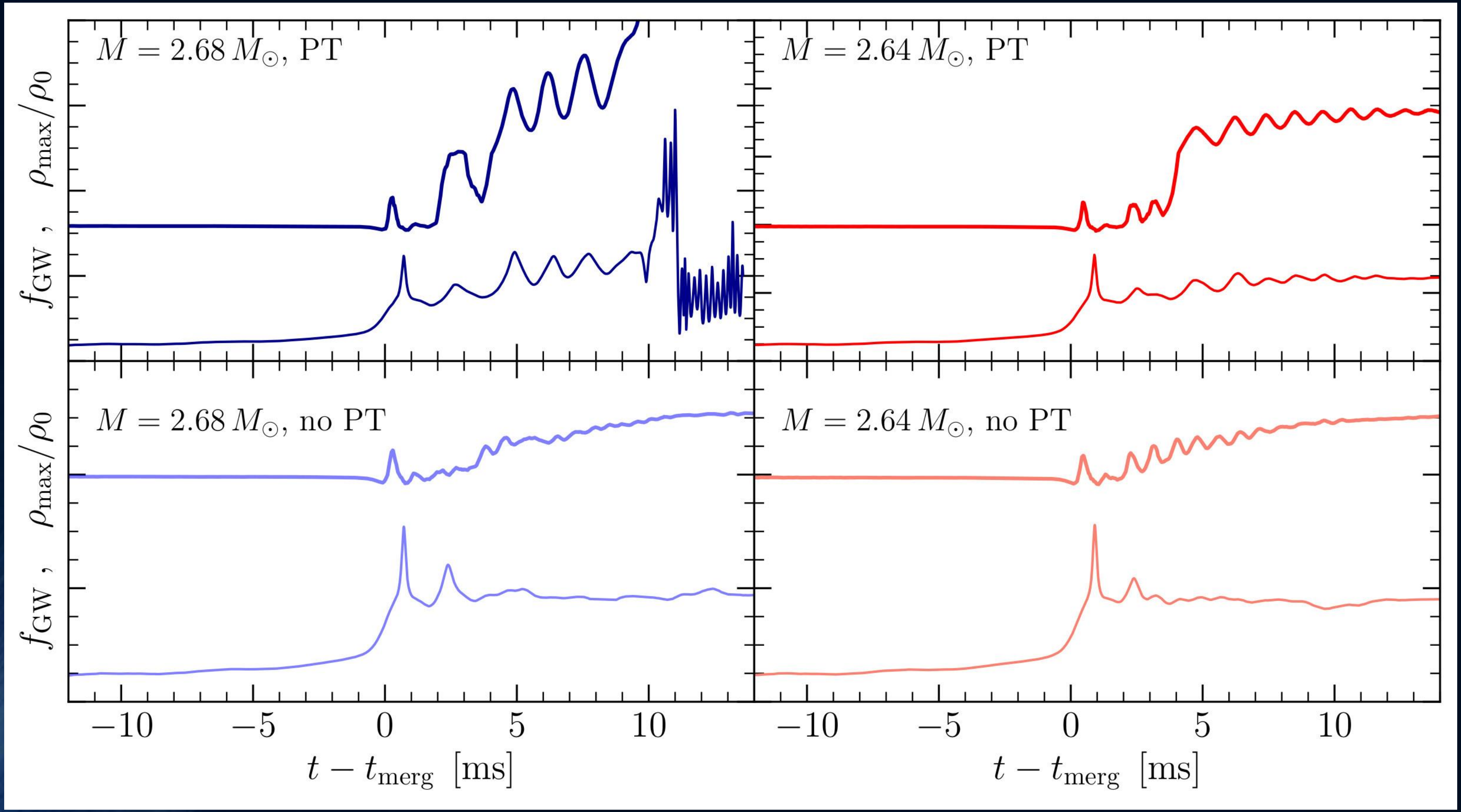

Evolution of the central rest-mass density (top)
and instantaneous gravitational wave frequency (bottom).

arXiv:1912.09340v1

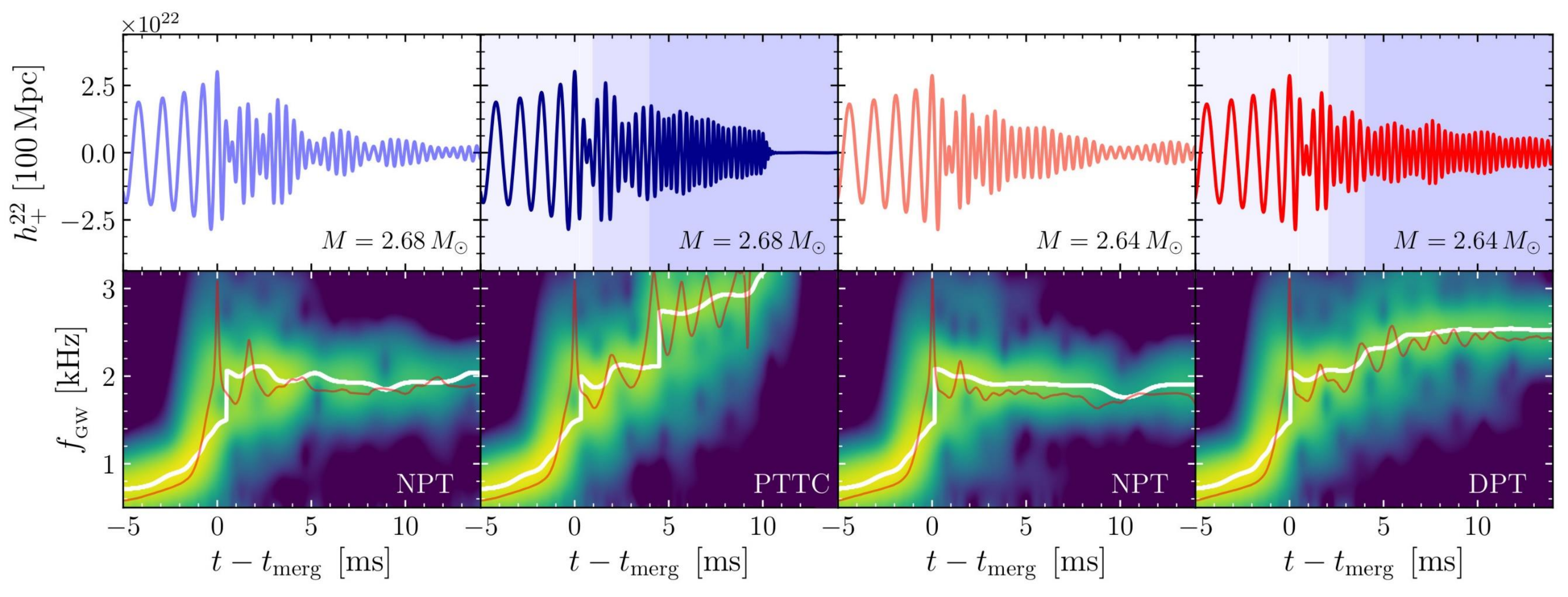

Strain h+ (top) and its spectrogram (bottom) for the four BNSs considered. In the top panels the different shadings mark the times when the HMNS core enters the mixed and quark phases the NPT models are always purely hadronic. In the bottom panels, the white lines trace the maximum of the spectrograms, while the red lines show the instantaneous gravitational-wave frequency.

In frequency space

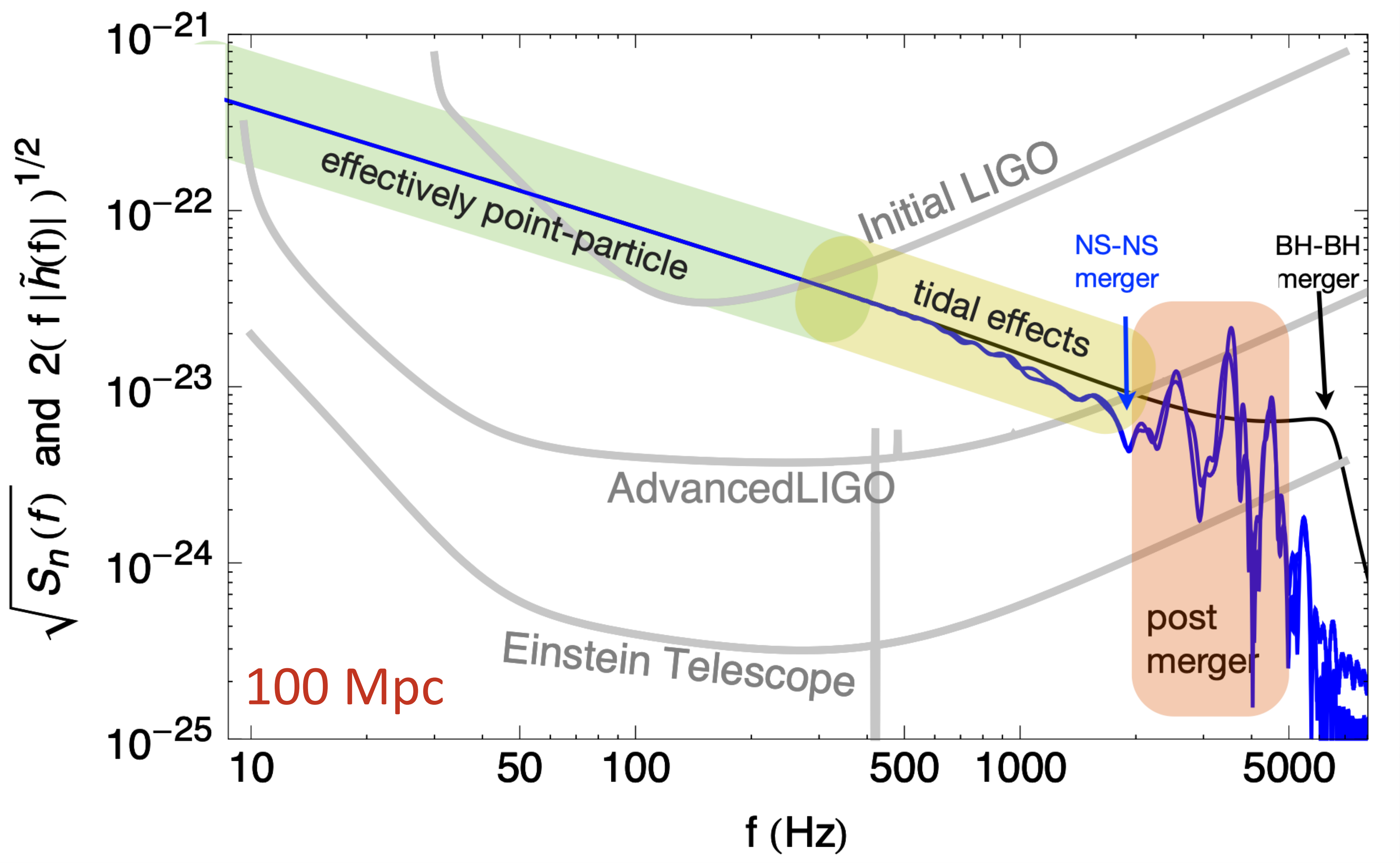

Read et al. (2013)

DPT

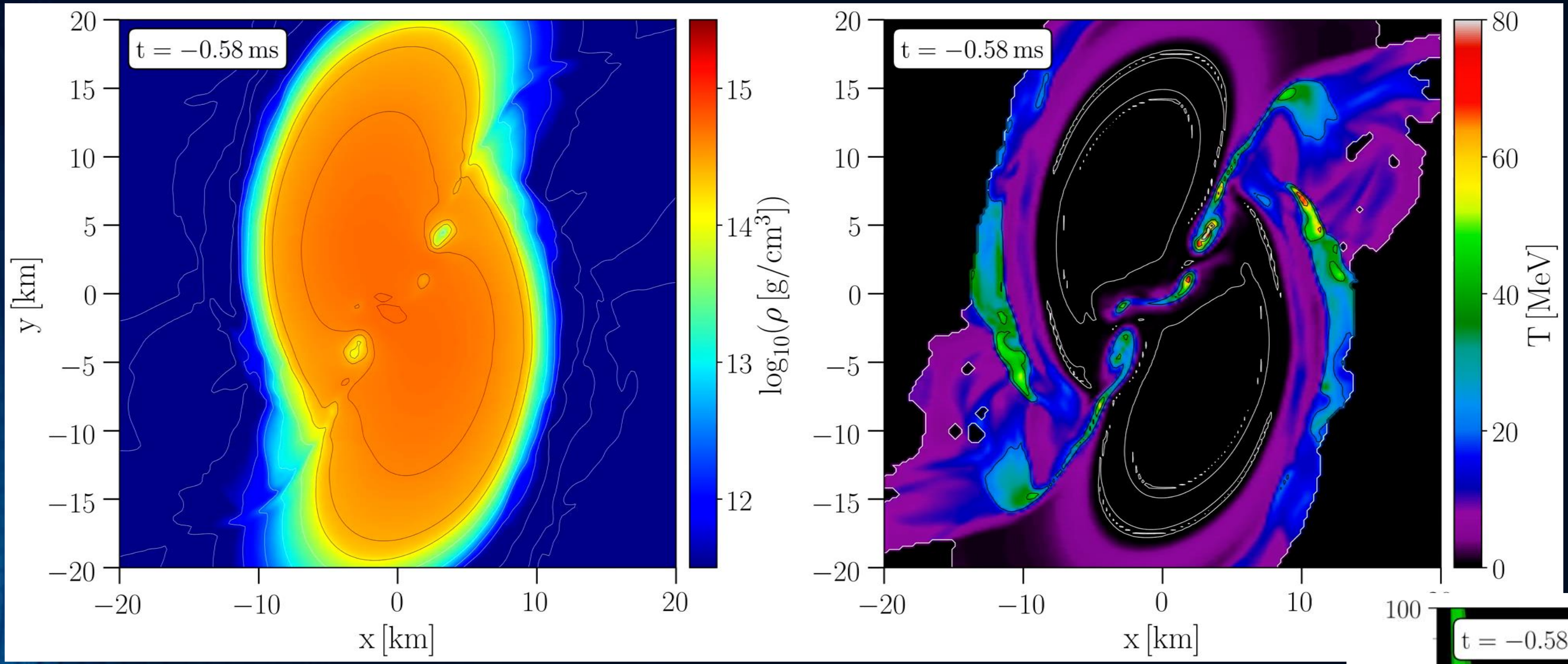

t = −0.58 ms
t = −0.58 ms
y [km]
x [km]
x [km]
$\log_{10}(\rho\,[\mathrm{g/cm^3}])$
T [MeV]

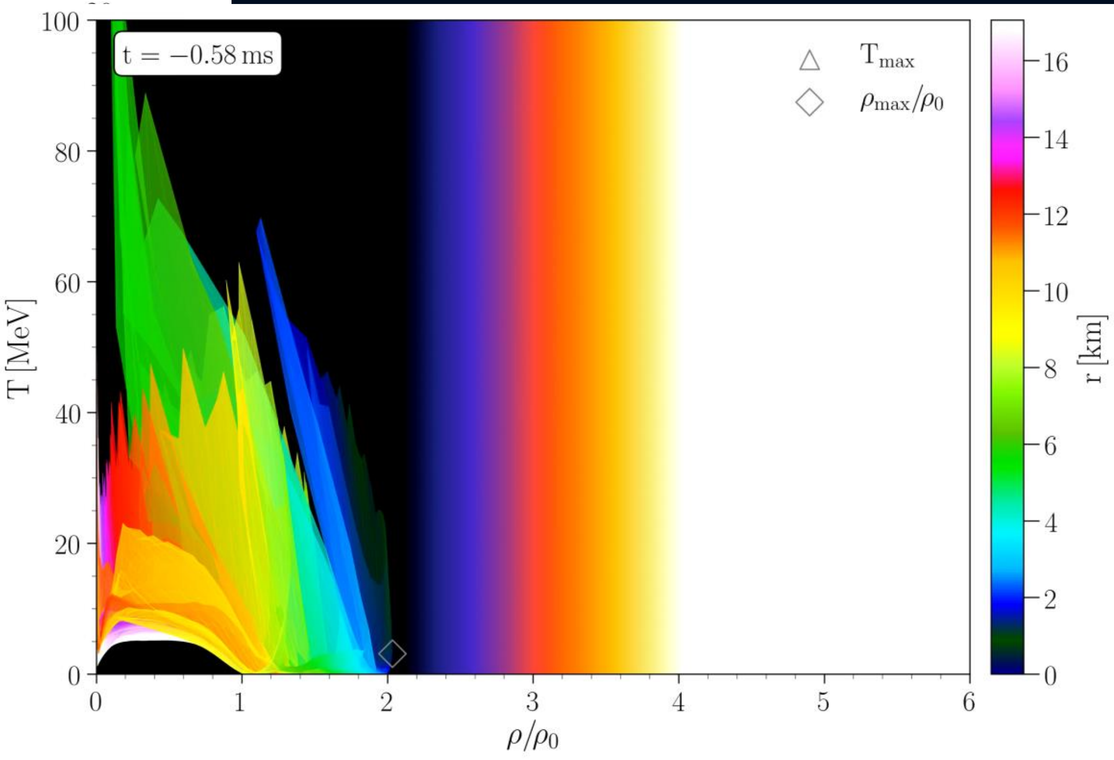

t = −0.58 ms
T_{max}
ρ_{max}/ρ_0
T [MeV]
ρ/ρ_0
r [km]

DPT

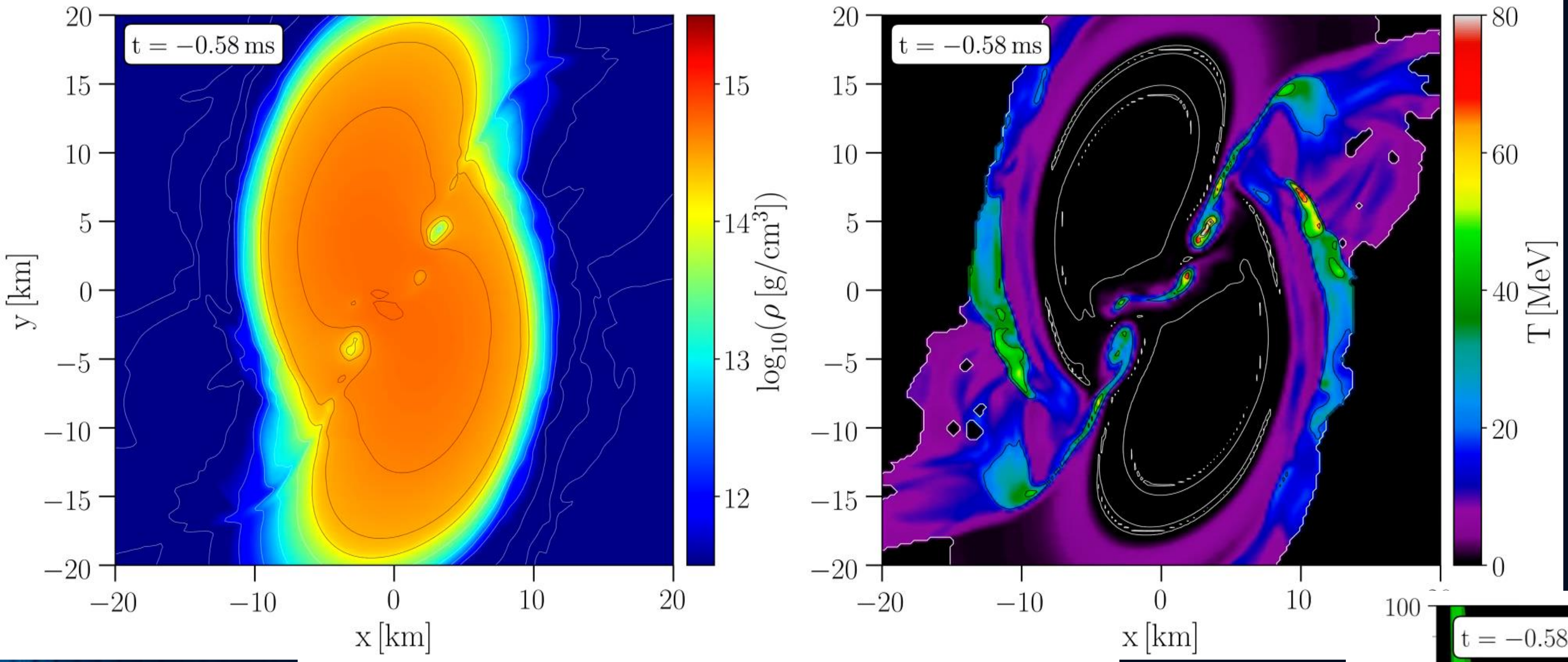

t = −0.58 ms
y [km]
x [km]
log10(ρ [g/cm3])
t = −0.58 ms
x [km]
T [MeV]

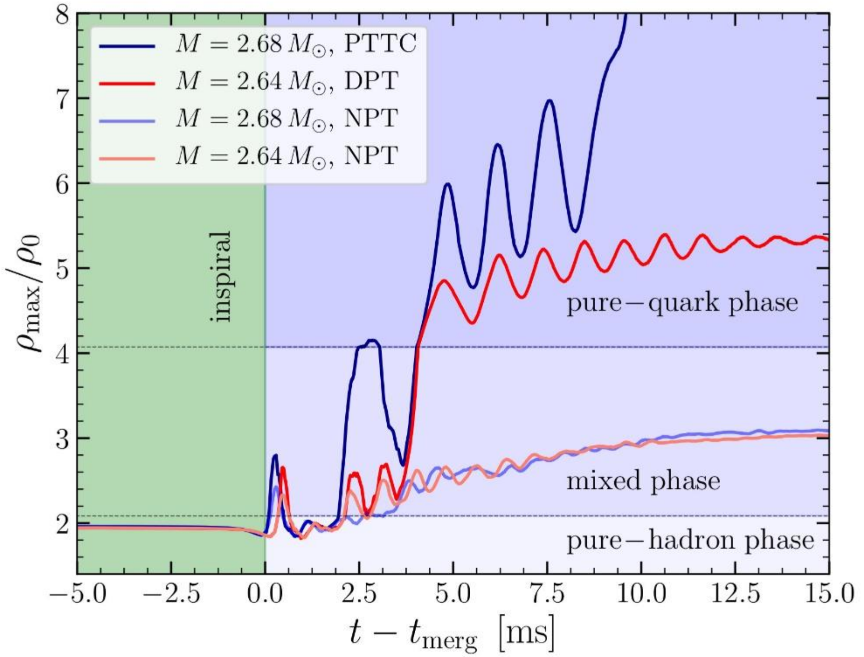

M = 2.68 M⊙, PTTC
M = 2.64 M⊙, DPT
M = 2.68 M⊙, NPT
M = 2.64 M⊙, NPT
inspiral
pure−quark phase
mixed phase
pure−hadron phase
ρmax/ρ0
t − tmerg [ms]

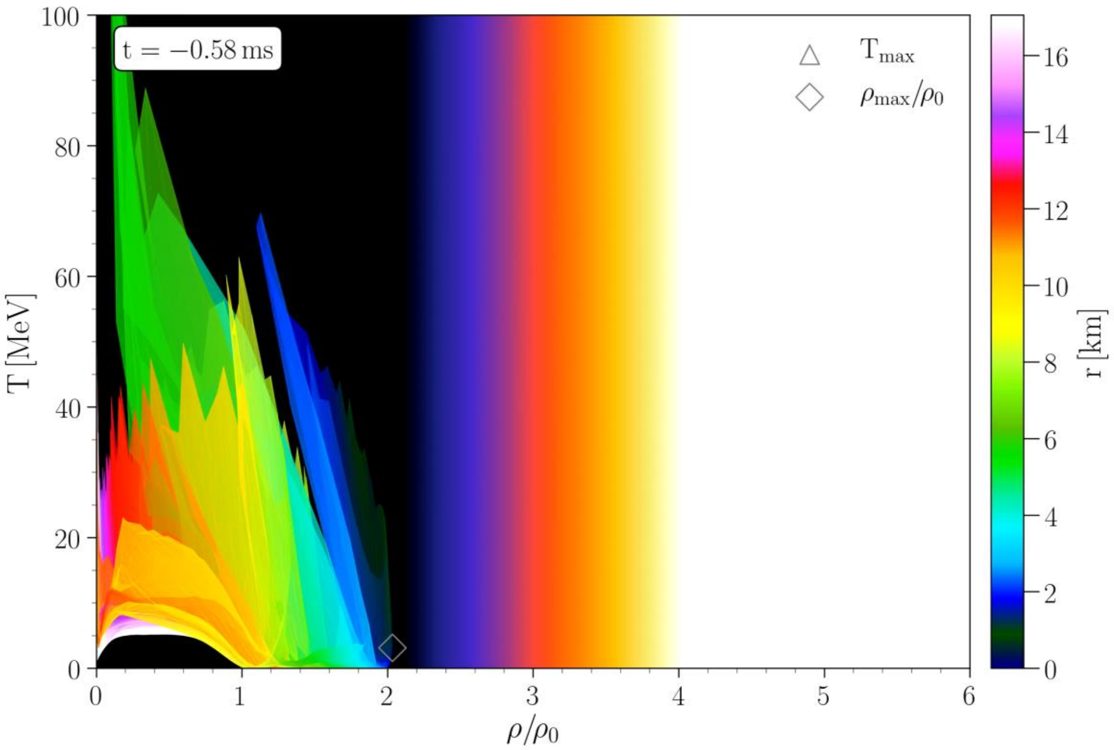

t = −0.58 ms
Tmax
ρmax/ρ0
T [MeV]
ρ/ρ0
r [km]

NPT

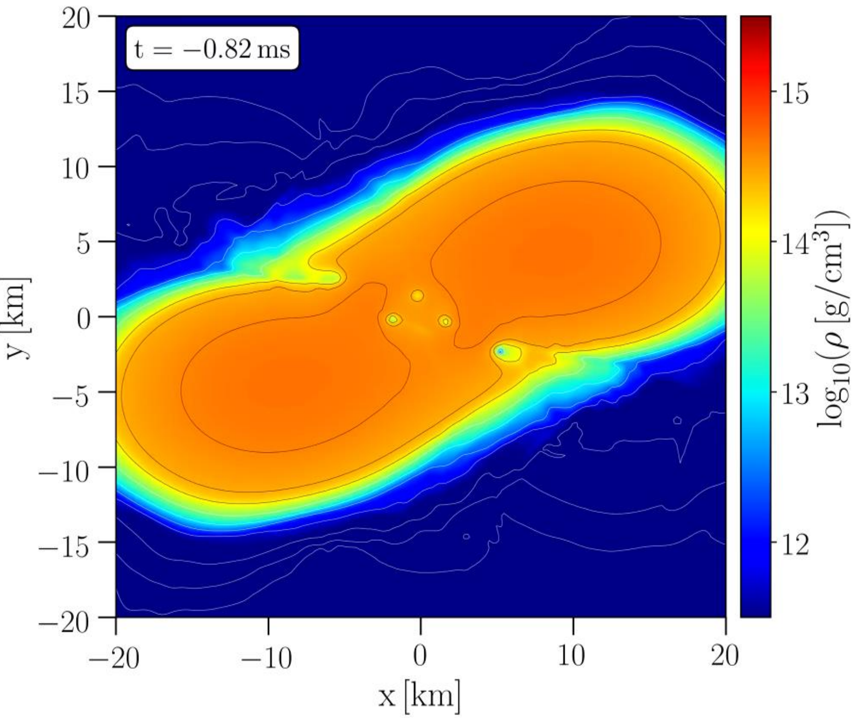

t = −0.82 ms
y [km]
x [km]
$\log_{10}(\rho\,[\mathrm{g/cm^3}])$

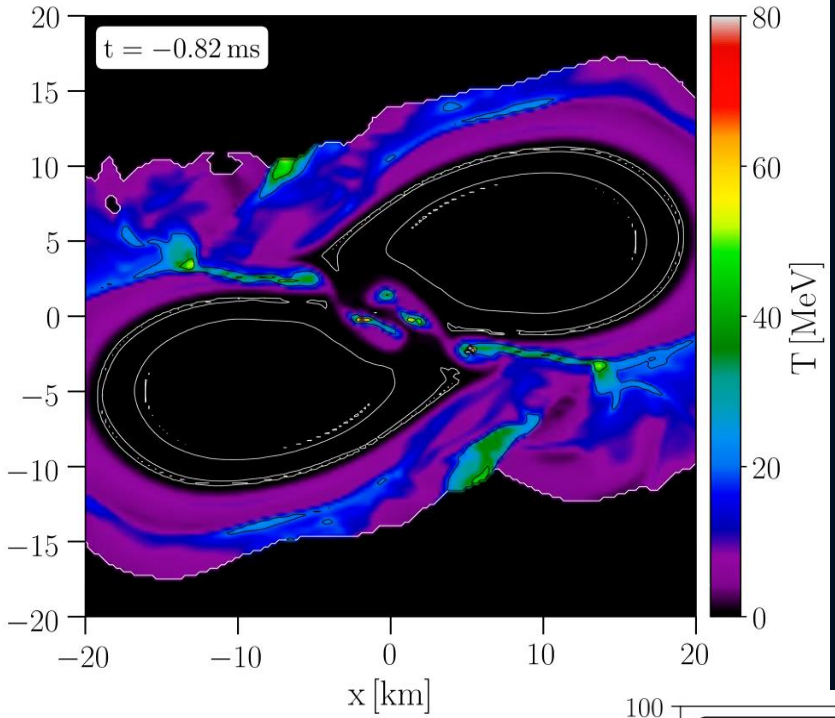

t = −0.82 ms
x [km]
T [MeV]

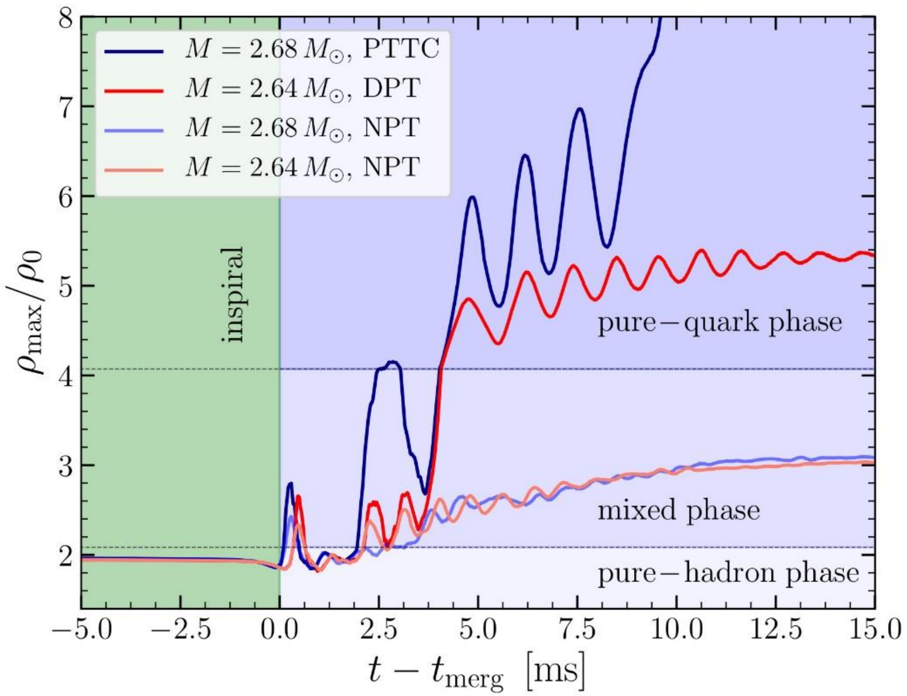

$M = 2.68\,M_\odot$, PTTC
$M = 2.64\,M_\odot$, DPT
$M = 2.68\,M_\odot$, NPT
$M = 2.64\,M_\odot$, NPT
inspiral
pure−quark phase
mixed phase
pure−hadron phase
$\rho_{\max}/\rho_0$
$t - t_{\rm merg}$ [ms]

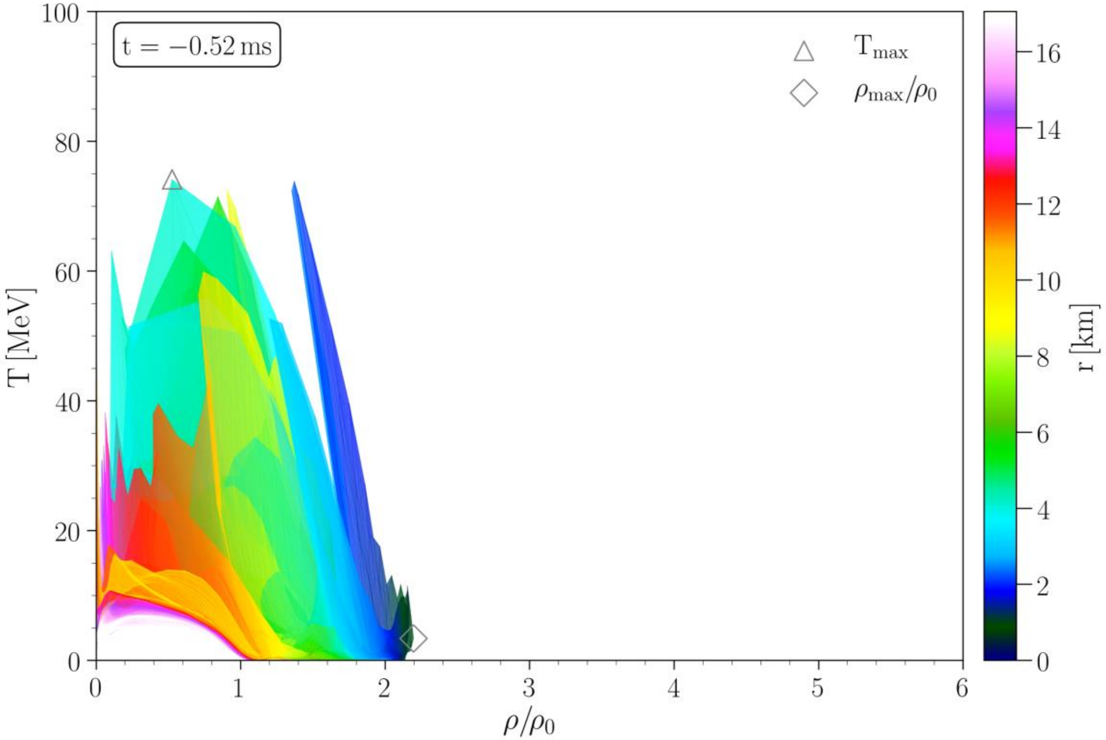

t = −0.52 ms
$T_{\max}$
$\rho_{\max}/\rho_0$
T [MeV]
ρ/ρ_0
r [km]

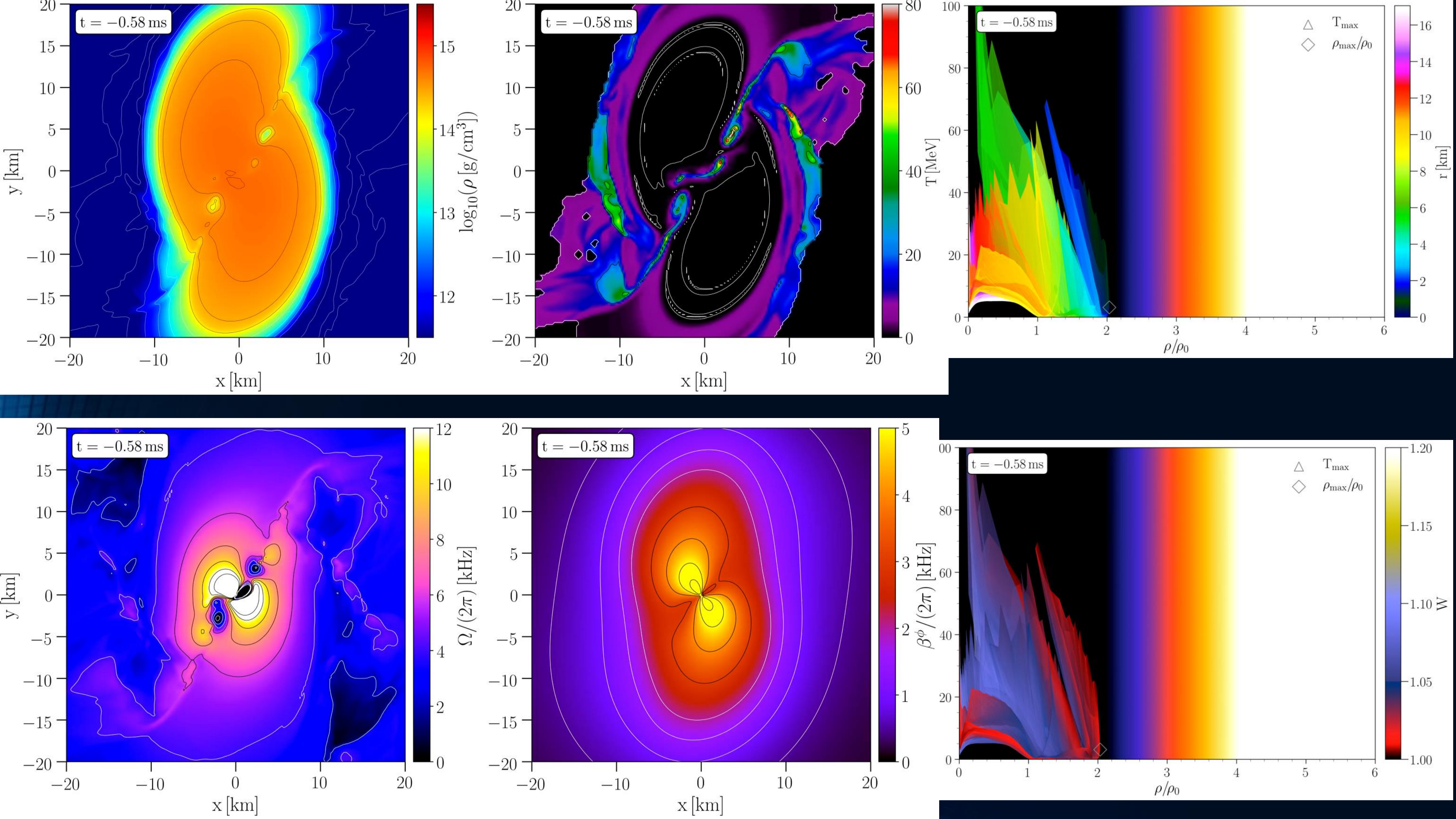
t = −0.58 ms
x [km]
y [km]
log10(ρ [g/cm3])
T [MeV]
ρ/ρ0
r [km]
Tmax
ρmax/ρ0
Ω/(2π) [kHz]
β^φ/(2π) [kHz]
W

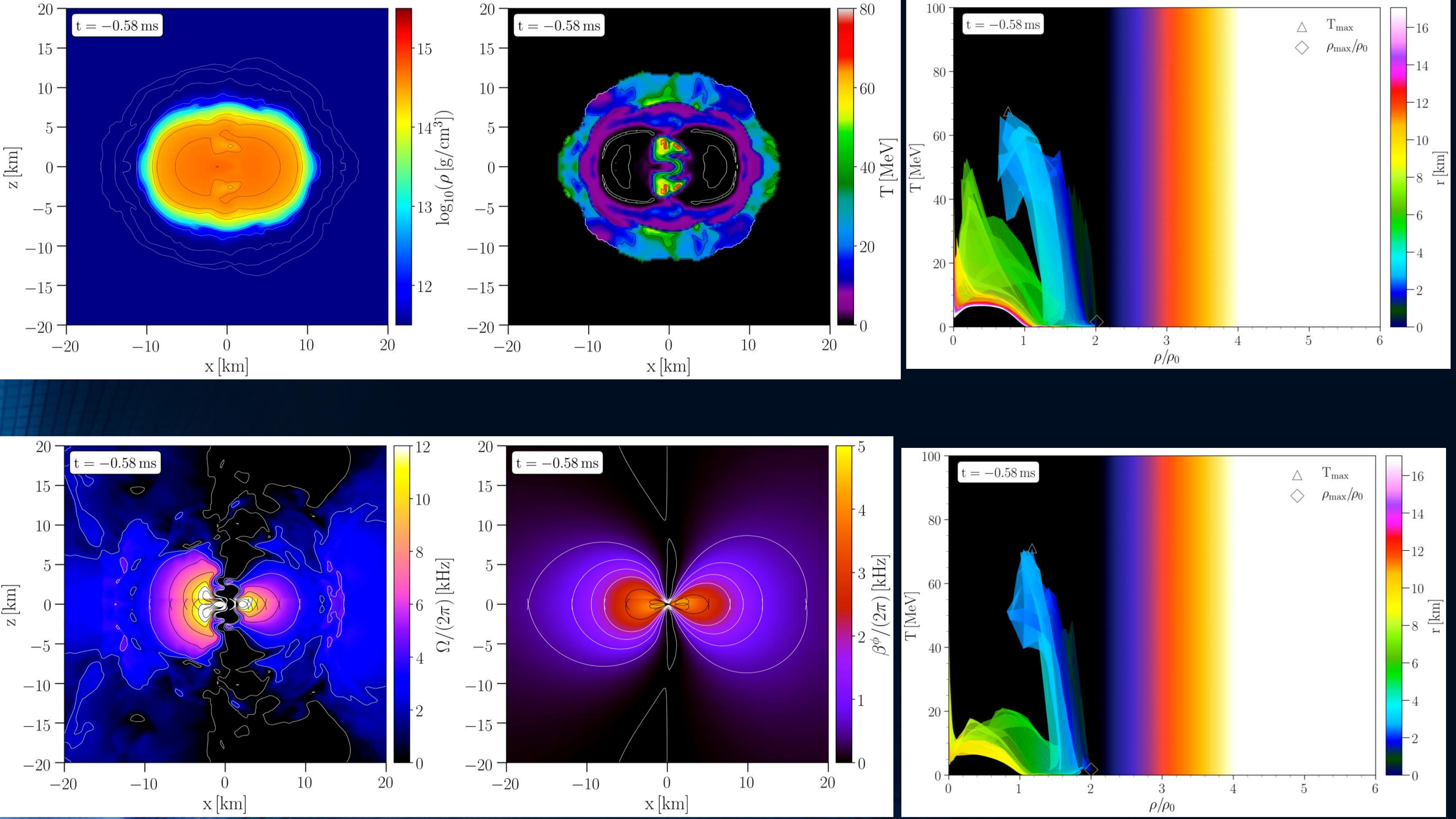
t = −0.58 ms
z [km]
x [km]
log10(ρ [g/cm³])
T [MeV]
Ω/(2π) [kHz]
β^φ/(2π) [kHz]
T [MeV]
ρ/ρ0
r [km]
T_max
ρ_max/ρ0

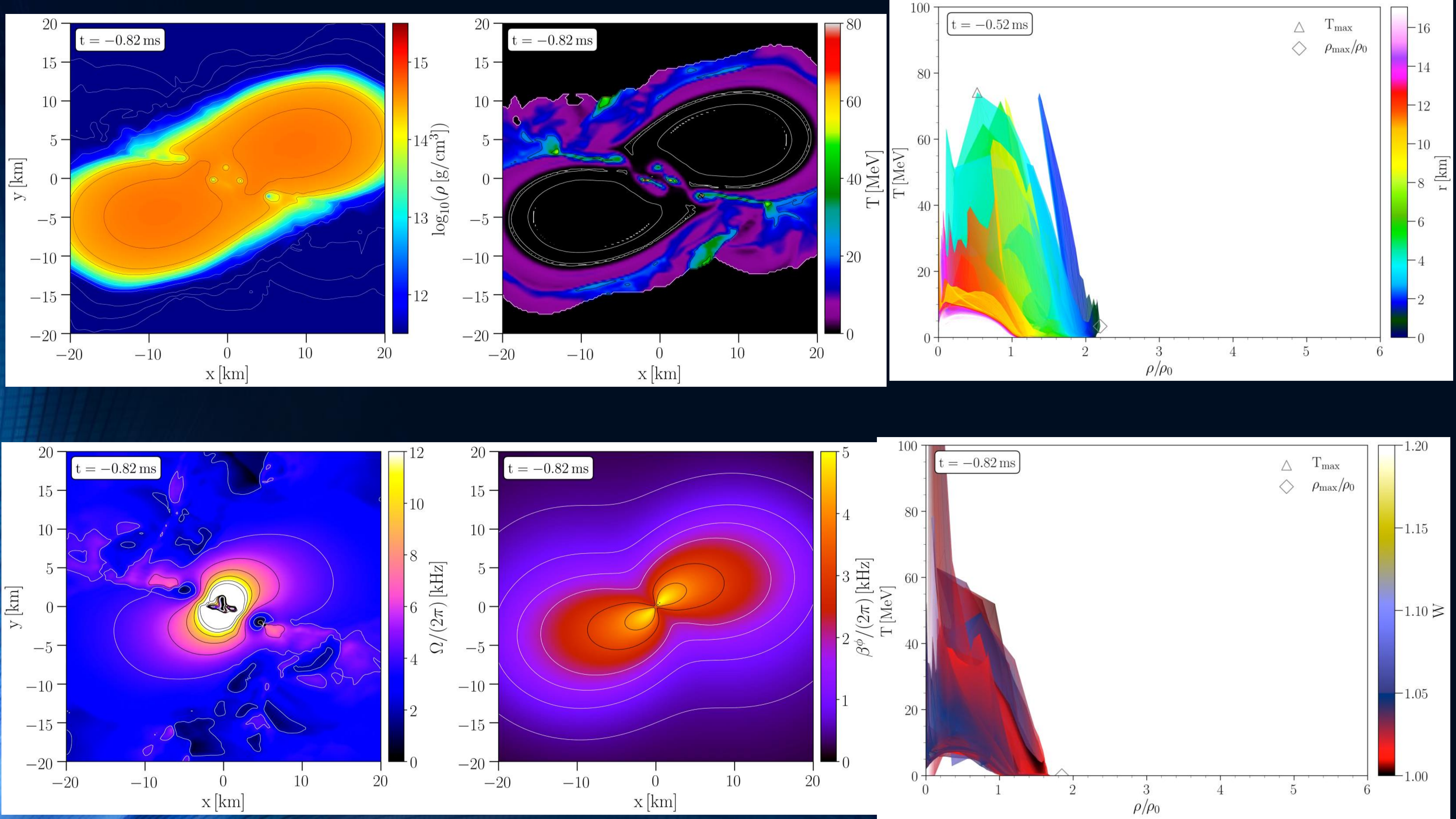

t = −0.82 ms
y [km]
x [km]
log10(ρ [g/cm³])
T [MeV]
t = −0.52 ms
T_max
ρ_max/ρ_0
ρ/ρ_0
r [km]
Ω/(2π) [kHz]
β^φ/(2π) [kHz]
W

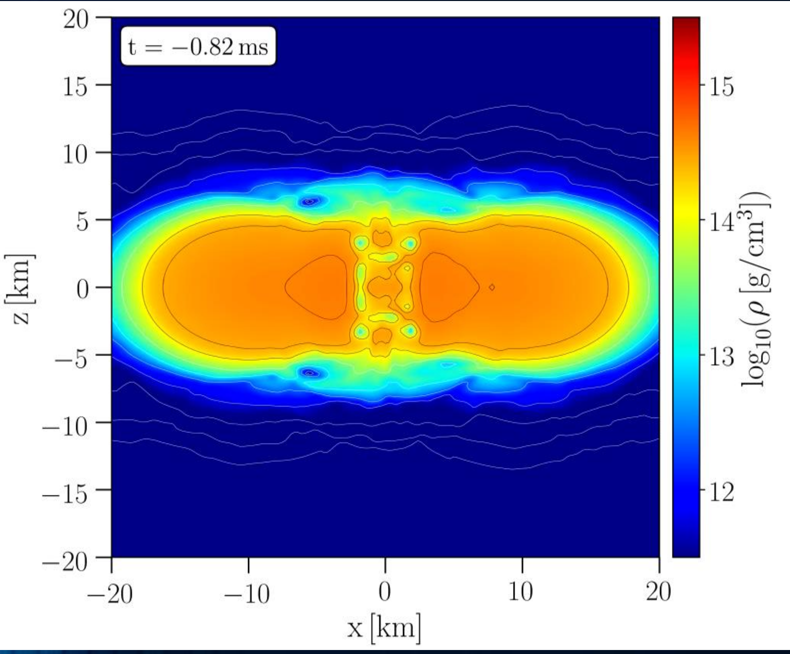
t = −0.82 ms
z [km]
x [km]
log10(ρ [g/cm3])
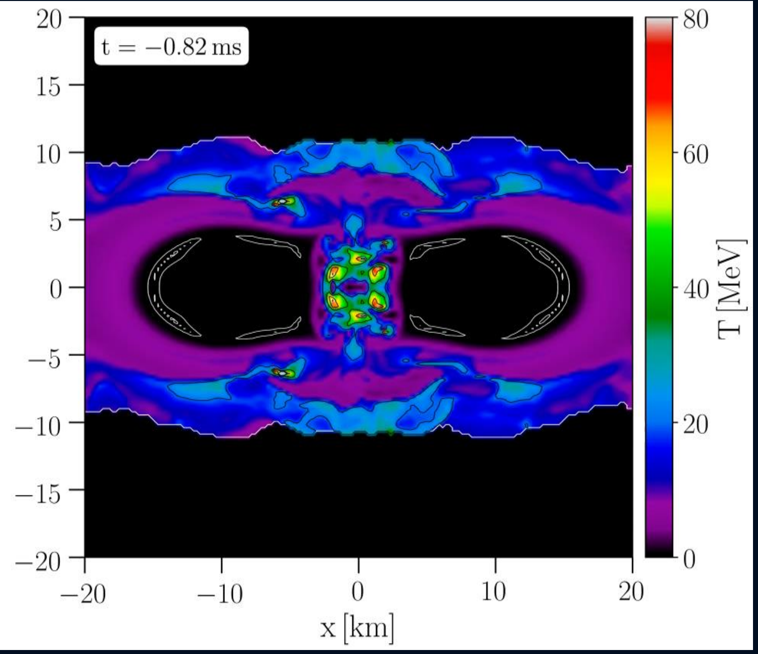
t = −0.82 ms
x [km]
T [MeV]
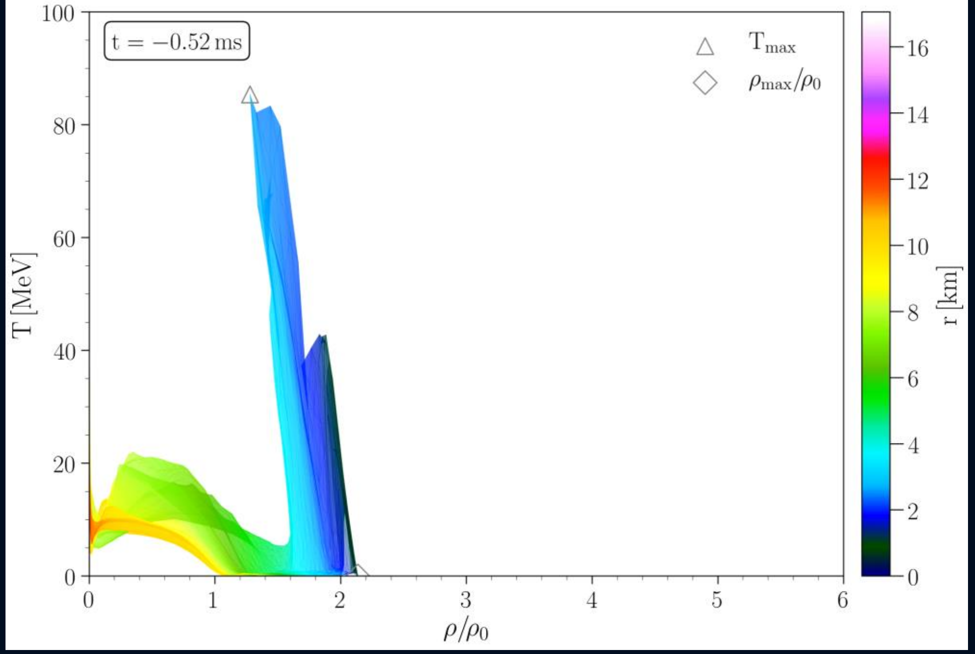
t = −0.52 ms
T_max
ρ_max/ρ_0
T [MeV]
ρ/ρ_0
r [km]
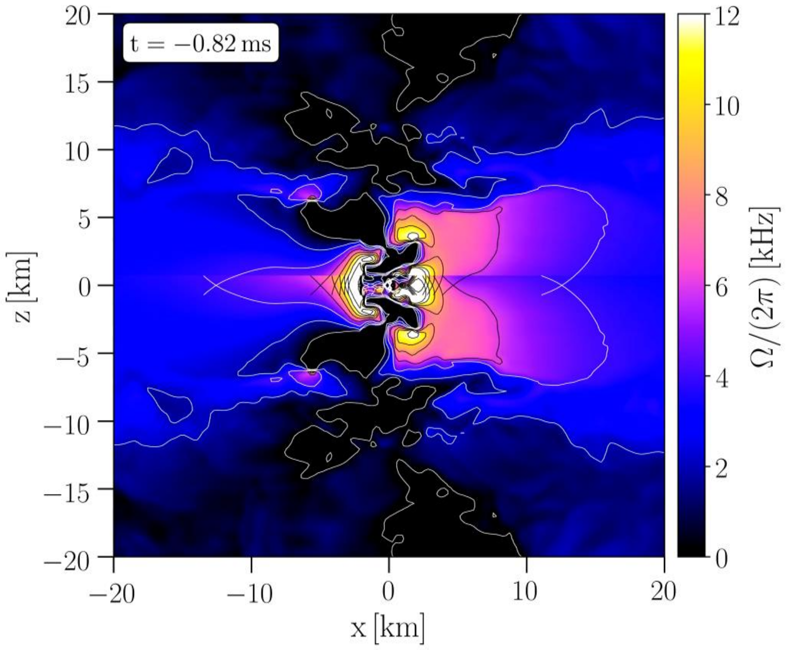
t = −0.82 ms
z [km]
x [km]
Ω/(2π) [kHz]
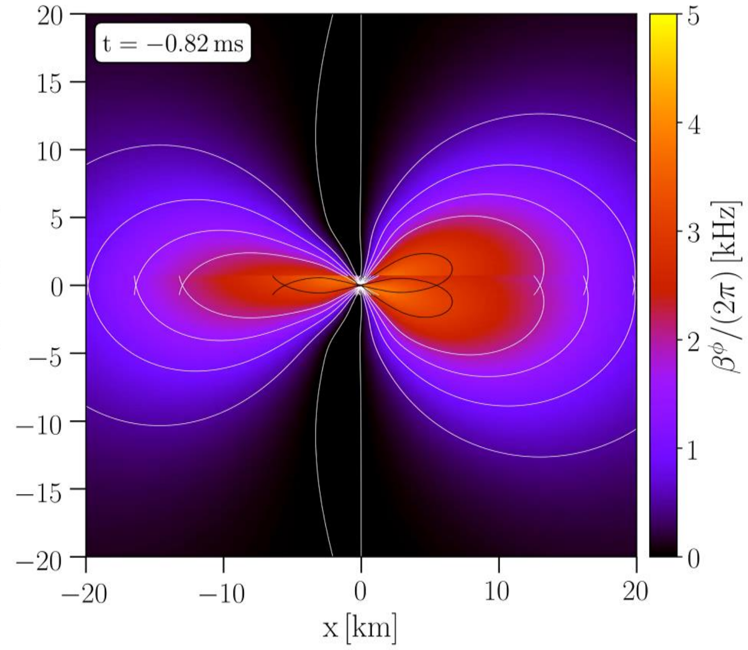
t = −0.82 ms
x [km]
β^φ/(2π) [kHz]

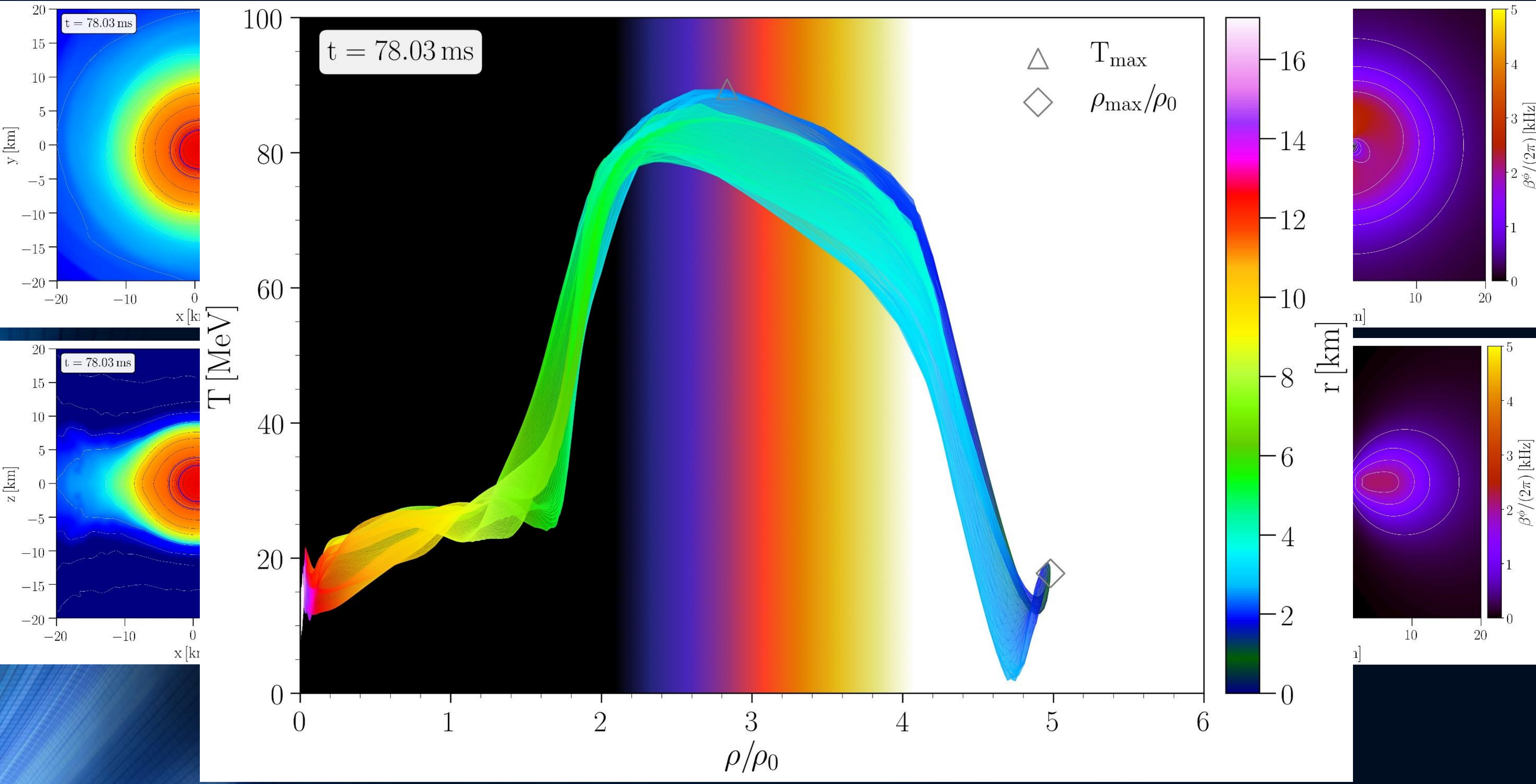

t = 78.03 ms
T_{max}
ρ_{max}/ρ_0
T [MeV]
ρ/ρ_0
r [km]
y [km]
z [km]
x [km]
$\beta^\phi/(2\pi)$ [kHz]

Gravitational-wave emissiom

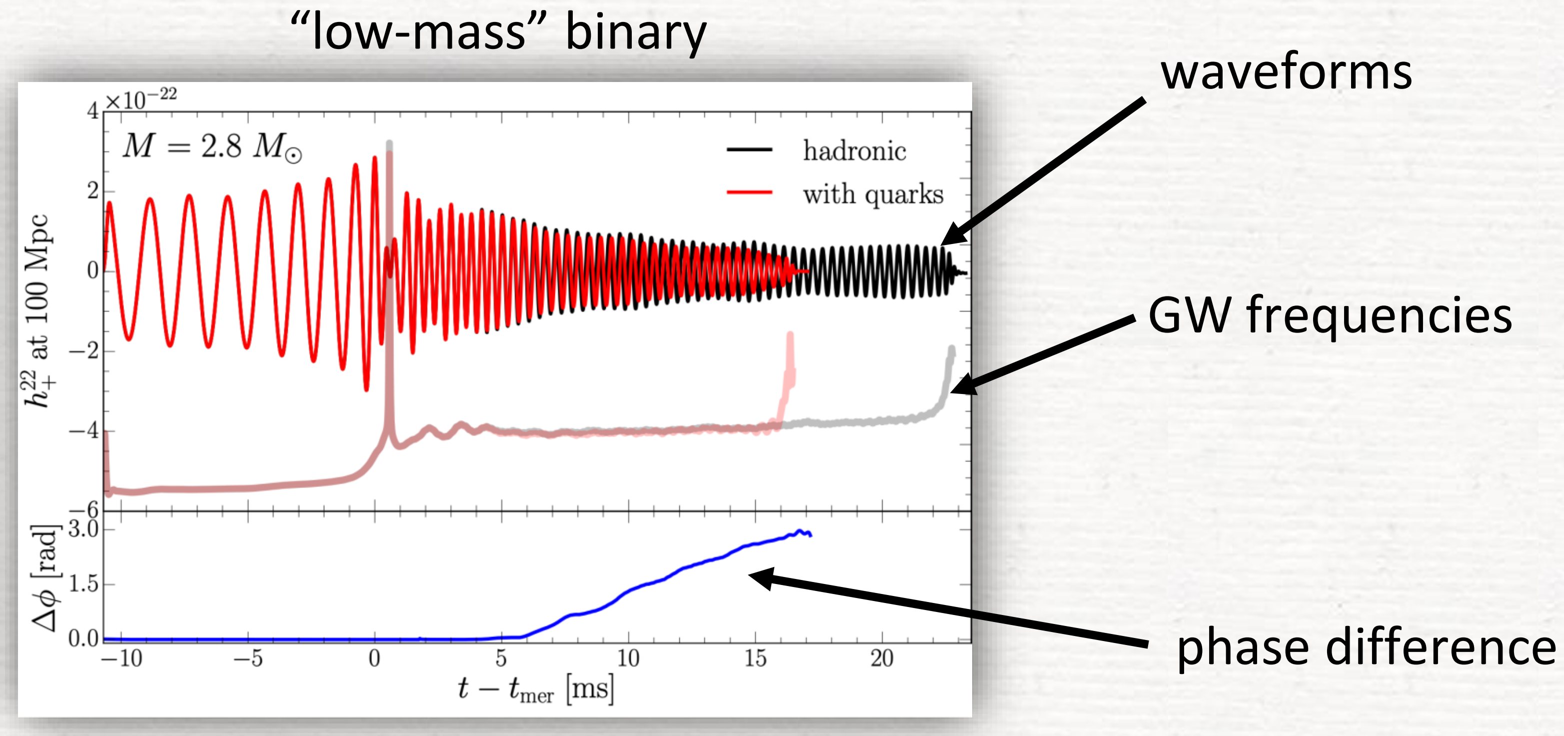

- In **low-mass binary**, after ~ 5 ms, quark fraction is large enough to change quadrupole moment and yield differences in the waveforms.
- Note the phase difference is **zero** in the inspiral.
- Sudden softening of the phase transition leads to collapse and **large difference** in phase evolution.

Gravitational-wave emissiom

"low-mass" binary "high-mass" binary

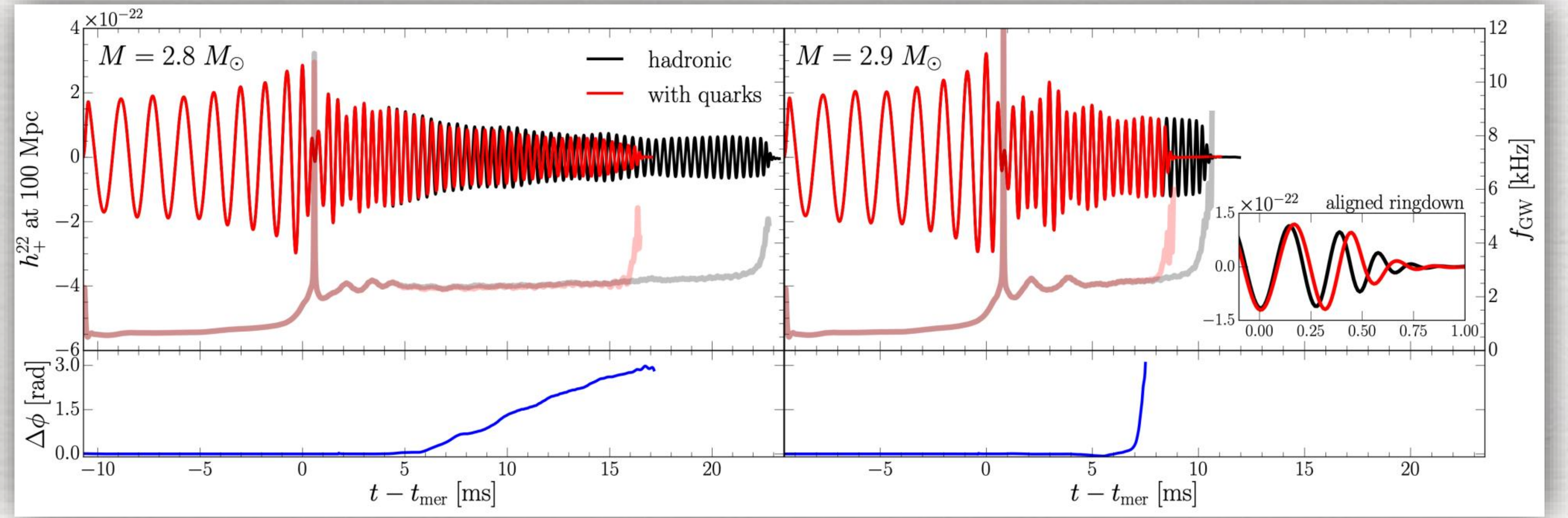

- In **low-mass binary**, after ~ 5 ms, quark fraction is large enough to change quadrupole moment and yield differences in the waveforms.
- In **high-mass binary**, phase transition takes place rapidly after ~ 5 ms.
- Waveforms are similar but **ringdown** is different (free fall for PT).

Observing mismatch between **inspiral** (fully hadronic) and **post-merger** (phase transition): clear signature of a PT.

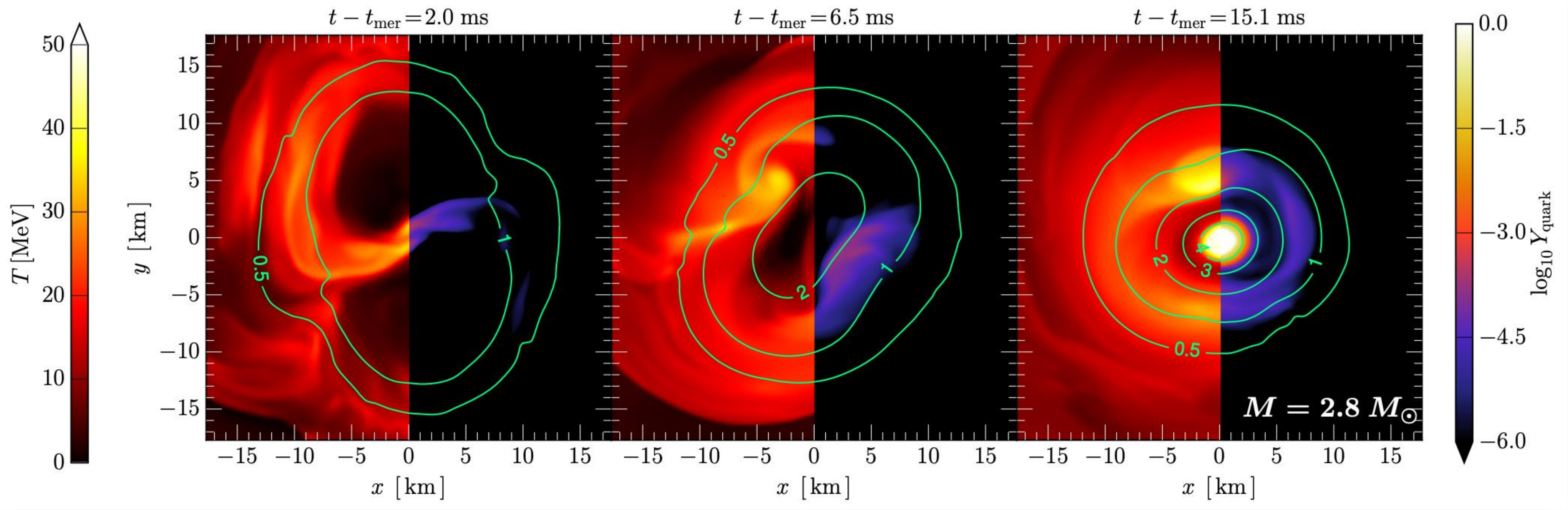

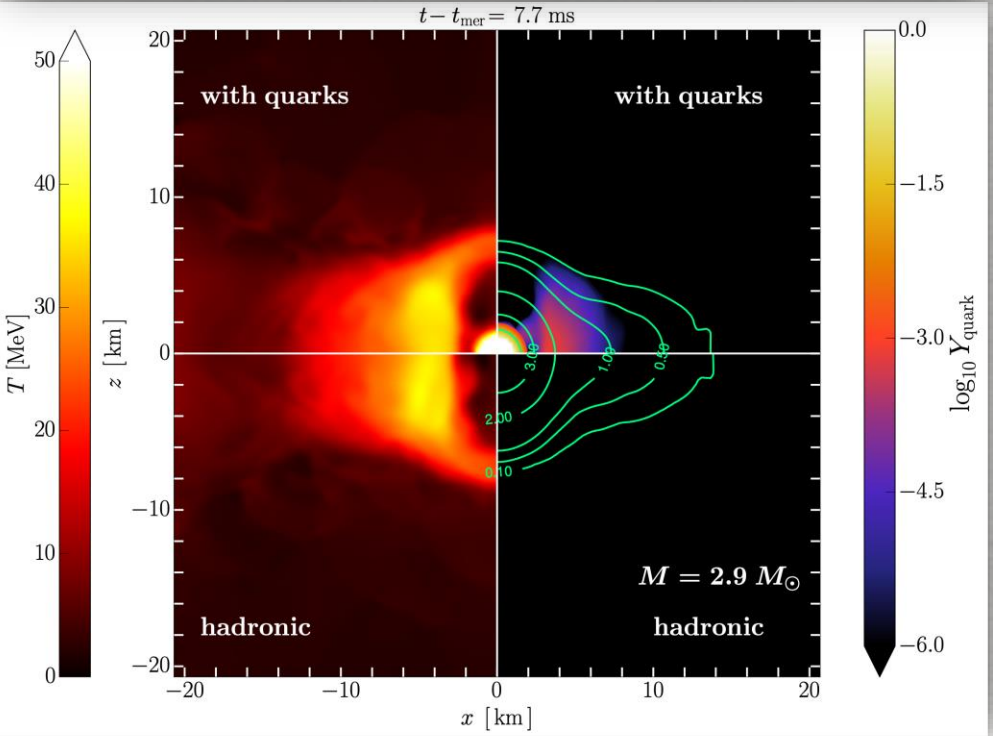

- EOS based on Chiral Mean Field (CMF) model, based on a nonlinear SU(3) sigma model.
- Quarks appear at sufficiently large temperatures and densities.
- For EOS without quarks, the dynamics is very similar, but no PT.

Binary Hybrid Star Mergers and the QCD Phase Diagram

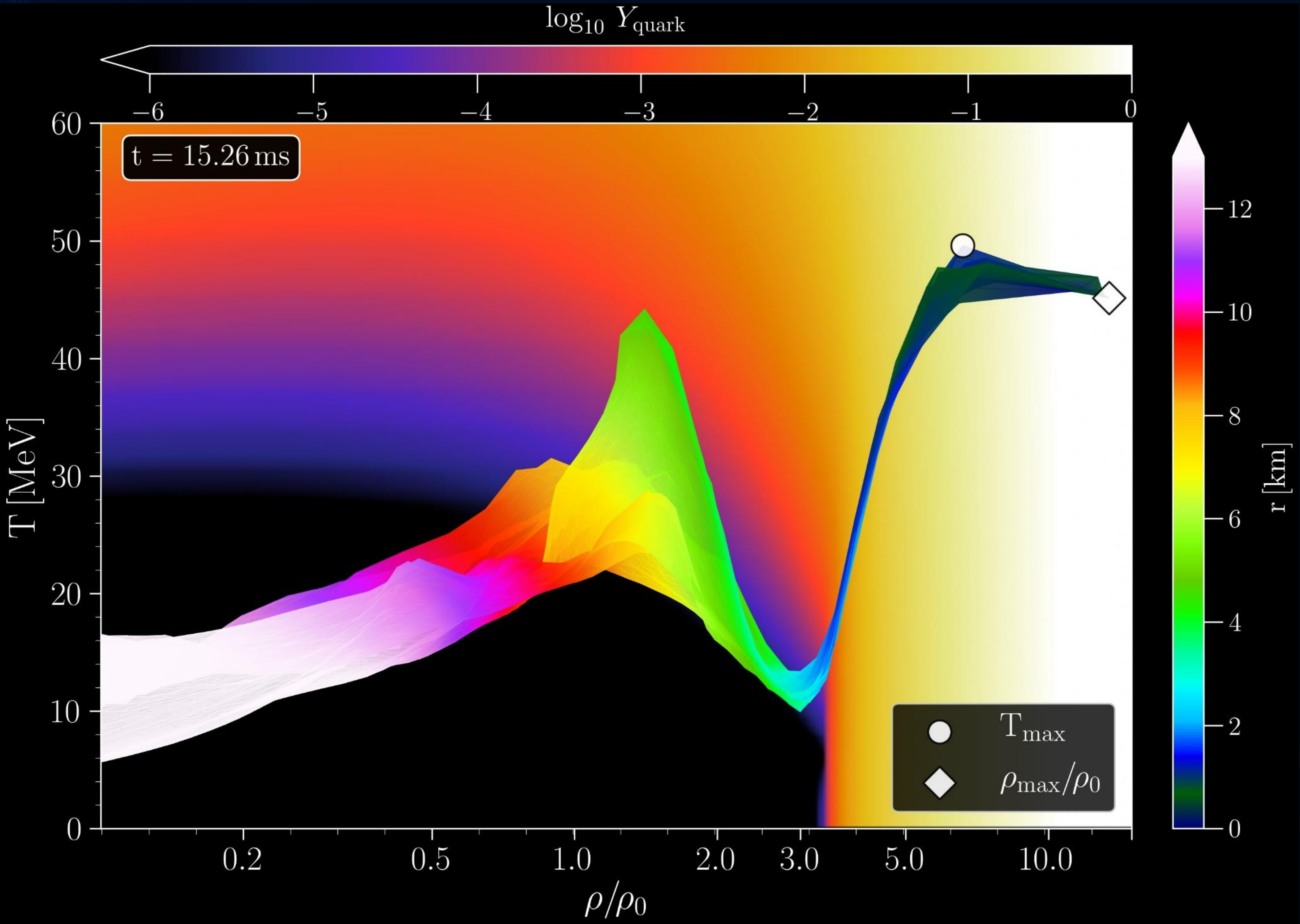

Hot and dense matter inside the inner area of a collapsing hypermassive hybrid star in the style of a (T- ρ) QCD phase diagram plot at a time right before the apparent horizont is formed in its center

The color-coding (right side) indicate the radial position r of the corresponding (T- ρ) fluid element measured from the origin of the simulation (x , y) = (0 , 0) on the equatorial plane at z = 0.
The color-coding (top) indicates the fraction of deconfined quarks.

The open triangle marks the maximum value of the temperature while the open diamond indicates the maximum of the density.

Late Inspiral Phase

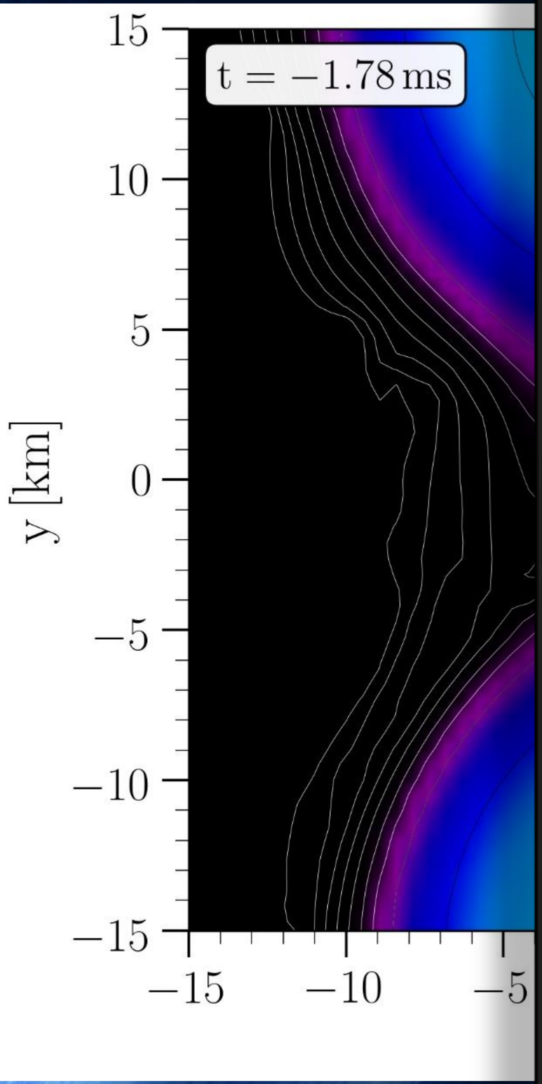

Rest mass density

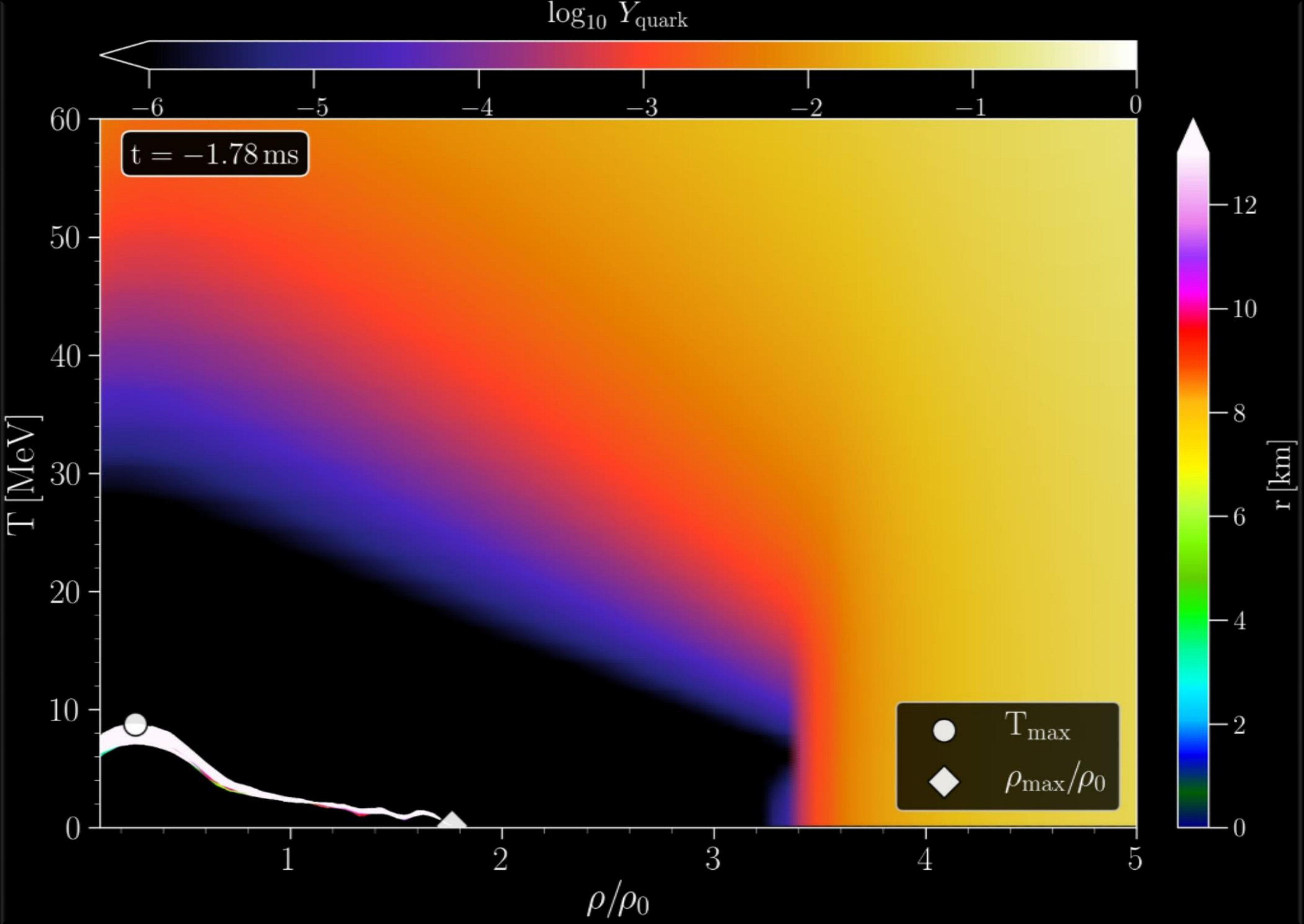

Merger Phase

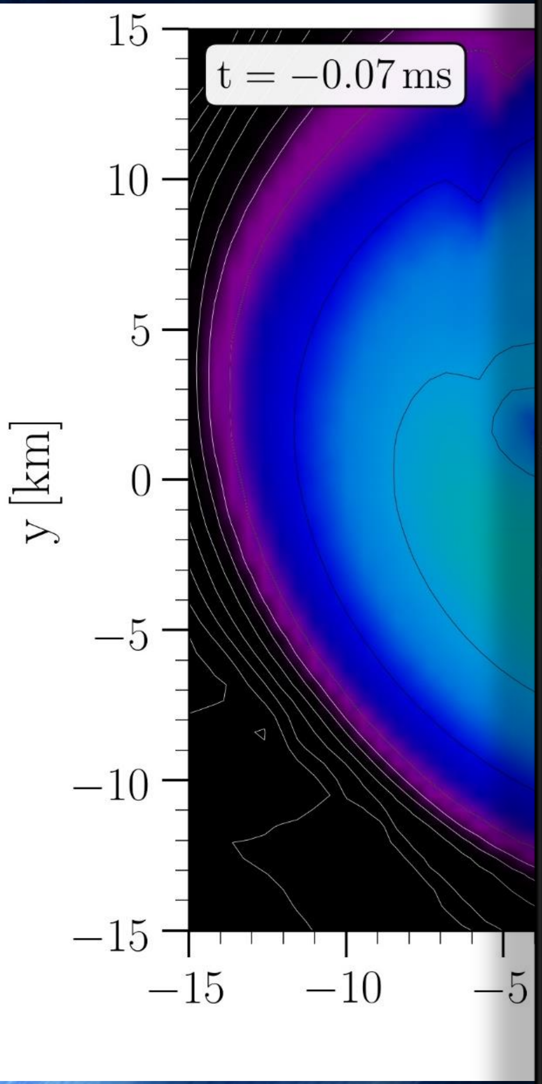

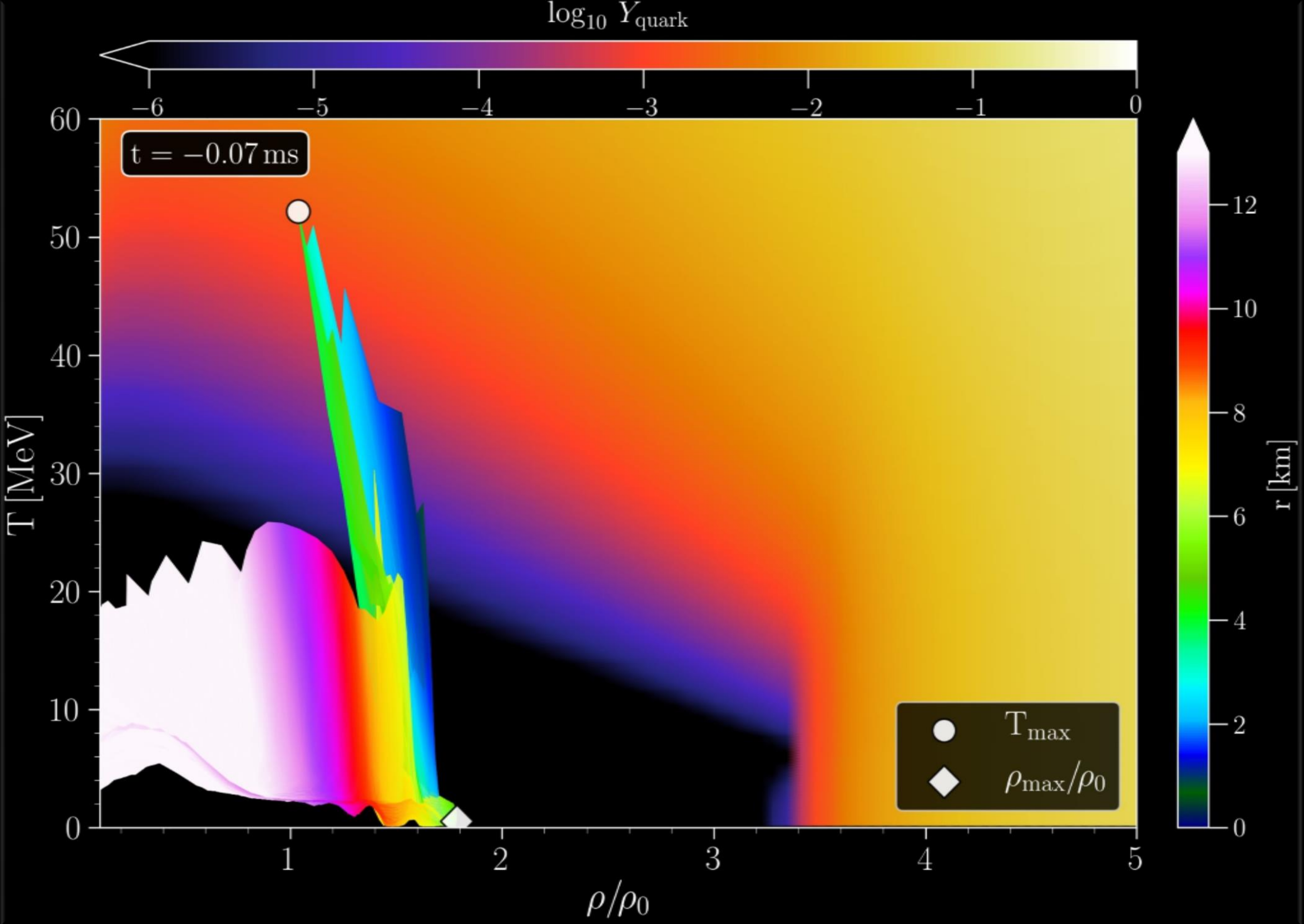

Rest mass density

Post Merger Phase

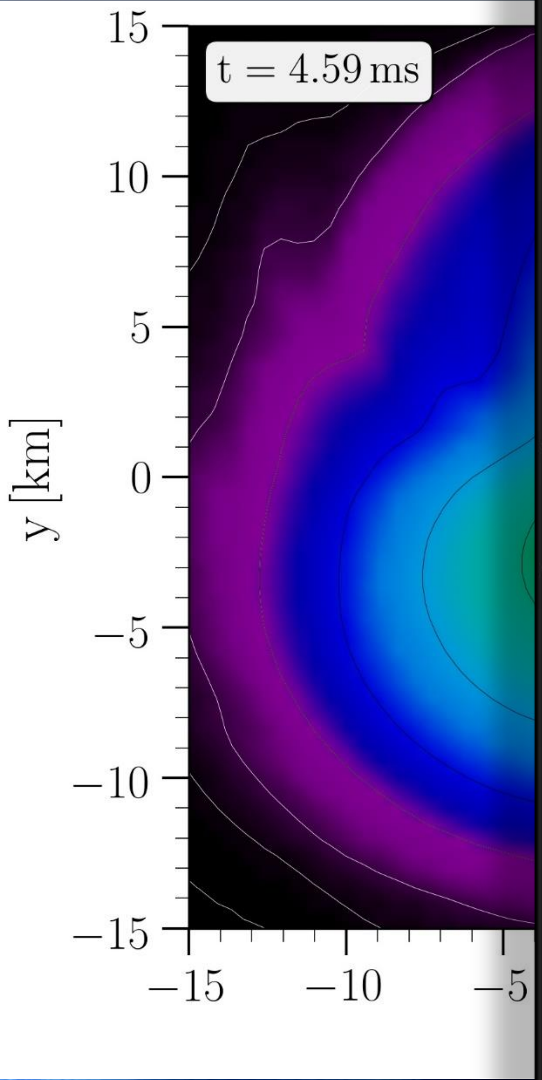

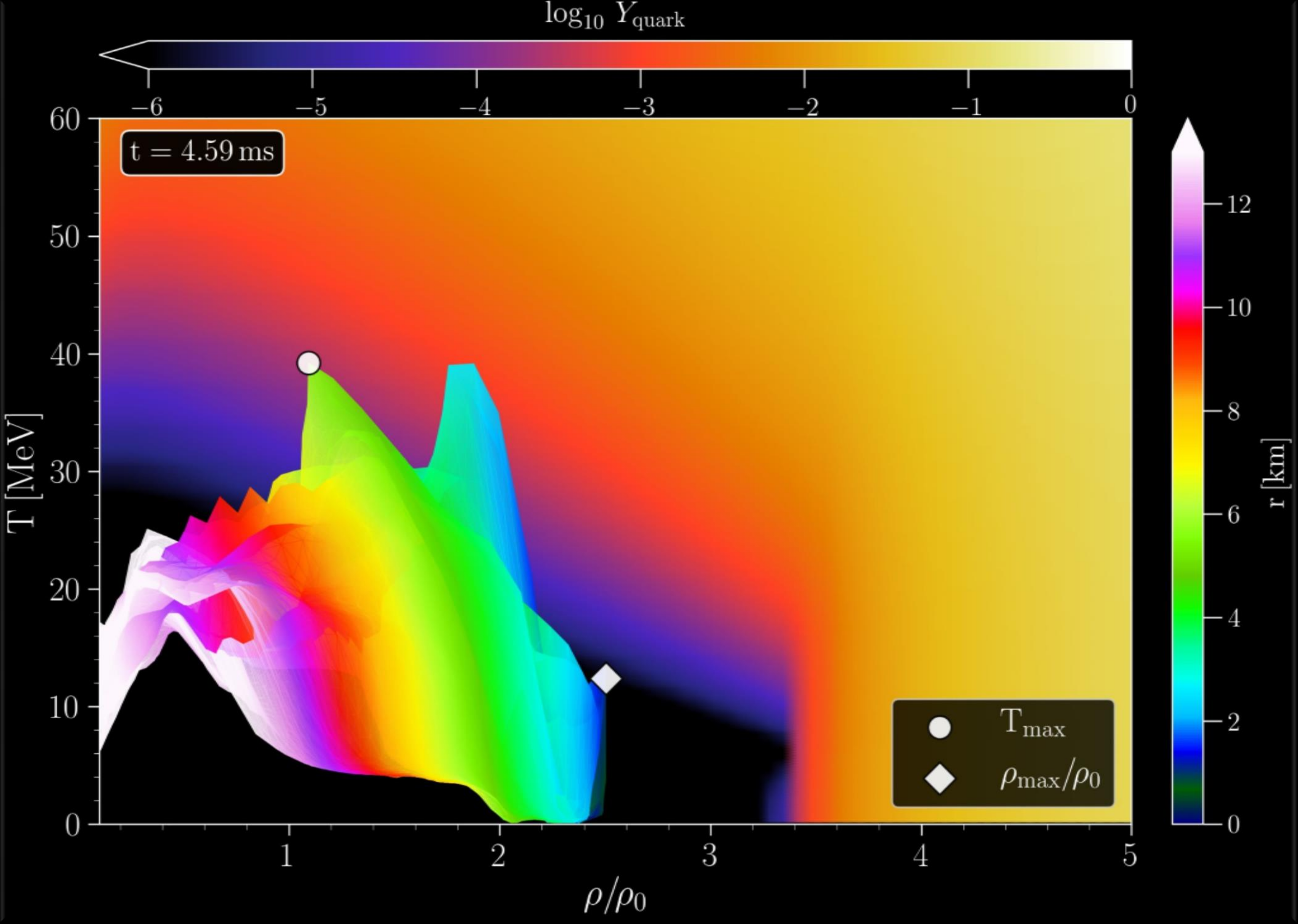

Rest mass density

Der Ereignishorizont eines Schwarzen Loches

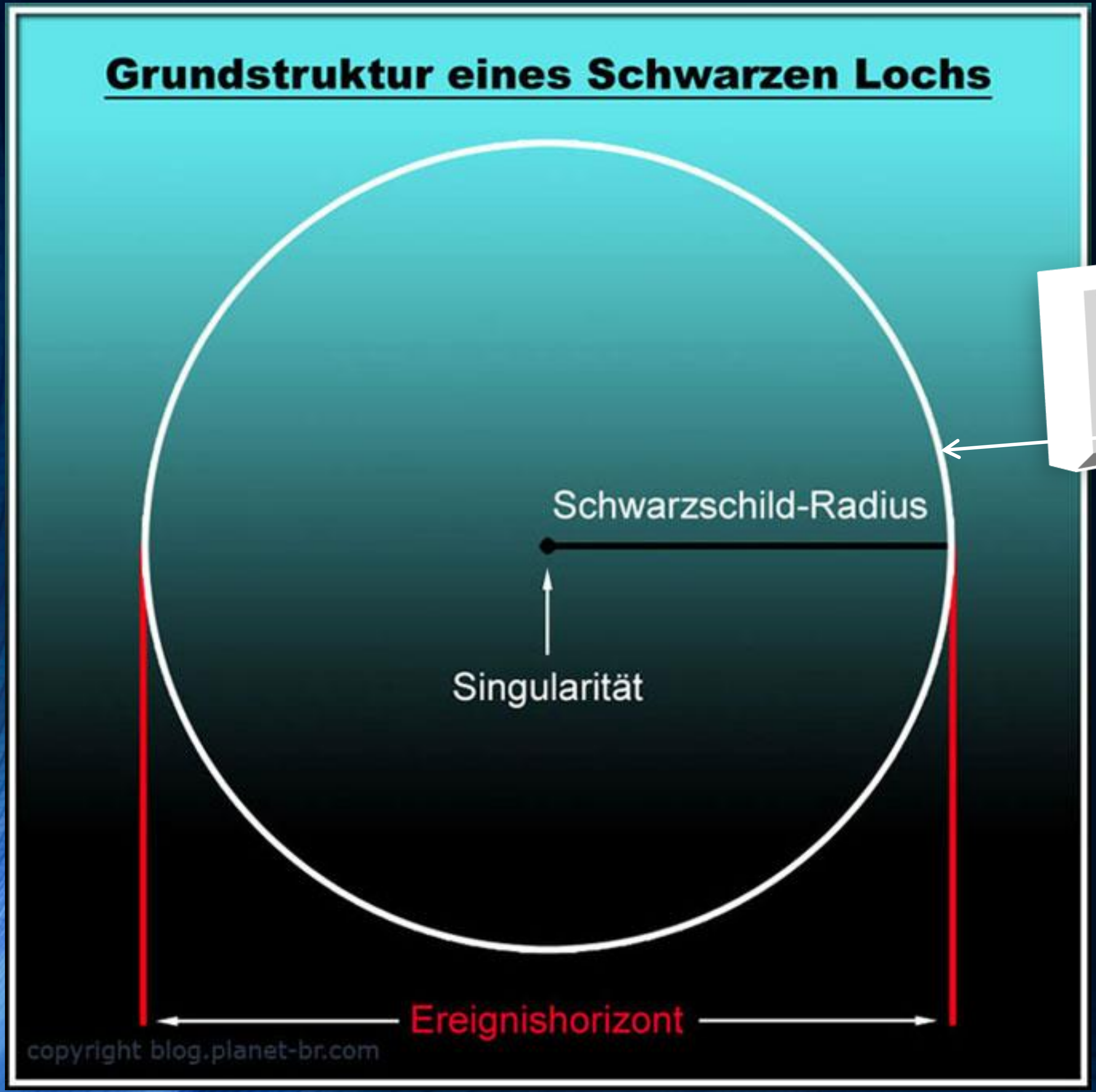

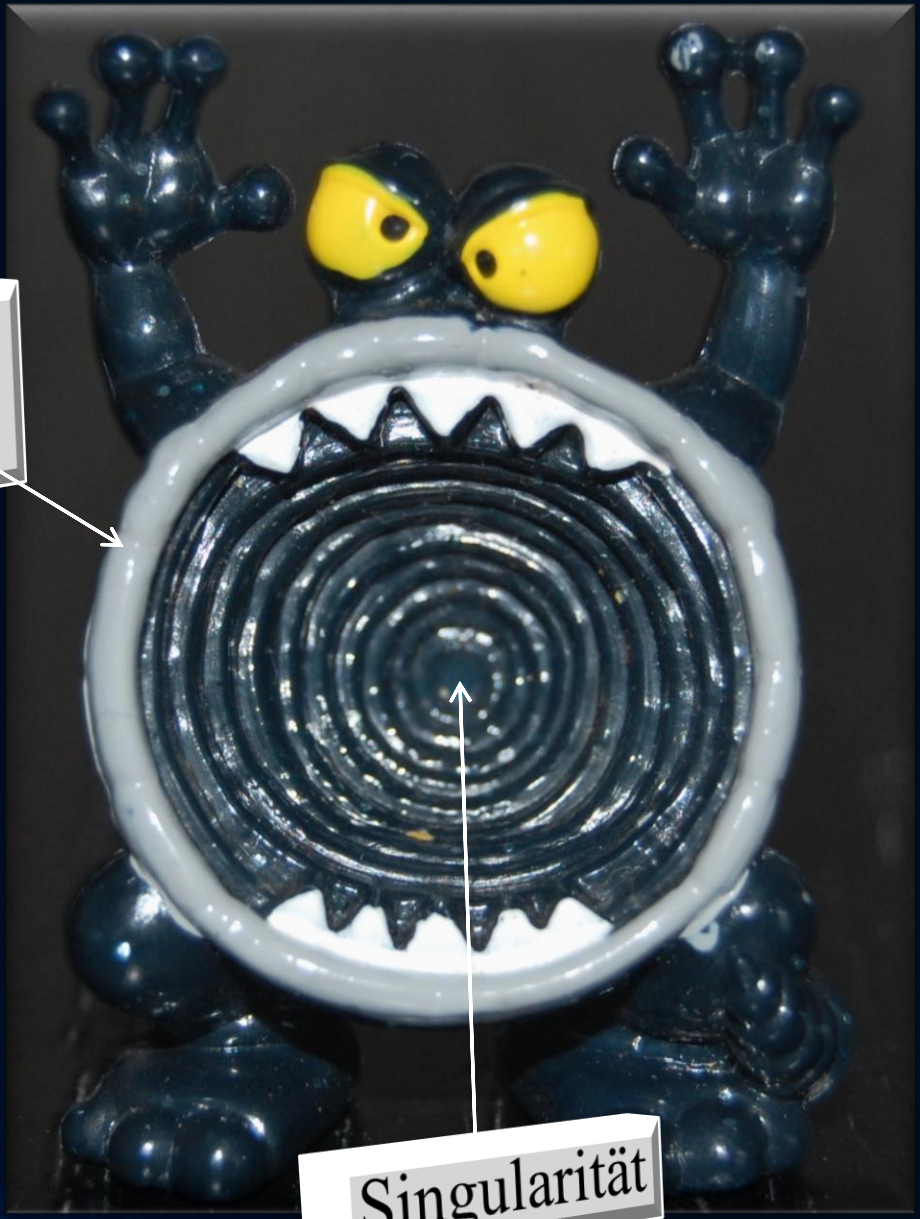

Der deutsche Bundestag in Berlin
Die wohl beste Veranschaulichung eines schwarzen Loches

Der Raumzeit-Tricher
im Reichstagsgebäude

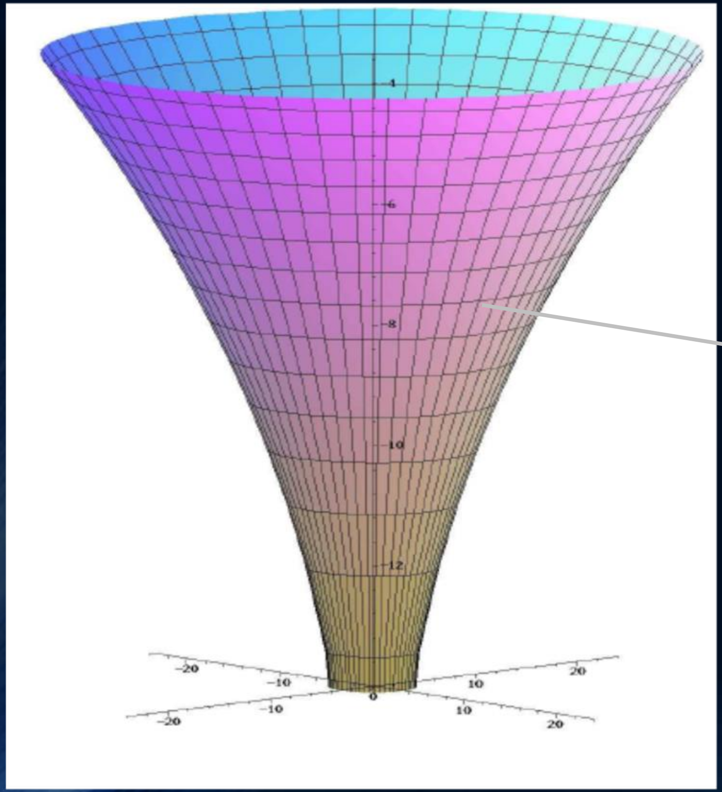

Schwarze Löcher und der deutsche Reichstag

Der deutsche Bundestag in Berlin

Die wohl beste Veranschaulichung eines schwarzen Loches